Outline

Surface, interface, and nanoscience—short introduction

Some surface concepts and techniques→why photoemission?

Synchrotron radiation: experimental aspects

Electronic structure—a brief review

The basic synchrotron radiation techniques: more details

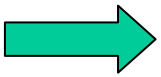

--Instrumentation for PS

Core-level photoemission

Valence-level photoemission

Microscopy with photoemission

Electron Spectroscopy—A typical configuration

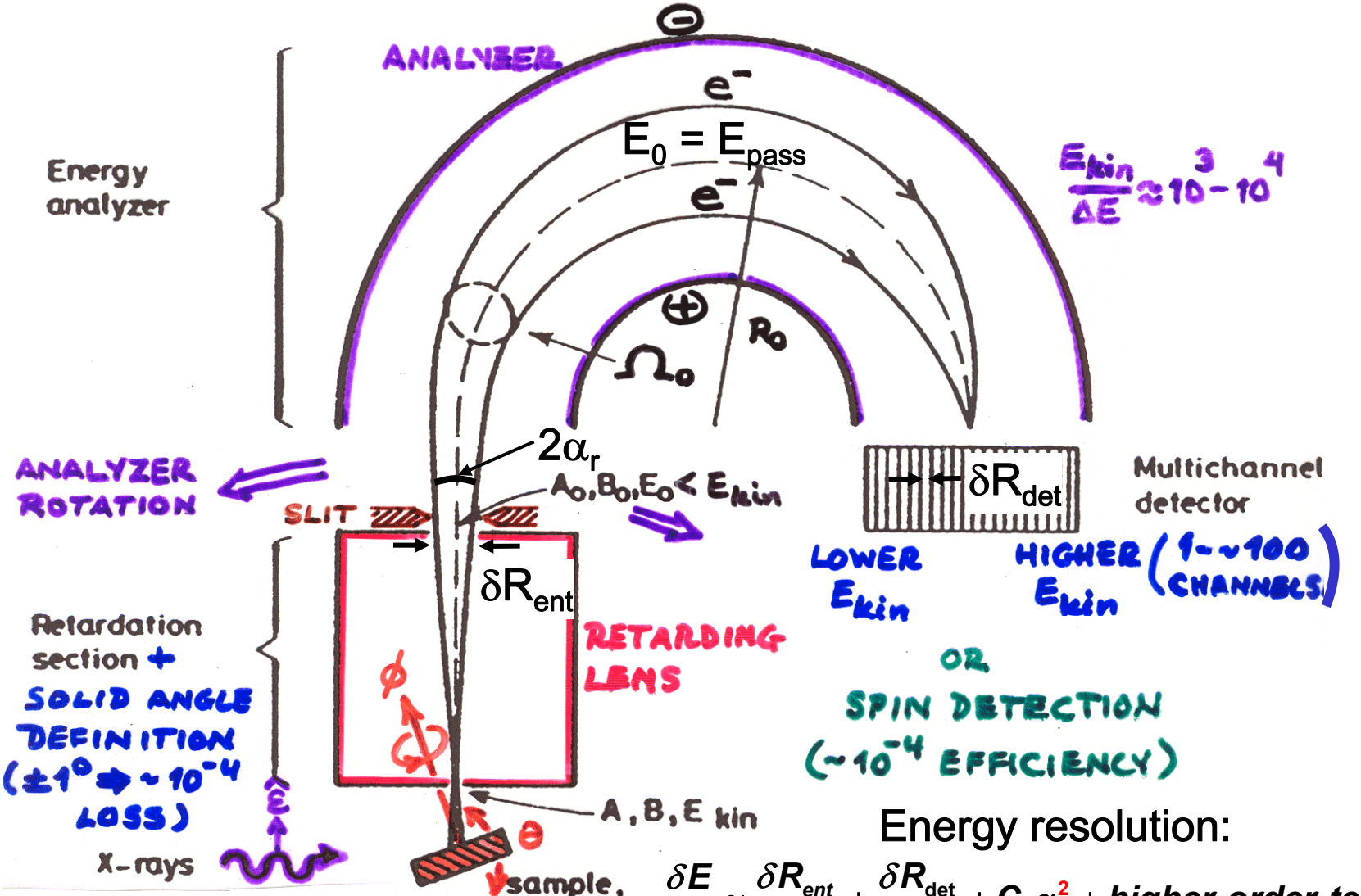

Energy resolution:

$$\frac{\delta E}{E_0} \approx \frac{\delta R_{ent}}{2R_0} + \frac{\delta R_{det}}{2R_0} + C_r \alpha_r^2 + \textit{higher order terms}$$

$C_r \approx 1.0$; α_z out of plane, much less critical

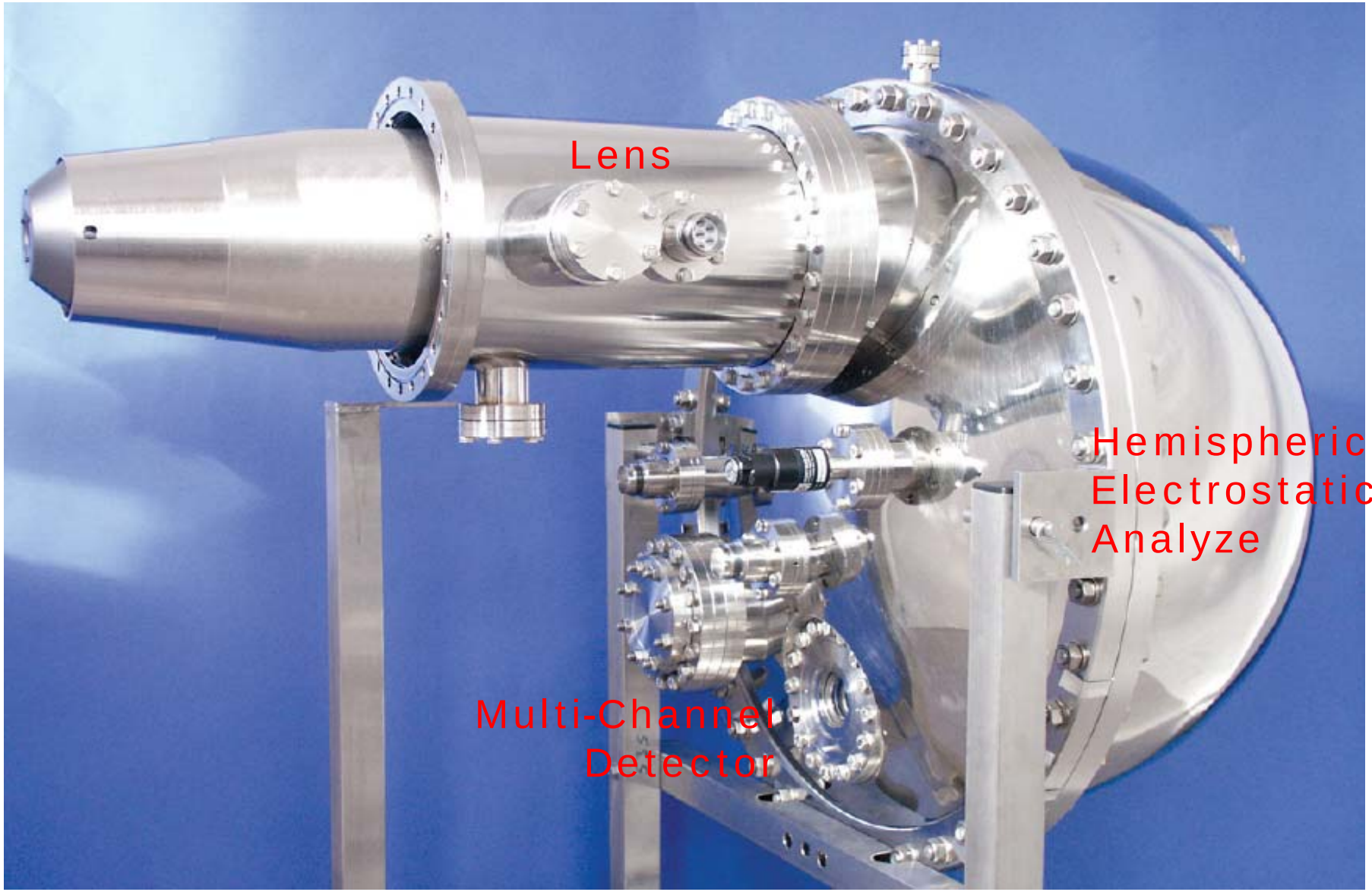

Nilsson et al., Journal of Electron Spectroscopy and Related Phenomena 70 (1994) 117-128

The Scienta R4000
(plus SPECS, MBS)

With proper lens imaging in vertical angle- an energy vs angle image at detector

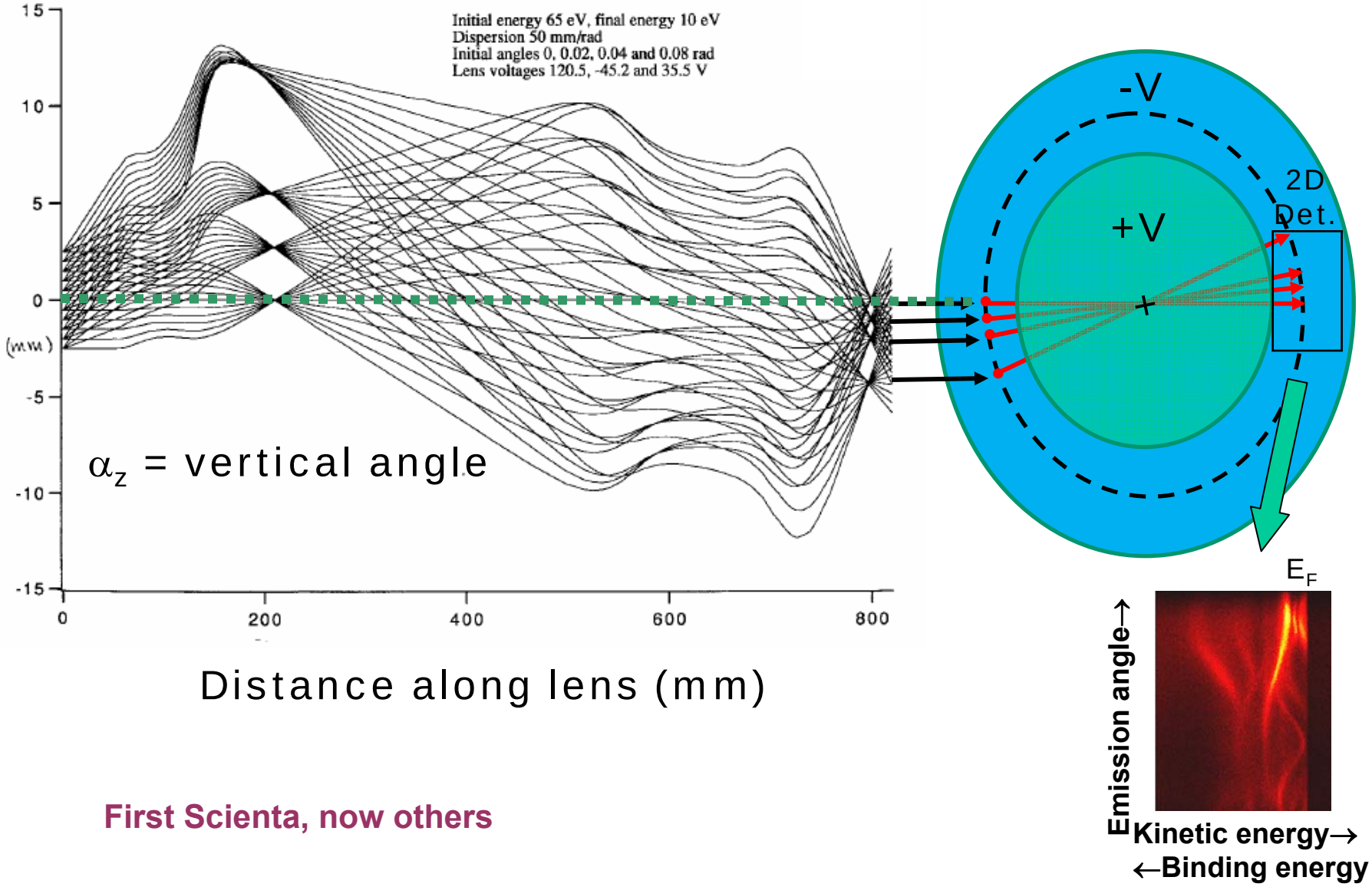

First Scienta, now others

MULTICHANNEL DETECTION GEOMETRIES

Multiple channeltrons: brute force

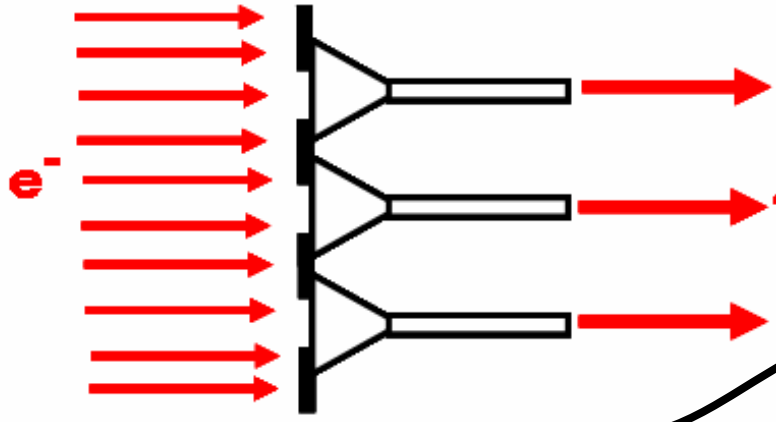

10^6-10^8 e^-

Up to ~ 1-5 MHz per channel

Crossed-wires—2D
Up to ~ 1GHz

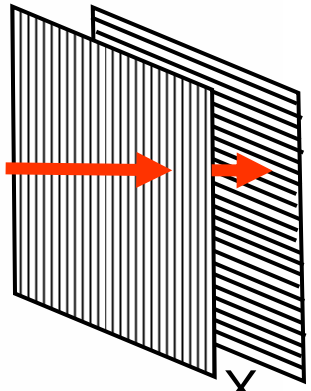

Microchannel plates (MCPs) and

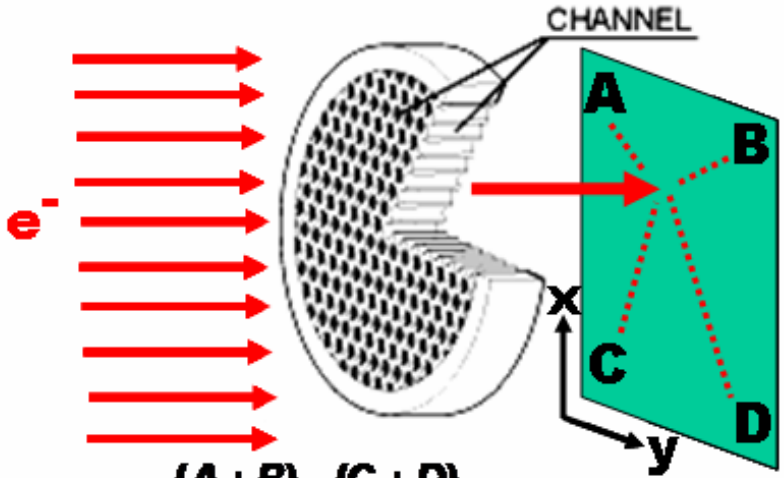

$$x = \frac{(A+B)-(C+D)}{A+B+C+D}$$

$$y = \frac{(B+D)-(A+C)}{A+B+C+D}$$

Resistive Anode—2D: Up to ~1 MHz

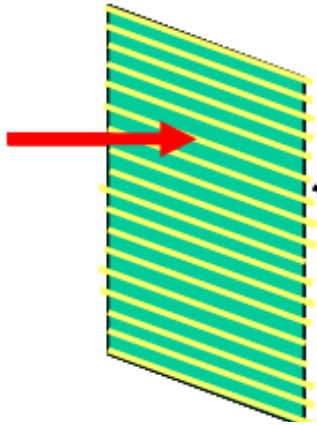

To IC channel

Individual Collectors—1D (Elettra and the ALS): Up to ~ 1GHz

The Microchannel Plate Electron (and Photon) Multiplier

Diam.
Down to 5
microns

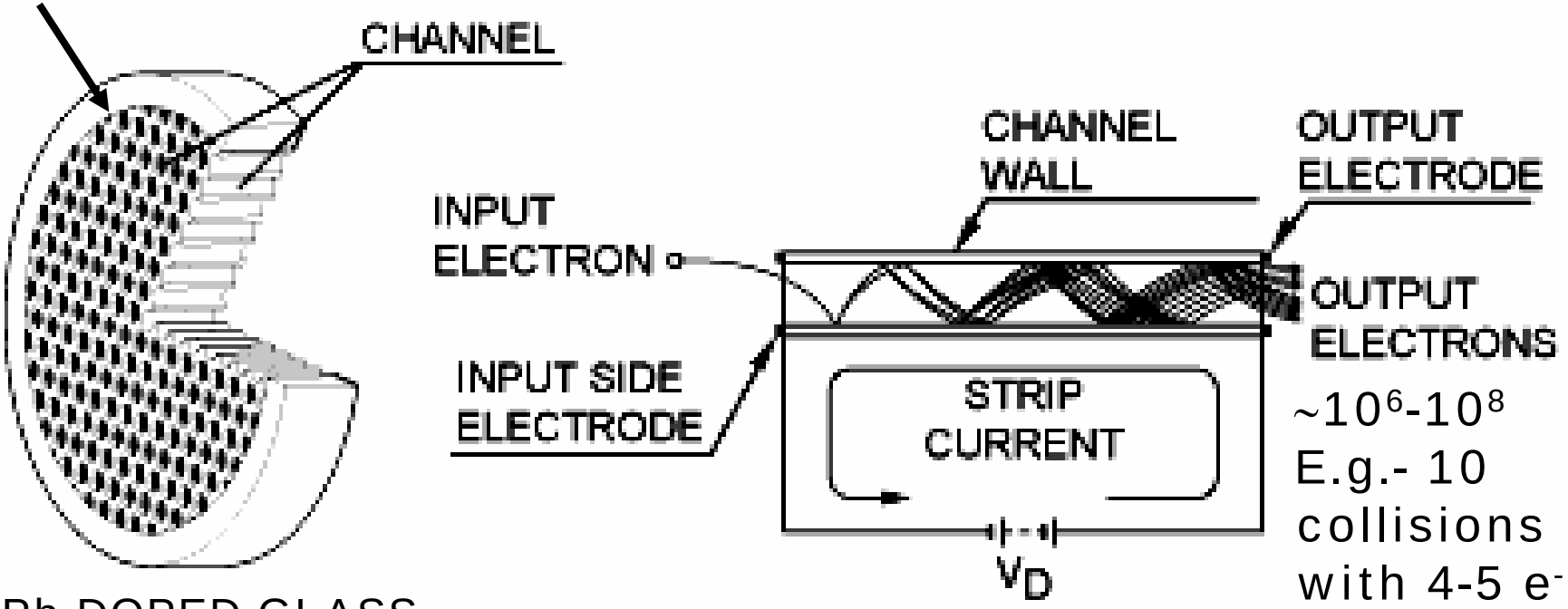

Pb-DOPED GLASS

~10^6-10^8
E.g.- 10
collisions
with 4-5 e^-
each

Next Generation Detection: ALS High-Speed Detector—1D

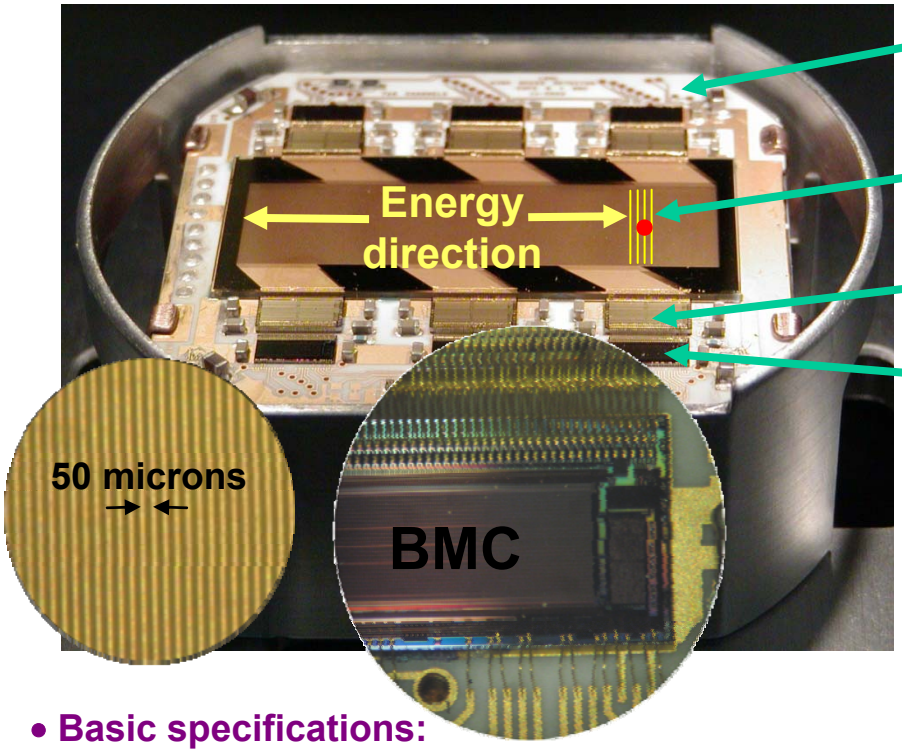

Ceramic substrate

768 collector strips

Amplifier/discriminator chip (CAFE-M) from HEP

Buffered multichannel counter chip (BMC)

Microchannel plates

e^- or $h\nu$

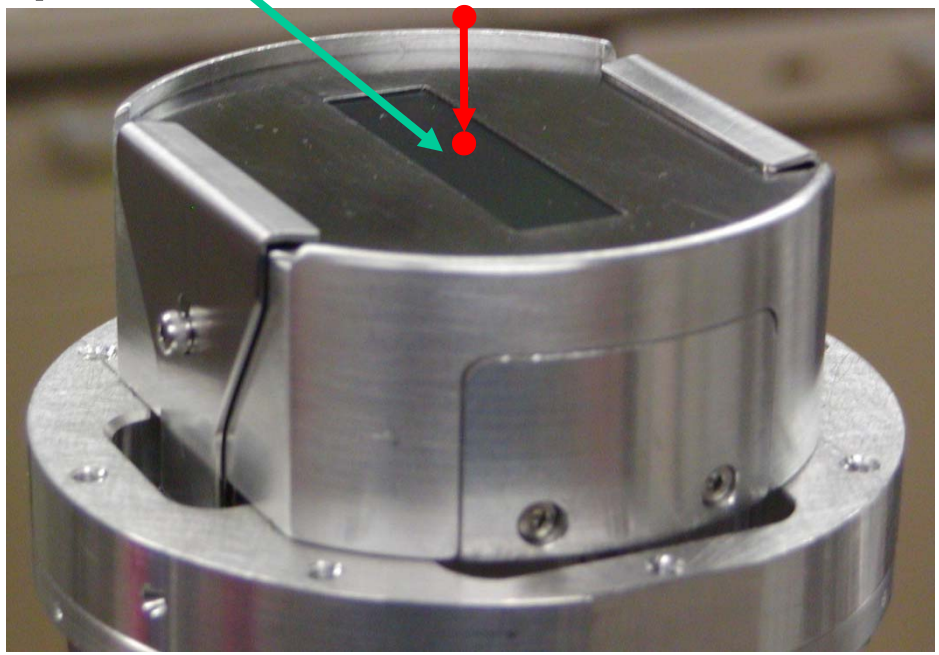

- Basic specifications:
  - 768 channels along one dimension
  - ~75 micron spatial resolution
  - >2 GHz overall linear count-rate→ 100-1000x faster than present
  - spectral readout in as little as 200 μs→ time-resolved measurements
  - programmable, robust
- Operating since July, 2003, final improvements underway: HV insulation, memory buffering
- Reinstallation for fulltime usage: 2008-09

ALS High-Speed Detector: Some First Data in 2004

Photoelectron Diffraction from NiO(001)

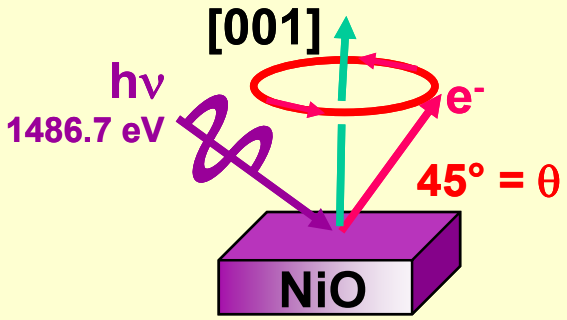

O 1s Spectrum

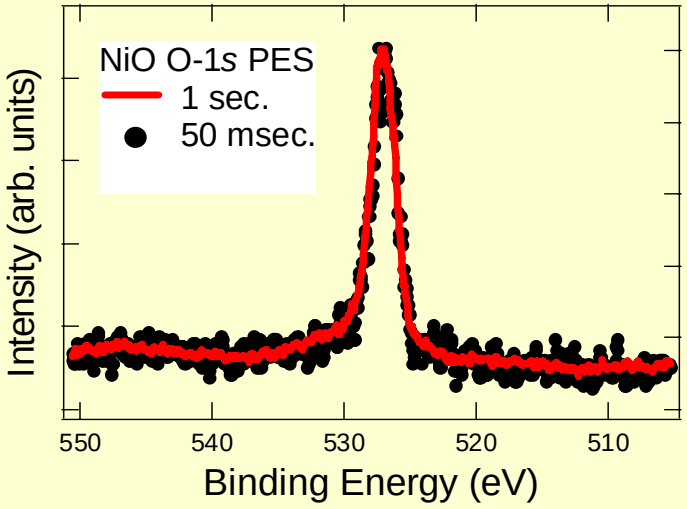

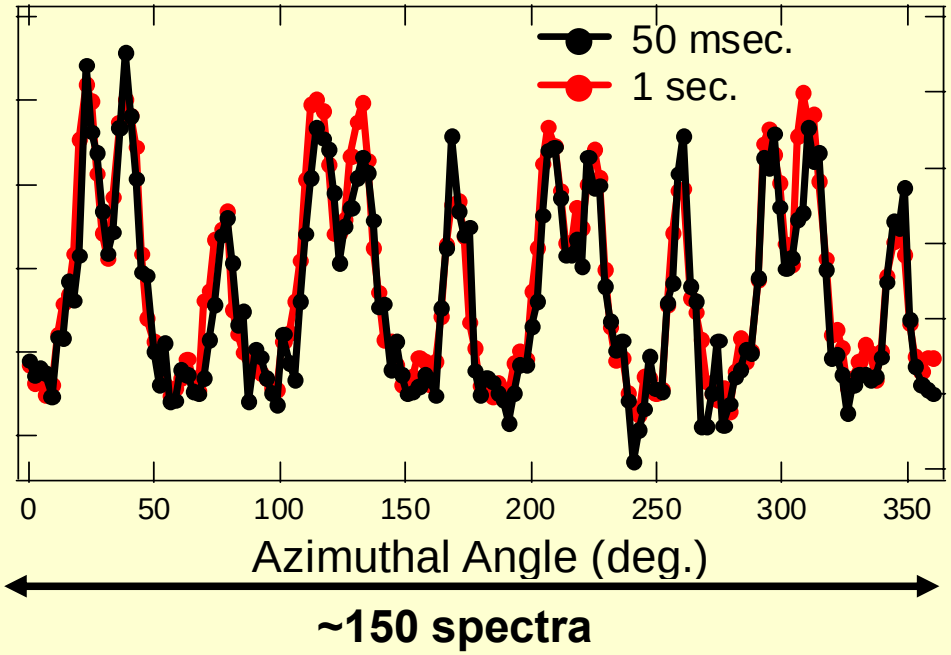

~150 spectra

Total 2 min. @ 50 msec/spectrum
→7 sec. without CPU process time.
With future data buffering:
→ 30 ms total @ 200 μs/spectrum

To be reinstalled for permanent use in 2008-2009

The MicroMott Electron Spin Detector

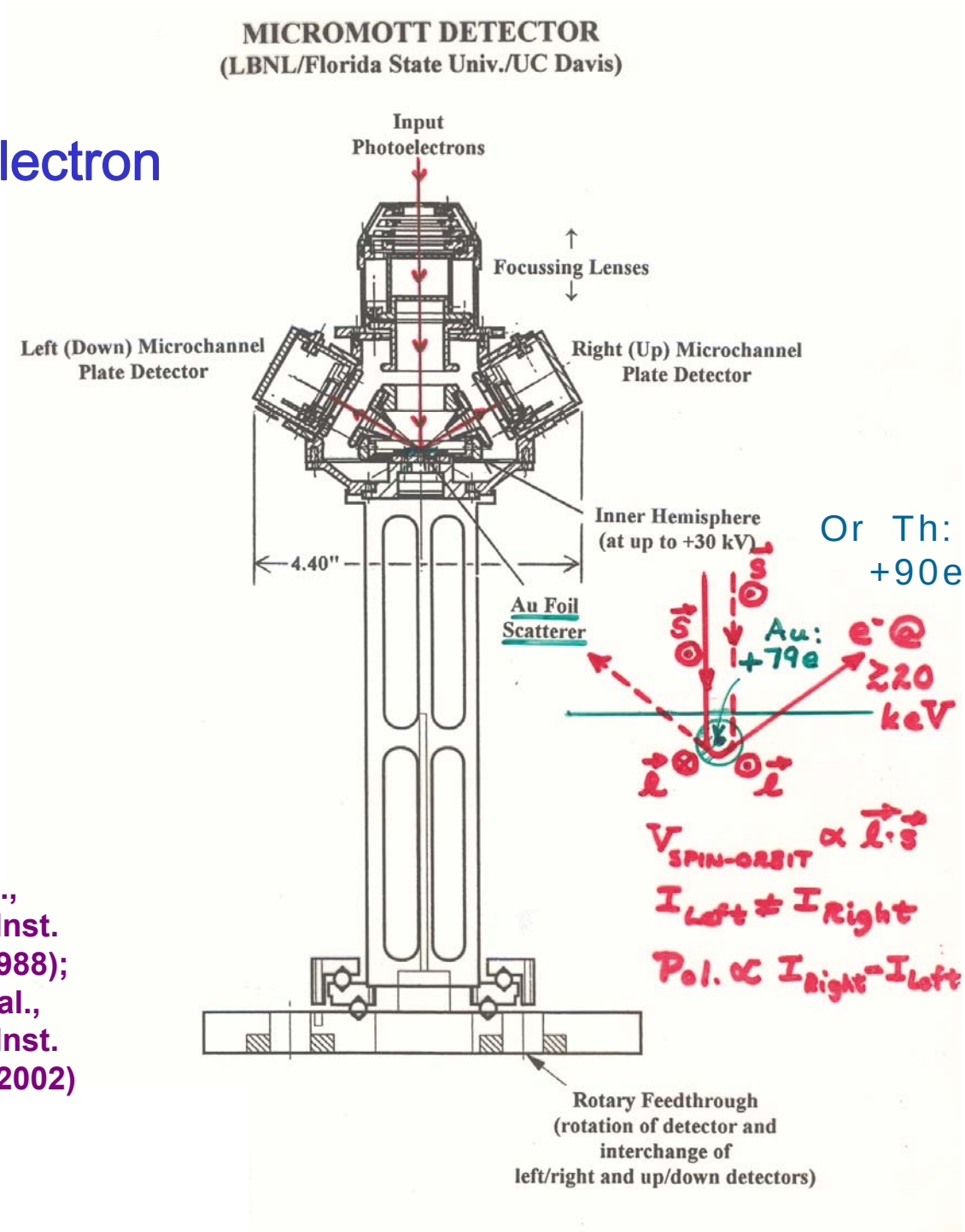

Or Th: or U:
+90e +92e

Tang et al.,
Rev. Sci. Inst.
59, 504 (1988);
Huang et al.,
Rev. Sci. Inst.
73, 3778 (2002)

Multi-Technique Spectrometer/ Diffractometer (Soft X-Ray/XUV)

Light from ALS elliptically polarized undulator (80-1500 eV)

New refocussing mirror (August '07)

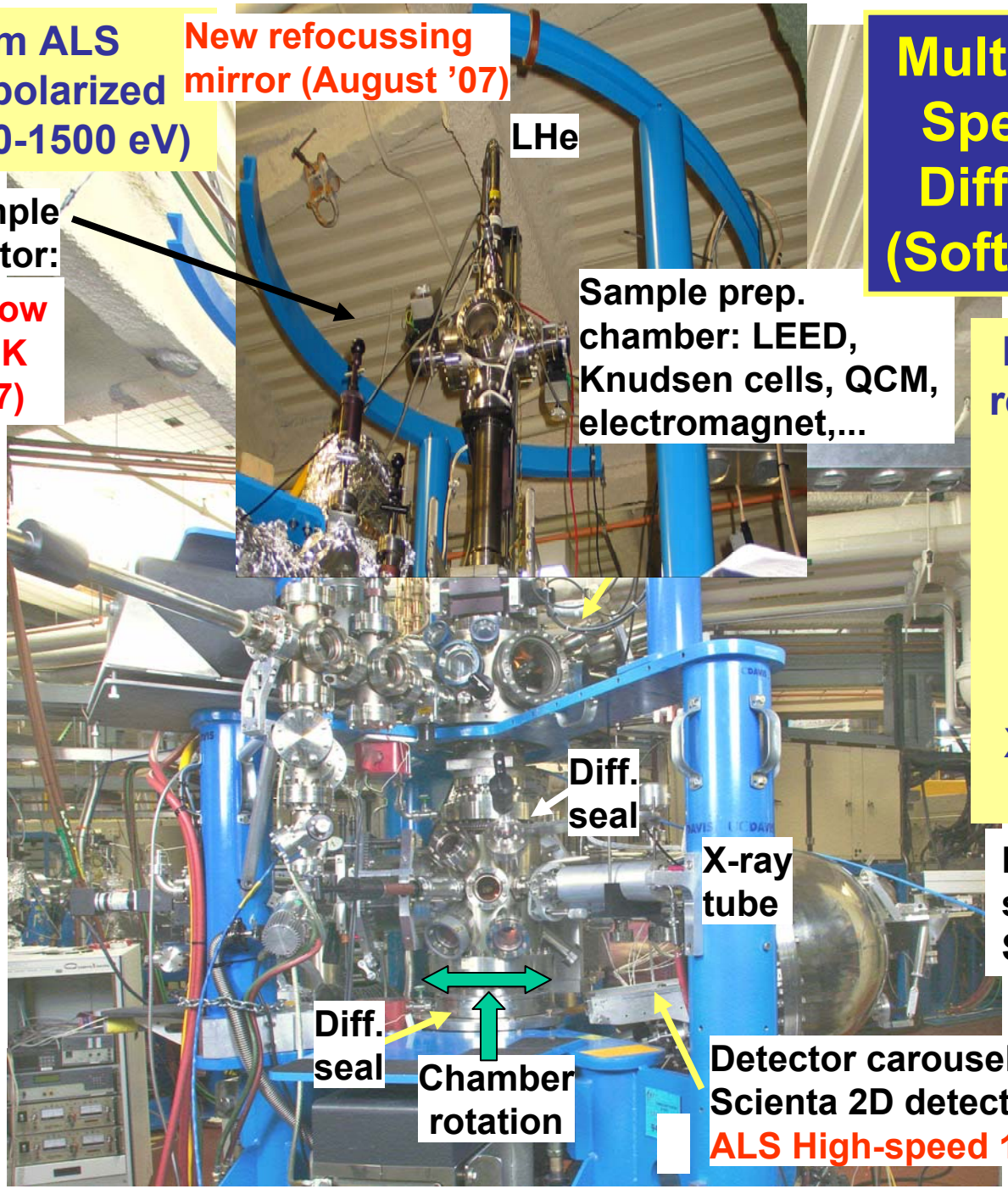

Permits using all relevant soft x-ray spectroscopies on a single sample: PS, PD, PH; XAS (e^- or photon detection), XES/REXS/RIXS, with MCD, MLD

Electron spectrometer: Scienta SES "2002"

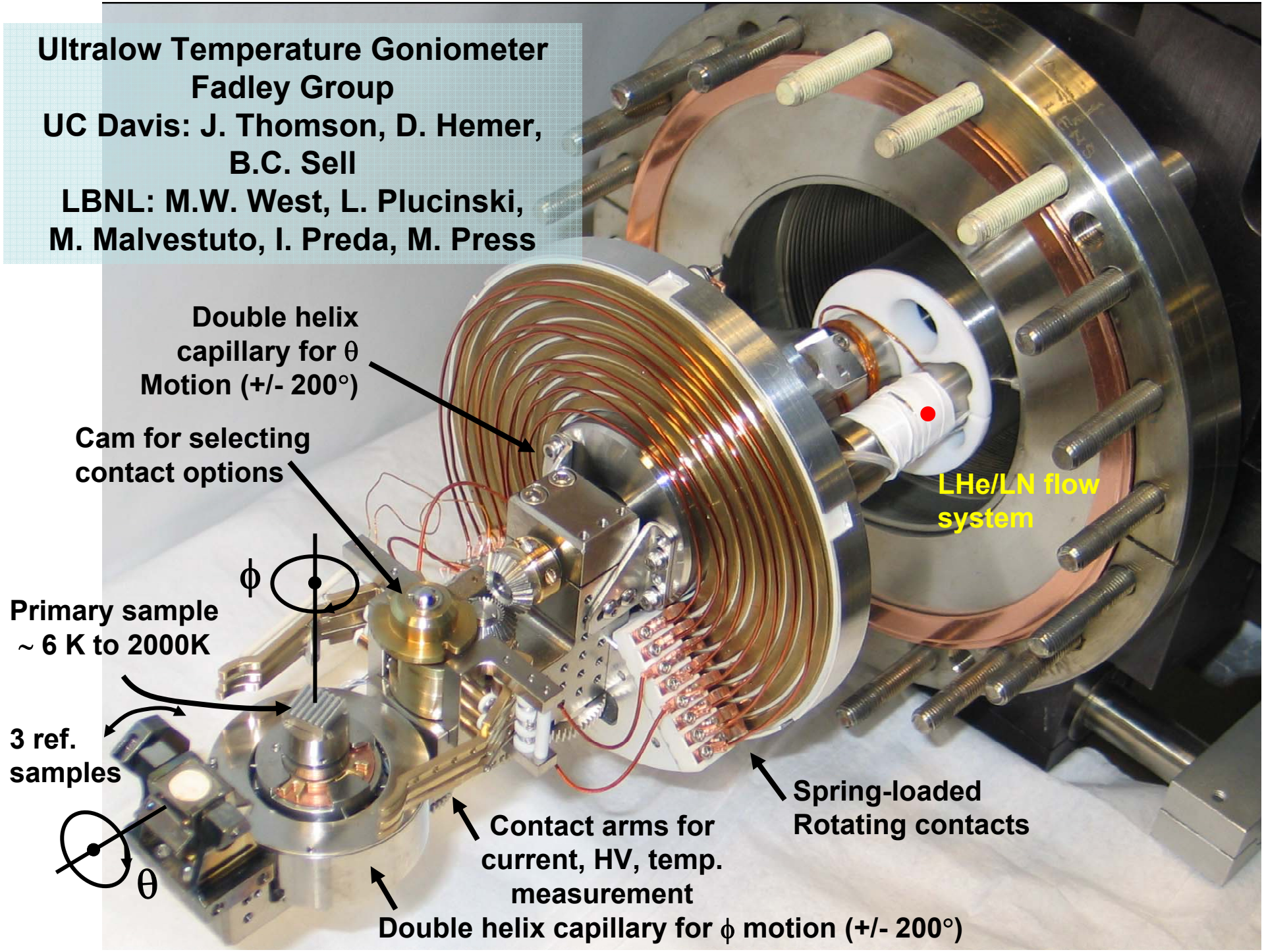
Ultralow Temperature Goniometer
Fadley Group
UC Davis: J. Thomson, D. Hemer, B.C. Sell
LBNL: M.W. West, L. Plucinski, M. Malvestuto, I. Preda, M. Press
Double helix capillary for θ Motion (+/- 200°)
Cam for selecting contact options
LHe/LN flow system
ϕ
Primary sample ~ 6 K to 2000K
3 ref. samples
θ
Spring-loaded Rotating contacts
Contact arms for current, HV, temp. measurement
Double helix capillary for ϕ motion (+/- 200°)

First cooldown tests, temp. read with Si diode in contact with Cu cryogen reservoir just under sample

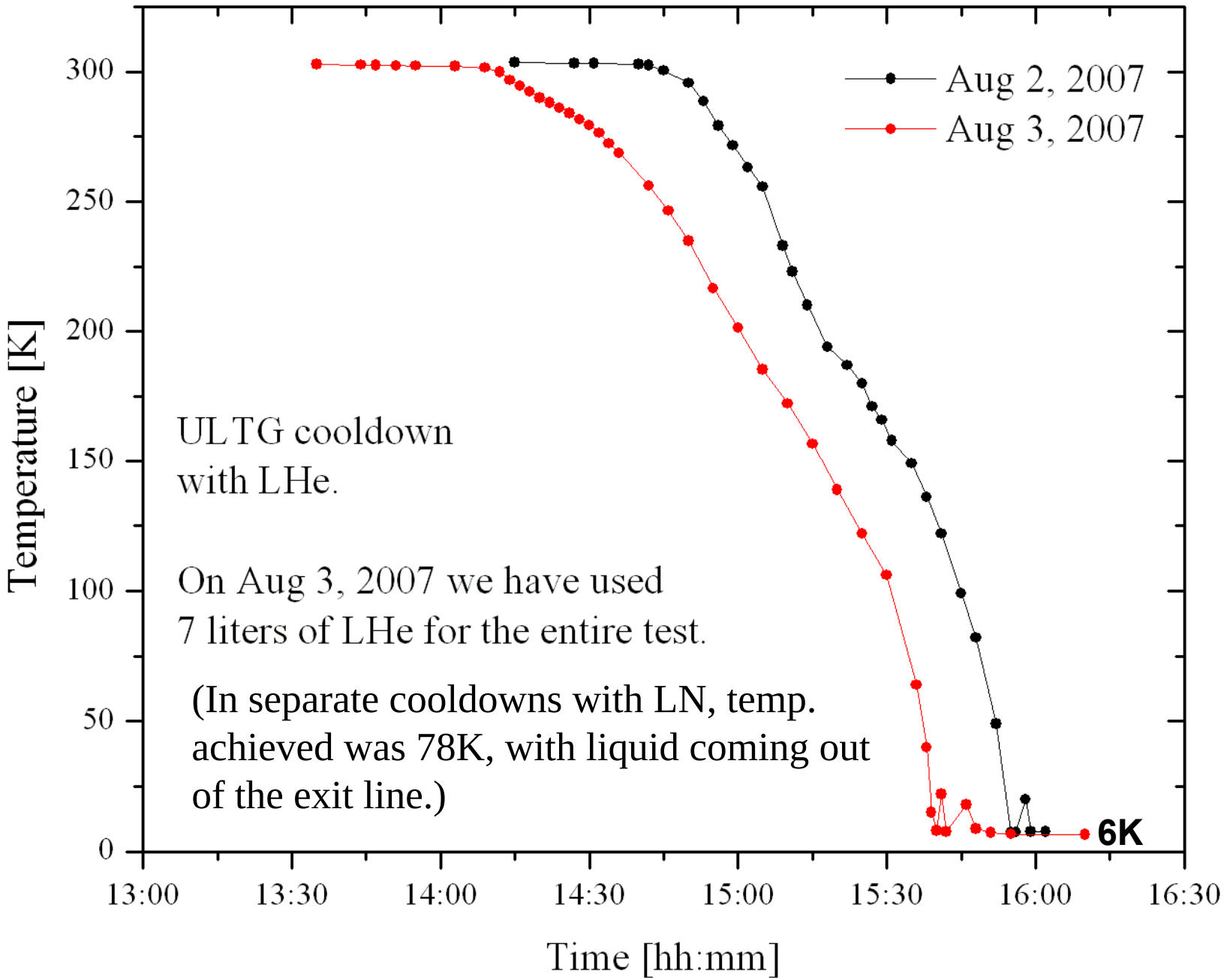

Measuring Electron Binding Energies: Basic energetics

$$h\nu = E_{binding}^{Vacuum} + E_{kinetic} = E_{binding}^{Fermi} + \varphi_{spectrometer} + E_{kinetic}$$

One-Electron Picture of Photoemission from a Surface

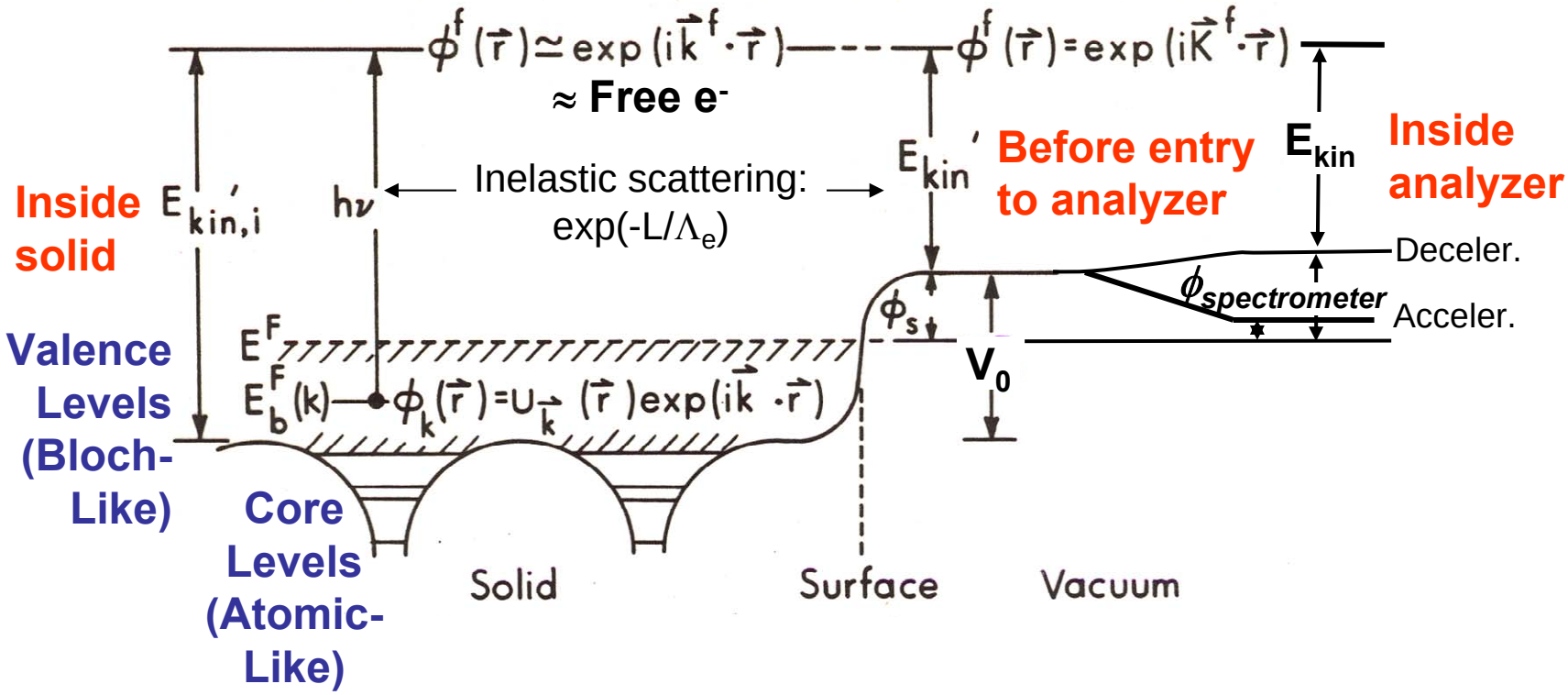

Measuring Electron Binding Energies

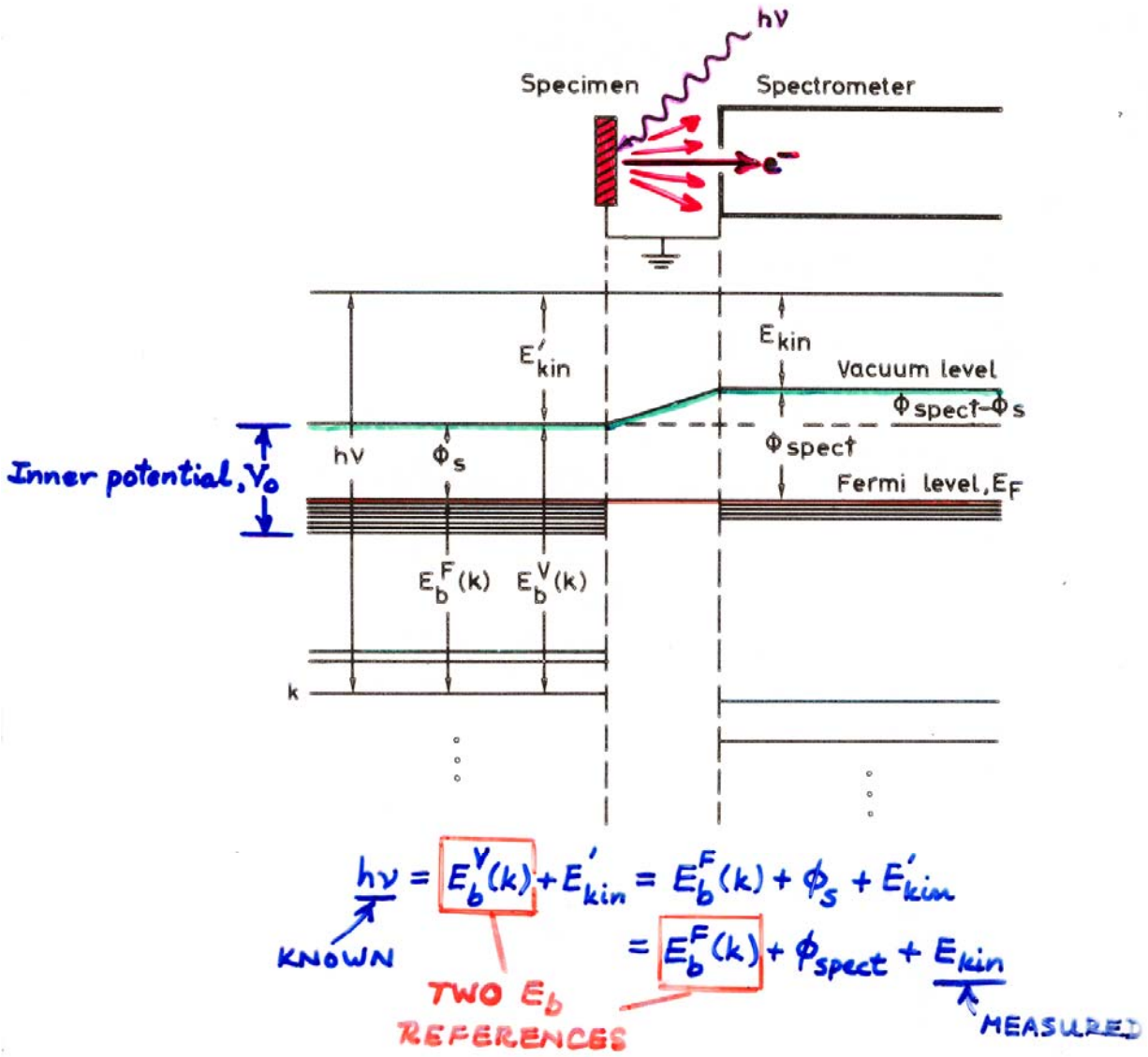

Figure 3 -- Energy level diagram for a metallic specimen in electrical equilibrium with an electron spectrometer. The closely spaced levels near the Fermi level E_F represent the filled portions of the valence bands in specimen and spectrometer. The deeper levels are core levels. An analogous diagram also applies to semiconducting or insulating specimens, with the only difference being that E_F lies somewhere between the filled valence bands and the empty conduction bands above.

"Basic Concepts of XPS"
Figure 3

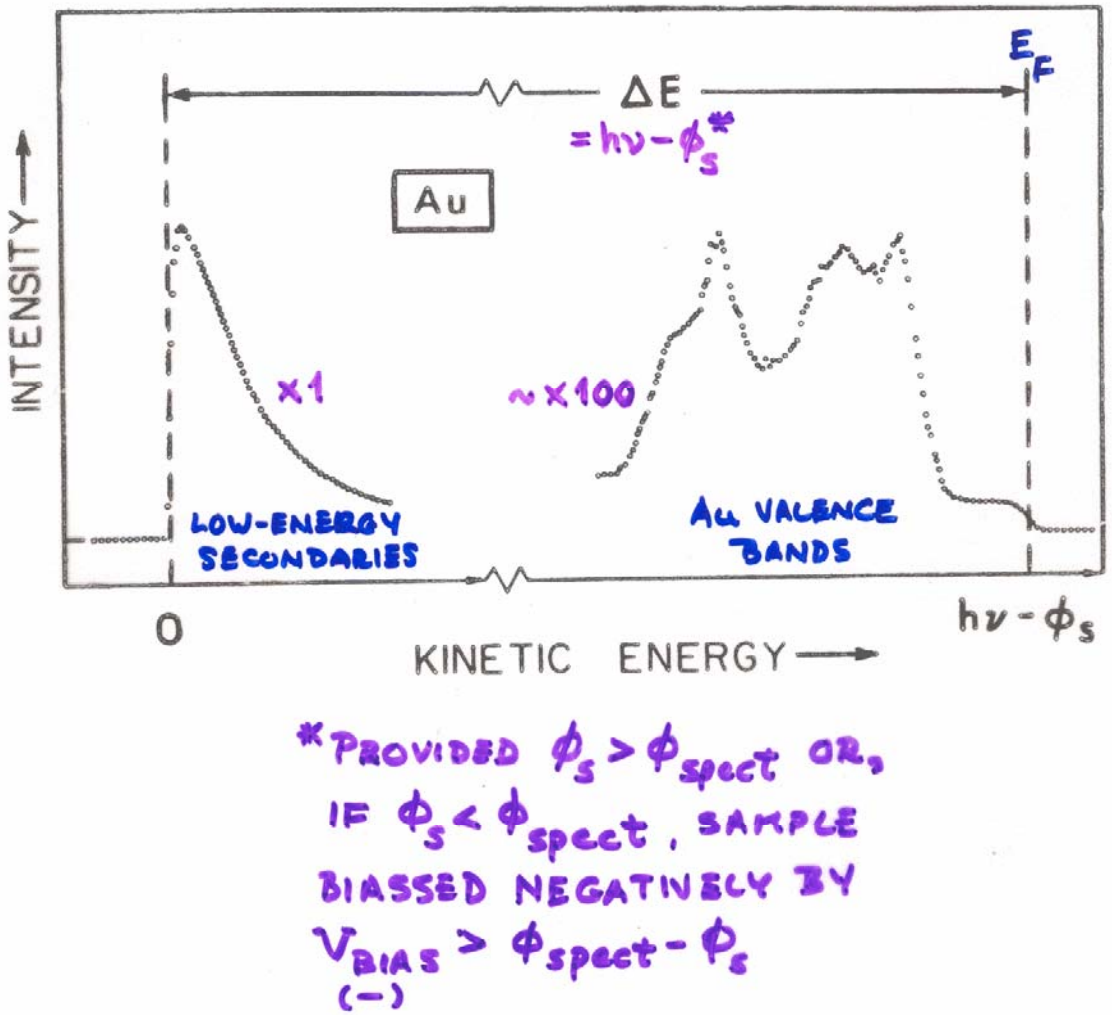

Figure 4 -- Full XPS spectral scan for a polycrystalline Au specimen, showing both the cutoff of the secondary electron peak at zero kinetic energy and the high-energy cutoff for emission from levels at the metal Fermi level. The measureable distance ΔE thus equals $h\nu - \phi_s$, provided that suitable specimen biasing has been utilized. For this case, $h\nu$ was 1253.6 eV and ϕ_s was 5.1 eV. (From Baer, reference 56).

"Basic Concepts of XPS"
Figure 3

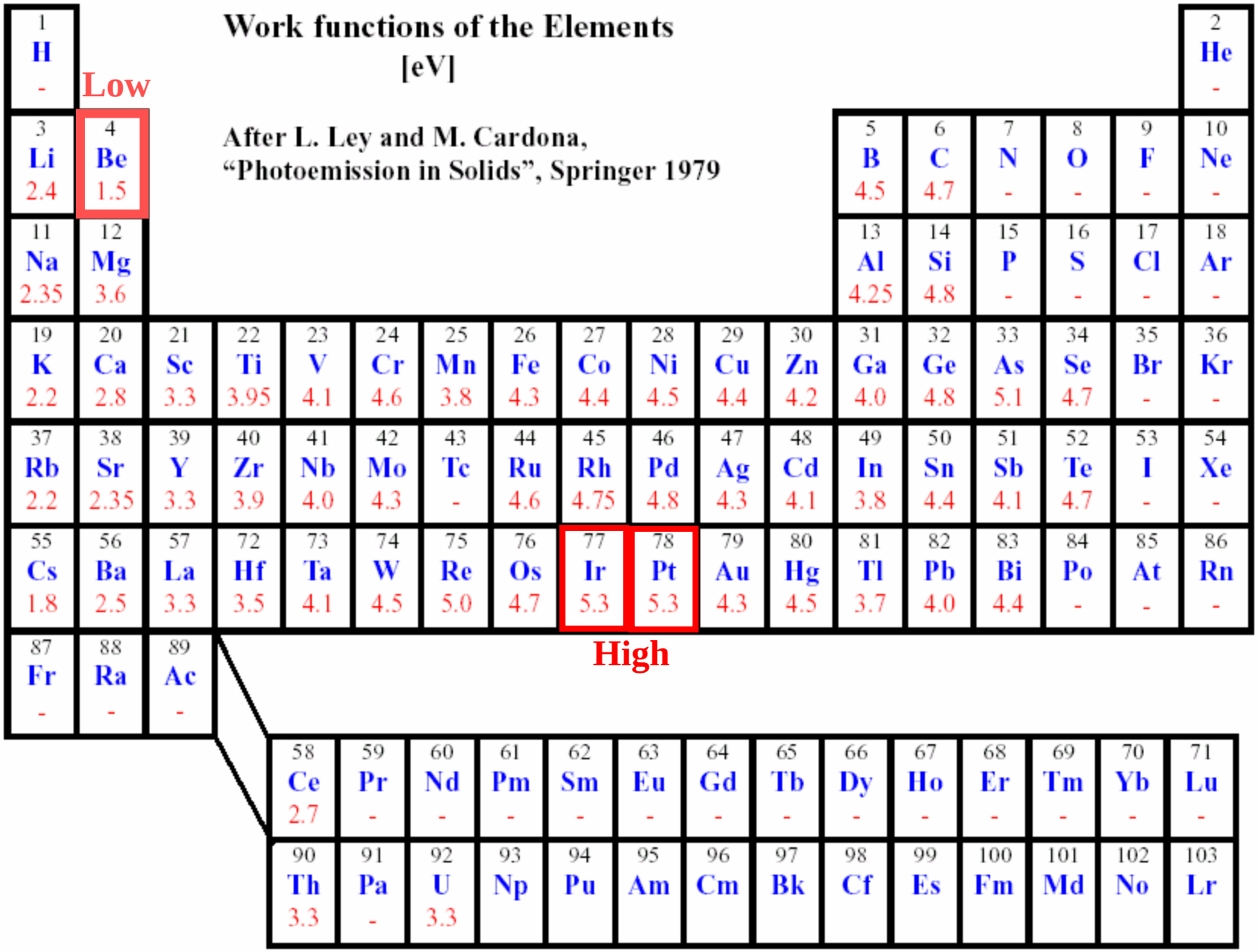
Work functions of the Elements
[eV]
After L. Ley and M. Cardona,
"Photoemission in Solids", Springer 1979
Low
High
1 H -
2 He -
3 Li 2.4
4 Be 1.5
5 B 4.5
6 C 4.7
7 N -
8 O -
9 F -
10 Ne -
11 Na 2.35
12 Mg 3.6
13 Al 4.25
14 Si 4.8
15 P -
16 S -
17 Cl -
18 Ar -
19 K 2.2
20 Ca 2.8
21 Sc 3.3
22 Ti 3.95
23 V 4.1
24 Cr 4.6
25 Mn 3.8
26 Fe 4.3
27 Co 4.4
28 Ni 4.5
29 Cu 4.4
30 Zn 4.2
31 Ga 4.0
32 Ge 4.8
33 As 5.1
34 Se 4.7
35 Br -
36 Kr -
37 Rb 2.2
38 Sr 2.35
39 Y 3.3
40 Zr 3.9
41 Nb 4.0
42 Mo 4.3
43 Tc -
44 Ru 4.6
45 Rh 4.75
46 Pd 4.8
47 Ag 4.3
48 Cd 4.1
49 In 3.8
50 Sn 4.4
51 Sb 4.1
52 Te 4.7
53 I -
54 Xe -
55 Cs 1.8
56 Ba 2.5
57 La 3.3
72 Hf 3.5
73 Ta 4.1
74 W 4.5
75 Re 5.0
76 Os 4.7
77 Ir 5.3
78 Pt 5.3
79 Au 4.3
80 Hg 4.5
81 Tl 3.7
82 Pb 4.0
83 Bi 4.4
84 Po -
85 At -
86 Rn -
87 Fr -
88 Ra -
89 Ac -
58 Ce 2.7
59 Pr -
60 Nd -
61 Pm -
62 Sm -
63 Eu -
64 Gd -
65 Tb -
66 Dy -
67 Ho -
68 Er -
69 Tm -
70 Yb -
71 Lu -
90 Th 3.3
91 Pa -
92 U 3.3
93 Np
94 Pu
95 Am
96 Cm
97 Bk
98 Cf
99 Es
100 Fm
101 Md
102 No
103 Lr

Electron Work Functions of the Elements

From the CRC-Handbook, 73rd edition (1993)

Element	Surface crystallographic orientation	Work function (eV)
Ag	polycrystalline	4.26
	(100)	4.64
	(110)	4.52
	(111)	4.74
Al	polycrystalline	4.28
	(100)	4.41
	(110)	4.06
	(111)	4.24
As		3.75
Au	polycrystalline	5.1
	(100)	5.47
	(110)	5.37
	(111)	5.31
B		4.45
Ba		2.7
Be		4.98
Bi		4.22
C		5.0

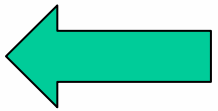

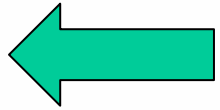

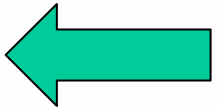

Depends on surface orientation

Measuring Electron Binding Energies: Charging Effects For Insulators

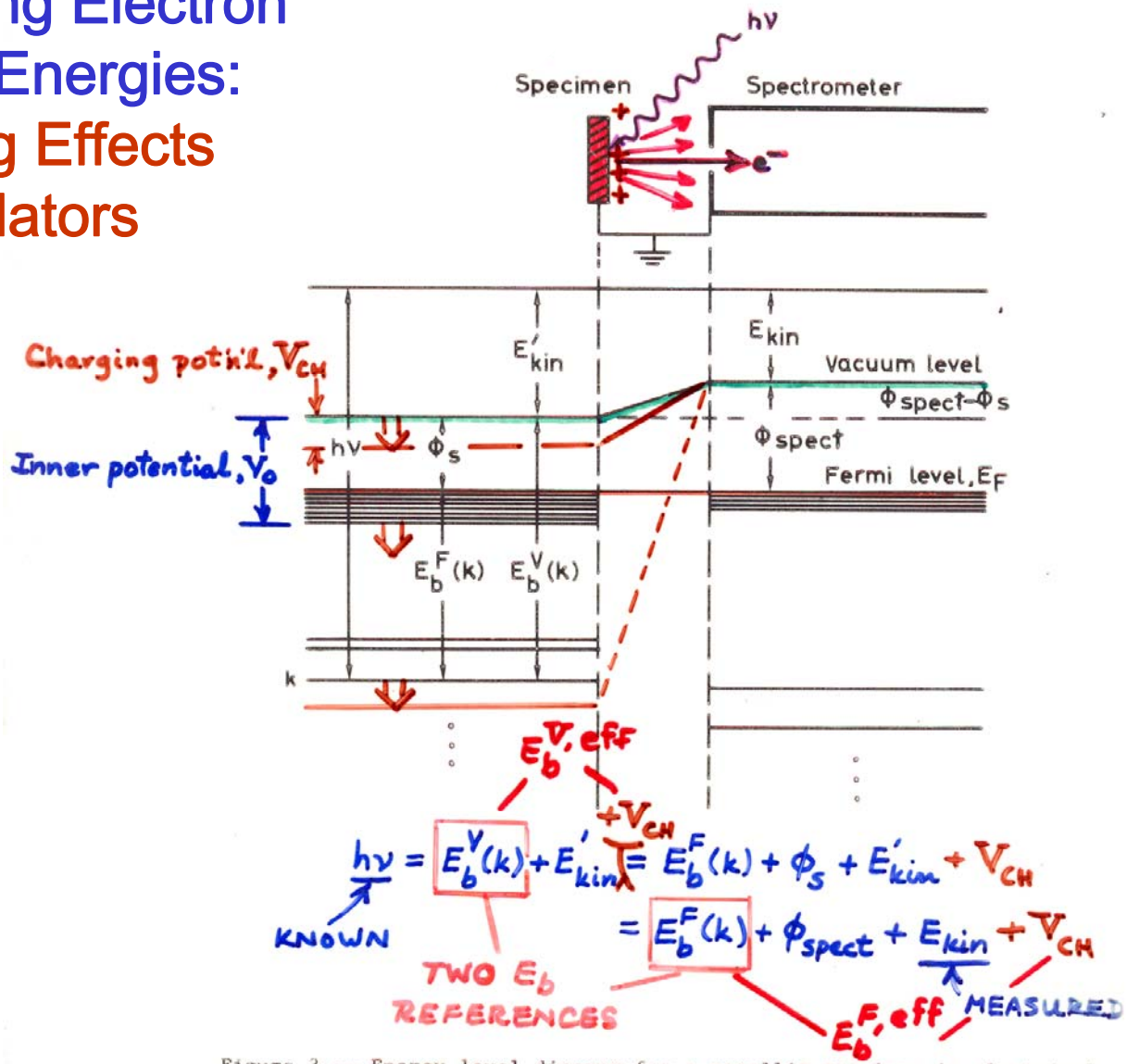

Figure 3 -- Energy level diagram for a metallic specimen in electrical equilibrium with an electron spectrometer. The closely spaced levels near the Fermi level E_F represent the filled portions of the valen bands in specimen and spectrometer. The deeper levels are core levels. An analogous diagram also applies to semiconducting or insulating specimens, with the only difference being that E_F lies somewhere between the filled valence bands and the empty conduction bands above.

"Basic Concepts of XPS" Figure 3

BEST CURRENT SOLUTION TO AN OLD PROBLEM: CHARGING IN INSULATORS

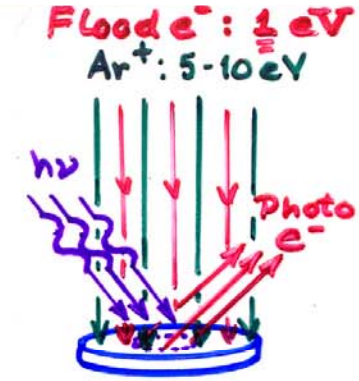

PET:

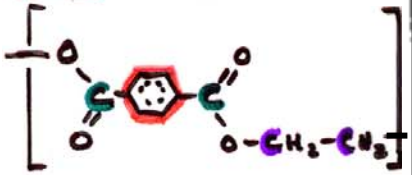

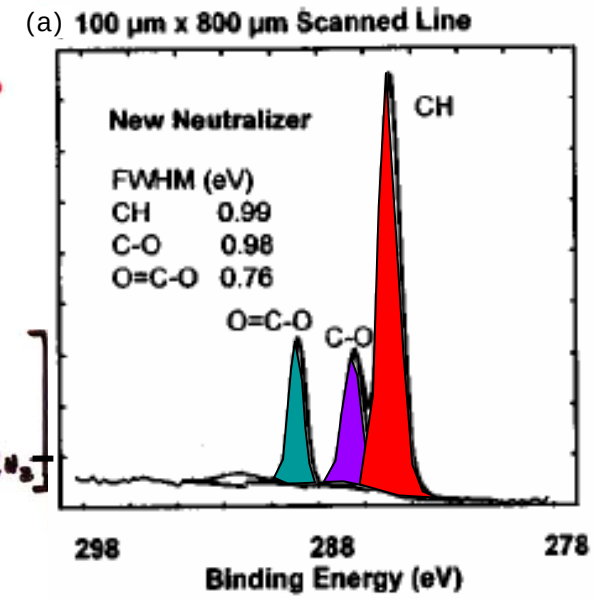

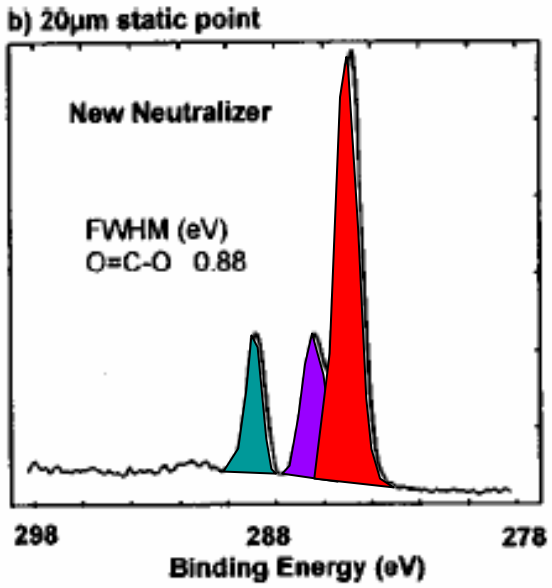

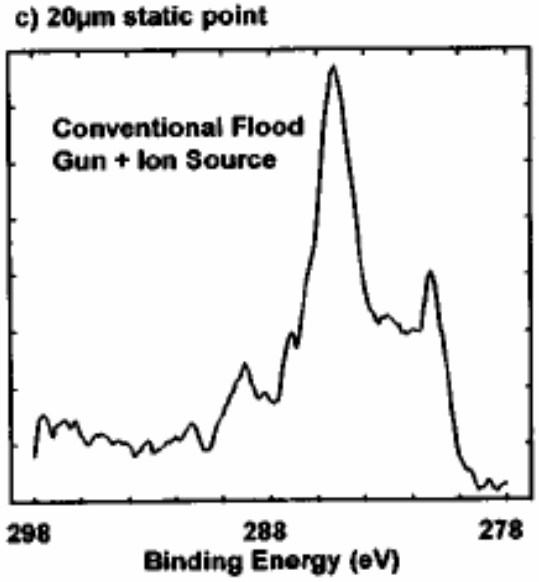

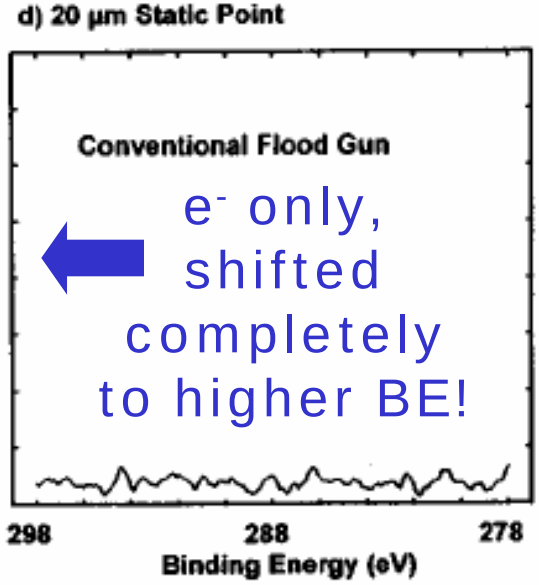

e⁻ only, shifted completely to higher BE!

P. LARSON, M. KELLY, J. VAC. SCI. TECH. 16, 3483 ('98)

Basic energetics

$$h\nu = E^{Vacuum}_{binding} + E_{kinetic} = E^{Fermi}_{binding} + \varphi_{spectrometer} + E_{kinetic}$$

One-Electron Picture of Photoemission from a Surface

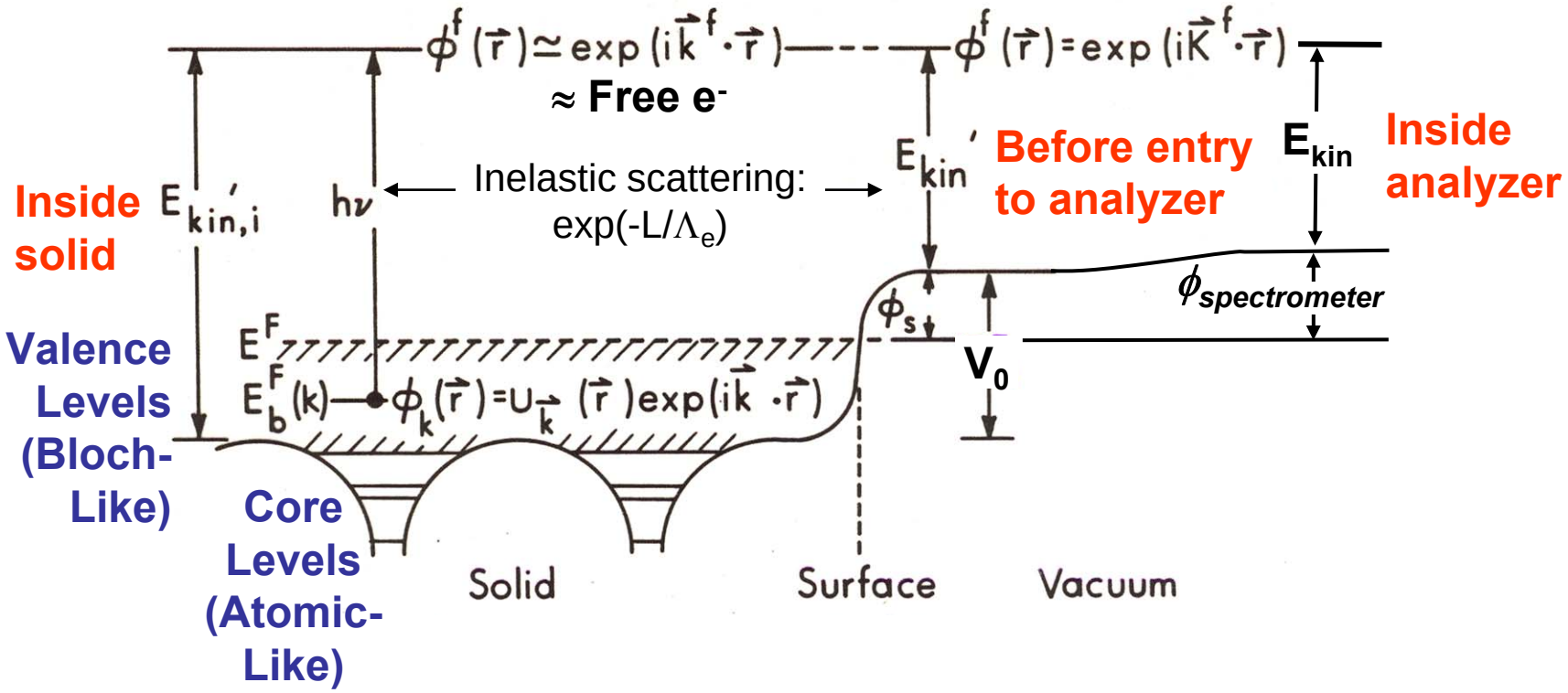

One-Electron Picture of Photoemission from a Surface—3D

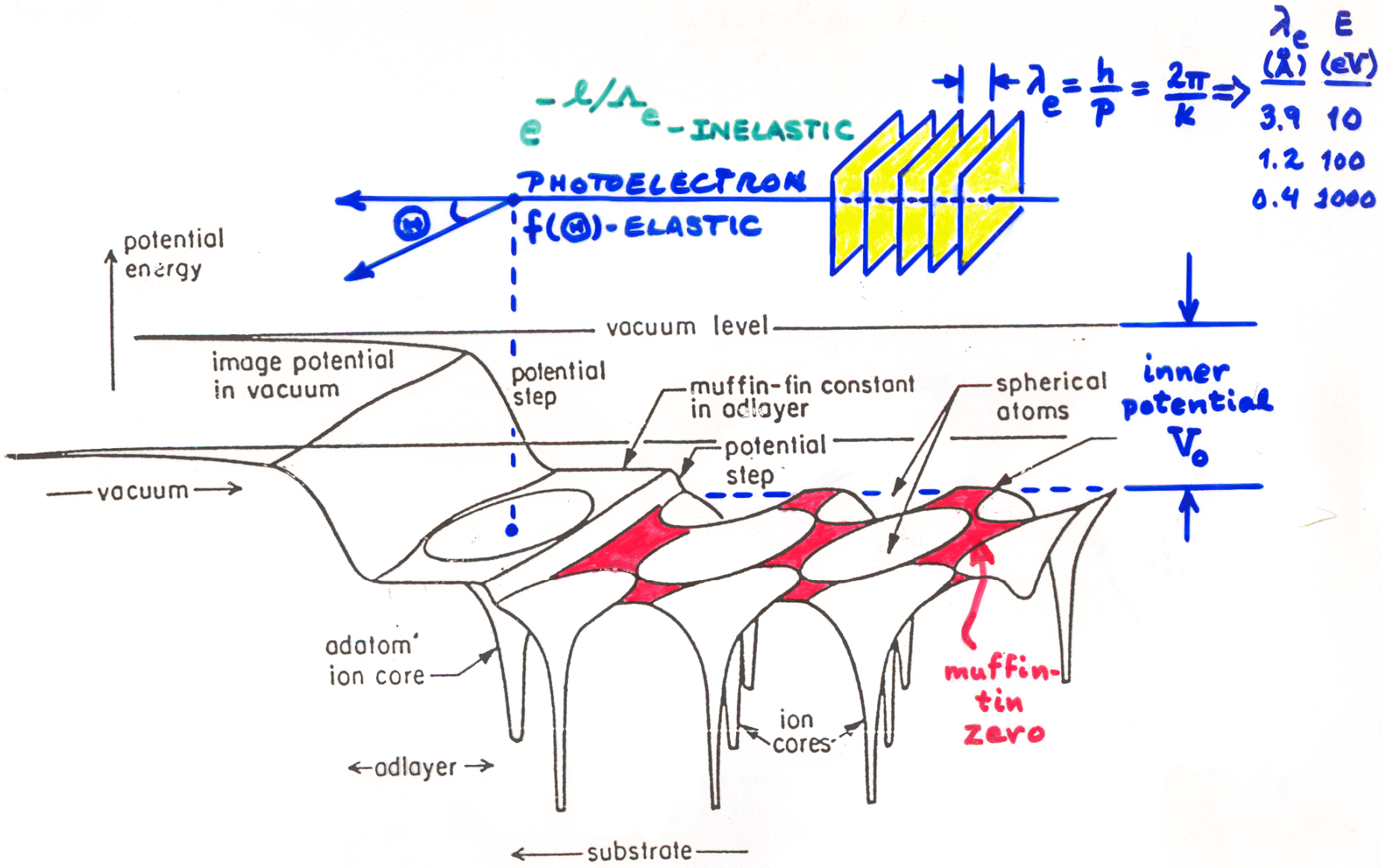

CALCULATION OF V_0 FOR AN IDEAL METAL

Fig. 4.2. Electron density profile at a jellium surface for two choices of the background density, r_s (Lang & Kohn, 1970).

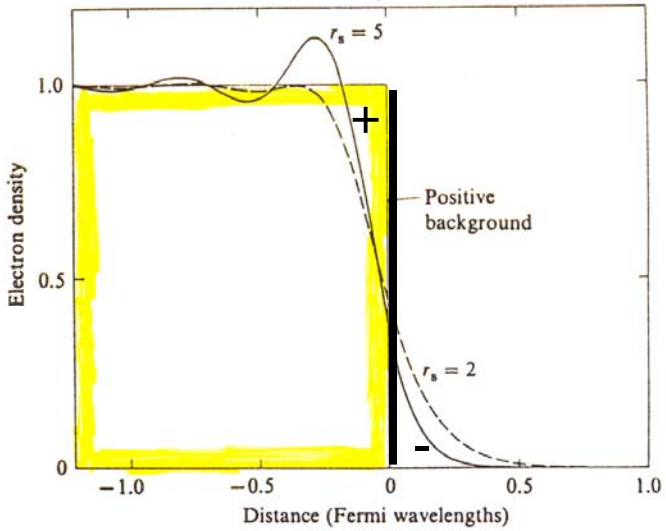

$Q = CV_{retard}$

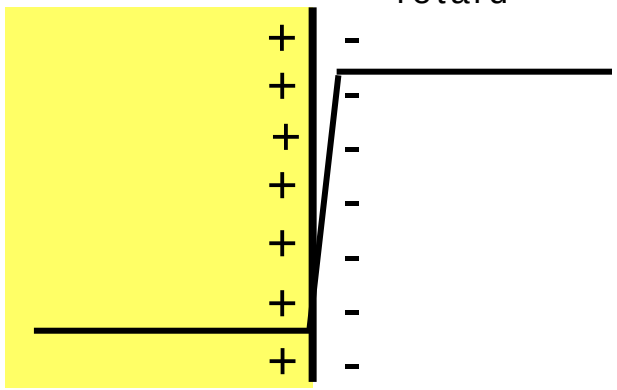

Fig. 4.3. Electrostatic potential, $v(z)$, and total effective one-electron potential, $v_{eff}(z)$, near a jellium surface (Lang & Kohn, 1970).

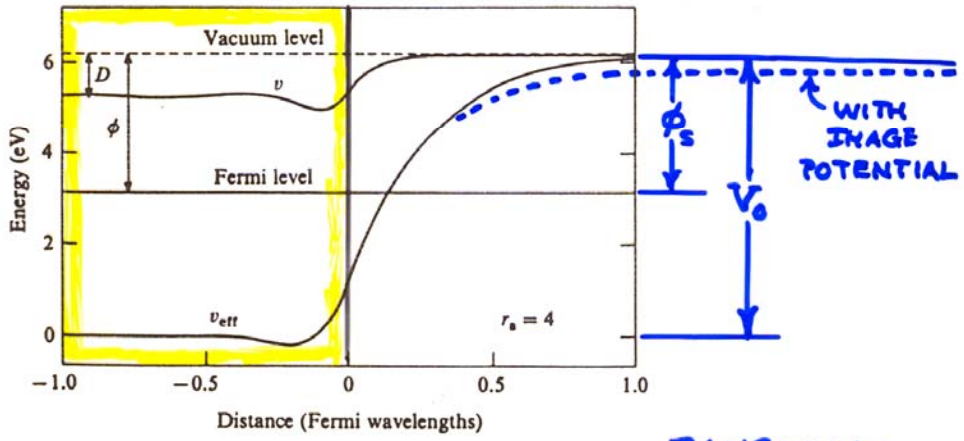

ZANGWILL, "SURFACE PHYSICS"

The electronic structure of a transition metal—fcc Cu

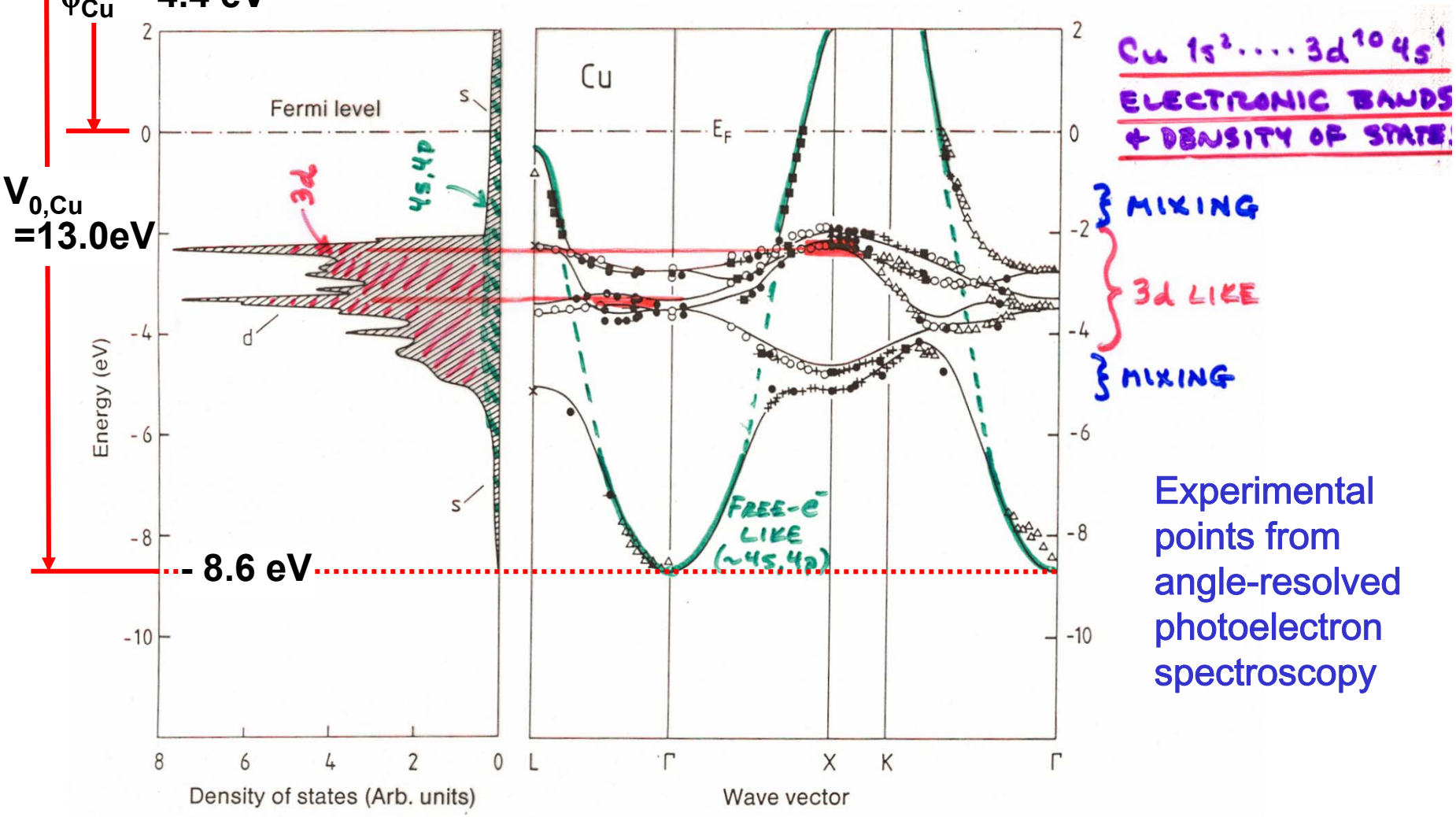

Experimental points from angle-resolved photoelectron spectroscopy

Fig. 7.12. Bandstructure $E(k)$ for copper along directions of high crystal symmetry (*right*). The experimental data were measured by various authors and were presented collectively by Courths and Hüfner [7.4]. The full lines showing the calculated energy bands and the density of states (*left*) are from [7.5]. The experimental data agree very well, not only among themselves, but also with the calculation

Outline

Surface, interface, and nanoscience—short introduction

Some surface concepts and techniques→photoemission

Synchrotron radiation: experimental aspects

Electronic structure—a brief review

The basic synchrotron radiation techniques

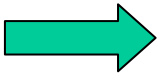

Core-level photoemission:
peak intensities and surface analysis

Valence-level photoemission

Microscopy with photoemission

PHOTOELECTRON INTENSITIES—THE 3-STEP MODEL

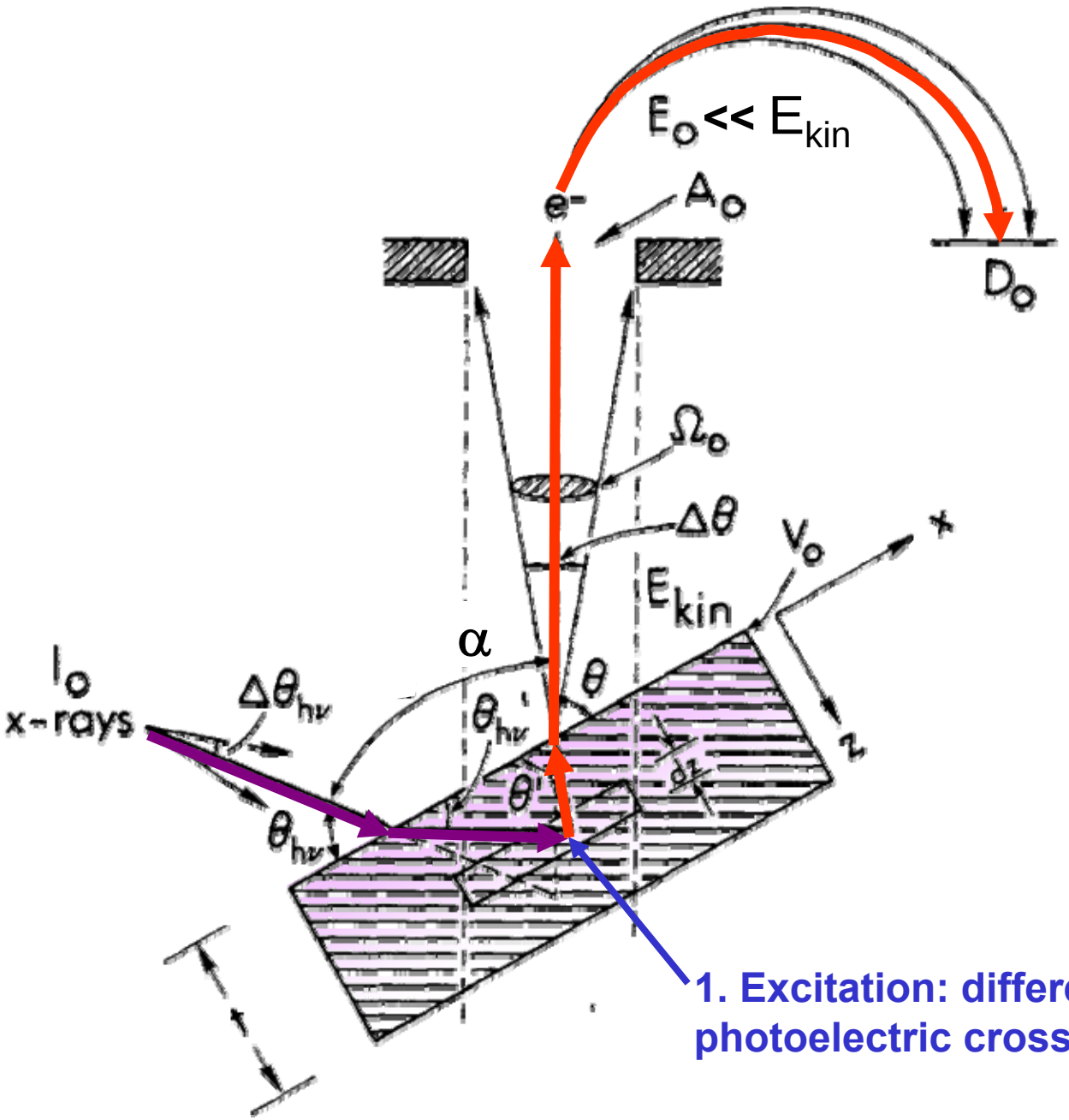

1. Excitation: differential photoelectric cross section ($d\sigma/d\Omega$)

PHOTOELECTRON EMISSION - BASIC MATRIX ELEMENTS + SELECTION RULES:

- **ATOMIC-LIKE (LOCALIZED) STATES ⇒ CORE:**

$$\varphi_i(\vec{r}) = \varphi_{n_i \ell_i m_i}(r,\theta,\phi) = R_{n_i \ell_i}(r) Y_{\ell_i m_i}(\theta,\phi)$$

PLUS SPIN:
$\alpha(\sigma) = m_{si} = +½ = \uparrow$
$\beta(\sigma) = m_{si} = -½ = \downarrow$

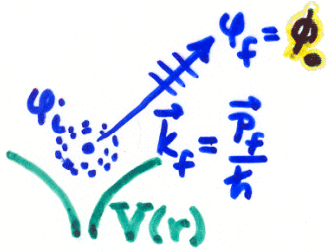

$$\varphi_f(\vec{r},\vec{k}_f) = \varphi_{E_f}(\vec{r},\vec{k}_f) \begin{cases}\alpha(\sigma)\\ \beta(\sigma)\end{cases}$$

$$= 4\pi \sum_{\ell_f, m_f} i^{\ell_f} e^{-i\delta_{\ell_f}} Y^*_{\ell_f m_f}(\theta_{k_f}, \phi_{k_f}) Y_{\ell_f m_f}(\theta,\phi) R_{E_f \ell_f}(r) \begin{cases}\alpha(\sigma)\\ \beta(\sigma)\end{cases}$$

(δ_{ℓ_f}: PHASE SHIFT OF ℓ_f WAVE IN V(r))

DIPOLE APPROX.: INT. $\propto |\langle \varphi_f | \hat{\varepsilon}\cdot\vec{r} | \varphi_i \rangle|^2 = |\hat{\varepsilon}\langle \varphi_f | \vec{r} | \varphi_i \rangle|^2 \Rightarrow$

EQUIVALENT WITHIN CONSTANT FACTOR: $\vec{r} \leftrightarrow \vec{p} \leftrightarrow \vec{\nabla}V(r)$

- $\Delta\ell = \ell_f - \ell_i = \pm 1$ — TWO CHANNELS
- $\Delta m = m_f - m_i = 0, \pm 1$ — LINEAR POLARIZ.
- $\Delta m = \pm 1$, CIRCULAR POLARIZATION

$\Delta m_s = m_{sf} - m_{si} = 0$!

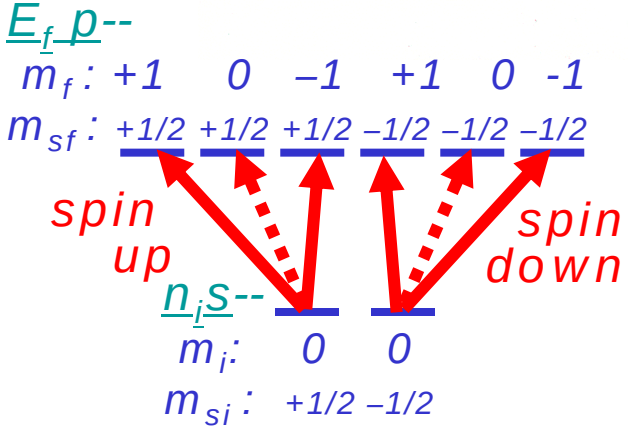

FOR A GIVEN $n_i l_i m_i m_{si}$: SUM OVER DEGENERATE INITIAL STATES $m_i m_{si}$ AND AVERAGE OVER FINAL STATES $E_f l_f m_f m_{sf}$ ACCESSED FROM EACH m_i TO YIELD DIFFERENTIAL SUBSHELL PHOTOELECTRIC CROSS SECTION :

$$d\sigma_{n_i \ell_i} / d\Omega$$

$\propto$ PROBABILITY PER UNIT SOLID ANGLE OF EXCITING ONE ELECTRON FROM SUBSHELL $n_i l_i$ INTO THE DIRECTION k_f

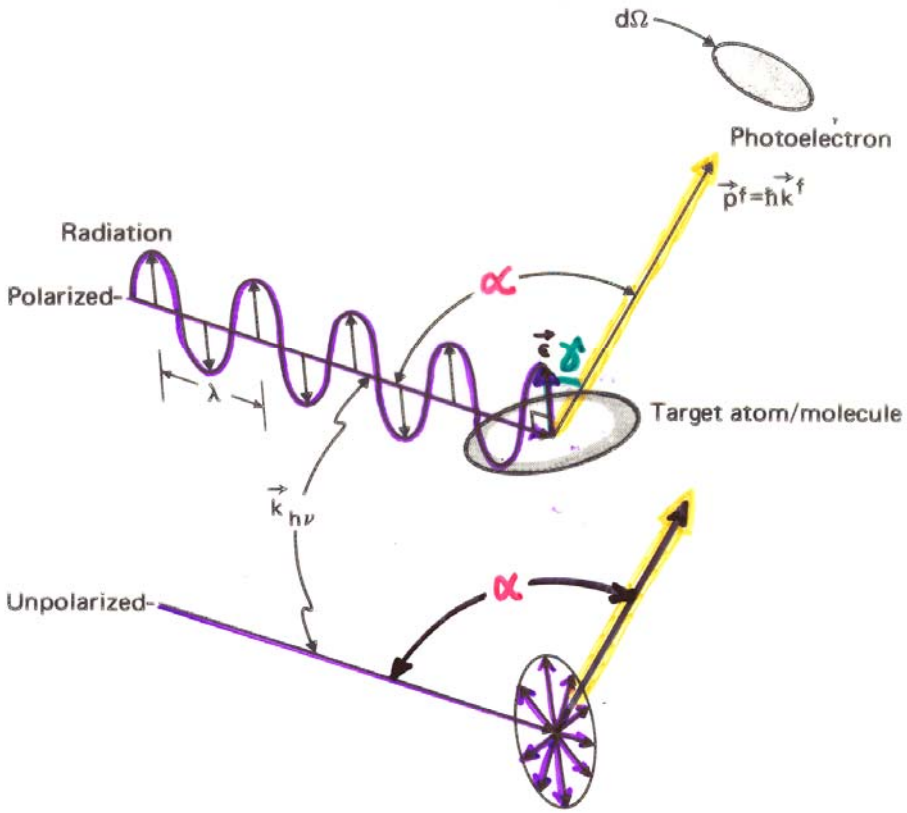

FOR ATOMIC-LIKE EMISSION:

LIN. POLARIZED: $$\frac{d\sigma_{nl}(E_f)}{d\Omega} = \frac{\sigma_{nl}(E_f)}{4\pi}\left[1 + \beta_{nl}(E^f)\left(\frac{3}{2}\cos^2\gamma - \frac{1}{2}\right)\right]$$

UNPOLARIZED: $$\frac{d\sigma_{nl}(E_f)}{d\Omega} = \frac{\sigma_{nl}(E_f)}{4\pi}\left[1 + \frac{1}{2}\beta_{nl}(E^f)\left(\frac{3}{2}\sin^2\alpha - 1\right)\right]$$

Figure 7 -- General geometry for defining the differential cross section $d\sigma/d\Omega$, showing both polarized and unpolarized incident radiation. The polarization vector $\vec{e}$ is parallel to the electric field $\vec{E}$ of the radiation. In order for the dipole approximation to be valid, the radiation wave length λ should be much larger than typical target dimensions (that is, the opposite of what is shown here).

WITH:

σ_{nl} = TOTAL CROSS SECTION

β_{nl} = ASYMMETRY PARAMETER

σ_{nl}, β_{nl} TABULATIONS IN: GOLDBERG ET AL., J. ELECT. SPECT. & YEH, LINDAU, AT. NUC. DATA 32, 1 ('85) \ 21, 285 ('91)

TOTAL SUBSHELL CROSS SECTION: $\int_{4\pi} \frac{d\sigma_{nl}}{d\Omega} d\Omega =$

$$\sigma_{nl}(E^f) = \frac{4\pi\alpha_0 a_0^2}{3} (h\nu)[lR_{l-1}^2(E^f) + (l+1)R_{l+1}^2(E^f)]$$

= SUM OVER ALL m_l, m_s IN SUBSHELL nl

RADIAL MATRIX ELEMENTS TO $l \pm 1$ CHANNELS:

$$R_{l\pm1}(E^f) = \int_0^\infty R_{nl}(r) r R_{E^f,\, l\pm1}(r) r^2\, dr = \int_0^\infty P_{nl}(r) r P_{E^f,\, l\pm1}(r)\, dr$$

DIFFERENTIAL CROSS SECTION: UNPOLARIZED

$$\frac{d\sigma_{nl}}{d\Omega}(E^f) = \frac{\sigma_{nl}}{4\pi}[1 - \tfrac{1}{2}\beta_{nl}(E^f) P_2(\cos\alpha)]$$

$$= \frac{\sigma_{nl}}{4\pi}[1 + \tfrac{1}{2}\beta_{nl}(E^f)(\tfrac{3}{2}\sin^2\alpha - 1)]$$

$$= A + B\sin^2\alpha$$

ASYMMETRY PARAMETER:

TERM FOR $l \pm 1$ INTERFERENCE

$$\beta_{nl}(E^f) = \frac{\{l(l-1)R_{l-1}^2(E^f) + (l+1)(l+2)R_{l+1}^2(E^f) - 6l(l+1)R_{l+1}(E^f)R_{l-1}(E^f)\cos[\delta_{l+1}(E^f) - \delta_{l-1}(E^f)]\}}{(2l+1)[lR_{l-1}^2(E^f) + (l+1)R_{l+1}^2(E^f)]}$$

$\delta_{l\pm1}(E^f)$ = CONTINUUM ORBITAL PHASE SHIFTS IN ATOMIC POTENTIAL $V(r)$

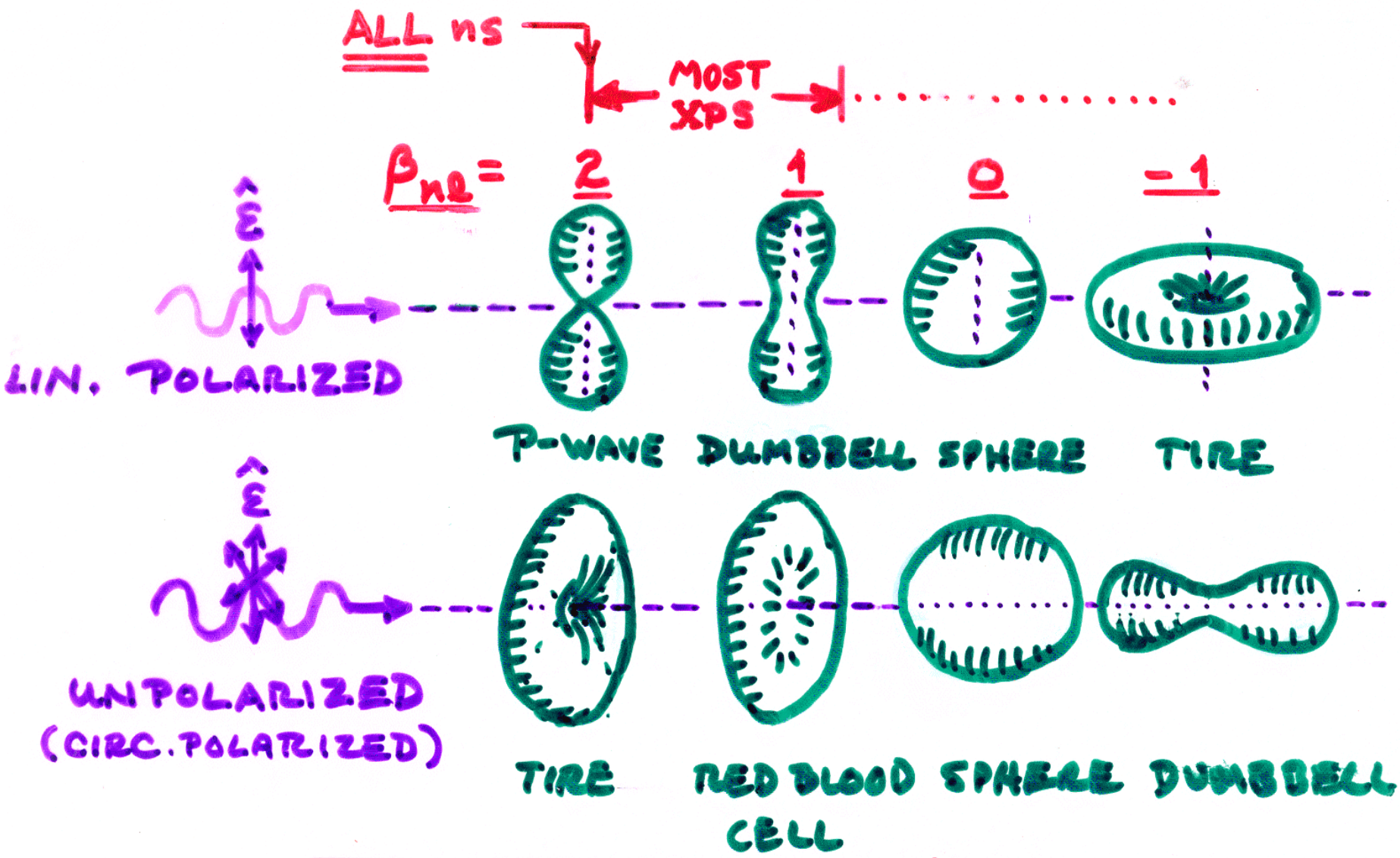
ALL ns
MOST XPS
β_{nR} = 2 1 0 -1
$\hat{\varepsilon}$
LIN. POLARIZED
P-WAVE DUMBBELL SPHERE TIRE
$\hat{\varepsilon}$
UNPOLARIZED
(CIRC. POLARIZED)
TIRE RED BLOOD CELL SPHERE DUMBBELL
RANGE OF SHAPES OF $\frac{d\sigma}{d\Omega}$

PHOTOELECTRIC CROSS SECTIONS FOR Mn

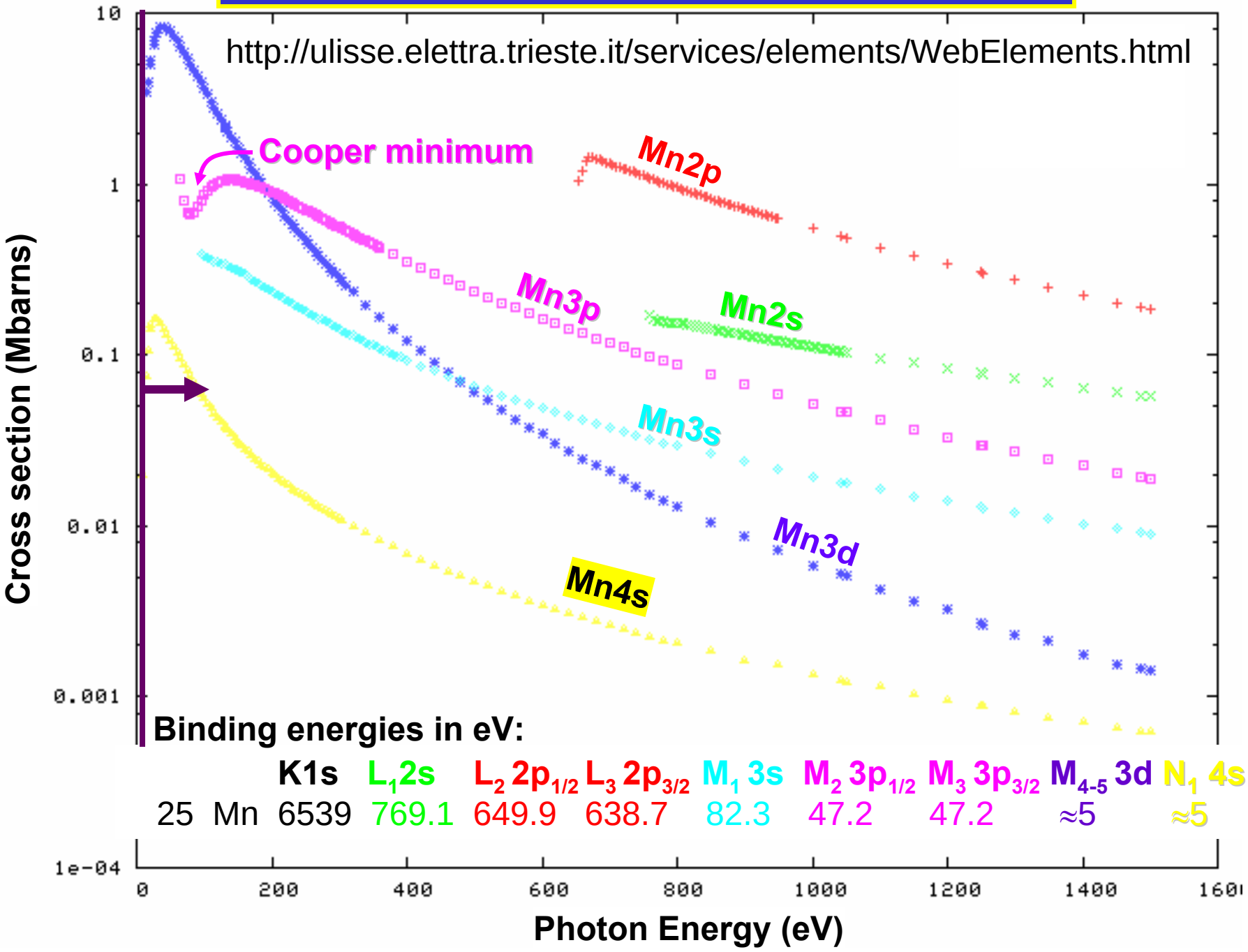

Binding energies in eV:

		K1s	L_1 2s	L_2 $2p_{1/2}$	L_3 $2p_{3/2}$	M_1 3s	M_2 $3p_{1/2}$	M_3 $3p_{3/2}$	M_{4-5} 3d	N_1 4s
25	Mn	6539	769.1	649.9	638.7	82.3	47.2	47.2	≈5	≈5

GRAPH I. Atomic Subshell Photoionization Cross Sections for 0–1500 eV, $1 \leq Z \leq 103$

See page 6 for Explanation of Graphs

PHOTOELECTRIC CROSS SECTIONS FOR C

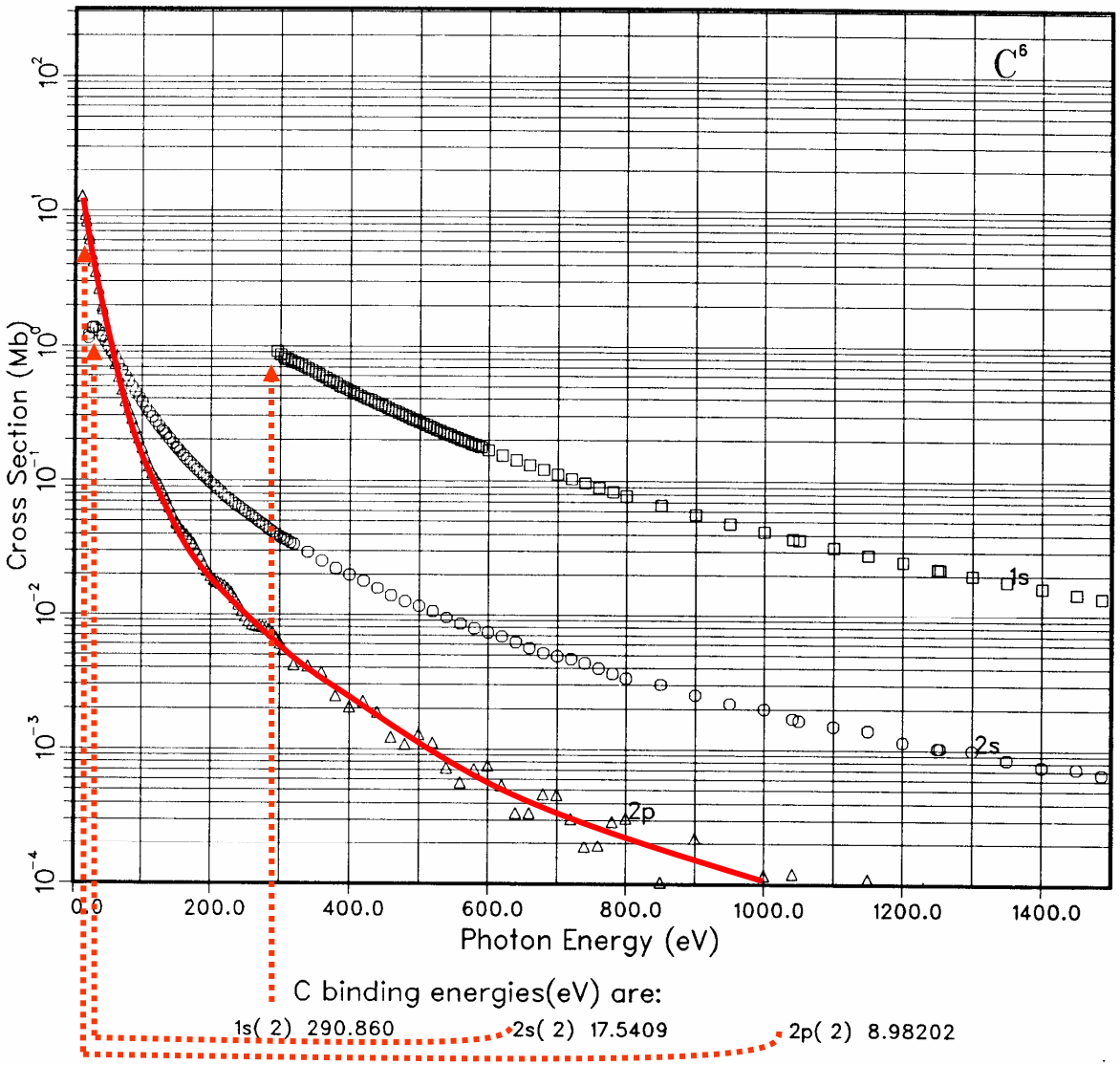

Plus other Examples from Yeh and Lindau in Sec. 1.5 of X-Ray Data Booklet, and plots for all elements at: http://ulisse.elettra.trieste.it/elements/WebElements.html

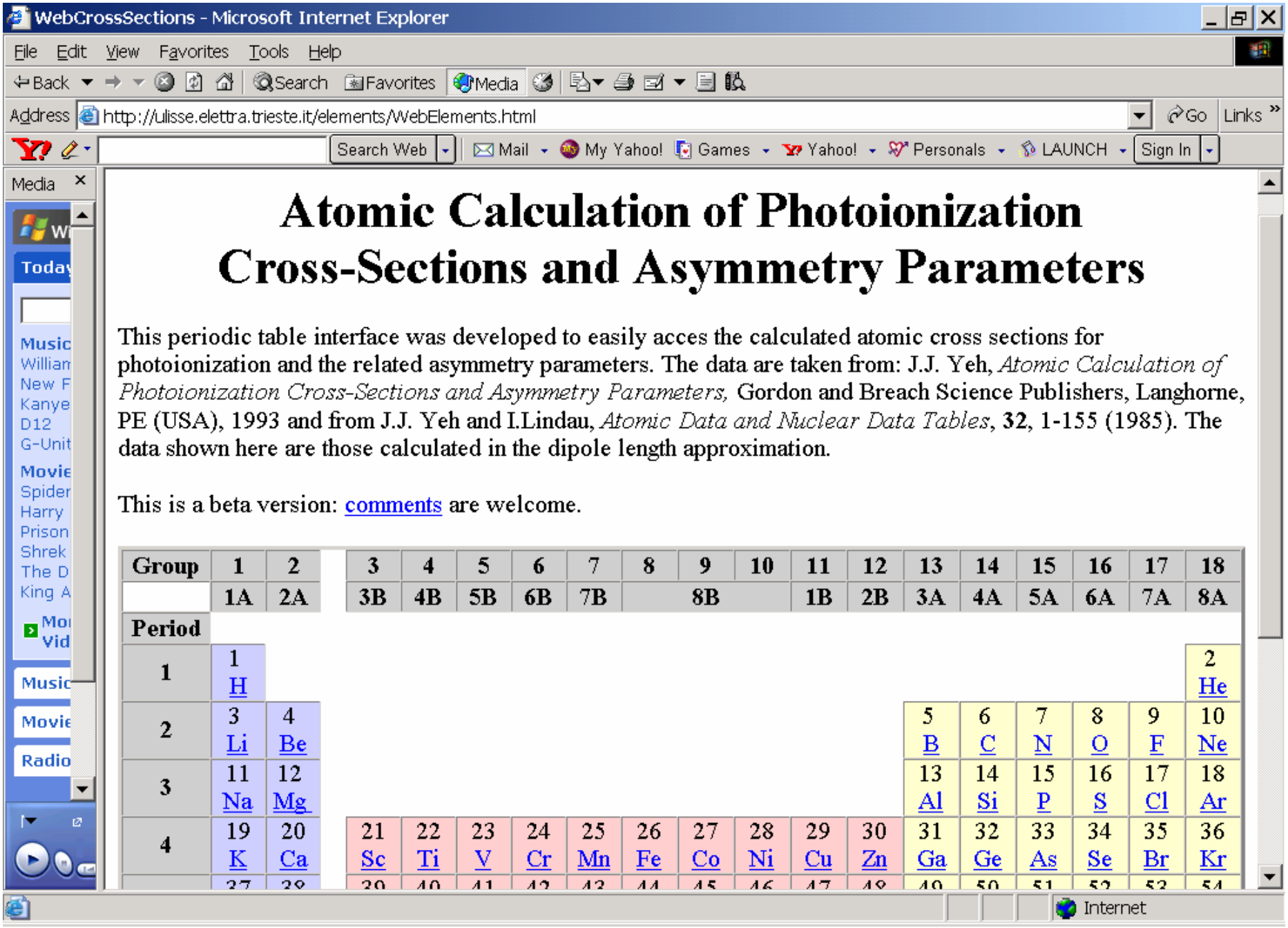
WebCrossSections - Microsoft Internet Explorer
File Edit View Favorites Tools Help
Back Search Favorites Media
Address http://ulisse.elettra.trieste.it/elements/WebElements.html
Go Links
Search Web Mail My Yahoo! Games Yahoo! Personals LAUNCH Sign In
Media
Atomic Calculation of Photoionization Cross-Sections and Asymmetry Parameters
This periodic table interface was developed to easily acces the calculated atomic cross sections for photoionization and the related asymmetry parameters. The data are taken from: J.J. Yeh, Atomic Calculation of Photoionization Cross-Sections and Asymmetry Parameters, Gordon and Breach Science Publishers, Langhorne, PE (USA), 1993 and from J.J. Yeh and I.Lindau, Atomic Data and Nuclear Data Tables, 32, 1-155 (1985). The data shown here are those calculated in the dipole length approximation.
This is a beta version: comments are welcome.
Group 1 2 3 4 5 6 7 8 9 10 11 12 13 14 15 16 17 18
1A 2A 3B 4B 5B 6B 7B 8B 1B 2B 3A 4A 5A 6A 7A 8A
Period
1 1 H 2 He
2 3 Li 4 Be 5 B 6 C 7 N 8 O 9 F 10 Ne
3 11 Na 12 Mg 13 Al 14 Si 15 P 16 S 17 Cl 18 Ar
4 19 K 20 Ca 21 Sc 22 Ti 23 V 24 Cr 25 Mn 26 Fe 27 Co 28 Ni 29 Cu 30 Zn 31 Ga 32 Ge 33 As 34 Se 35 Br 36 Kr
Internet

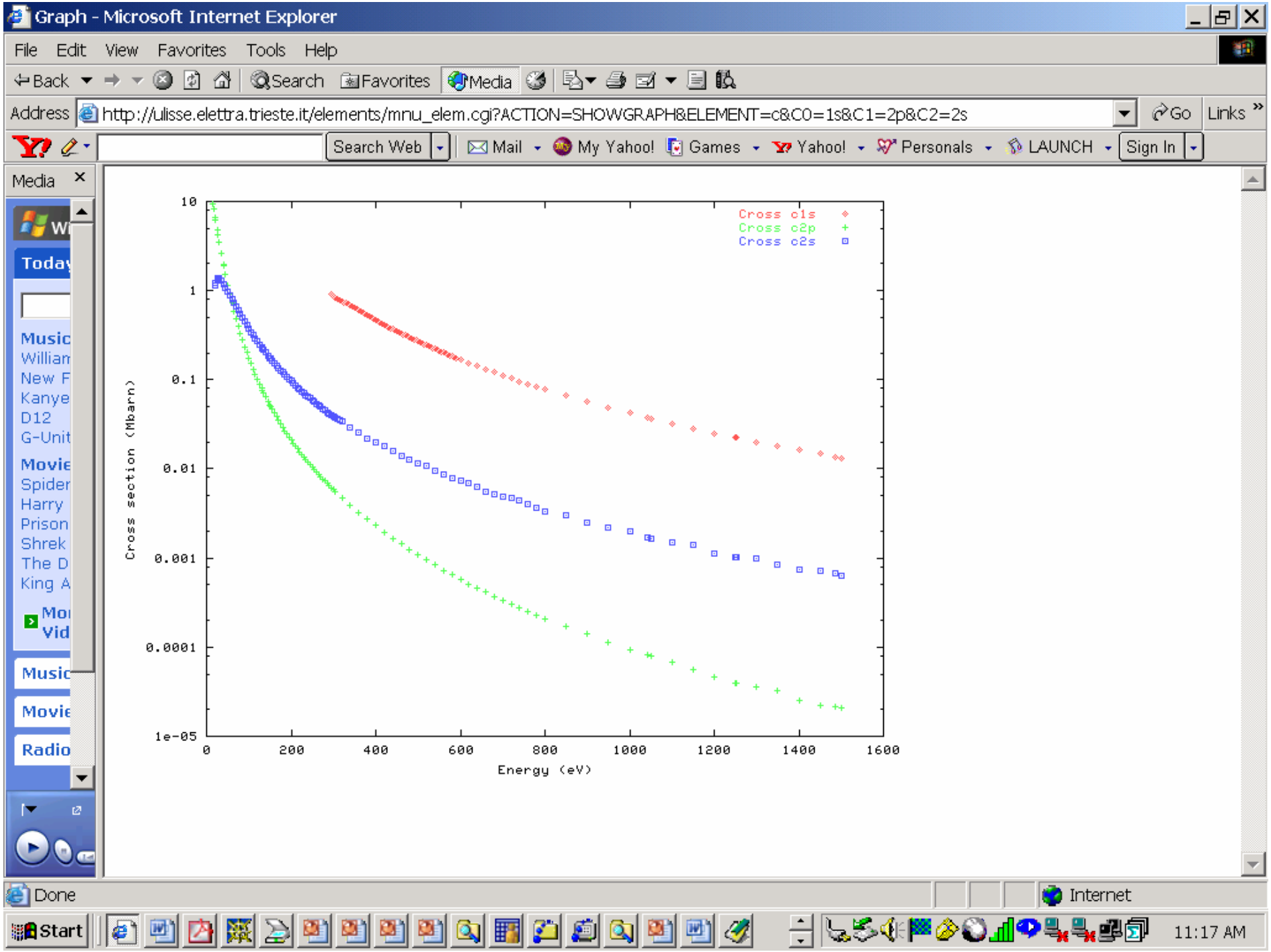
Graph - Microsoft Internet Explorer
File Edit View Favorites Tools Help
Back Search Favorites Media
Address http://ulisse.elettra.trieste.it/elements/mnu_elem.cgi?ACTION=SHOWGRAPH&ELEMENT=c&C0=1s&C1=2p&C2=2s
Go Links
Search Web Mail My Yahoo! Games Yahoo! Personals LAUNCH Sign In
Media
Cross c1s
Cross c2p
Cross c2s
Cross section (Mbarn)
Energy (eV)
10
1
0.1
0.01
0.001
0.0001
1e-05
0
200
400
600
800
1000
1200
1400
1600
Done
Internet
Start
11:17 AM

GRAPH I. Atomic Subshell Photoionization Cross Sections for 0–1500 eV, $1 \leq Z \leq 103$

See page 6 for Explanation of Graphs

PHOTOELECTRIC CROSS SECTIONS FOR H

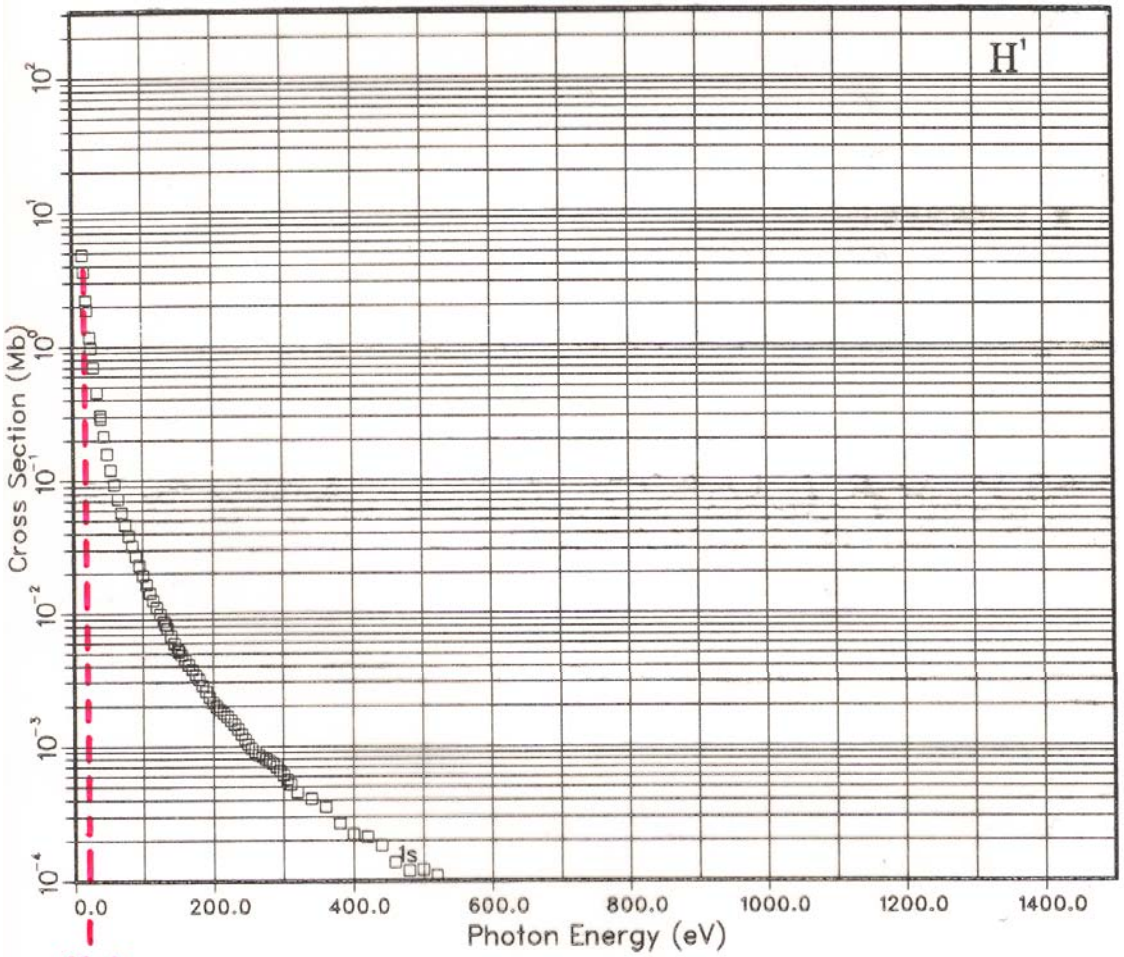

H binding energies(eV) are:

1s(1) 13.6050

13.6 eV = THRESHOLD FOR e^- EMISSION

GRAPH I. Atomic Subshell Photoionization Cross Sections for 0–1500 eV, $1 \leq Z \leq 103$

See page 6 for Explanation of Graphs

PHOTOELECTRIC CROSS SECTIONS FOR Ne

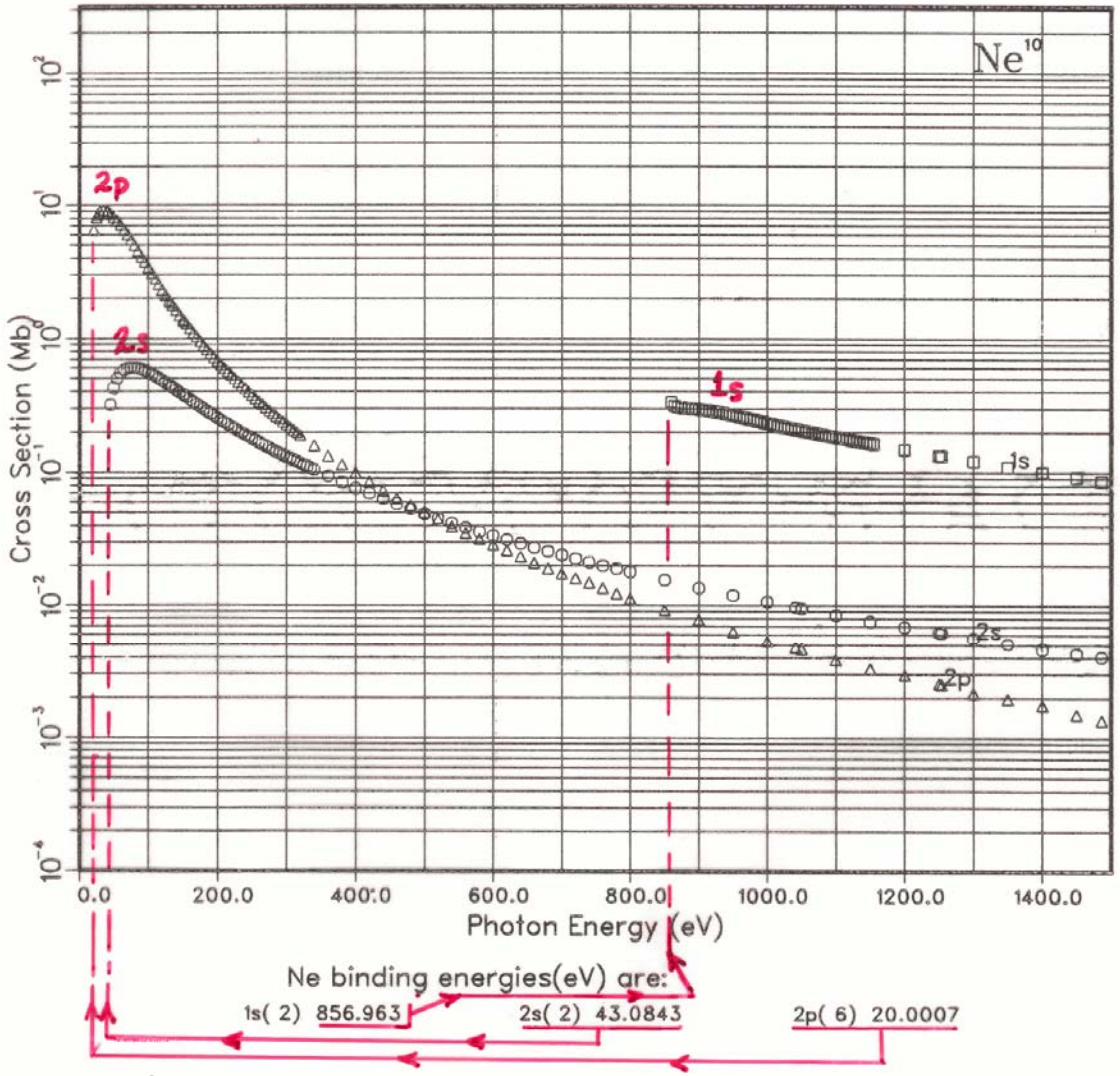

GRAPH I. Atomic Subshell Photoionization Cross Sections for 0–1500 eV, $1 \leq Z \leq 103$

See page 6 for Explanation of Graphs

PHOTOELECTRIC CROSS SECTIONS FOR Ag

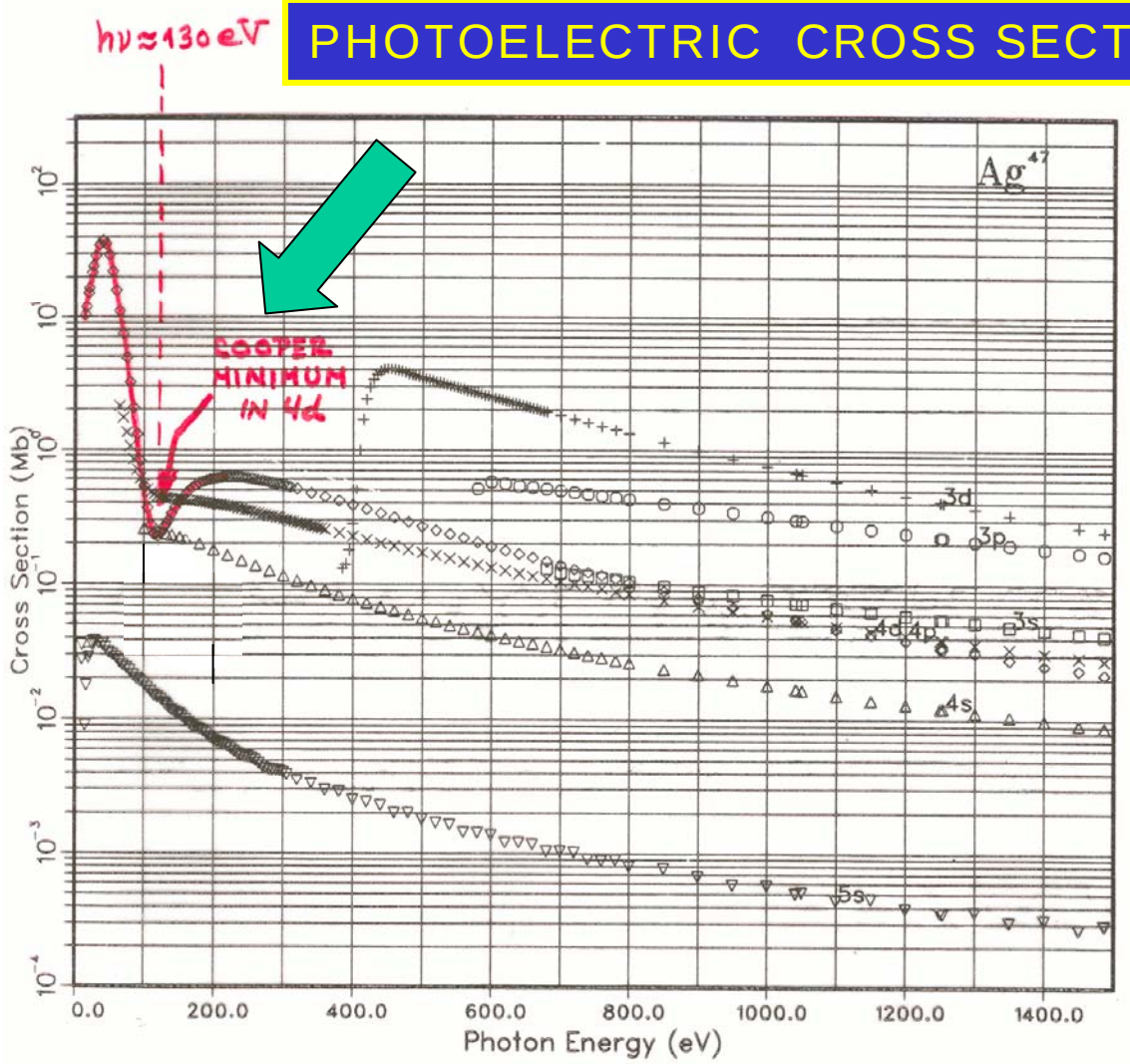

Ag binding energies(eV) are:

1s(2) 24693.5	2s(2) 3591.17	2p(6) 3352.94
3s(2) 665.102	3p(6) 567.203	4s(2) 94.2146
3d(10) 384.360	4p(6) 62.9041	4d(10) 12.6499
5s(1) 6.42700		

COOPER MINIMUM IN Ag 4d (Z = 47) CROSS SECTION : Expt. & Theory

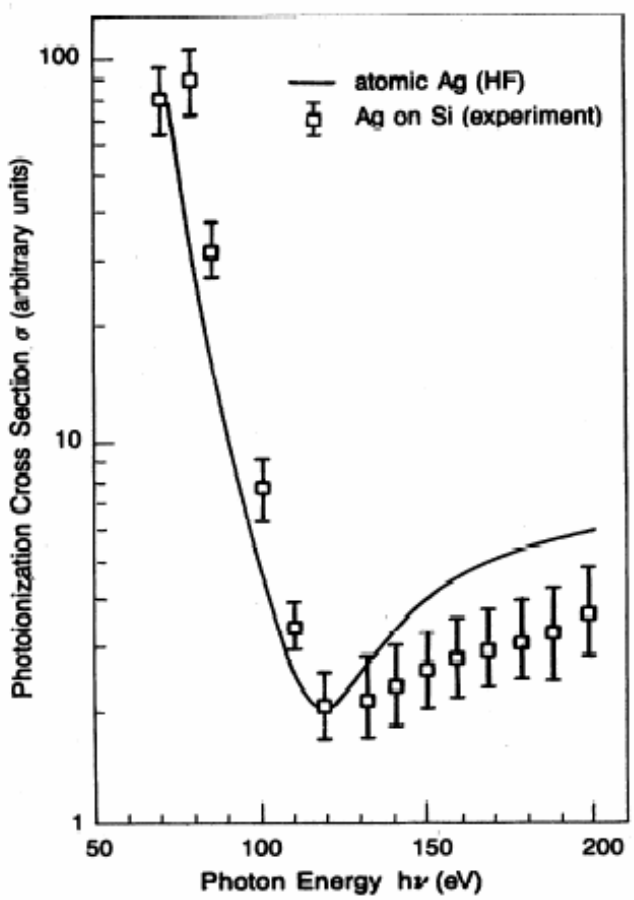

FIG. 5. Partial photoionization cross section for 4*d* electrons of Ag in logarithmic scale. Our experimental data for the Ag/Si interface (squares) are compared with the Hartree-Fock results for atomic Ag by Yeh and Lindau (solid line). Note that our experimental data are normalized at the minimum to the theoretical value.

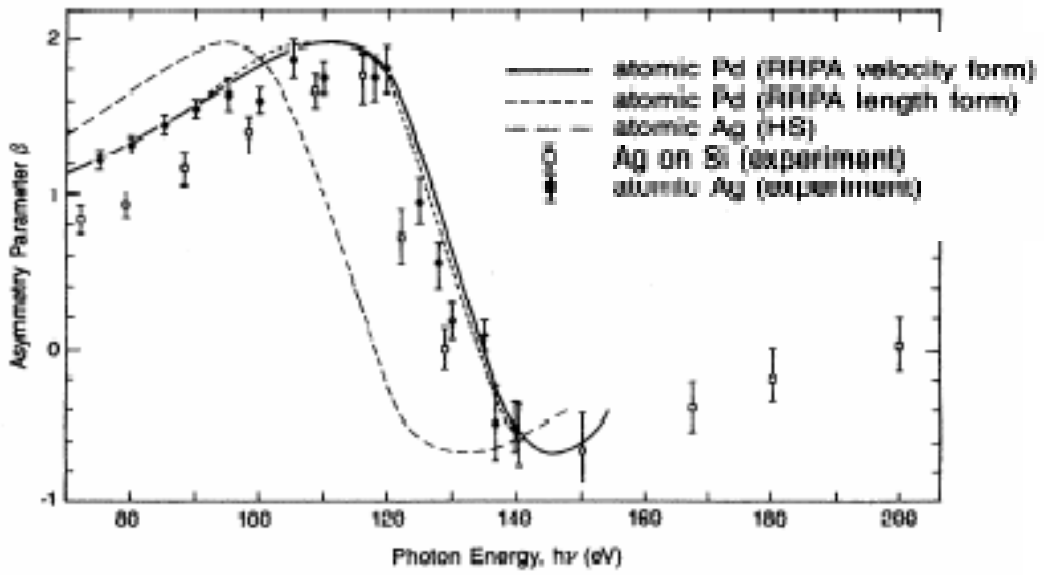

FIG. 6. Asymmetry parameter for 4*d* electrons of Ag. Our experimental data for the Ag/Si interface (squares) are compared with the data for atomic Ag (circles), the RRPA prediction for atomic Pd by Radojevic and Johnson (solid line, velocity form; short-dashed line, length form), and the HS calculations for atomic Ag by Manson (long-dashed line).

M. Ardehali et al., Phys. Rev. B 39, 8107 (1989)

TOTAL SUBSHELL CROSS SECTION: $\int_{4\pi} \frac{d\sigma_{nl}}{d\Omega} d\Omega =$

$$\sigma_{nl}(E^f) = \frac{4\pi\alpha_0 a_0^2}{3}(h\nu)\left[lR_{l-1}^2(E^f) + (l+1)R_{l+1}^2(E^f)\right]$$

= SUM OVER ALL m_l, m_s IN SUBSHELL nl

RADIAL MATRIX ELEMENTS TO $l \pm 1$ CHANNELS:

$$R_{l\pm1}(E^f) = \int_0^\infty R_{nl}(r) r R_{E^f,\, l\pm1}(r) r^2\, dr = \int_0^\infty P_{nl}(r) r P_{E^f,\, l\pm1}(r)\, dr$$

DIFFERENTIAL CROSS SECTION: UNPOLARIZED

$$\frac{d\sigma_{nl}}{d\Omega}(E^f) = \frac{\sigma_{nl}}{4\pi}\left[1 - \tfrac{1}{2}\beta_{nl}(E^f) P_2(\cos\alpha)\right]$$

$$= \frac{\sigma_{nl}}{4\pi}\left[1 + \tfrac{1}{2}\beta_{nl}(E^f)\left(\tfrac{3}{2}\sin^2\alpha - 1\right)\right]$$

$$= A + B\sin^2\alpha$$

ASYMMETRY PARAMETER:

TERM FOR $l \pm 1$ INTERFERENCE

$$\beta_{nl}(E^f) = \frac{\{l(l-1)R_{l-1}^2(E^f) + (l+1)(l+2)R_{l+1}^2(E^f) - 6l(l+1)R_{l+1}(E^f)R_{l-1}(E^f)\cos\left[\delta_{l+1}(E^f) - \delta_{l-1}(E^f)\right]\}}{(2l+1)\left[lR_{l-1}^2(E^f) + (l+1)R_{l+1}^2(E^f)\right]}$$

$\delta_{l\pm1}(E^f)$ = CONTINUUM ORBITAL PHASE SHIFTS IN ATOMIC POTENTIAL $V(r)$

COOPER MINIMUM IN In 4d (Z = 49) CROSS SECTION—Radial Matrix Element Variation

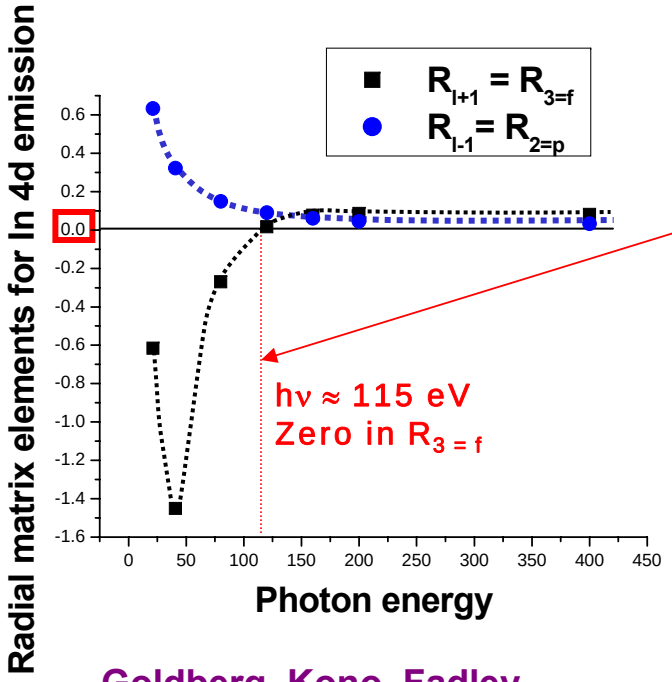

Goldberg, Kono, Fadley
J. Elect. Spect. 21, 285 ('81)

GRAPH I. Atomic Subshell Photoionization Cross Sections for 0–1500 eV, $1 \leq Z \leq 103$
See page 6 for Explanation of Graphs

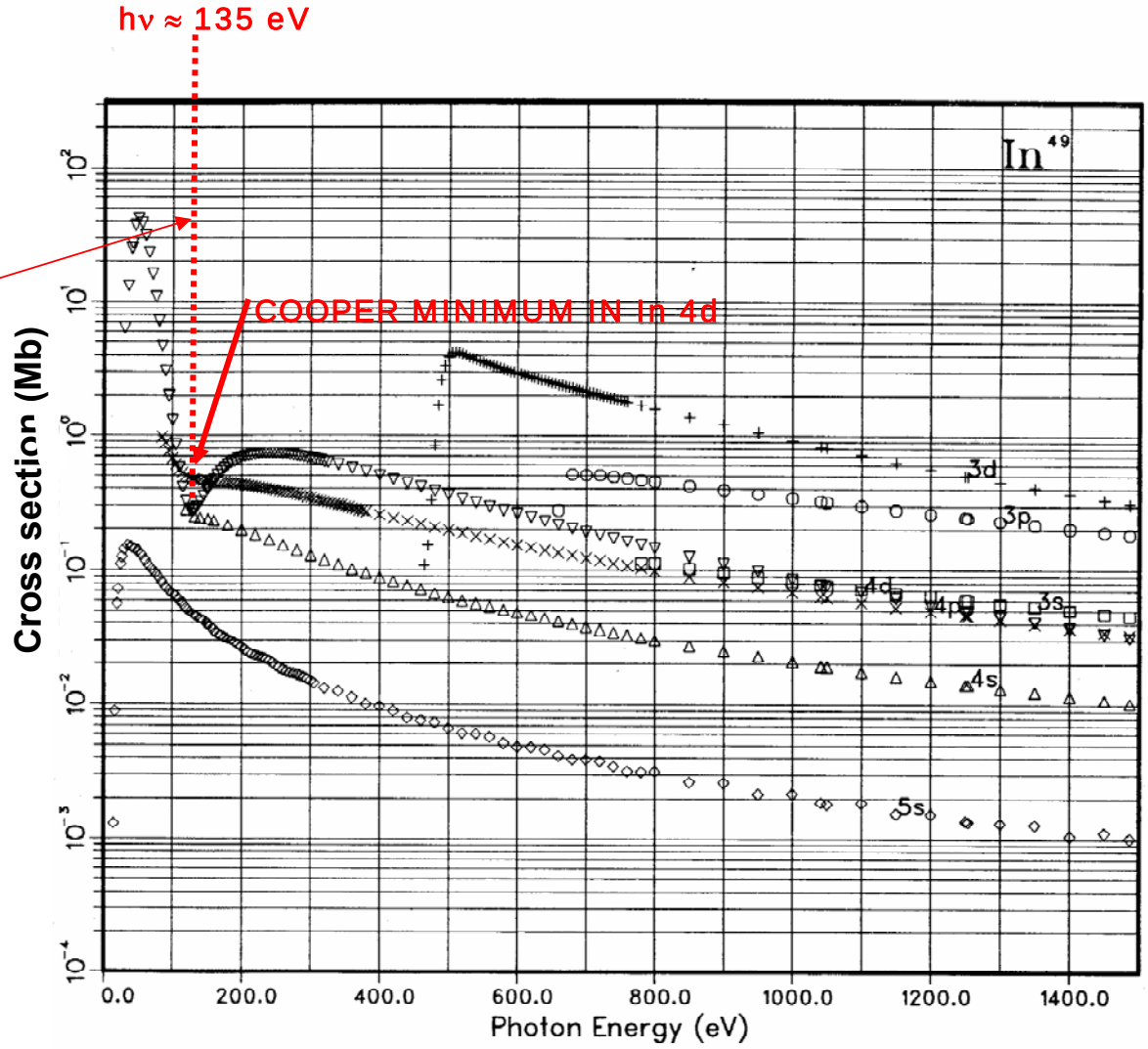

In binding energies(eV) are:

1s(2) 26971.5	2s(2) 3983.01	2p(6) 3731.41
3s(2) 764.232	3p(6) 659.286	4s(2) 118.953
3d(10) 462.909	4p(6) 84.0558	5s(2) 10.1384
4d(10) 26.2168	5p(1) 4.69781	

J. J. YEH and I. LINDAU Subshell Photoionization Cross Sections

ATOMIC & NUCLEAR DATA TABLES 32, 45 (1985)

GRAPH I. Atomic Subshell Photoionization Cross Sections for 0–1500 eV, $1 \leq Z \leq 103$

See page 6 for Explanation of Graphs

PHOTOELECTRIC CROSS SECTIONS FOR Mn

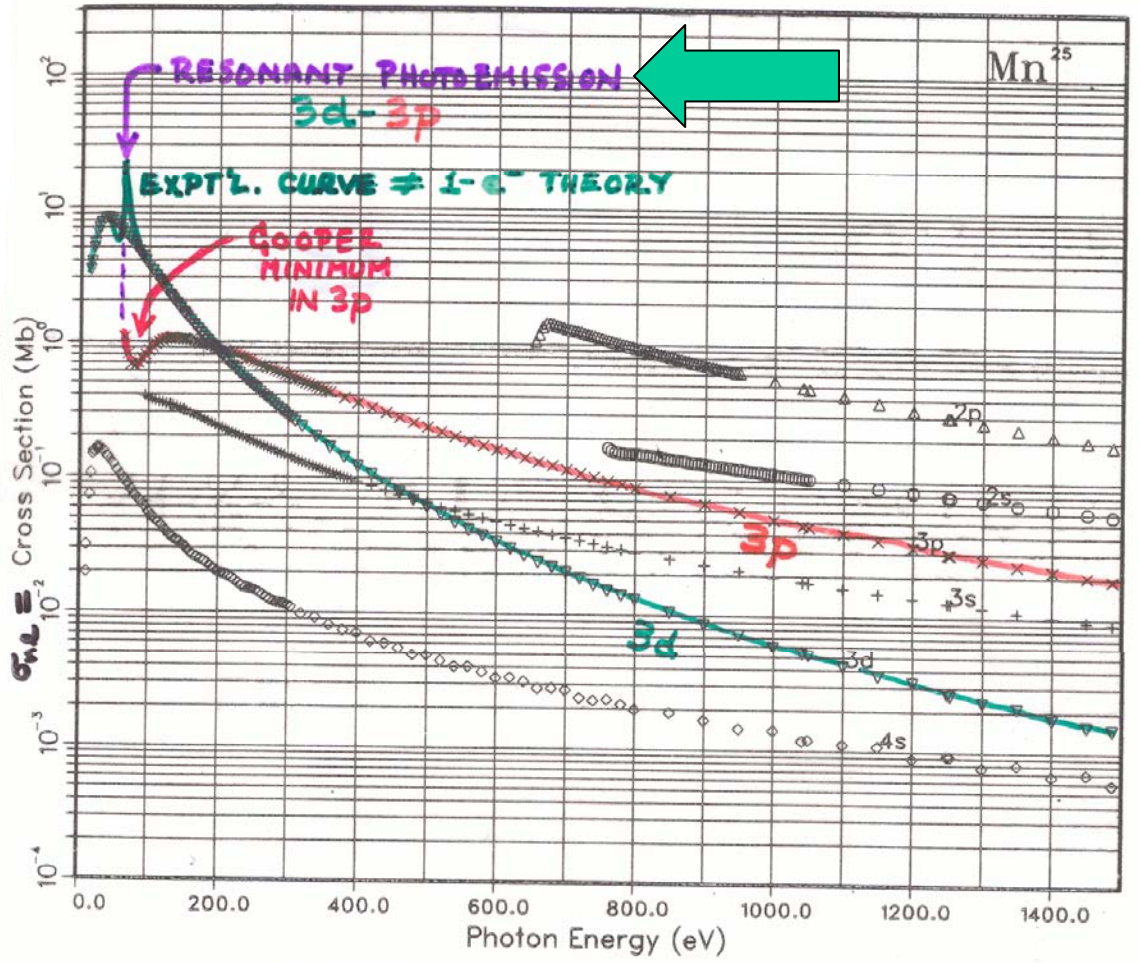

Mn binding energies(eV) are:

1s(2) 6455.26	2s(2) 755.155	2p(6) 653.681
3s(2) 90.8814	3p(6) 60.9150	4s(2) 7.14671
3d(5) 12.0486		

RESONANT PHOTOEMISSION FOR Mn-A MANY-ELECTRON EFFECT

Ex. – Mn atom: Mn3d emission, resonance with Mn3p

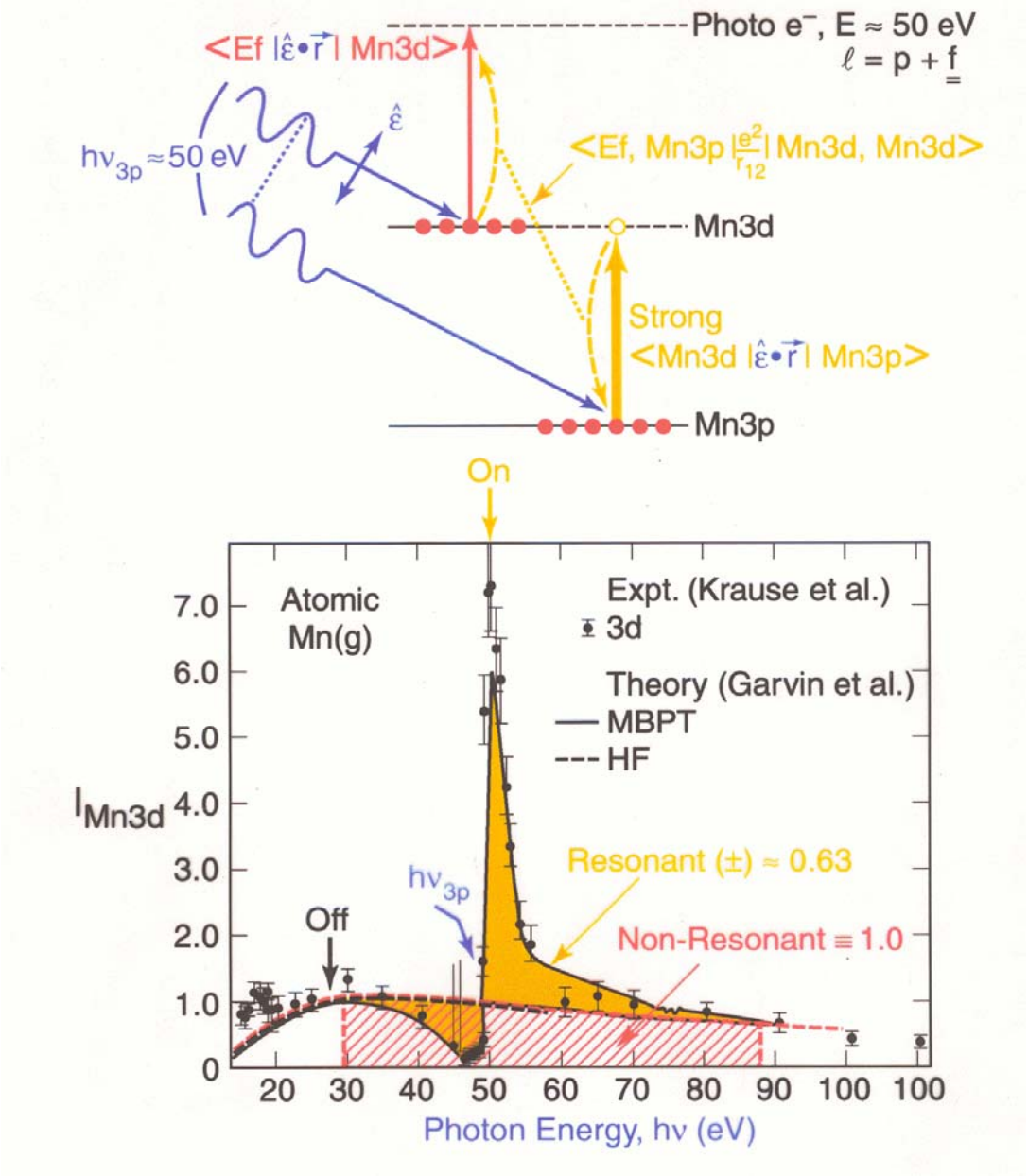

SINGLE-ATOM RESONANT PHOTOEMISSION:

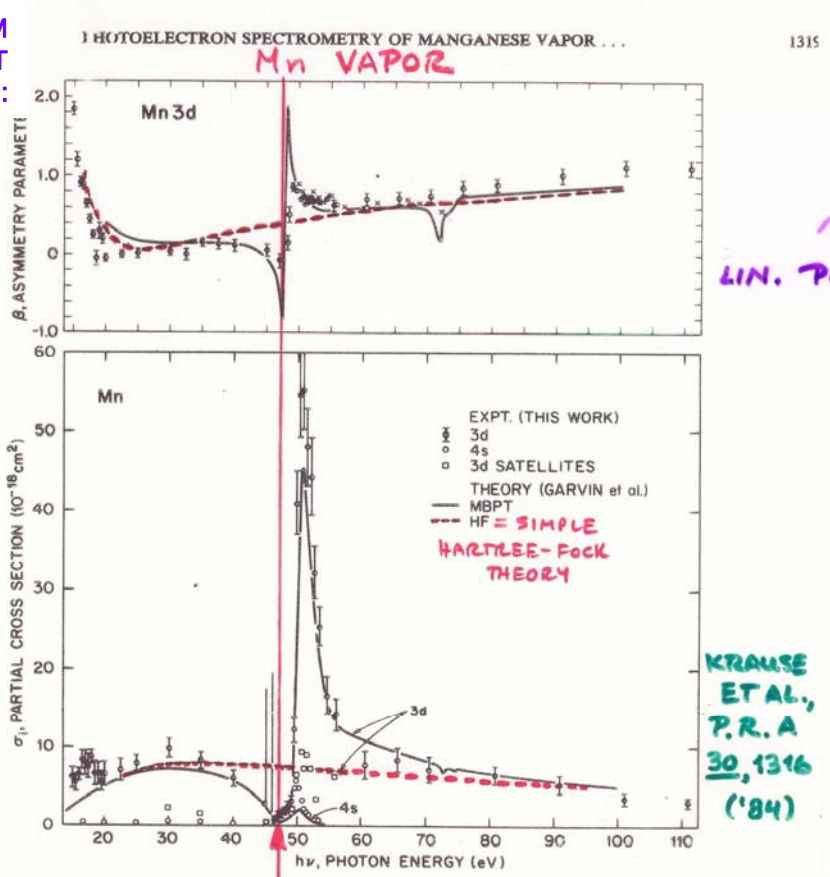

β_{3d}

σ_{3d}

KRAUSE ET AL., P.R.A 30, 1316 ('84)

FIG. 2. Angular distribution parameter β of $3d$ photoelectrons (upper panel) and partial cross sections of $4s$, $3d$ and satellite peaks (lower panel). Crosses ($\times$) for β are from Ref. 3, theory from Ref. 6. The resonance near 50 eV is due to the $3p \rightarrow 3d$ excitation into the partially filled $3d$ subshell of Mn.

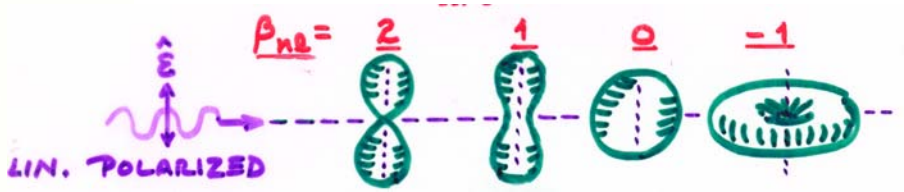

$h\nu = E_b^V(Mn\,3p)$

RESONANT PROCESS:

IF $h\nu \approx E_b$ OF nl' SUBSHELL INSIDE OF nl SUBSHELL OF INTEREST (E.G., 3p FOR 3d), TWO "CHANNELS" COUPLE -

USUAL 3d: $Mn^0 \ldots 3s^2 3p^6 3d^5 4s^2 \xrightarrow{h\nu} Mn^+ \ldots 3s^2 3p^6 3d^4 4s^2 + e^-$ (PHOTOELECTRON)

RESONANT 3p: $Mn^0 \ldots 3s^2 3p^6 3d^5 4s^2 \xrightarrow{h\nu} Mn^0 \ldots 3s^2 3p^5 3d^6 4s^2 e^-$

$\xrightarrow[\text{ZATION}]{\text{AUTOIONI-}}$ (≈AUGER) $Mn^+ \ldots 3s^2 3p^6 3d^4 4s^2$ + ELECTRON @ SAME E_{KIN} AS PHOTOELECTRON

COUPLING MUCH ENHANCES CROSS SECTION

MATRIX ELEMENTS IN THE SOFT X-RAY SPECTROSCOPIES: DIPOLE LIMIT

- ***Photoelectron spectroscopy/photoemission:***

$$I \propto \left|\hat{e} \bullet \left\langle \varphi_f(1) \middle| \vec{r} \middle| \varphi_i(1) \right\rangle\right|^2$$

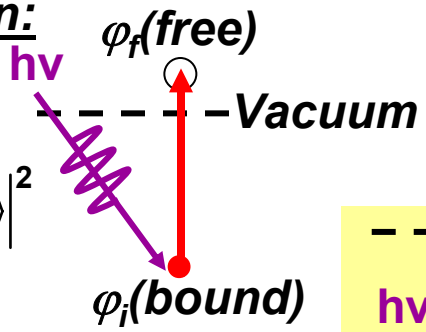

- ***Near-edge x-ray absorption:***

$$I \propto \left|\hat{e} \bullet \left\langle \varphi_f(1) \middle| \vec{r} \middle| \varphi_i(1) \right\rangle\right|^2$$

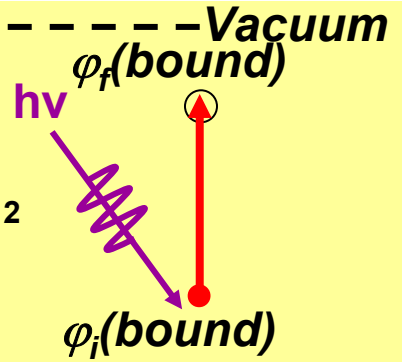

- ***Auger electron emission:***

$$I \propto \left| \left\langle \varphi_f(1)\varphi_1(2) \middle| \frac{e^2}{r_{12}} \middle| \varphi_3(1)\varphi_2(2) \right\rangle - \left\langle \varphi_1(1)\varphi_f(2) \middle| \frac{e^2}{r_{12}} \middle| \varphi_3(1)\varphi_2(2) \right\rangle \right|^2$$

Direct

Exchange

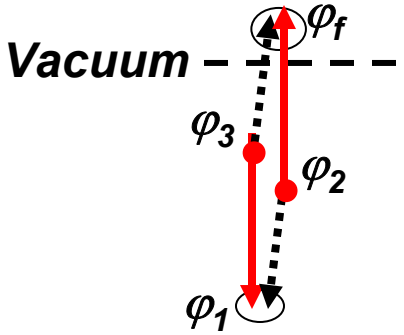

- ***X-ray emission:***

$$I \propto \left|\hat{e} \bullet \left\langle \varphi_f(1) \middle| \vec{r} \middle| \varphi_i(1) \right\rangle\right|^2$$

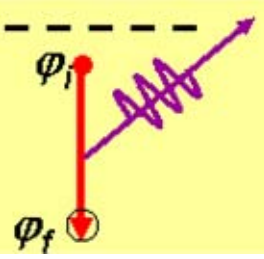

MATRIX ELEMENTS IN THE SOFT X-RAY SPECTROSCOPIES: RESONANT EFFECTS

- ***Resonant photoemission:***

$$I \propto \left| \langle \varphi_f(1) | \hat{e} \bullet \vec{r} | \phi_i(1) \rangle + \sum_m \langle \varphi_f(1)\varphi_1(2) | \frac{e^2}{r_{12}} | \varphi_i(1)\varphi_m(2) \rangle \langle \varphi_m(1) | \hat{e} \bullet \vec{r} | \varphi_1(1) \rangle \right|^2 \times \delta(h\nu - (E_m - E_1))$$

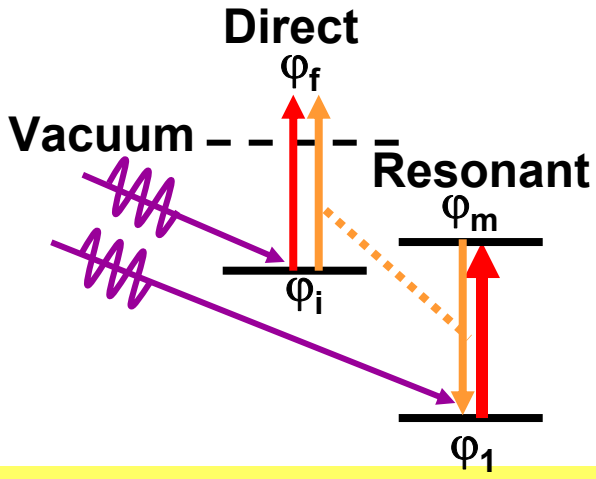

- ***Resonant inelastic x-ray scattering:***

$$I \propto \sum_f \left| \sum_m \frac{\langle \Psi_f(N) | \hat{e} \bullet \vec{r} | \Psi_m(N) \rangle \langle \Psi_m(N) | \hat{e} \bullet \vec{r} | \Psi_i(N) \rangle}{h\nu + E_i(N) - E_m(N) - i\Gamma} \right|^2 \times \delta(h\nu - (E_m(N) - E_i(N)))$$

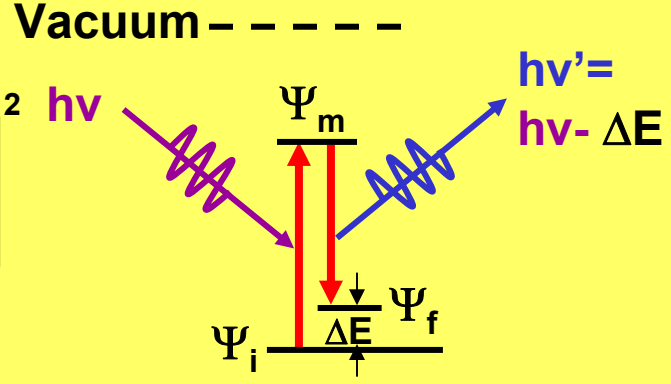

Multi-Atom Resonant Photoemission

Microscopic Q.M. picture

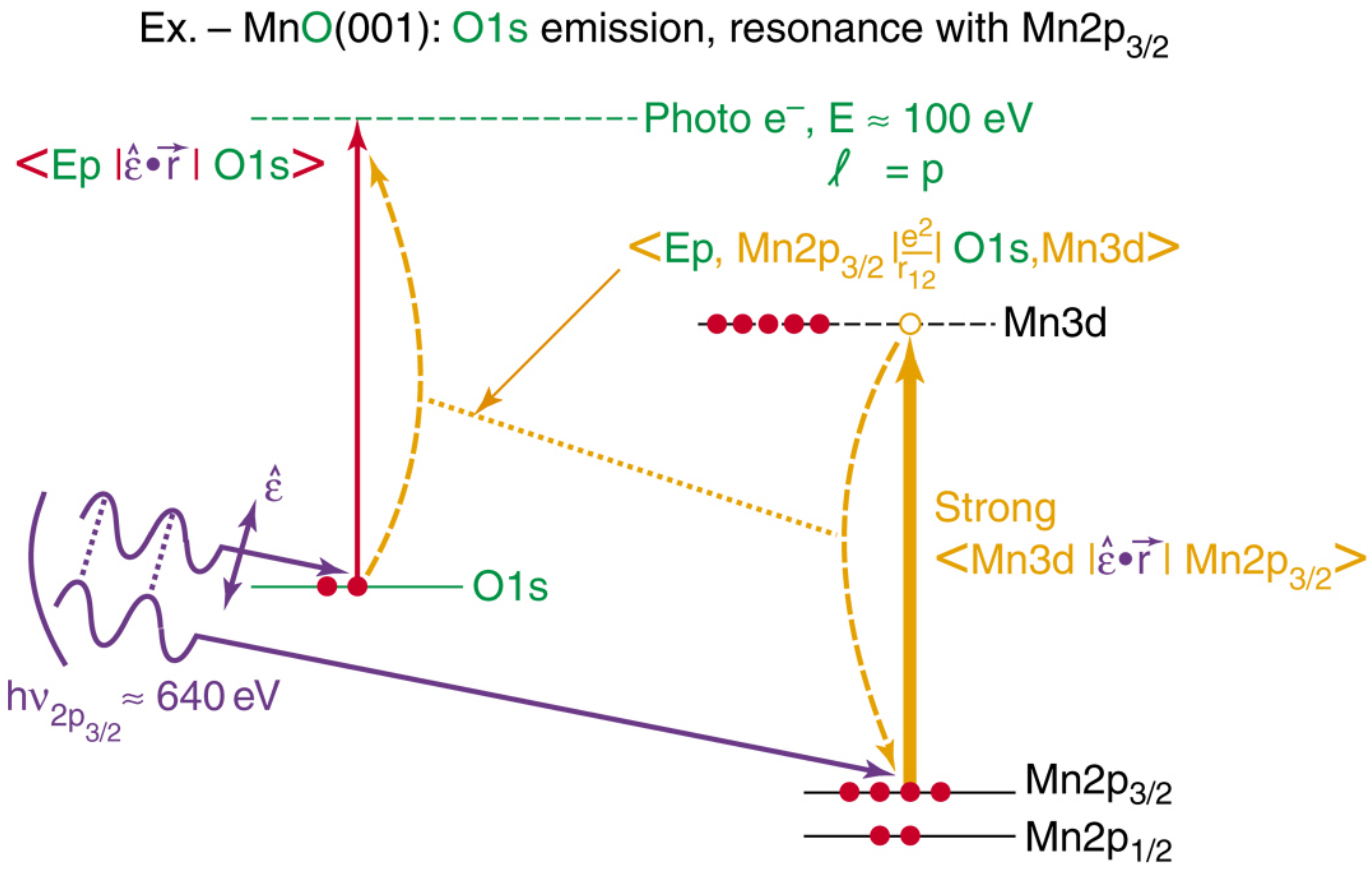

Kay et al.,
Science 281, 679 ('98);
Corrected picture in
PRB 61, 5119 ('01)←

Multi-Atom Resonant Photoemission—O 1s emission from NiO(001)

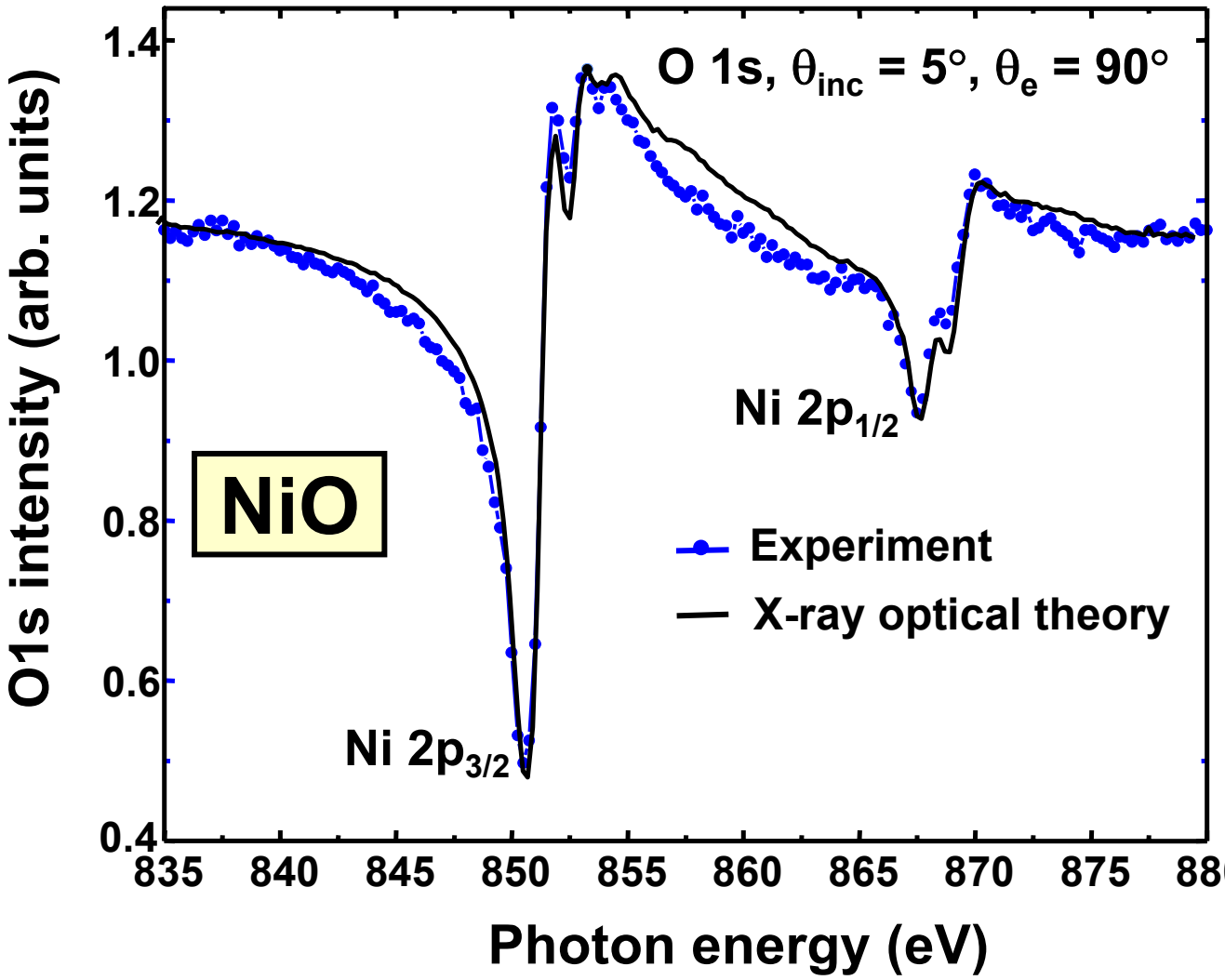

More later

Mannella et al., to be published

Effects beyond the dipole approximation

The differential cross section for photoionization of randomly oriented target atoms by 100% linearly polarized photons has the form:

$$\frac{d\sigma}{d\Omega} = \left(\frac{\sigma}{4\pi}\right)\left[\underbrace{1+\beta\, P_2(\cos\alpha)}_{\text{DIPOLE}} + \underbrace{(\delta+\gamma\cos^2\alpha)\sin\alpha\cos\phi}_{\text{NON-DIPOLE}}\right]$$

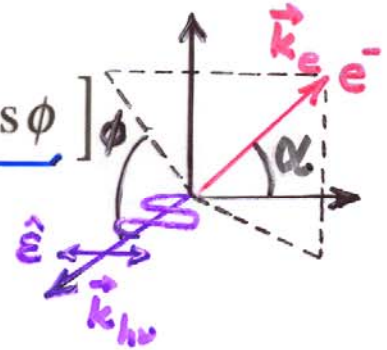

with:

$$P_2(\cos\alpha) = \frac{1}{2}(3\cos^2\alpha - 1)$$

σ: angle integrated cross section

γ: pole electron anisotropy parameter

β: electron anisotropy parameter

δ: non-dipole electron anisotropy parameter

$$\exp(i\vec{k}_{h\nu}\cdot\vec{r}) = \underbrace{1}_{\text{DIPOLE}} + \underbrace{i\vec{k}_{h\nu}\cdot\vec{r} - \tfrac{1}{2}(\vec{k}_{h\nu}\cdot r)^2 + \cdots}_{\text{NON-DIPOLE}}$$

Krause et al.
Lindle et al.
Krässig et al.

$k_{h\nu} = 2\pi/\lambda_{h\nu} = 0.75$ Å^{-1} @ 1.49 keV → $k_{h\nu} \bullet [\langle r_{nl}\rangle \approx 1$ Å$] \approx 0.75$—Non-dipole imp?

0.075 Å^{-1} @ 149 eV → $k_{h\nu} \bullet [\langle r_{nl}\rangle \approx 1$ Å$] \approx 0.075$—Dipole ~OK

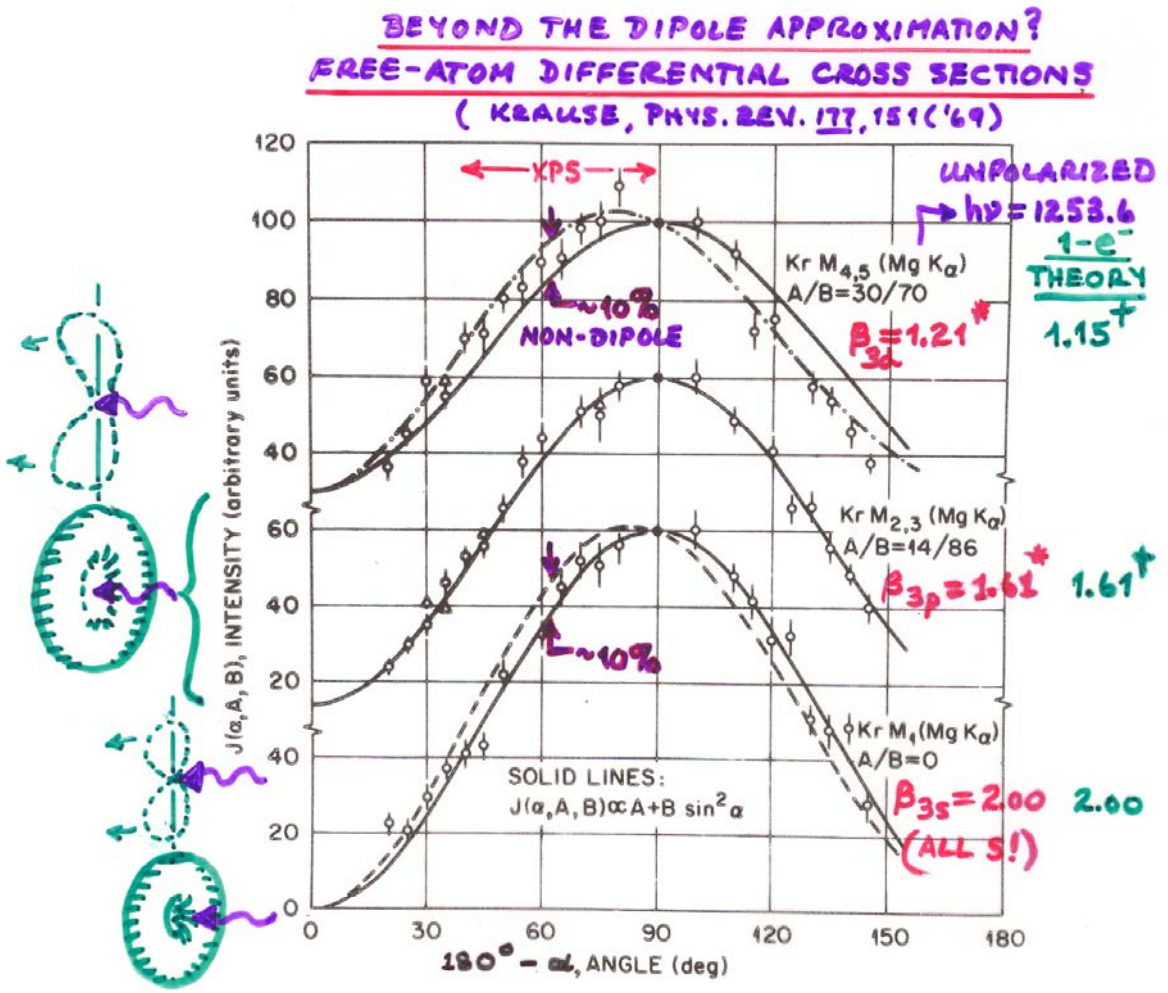

Figure 10 -- Experimental angular distributions of 3s (= M_1), 3p (= $M_{2,3}$), and 3d (= $M_{4,5}$) photoelectrons excited from gaseous Kr with MgKα X-rays. The curves represent least-squares fits to the data points of a relationship of the form of Equation (93), in which A and B were treated as empirical constants. (From Krause, reference 142.)

* FROM: $\beta_{nL} = \frac{4B}{(3A+2B)} = \frac{4}{(3A/B+2)}$

NEAR EQ. 93; FADLEY, "BASIC CONCEPTS OF XPS"

† FROM YEH & LINDAU TABLES

"Basic Concepts of XPS"
Figure 10

Non-dipole effects in 2p emission from Ne

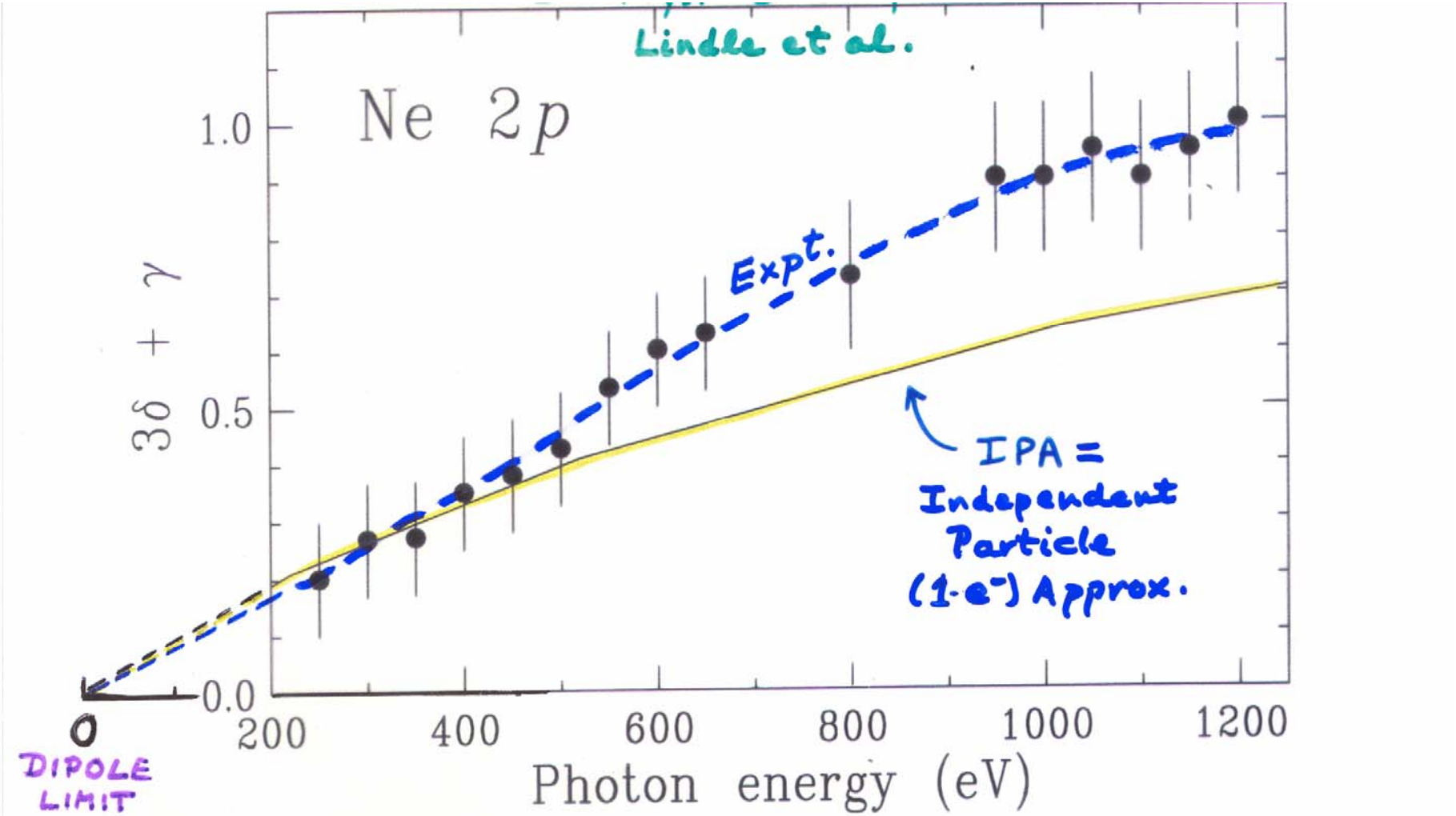

+ see Phys. Rev. Lett. 78, 4553 ('97): Lindle et al.
" " " 75, 4736 ('95): Krässig et al.

PHOTOELECTRON INTENSITIES—THE 3-STEP MODEL

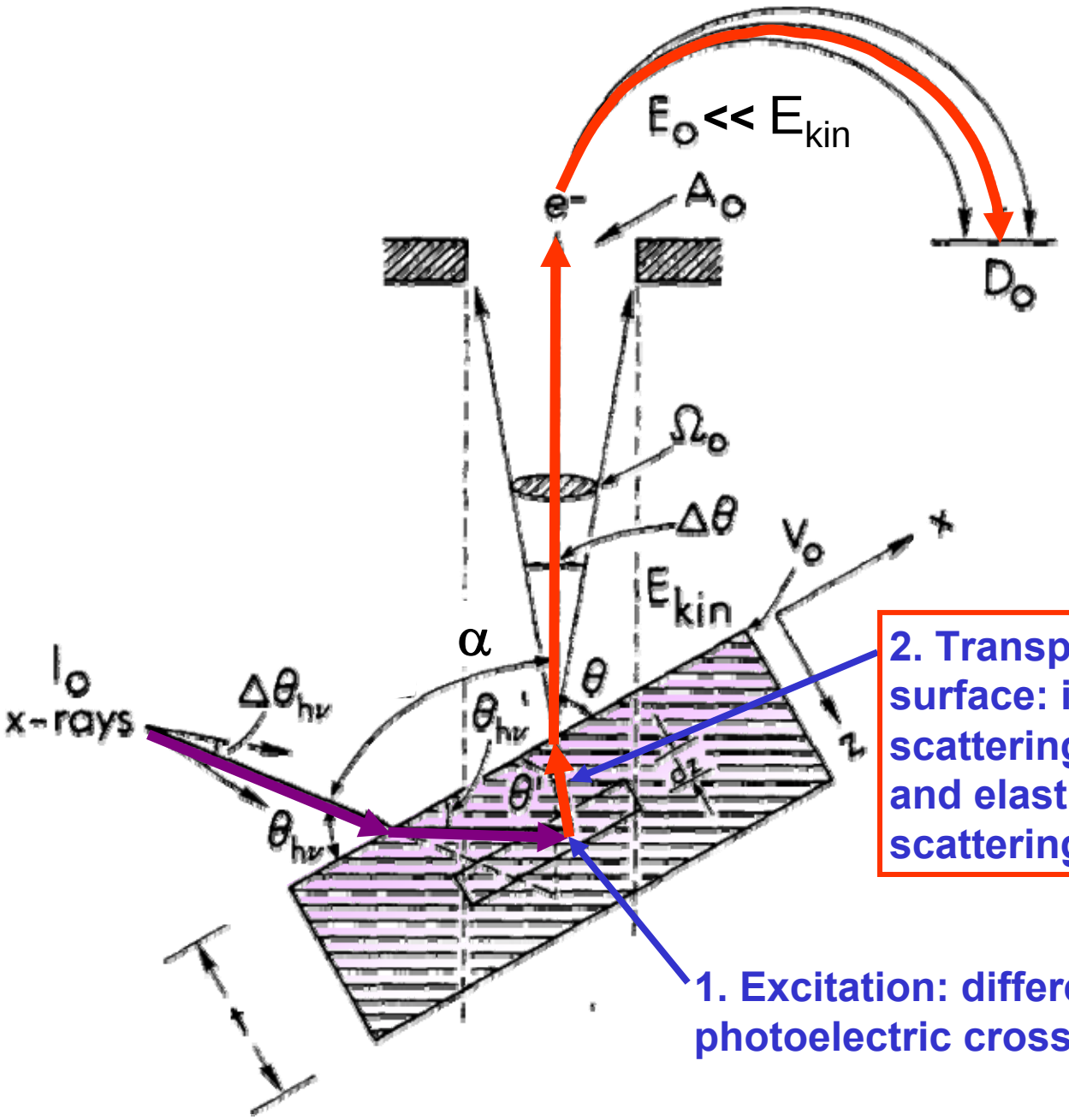

2. Transport to the surface: inelastic scattering (Λ_e) and elastic scattering (f(θ)--later)

1. Excitation: differential photoelectric cross section ($d\sigma/d\Omega$)

Electron inelastic attenuation length in solids—the "universal curve"
Photoemission is a surface sensitive experiment

Changing angle:
1st way to vary surface sensitivity

$$I(z) = I_0 e^{-\frac{z}{\Lambda_e \sin\Theta}}$$

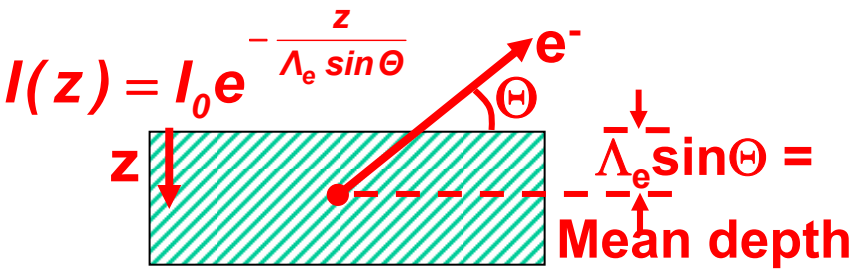

Graphite

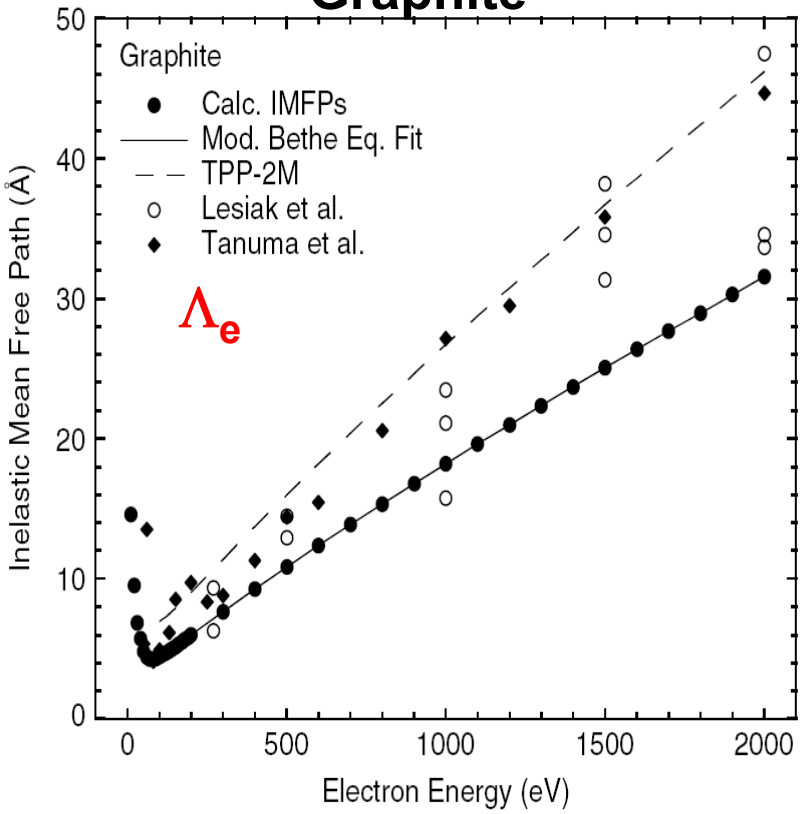

Germanium

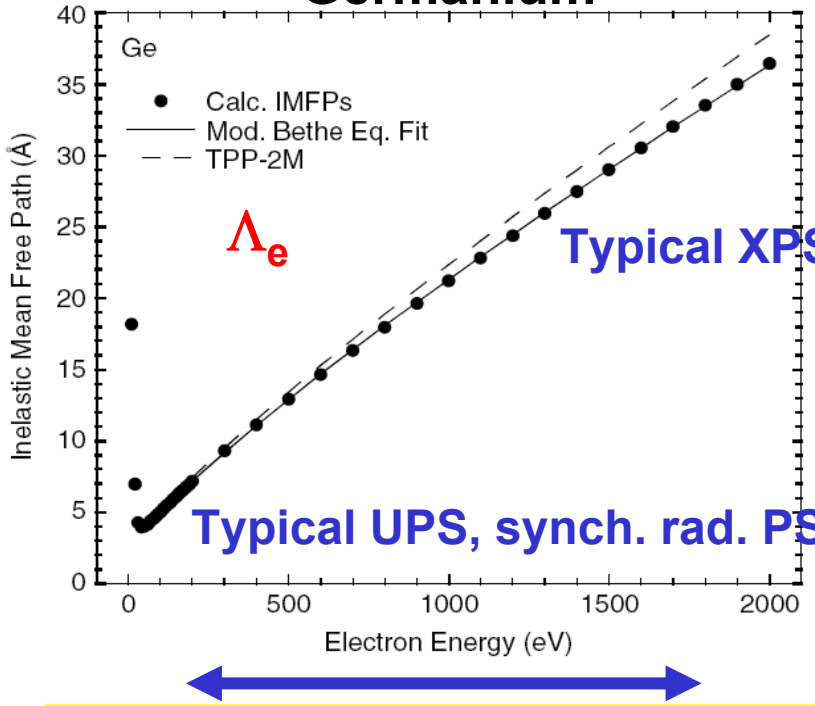

Changing photon energy:
2nd way to vary surface sensitivity

Inelastic mean free paths in solids

Database of experimental and theoretically estimated mean free paths at http://www.nist.gov/srd/webguide/nist71/71imfp.htm#elements

Plus estimation with the TPP-2M (TPP-2) formula of Tanuma, Powell, Penn:

Web calculation for elements from: http://www.ss.teen.setsunan.ac.jp/e-imfp2.html

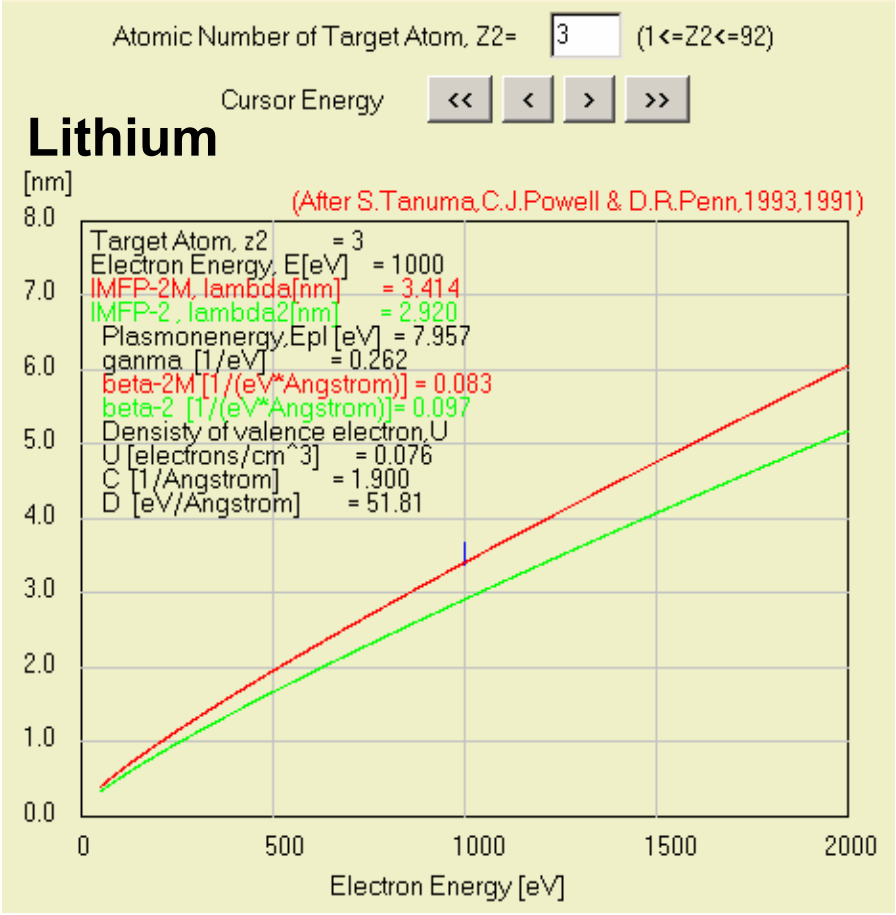

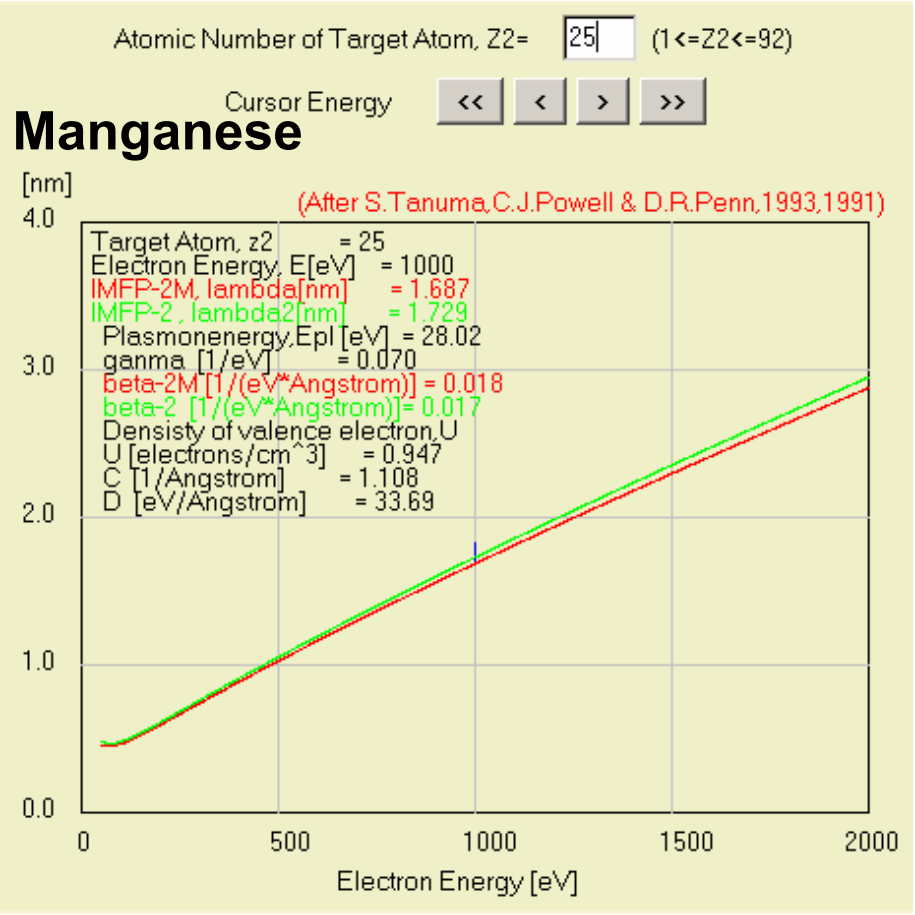

Inelastic mean free paths in solids

Estimation from the TPP-2M formula: any compound

$$\Lambda_e \approx \lambda = \frac{E}{E_p^2[\beta \ln(\gamma E) - (C/E) + (D/E^2)]}$$

where

$$\beta = -0.10 + 0.944/(E_p^2 + E_g^2)^{1/2} + 0.069\rho^{0.1}$$

$$\gamma = 0.191\rho^{-0.50}$$

$$C = 1.97 - 0.91U$$

$$D = 53.4 - 20.8U$$

$$U = N_v\rho/M = E_p^2/829.4$$

and $E_p = 28.8\ (N_v\rho/M)^{1/2}$ is the free-electron plasmon energy (in eV), ρ is the density (in g cm^{-3}), N_v is the number of valence electrons per atom (for an element) or molecule (for a compound), M is the atomic or molecular weight, and E_g is the bandgap energy (in eV). These equations are collectively known as the TPP-2M equation.

Tanuma, Powell, Penn, Surf. Interface Anal. 21, 165 (1994)

CORE PHOTOELECTRON INTENSITIES AND COMPOSITION

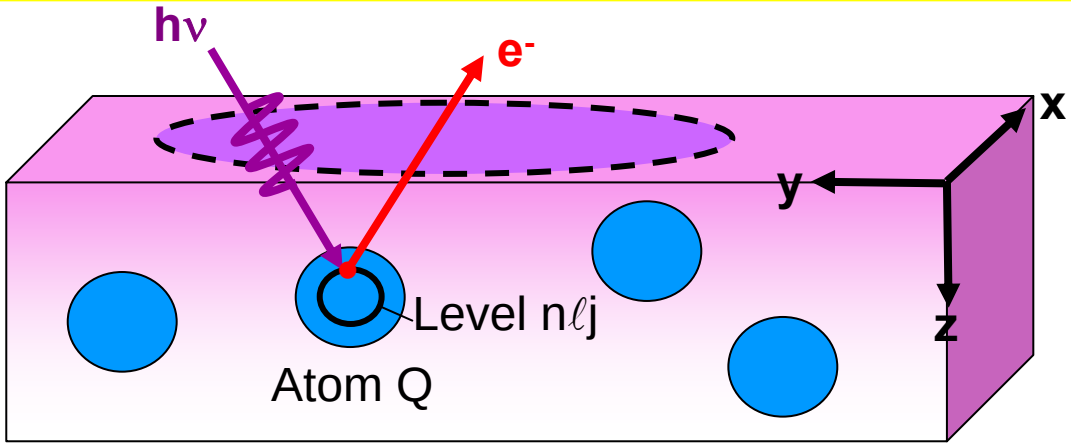

$$I(Qn\ell j) = C\int_0^{\infty} I_0(x,y,z)\rho_Q(x,y,z)\frac{d\sigma_{Qn\ell j}(h\nu)}{d\Omega}\exp\left[-\frac{z}{\Lambda_e \sin\theta}\right]\Omega(h\nu,x,y)\,dx\,dy\,dz$$

$I_{h\nu}(x,y,z)$ = x-ray flux

$\rho_Q(x,y,z)$ = density of atoms Q $\rightarrow$ quantitative analysis

$\frac{d\sigma_{Qn\ell j}(h\nu)}{d\Omega}$ = differential photoelectric cross section for subshell $Qn\ell j$

Λ_e = inelastic attenuation length

$\Omega(h\nu,x,y)$ = spectrometer acceptance solid angle

(a) Semi-infinite specimen, atomically clean surface, peak k with $E_{kin} \equiv E_k$:

$$N_k(\theta) = I_0 \Omega_0(E_k) A_0(E_k) D_0(E_k) \rho \, d\sigma_k/d\Omega \, \Lambda_e(E_k) \quad (115)$$

(NO θ DEP.)

This case corresponds to an optimal measurement on a homogeneous specimen for which no surface contaminant layer is present.

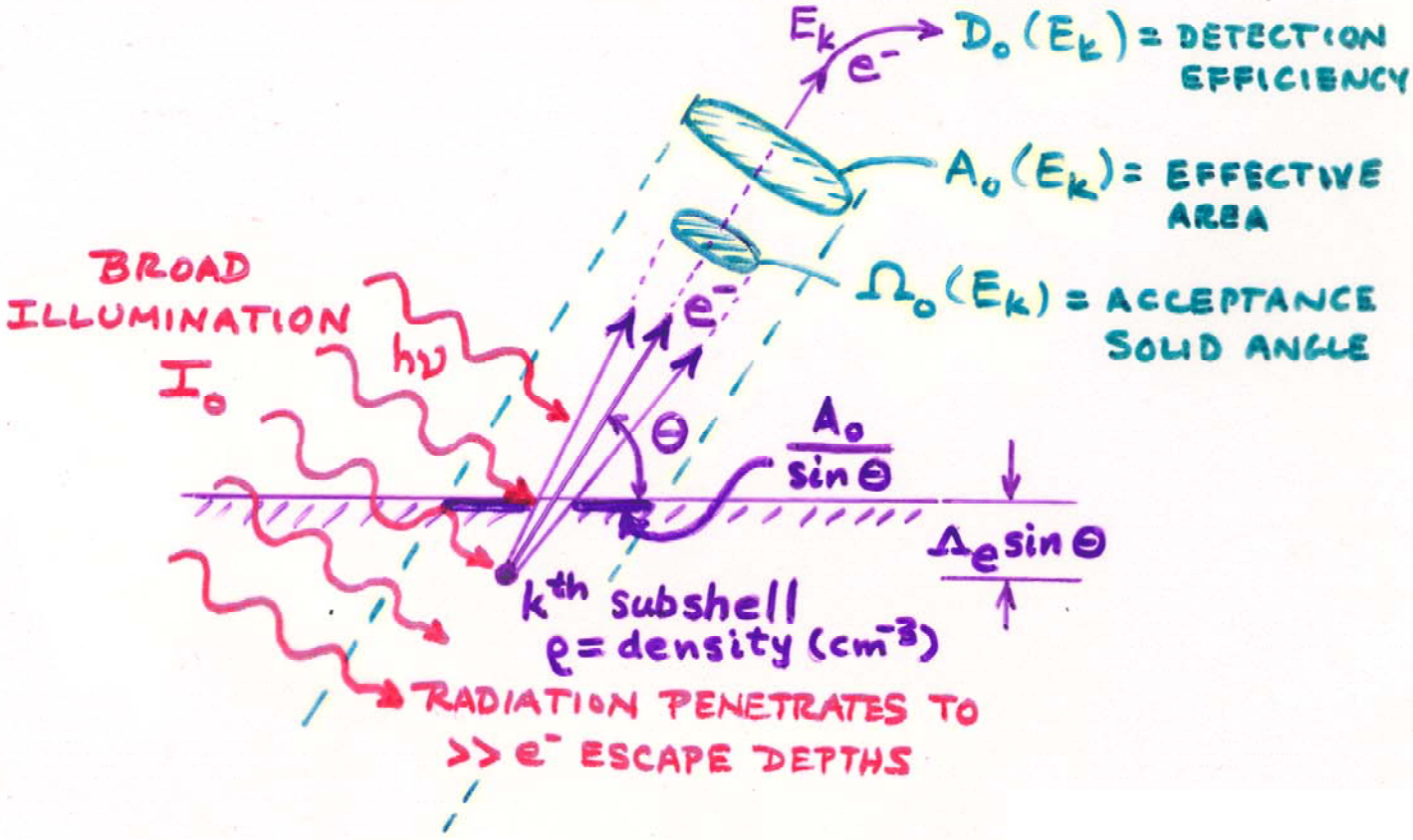

(b) Specimen of thickness t, atomically clean surface, peak k with $E_{kin} \equiv E_k$:

$$N_k(\theta) = I_0 \Omega_0(E_k) A_0(E_k) D_0(E_k) \rho \, d\sigma_k/d\Omega \, \Lambda_e(E_k) \times [1 - \exp(-t/\Lambda_e(E_k) \sin \theta)] \quad (116)$$

Here, the intensity of a peak originating in a specimen of finite thickness is predicted to increase with decreasing θ.

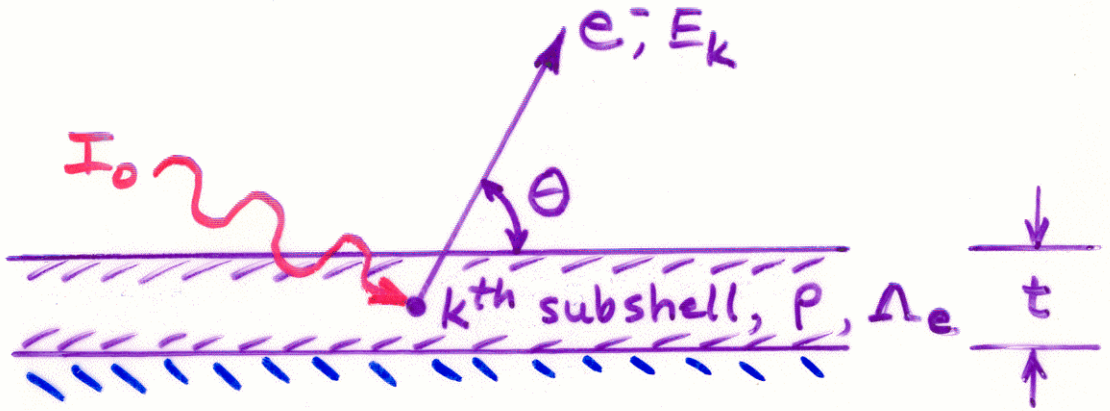

(c) Semi-infinite substrate with uniform overlayer of thickness t - Peak k from substrate with $E_{kin} \equiv E_k$:

$$N_k(\theta) = I_0 \Omega_0(E_k) A_0(E_k) D_0(E_k) \rho \, d\sigma_k/d\Omega \, \Lambda_e(E_k) \times \exp(-t/\Lambda_e'(E_k) \sin\theta) \quad (117)$$

Peak l from overlayer with $E_{kin} \equiv E_l$:

$$N_l(\theta) = I_0 \Omega_0(E_l) A_0(E_l) D_0(E_l) \rho' \, d\sigma_l/d\Omega \, \Lambda_e'(E_l) \times [1 - \exp(-t/\Lambda_e'(E_l) \sin\theta)] \quad (118)$$

where

$\Lambda_e(E_k)$ = an attenuation length in the substrate

$\Lambda_e'(E_k)$ = an attenuation length in the overlayer

ρ = an atomic density in the substrate

ρ' = an atomic density in the overlayer.

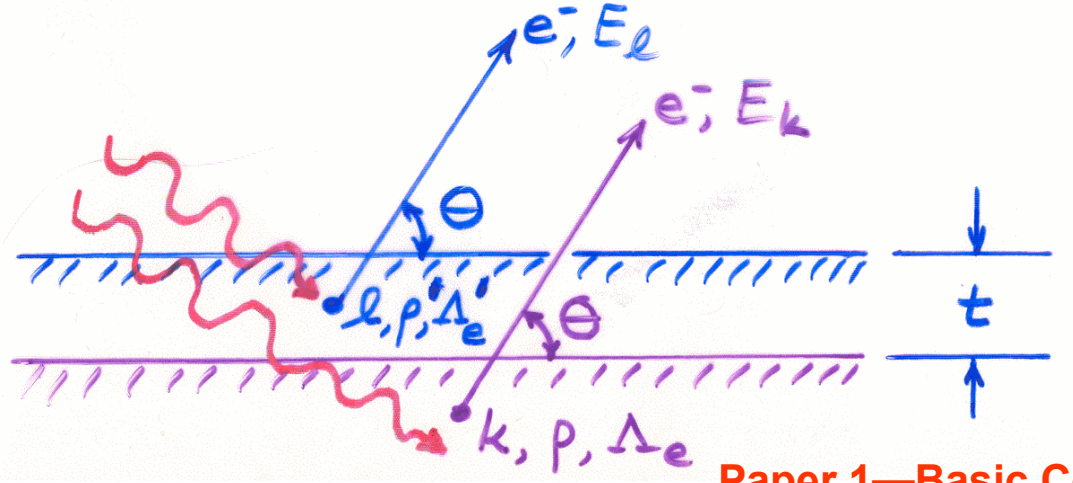

(d) Semi-infinite substrate with a non-attenuating overlayer at fractional monolayer coverage—Peak k from substrate: Eq. (115).

Peak l from overlayer:

$$N_l(\theta) = I_0 \Omega_0(E_l) A_0(E_l) D_0(E_l) s' (\mathrm{d}\sigma_l/\mathrm{d}\Omega)(\sin\theta)^{-1} \tag{120a}$$

Overlayer/substrate ratio:

$$\frac{N_l(\theta)}{N_k(\theta)} = \frac{\Omega_0(E_l) A_0(E_l) D_0(E_l) s' (\mathrm{d}\sigma_l/\mathrm{d}\Omega)}{\Omega_0(E_k) A_0(E_k) D_0(E_k) s\ \mathrm{d}\sigma_k/\mathrm{d}\Omega\ (\Lambda_e(E_k) \sin\theta/d)}$$

$$= \left[\frac{s'}{s}\right] \cdot \frac{D_0(E_l)\Omega_0(E_l)A_0(E_l)(\mathrm{d}\sigma_l/\mathrm{d}\Omega)d}{D_0(E_k)\Omega_0(E_k)A_0(E_k)\ \mathrm{d}\sigma_k/\mathrm{d}\Omega\ \Lambda_e \sin\theta} \tag{120b}$$

with

s' = the mean surface density of atoms in which peak l originates in cm^{-2}

s = the mean surface density of substrate atoms in $\mathrm{cm}^{-2} \equiv \rho_s$

s'/s = the fractional monolayer coverage of the atomic species in which peak l originates

d = the mean separation between layers of density s in the substrate (calculable from s/ρ).

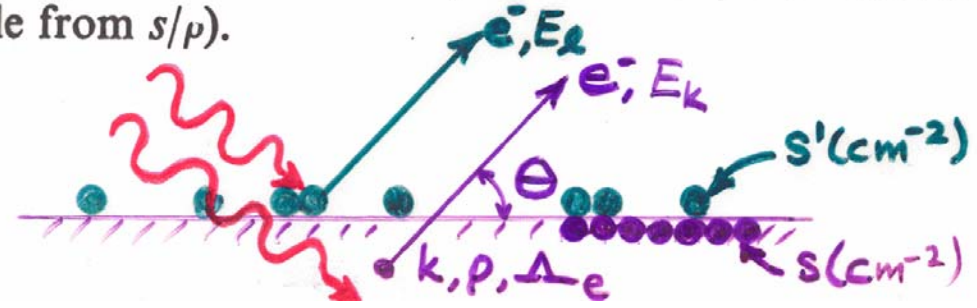

Table 4 Density and atomic concentration

The data are given at atmospheric pressure and room temperature, or at the stated temperature in deg K. (Crystal modifications as for Table 3.)

Atomic radius = r_{MT} = 0.5 n-n dist.

Average surface density = $\rho_S = (\rho_V)^{2/3}$

Density in g cm^{-3} (10^3kg m^{-3})
Concentration in 10^{22} cm^{-3} (10^{28} m^{-3})
Nearest-neighbor distance, in Å (10^{-10}m)

H 4K																	He 2K
0.088																	0.205 (at 37 atm)
Li 78K	Be											B	C	N 20K	O	F	Ne 4K
0.542	1.82											2.47	3.516	1.03			1.51
4.700	12.1											13.0	17.6				4.36
3.023	2.22												1.54			1.44	3.16
Na 5K	Mg											Al	Si	P	S	Cl 93K	Ar 4K
1.013	1.74											2.70	2.33			2.03	1.77
2.652	4.30											6.02	5.00				2.66
3.659	3.20											2.86	2.35			2.02	3.76
K 5K	Ca	Sc	Ti	V	Cr	Mn	Fe	Co	Ni	Cu	Zn	Ga	Ge	As	Se	Br 123K	Kr 4K
0.910	1.53	2.99	4.51	6.09	7.19	7.47	7.87	8.9	8.91	8.93	7.13	5.91	5.32	5.77	4.81	4.05	3.09
1.402	2.30	4.27	5.66	7.22	8.33	8.18	8.50	8.97	9.14	8.45	6.55	5.10	4.42	4.65	3.67	2.36	2.17
4.525	3.95	3.25	2.89	2.62	2.50	2.24	2.48	2.50	2.49	2.56	2.66	2.44	2.45	3.16	2.32		4.00
Rb 5K	Sr	Y	Zr	Nb	Mo	Tc	Ru	Rh	Pd	Ag	Cd	In	Sn	Sb	Te	I	Xe 4K
1.629	2.58	4.48	6.51	8.58	10.22	11.50	12.36	12.42	12.00	10.50	8.65	7.29	5.76	6.69	6.25	4.95	3.78
1.148	1.78	3.02	4.29	5.56	6.42	7.04	7.36	7.26	6.80	5.85	4.64	3.83	2.91	3.31	2.94	2.36	1.64
4.837	4.30	3.55	3.17	2.86	2.72	2.71	2.65	2.69	2.75	2.89	2.98	3.25	2.81	2.91	2.86	3.54	4.34
Cs 5K	Ba	La	Hf	Ta	W	Re	Os	Ir	Pt	Au	Hg 227	Tl	Pb	Bi	Po	At	Rn
1.997	3.59	6.17	13.20	16.66	19.25	21.03	22.58	22.55	21.47	19.28	14.26	11.87	11.34	9.80	9.31		
0.905	1.60	2.70	4.52	5.55	6.30	6.80	7.14	7.06	6.62	5.90	4.26	3.50	3.30	2.82	2.67	—	—
5.235	4.35	3.73	3.13	2.86	2.74	2.74	2.68	2.71	2.77	2.88	3.01	3.46	3.50	3.07	3.34		
Fr	Ra	Ac															
		10.07															
—	—	2.66															
		3.76															

Ce	Pr	Nd	Pm	Sm	Eu	Gd	Tb	Dy	Ho	Er	Tm	Yb	Lu
6.77	6.78	7.00		7.54	5.25	7.89	8.27	8.53	8.80	9.04	9.32	6.97	9.84
2.91	2.92	2.93	—	3.03	2.04	3.02	3.22	3.17	3.22	3.26	3.32	3.02	3.39
3.65	3.63	3.66		3.59	3.96	3.58	3.52	3.51	3.49	3.47	3.54	3.88	3.43
Th	Pa	U	Np	Pu	Am	Cm	Bk	Cf	Es	Fm	Md	No	Lr
11.72	15.37	19.05	20.45	19.81	11.87								
3.04	4.01	4.80	5.20	4.26	2.96	—	—	—	—	—	—	—	—
3.60	3.21	2.75	2.62	3.1	3.61								

Surface sensitivity enhancement for grazing exit angles

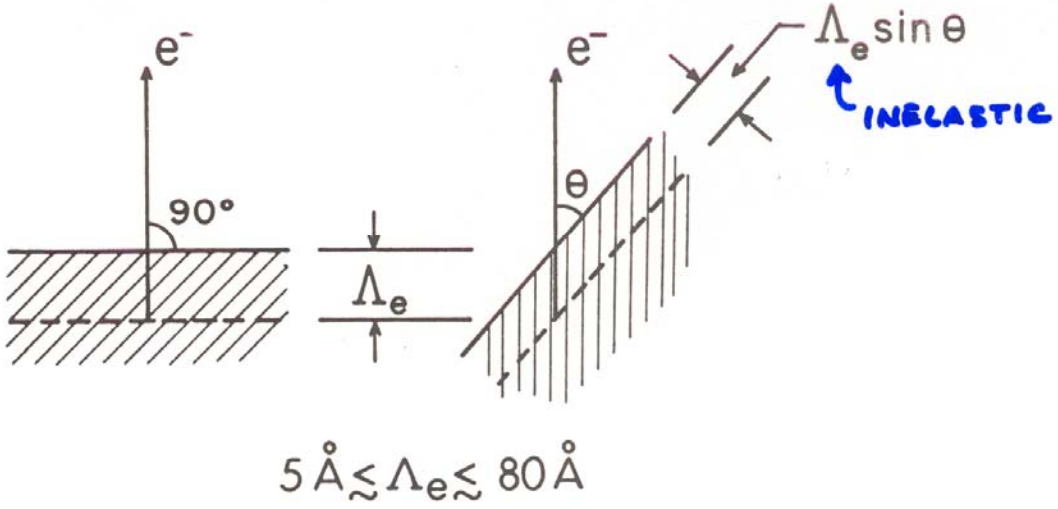

Fig. 5. Illustration of the basic mechanism producing surface sensitivity enhancement for low electron exit angles θ. The average depth for no-loss emission as measured perpendicular to the surface is $\Lambda_e \sin\theta$.

E.g.- Λ_e = 28 Å in Au(s) at 1400 eV

	θ	Mean Depth	No. layers
"BULK" →	90°	28 Å	~9
"SURFACE" →	10°	~4.4 Å	~1.5

... BUT REFRACTION AT SURFACE AND ELASTIC SCATTERING CAN REDUCE SURFACE ENHANCEMENT, ESP. AT LOW θ ≤ 30°

Surface sensitivity enhancement for grazing exit angles

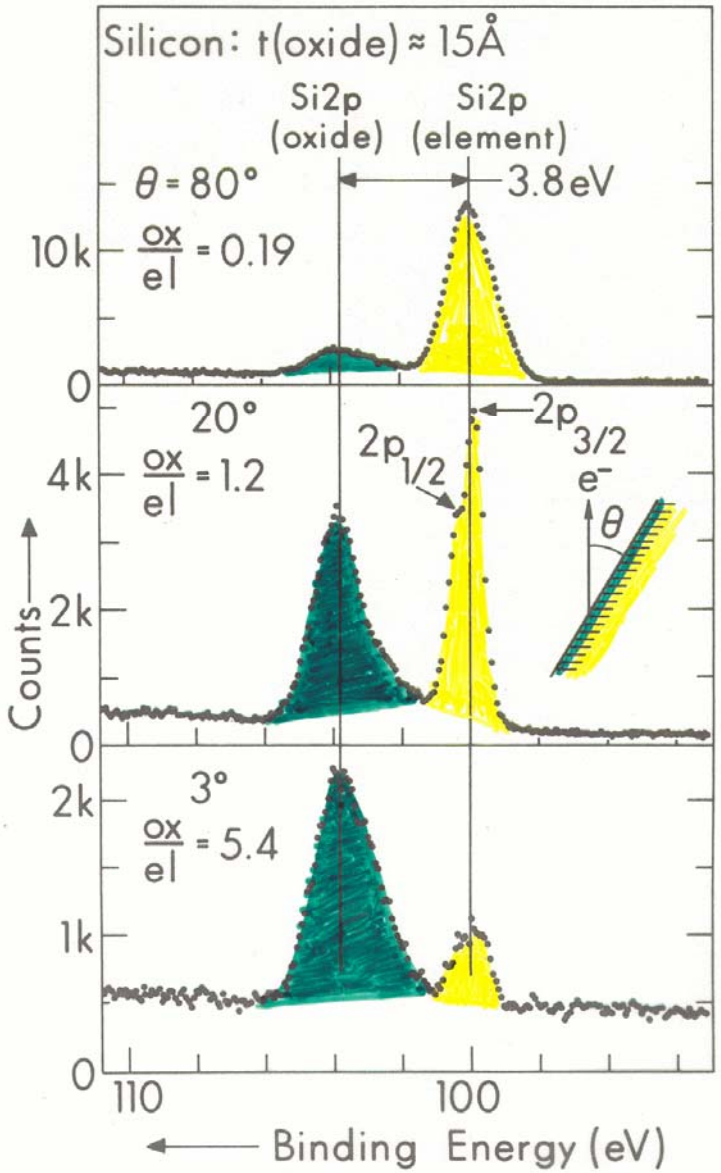

Fadley, Progress in Surface Science, 16, 275 ('84)

Fig. 7. Si2p spectra at three electron exit angles for a Si specimen with a 15-Å thick oxide overlayer. Note the complete reversal of the relative intensities of oxide and element between high and low θ. (From Hill et al., ref. (19).)

Surface sensitivity enhancement for grazing exit angles

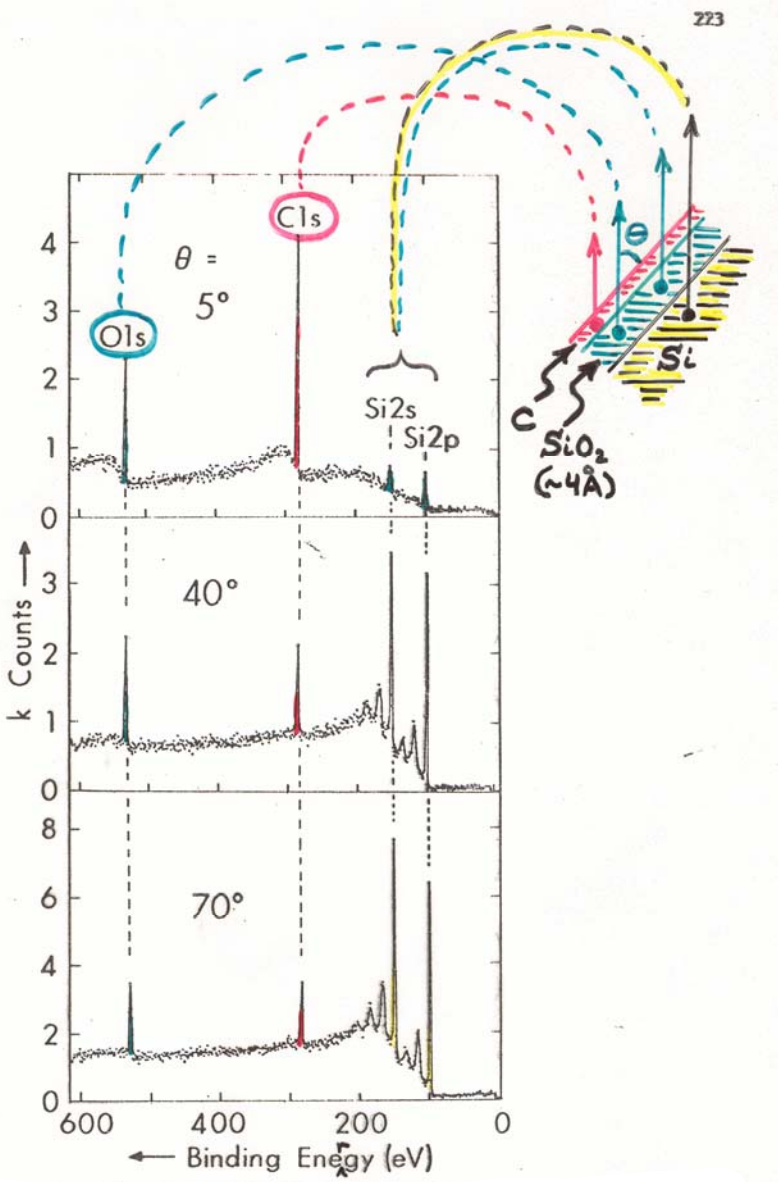

Figure 44 -- Broad-scan core spectra at low and high exit angles for a Si specimen with a thin oxide overlayer (~ 4Å) and an outermost carbon contaminant overlayer approximately 1-2 monolayers in thickness. The C1s and O1s signals are markedly enhanced in relative intensity at low θ due to the general effect presented in Figure 43. (From Fadley, reference 17.)

PHOTOELECTRON INTENSITIES—THE 3-STEP MODEL

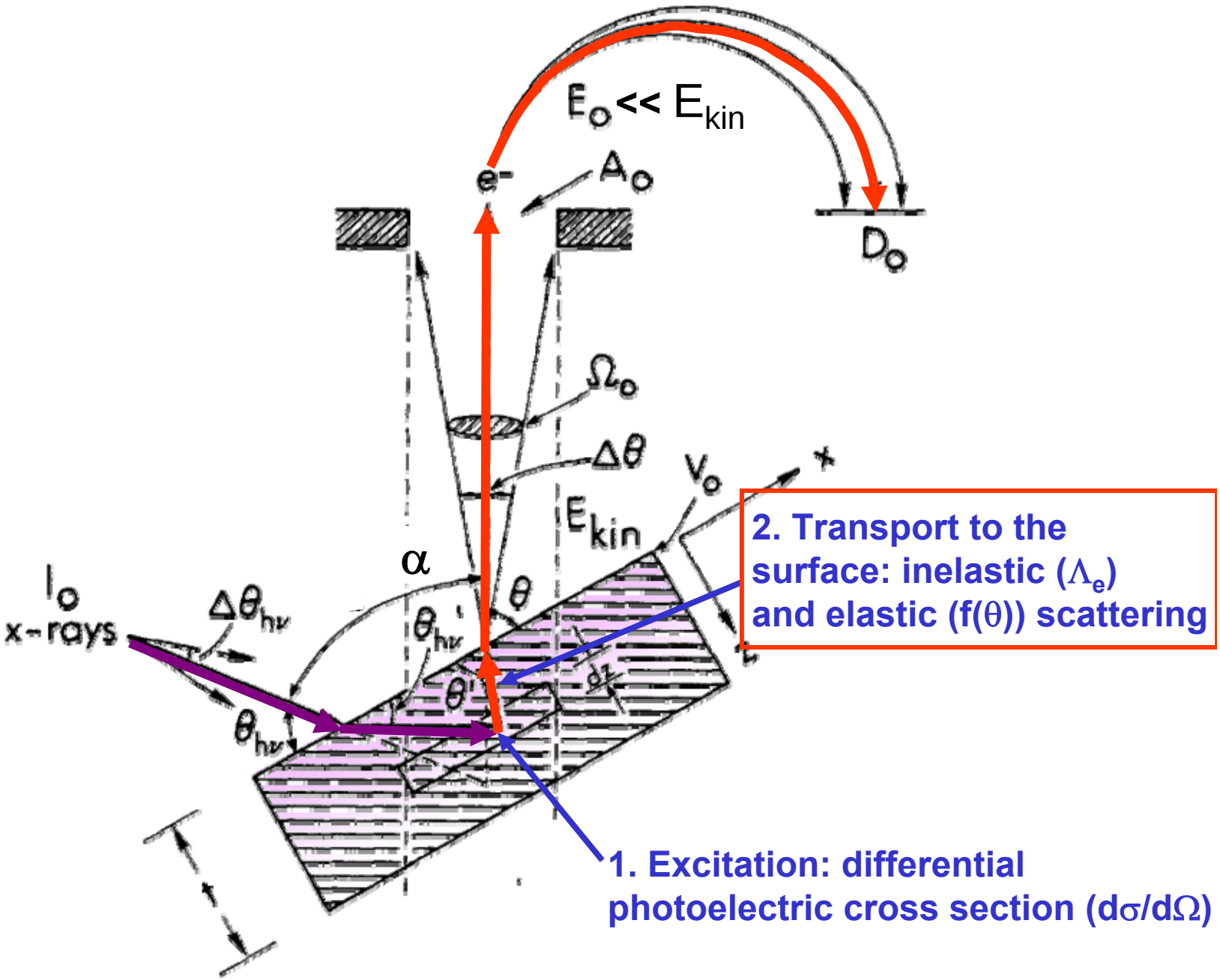

EFFECTS OF ELASTIC SCATTERING ON ANGULAR DISTRIBUTIONS: POLYCRYSTALLINE OR AMORPHOUS SAMPLE

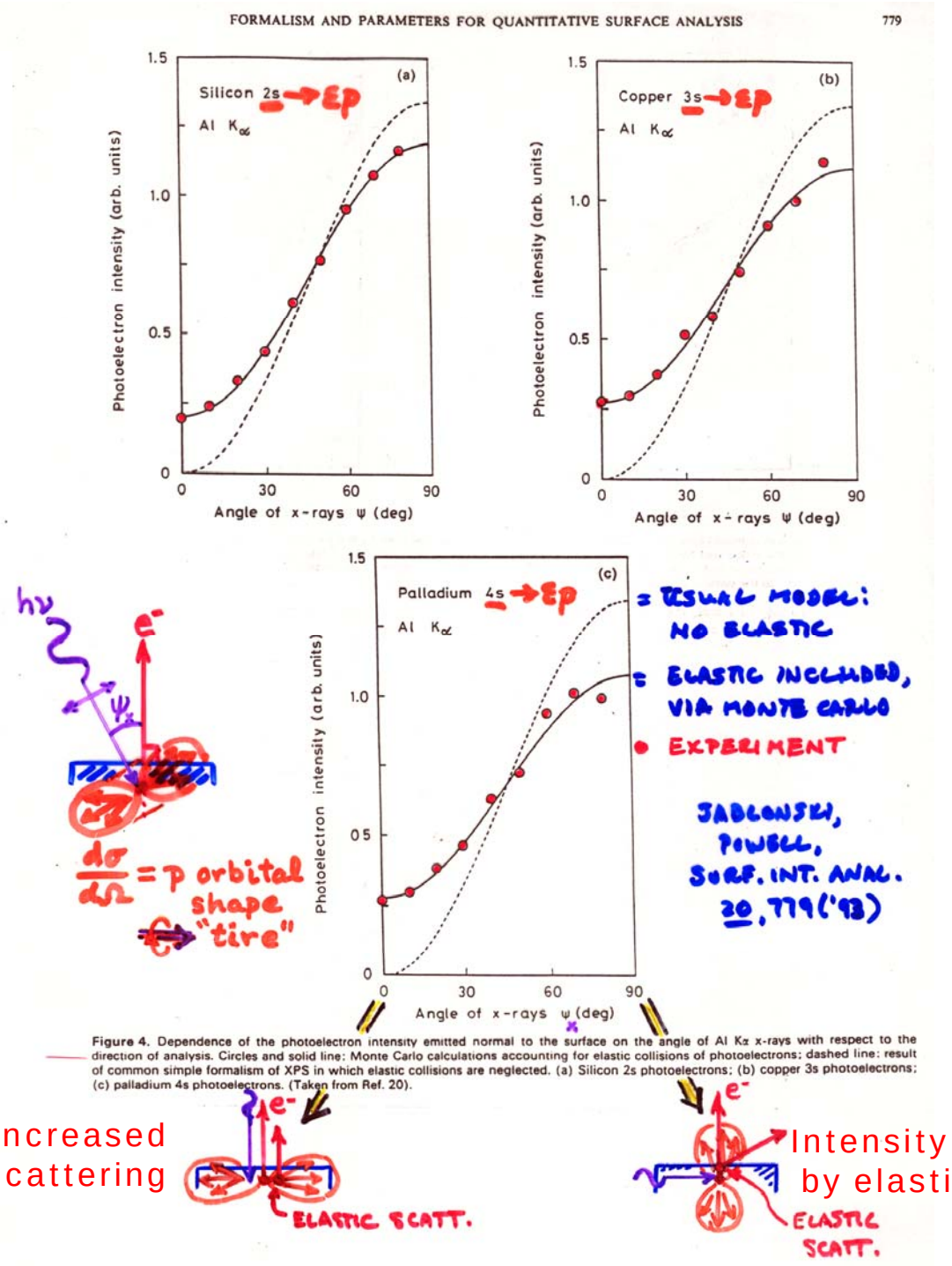

Figure 4. Dependence of the photoelectron intensity emitted normal to the surface on the angle of Al Kα x-rays with respect to the direction of analysis. Circles and solid line: Monte Carlo calculations accounting for elastic collisions of photoelectrons; dashed line: result of common simple formalism of XPS in which elastic collisions are neglected. (a) Silicon 2s photoelectrons; (b) copper 3s photoelectrons; (c) palladium 4s photoelectrons. (Taken from Ref. 20).

Intensity increased by elastic scattering

Intensity decreased by elastic scatt.

PHOTOELECTRON INTENSITIES—THE 3-STEP MODEL

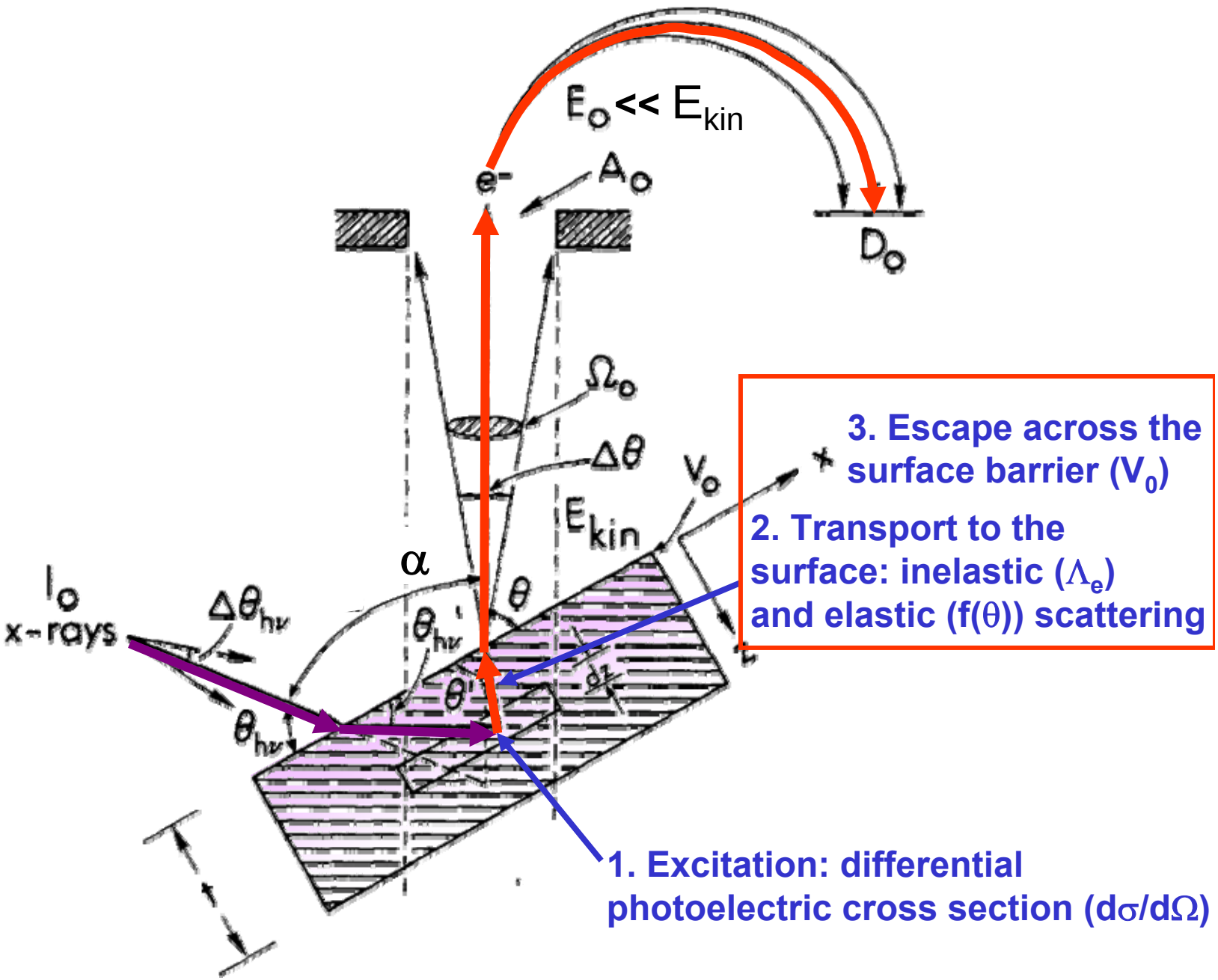

One-Electron Picture of Photoemission from a Surface

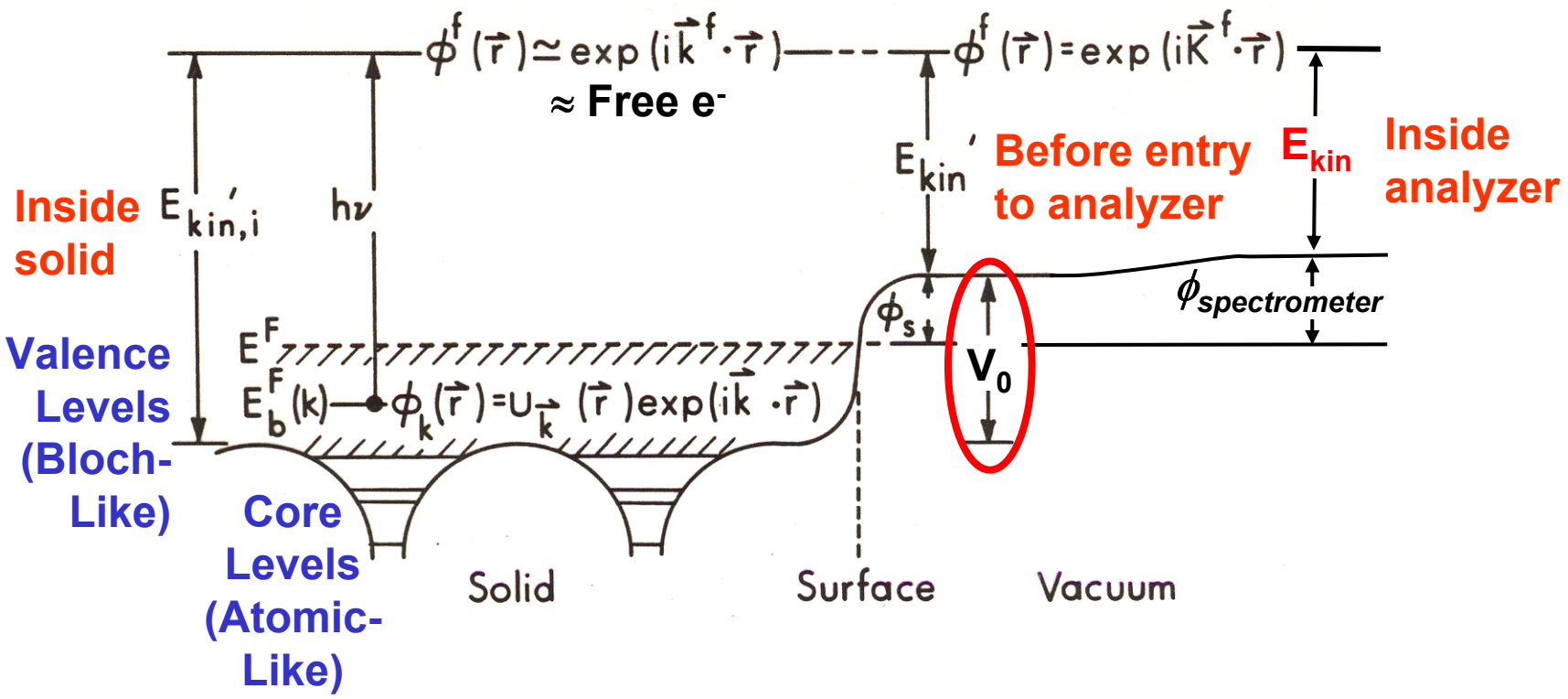

Electron Refraction at the Surface Due to the Inner Potential

$$\theta = \tan^{-1}\left[\sqrt{\sin^2\theta' - \frac{V_o}{E_{kin}}} \Big/ \cos\theta'\right]$$

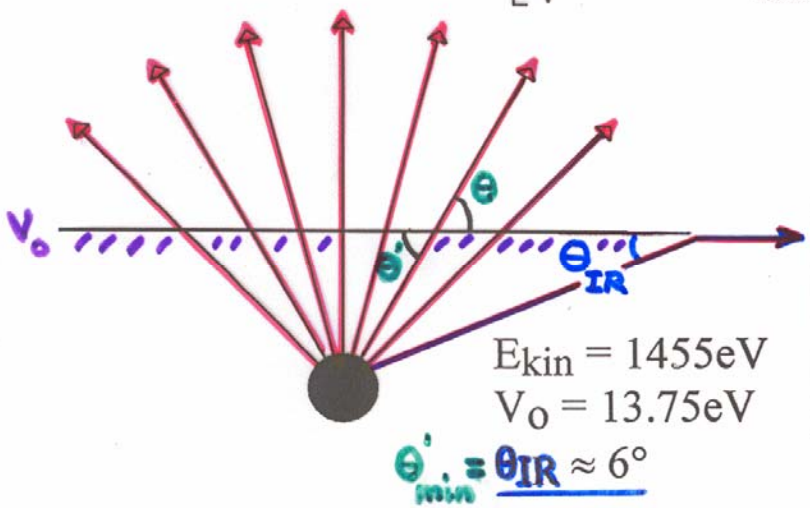

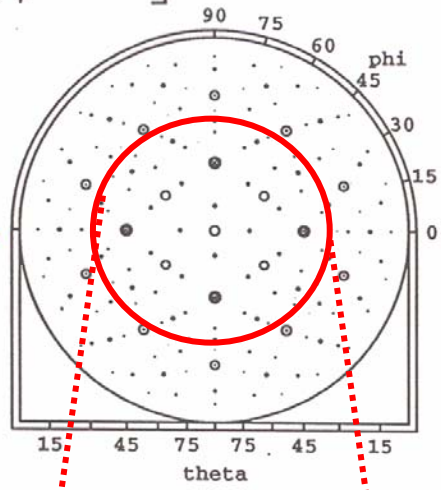

Observed Low-Index Directions Above W(110)

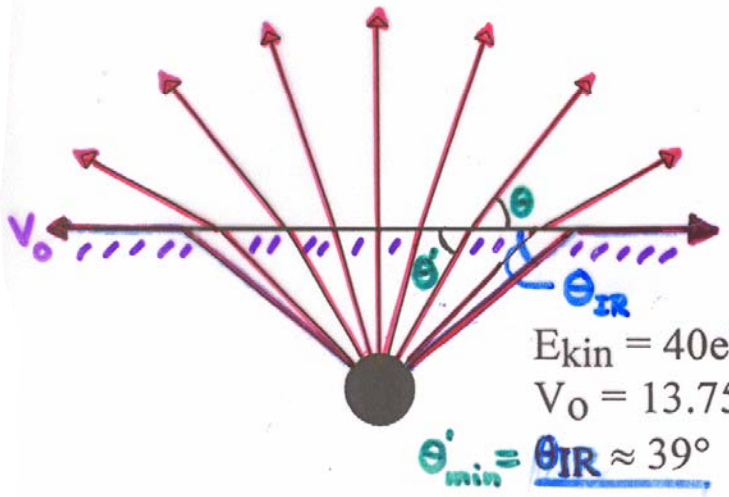

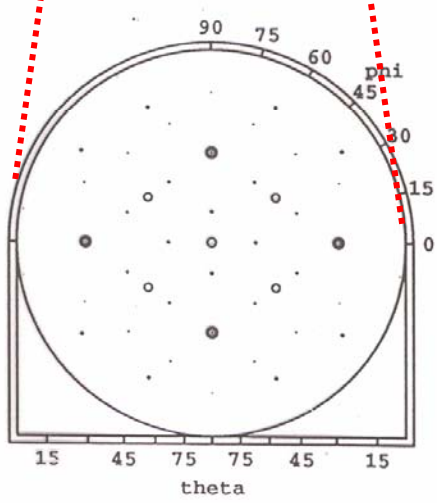

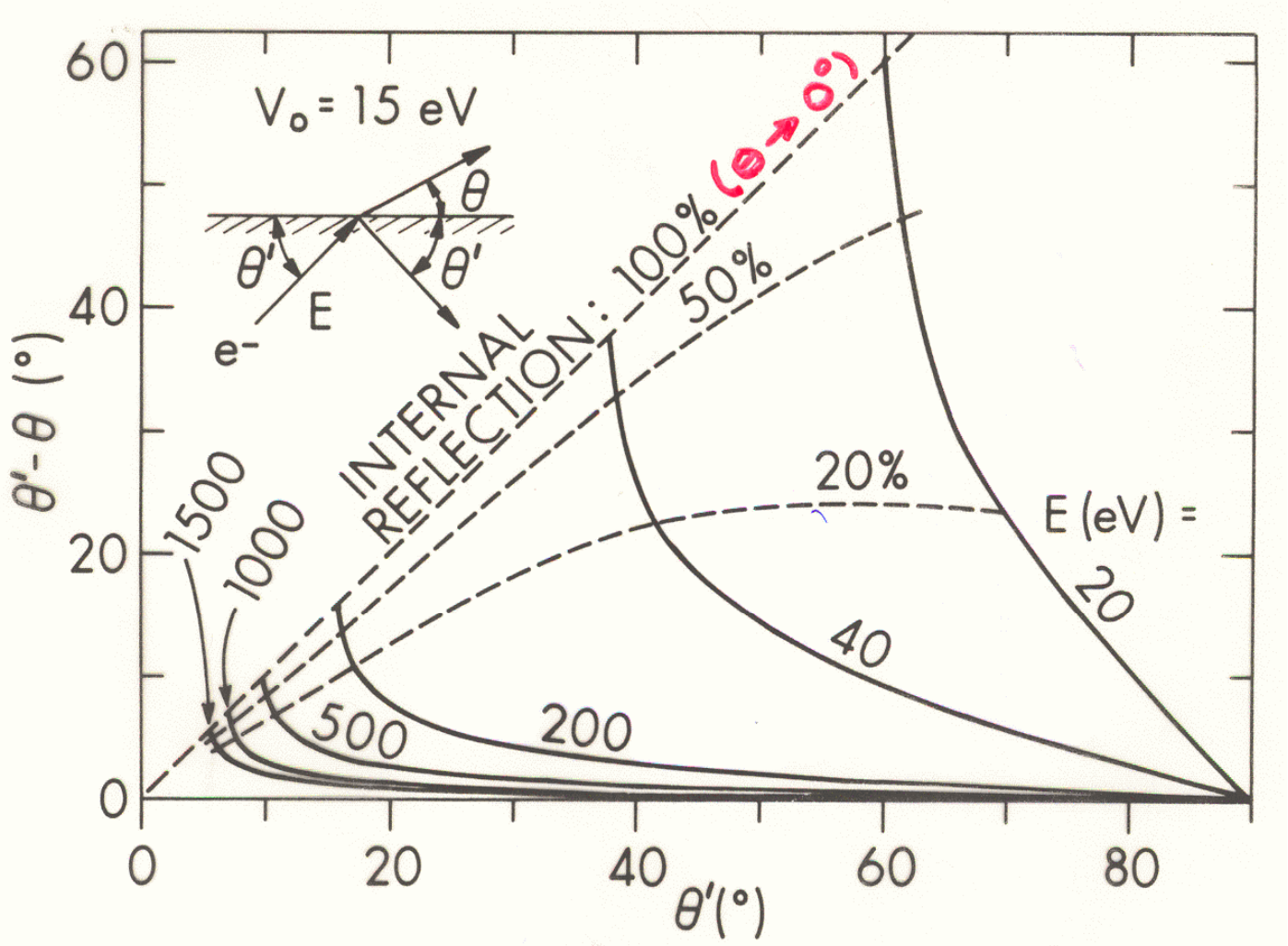

Fig. 14. Calculation of electron refraction effects for different electron kinetic energies and a typical V_o value of 15eV. The degree of refraction is indicated by the difference θ' (internal) — θ (external) Contours of equal probablility of internal reflection are also shown. (From ref. (5).)

Varying surface sensitivity for lower electron takeoff angles

Simplest interpretation:

Average emission depth = $\Lambda_{inelastic}\sin\theta_{takeoff}$

How valid?

$E_{kin} \approx$ 500-1000 eV

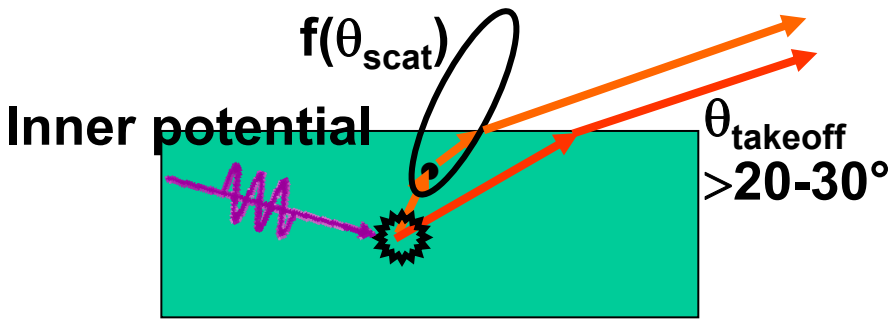

E.g.: A. Jablonski and C. J. Powell,
J. Vac. Sci. Tech. A 21, 274 (2003):
→ Mean Emission Depth (MED)
more relevant than $\Lambda_{inelastic}$

Varying surface sensitivity for lower electron takeoff angles

Simplest interpretation:

Average emission depth = $\Lambda_{inelastic}\sin\theta_{takeoff}$

How valid?

$E_{kin} \approx$ 500-1000 eV

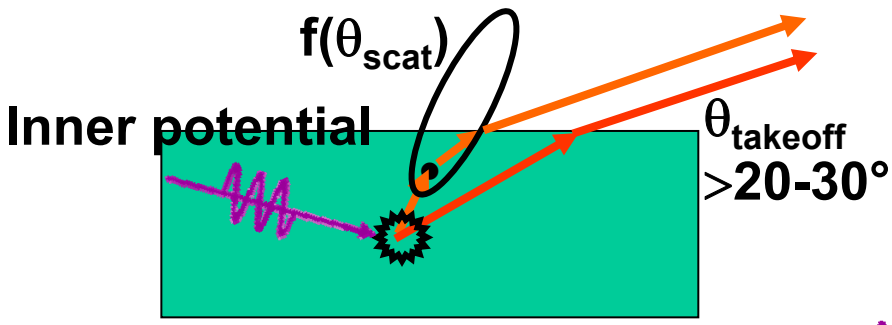

E.g.: A. Jablonski and C. J. Powell, J. Vac. Sci. Tech. A 21, 274 (2003):
→ Mean Emission Depth (MED) more relevant than $\Lambda_{inelastic}$

$E_{kin} \approx$ 10,000 eV

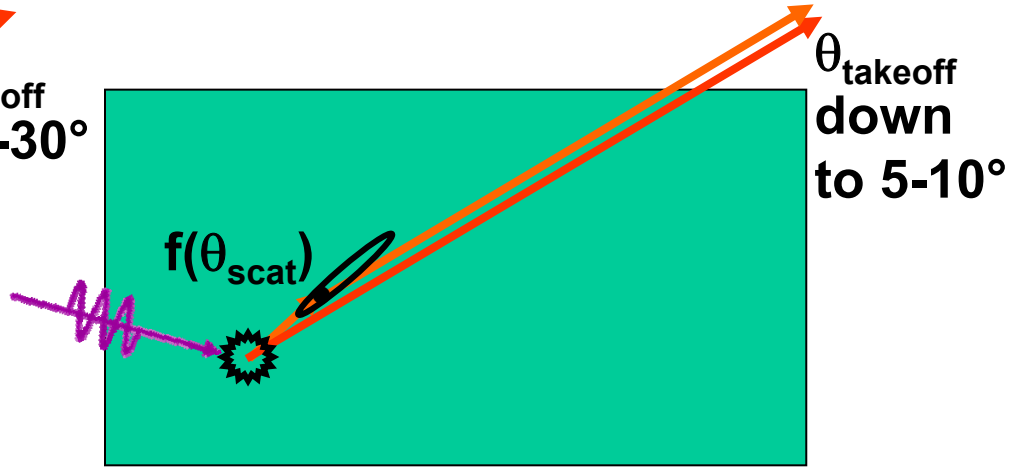

Simpler analysis

Cleaner bulk & surface distinction

C. J. Powell, W. Werner et al., priv. comm.;
C.S.F., Nucl. Inst. & Meth. A 547, 24 (2005)

Variable takeoff-angle Si 1s photoelectron spectra from NiGe(12-nm)/SiO_2(12-nm)/Si(100)

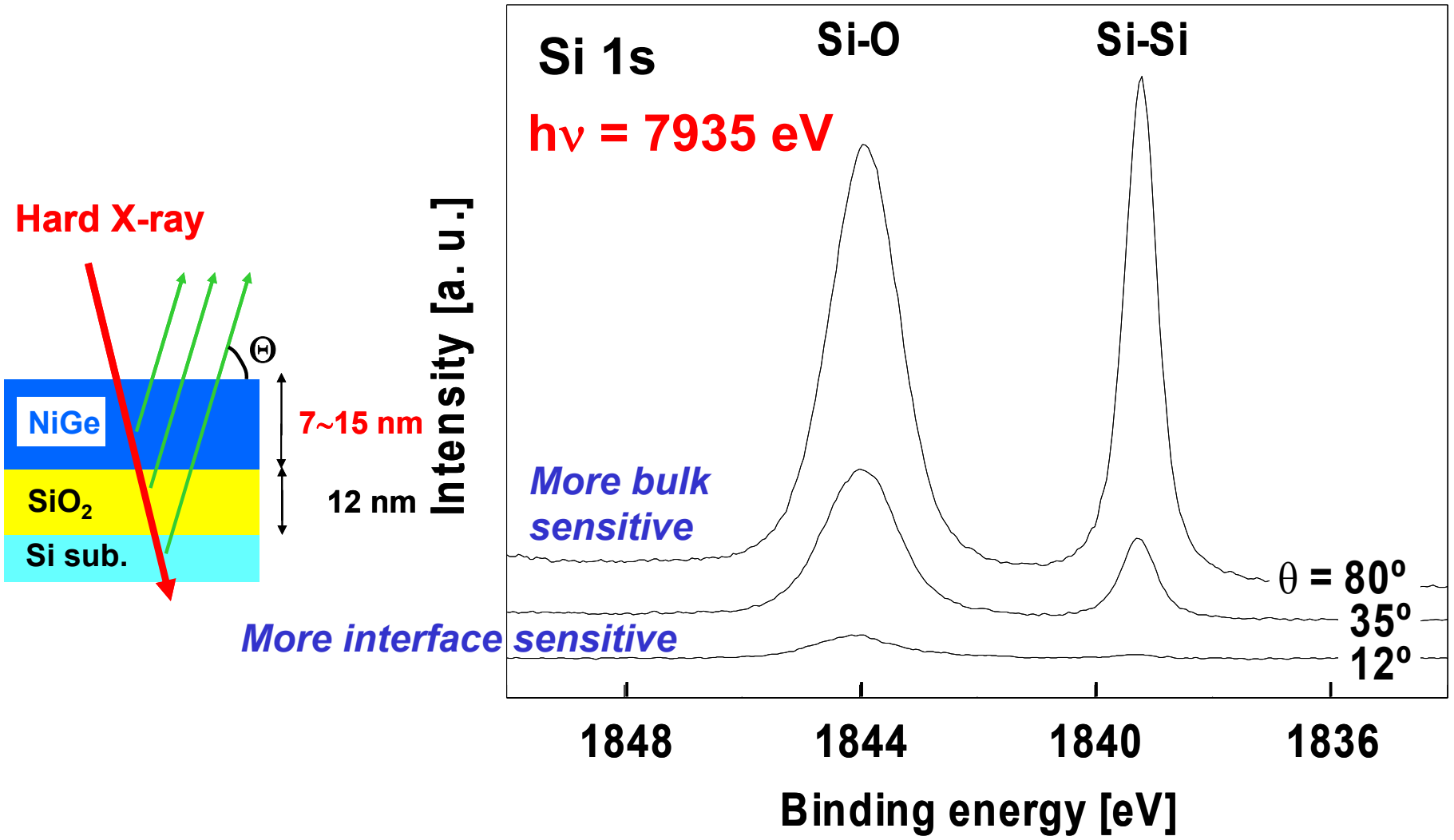

T. Hattori et al., Int. J. High Speed Electronics 16 (2006) 353
SPring8-Japan

Outline

Surface, interface, and nanoscience—short introduction

Some surface concepts and techniques→photoemission

Synchrotron radiation: experimental aspects

Electronic structure—a brief review

The basic synchrotron radiation techniques
+Instrumentation for PS and XES

Core-level photoemission:
photoelectron diffraction

Valence-level photoemission

Microscopy with photoemission

Some basic measurements:

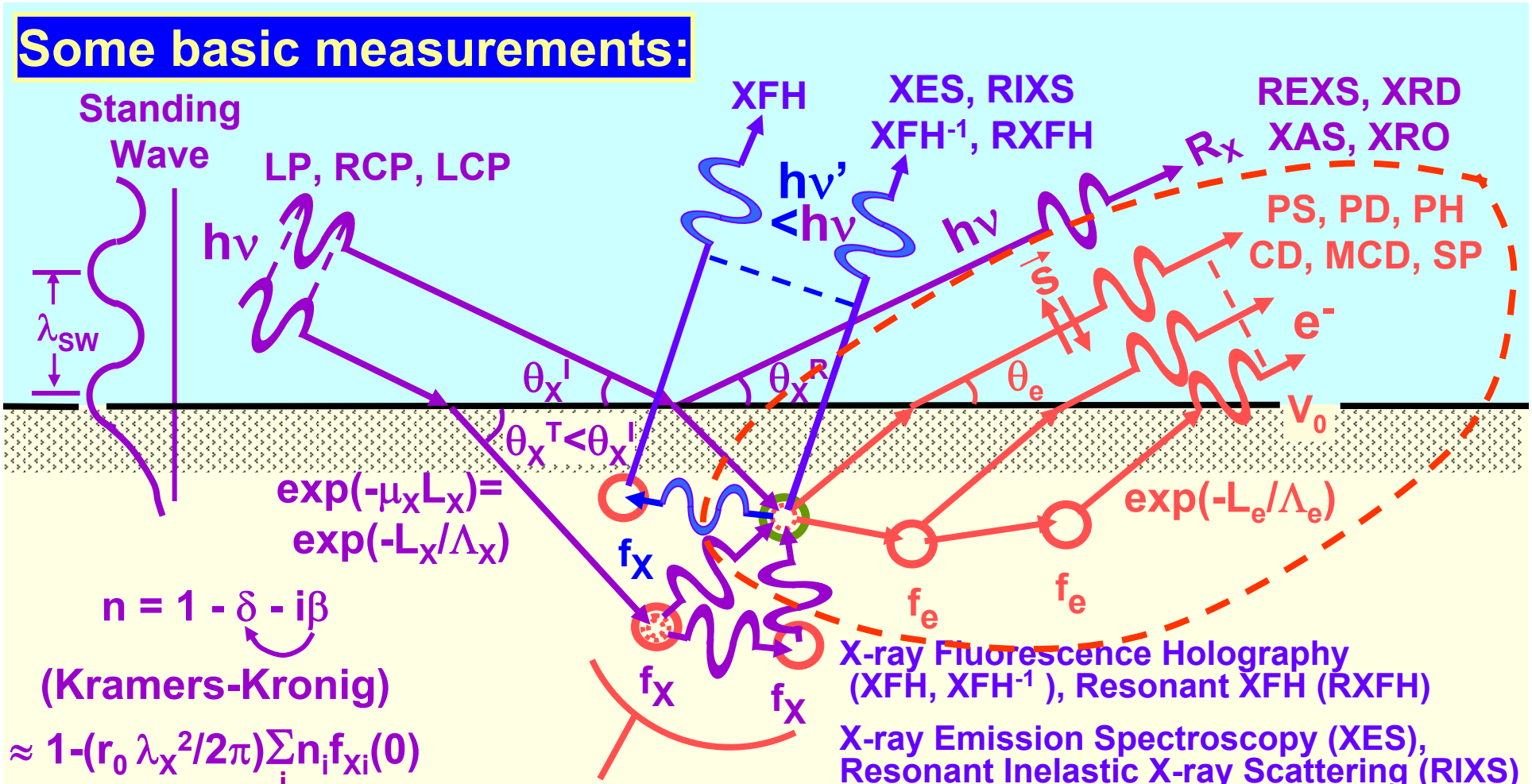

$n = 1 - \delta - i\beta$

(Kramers-Kronig)

$\approx 1-(r_0 \lambda_x^2/2\pi)\sum_i n_i f_{xi}(0)$

$\mu_x = 4\pi\beta/\lambda_x$

$\theta_x^R = \theta_x^I$

$\lambda_{SW} = \lambda_x/(2\sin\theta_x^I)$

$\theta_{CRIT}^I = (2\delta)^{1/2}$

X-ray Fluorescence Holography (XFH, XFH^{-1}), Resonant XFH (RXFH)

X-ray Emission Spectroscopy (XES), Resonant Inelastic X-ray Scattering (RIXS)

Resonant Elastic X-ray Scattering (REXS)

X-Ray Diffraction (XRD)

X-ray Absorption Spectroscopy (XAS)

X-Ray Optical measurements (XRO)

Photoelectron Spectroscopy (PS), Diffraction (PD), Holography (PH) + Circular Dichroism (CD), Magnetic CD (MCD), Spin Polarization (SP)

PHOTOELECTRON INTENSITIES—THE 3-STEP MODEL

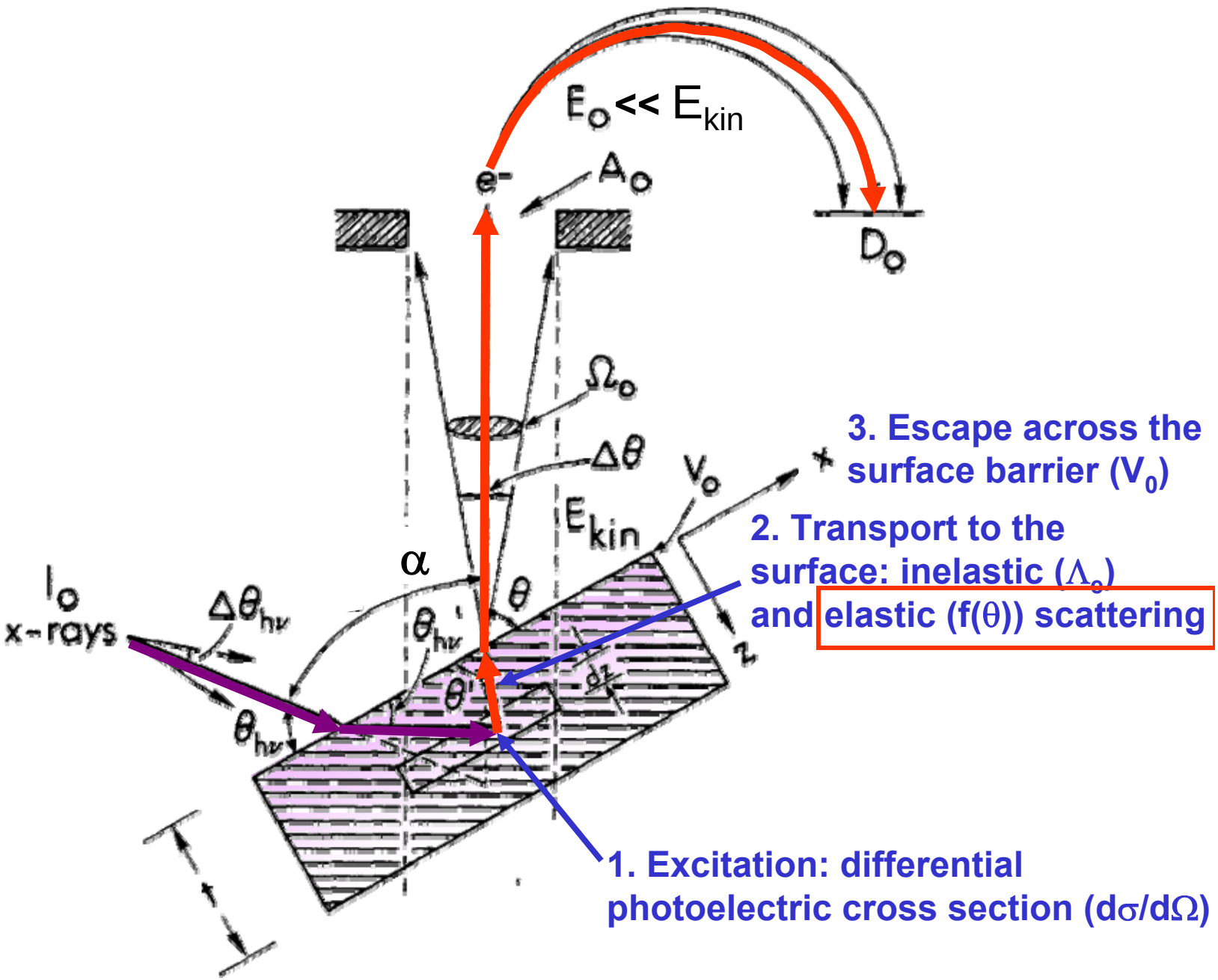

3. Escape across the surface barrier (V_0)

2. Transport to the surface: inelastic (Λ_e) and elastic ($f(\theta)$) scattering

1. Excitation: differential photoelectric cross section ($d\sigma/d\Omega$)

PHOTOELECTRON DIFFRACTION AND HOLOGRAPHY

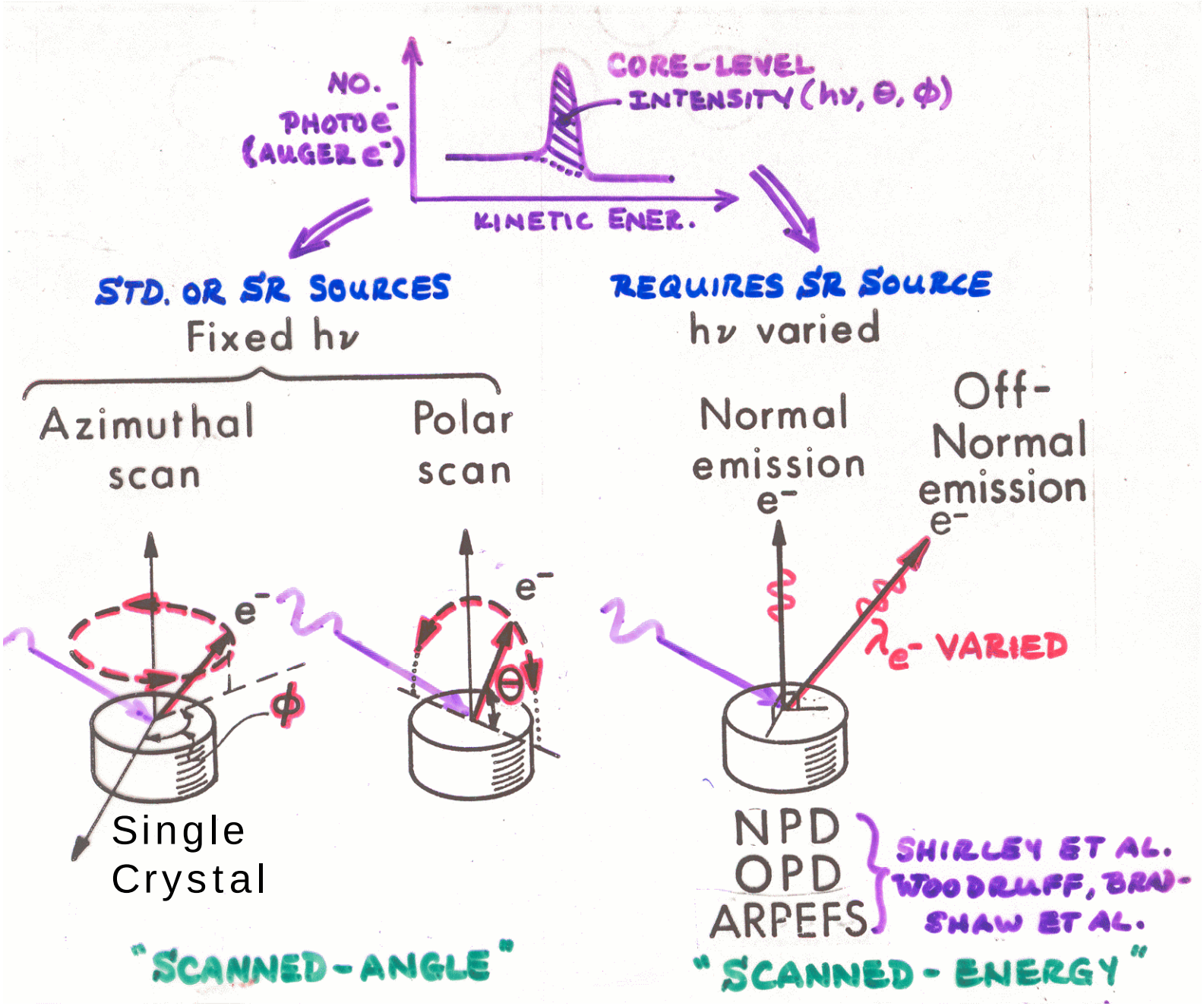

EFFECTS OF ELASTIC SCATTERING ON ANGULAR DISTRIBUTIONS: SINGLE-CRYSTAL SAMPLE→→ *PHOTOELECTRON DIFFRACTION And PHOTOELECTRON HOLOGRAPHY*

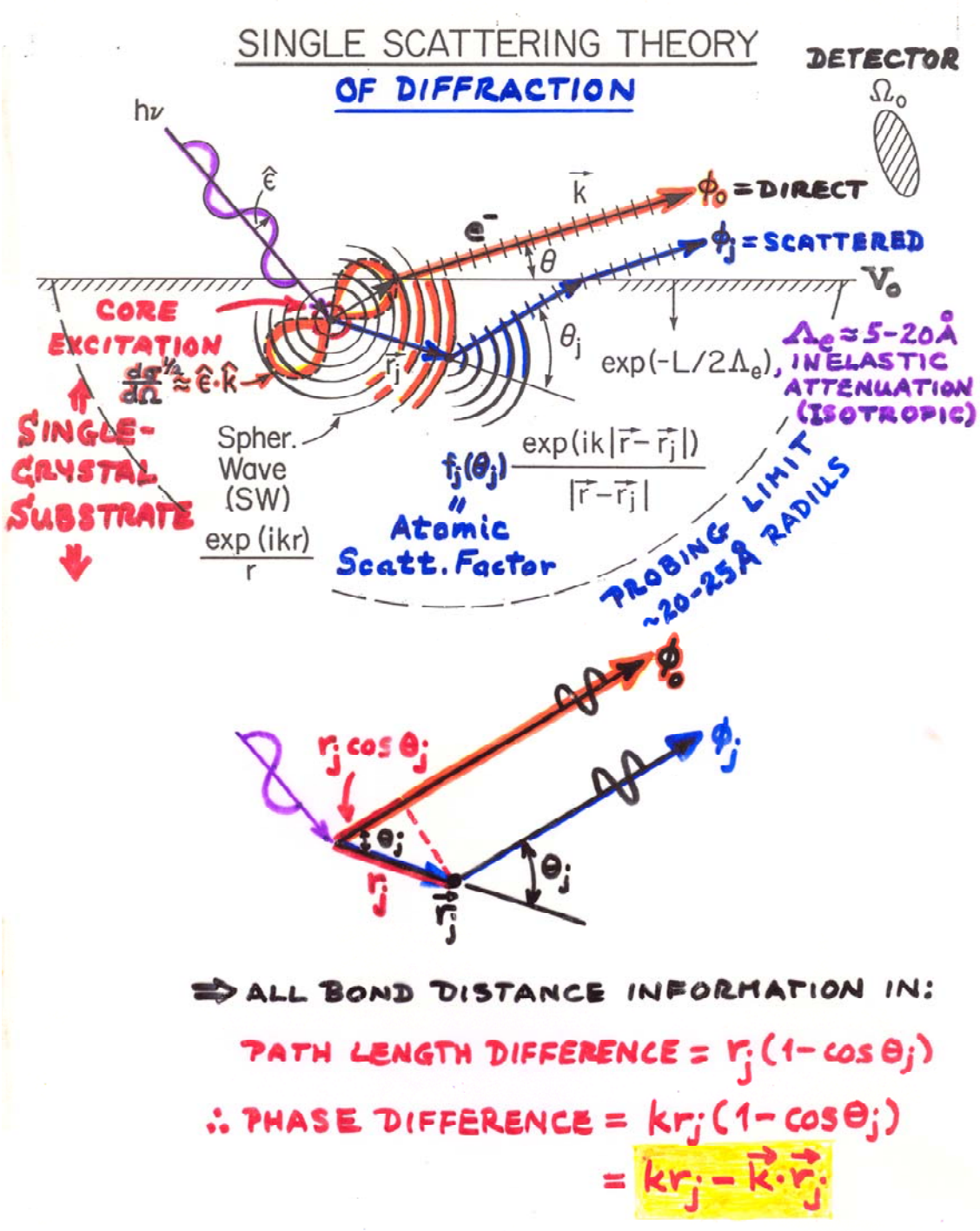

"Study of Surface Structures…"
Figure 3

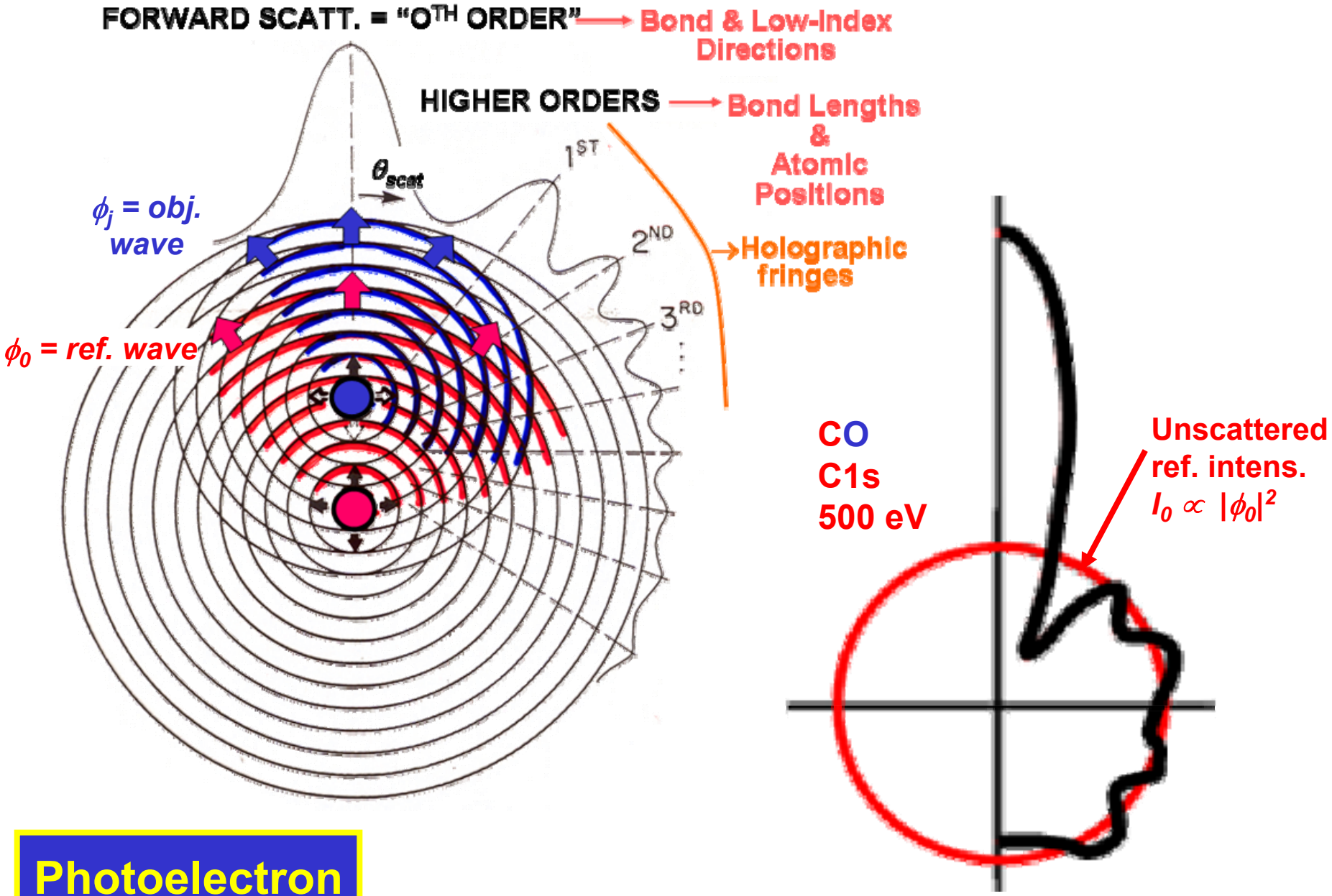

Photoelectron Diffraction

EDAC program: Javier Garcia de Abajo
http://maxwell.optica.csic.es/software/edac/index.html

SCANNED-ANGLE PHOTOELECTRON DIFFRACTION

Example:

Ge(111) - Ge3d Photoelectron Hologram

E_{kin} = 1458 eV

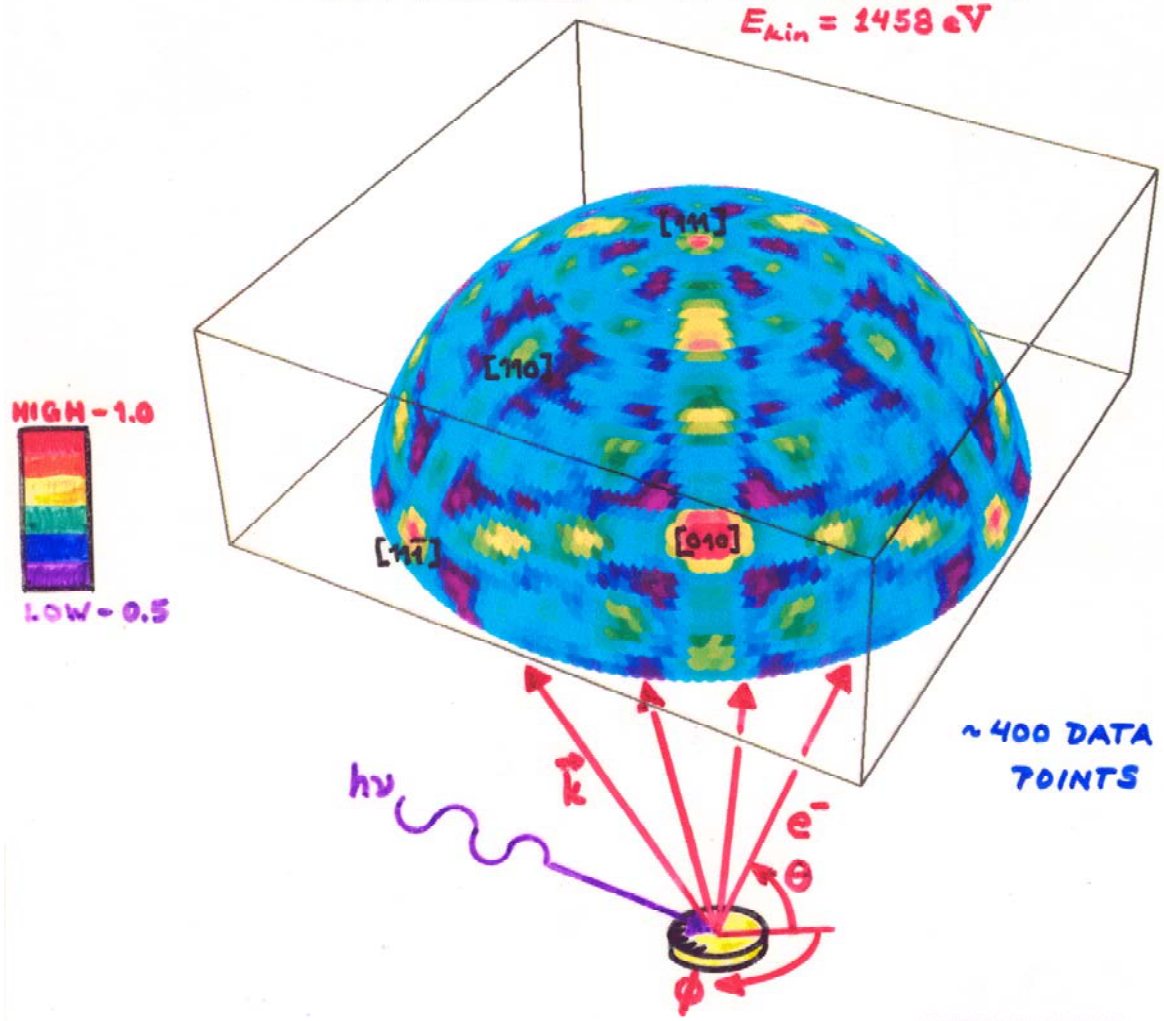

~400 DATA POINTS

TRAN ET AL., SURF. SCI. 281, 270('93) + BUDGE, YNZUNZA

SCANNED-ENERGY PHOTOELECTRON DIFF.

$(\sqrt{3}\times\sqrt{3})$ AL ON Si(111)

* 41 diffraction curves χ taken from Al 2p
* $\theta = 0 \sim 70°$, $\varphi = 0 \sim 60°$

} ~1100 DATA POINTS

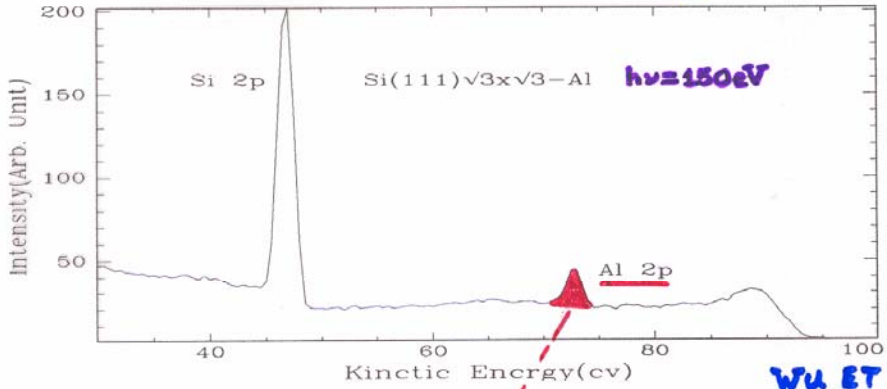

WU ET AL., P.R.L. 71, 261('93) P.R.B 51, 14549('95)

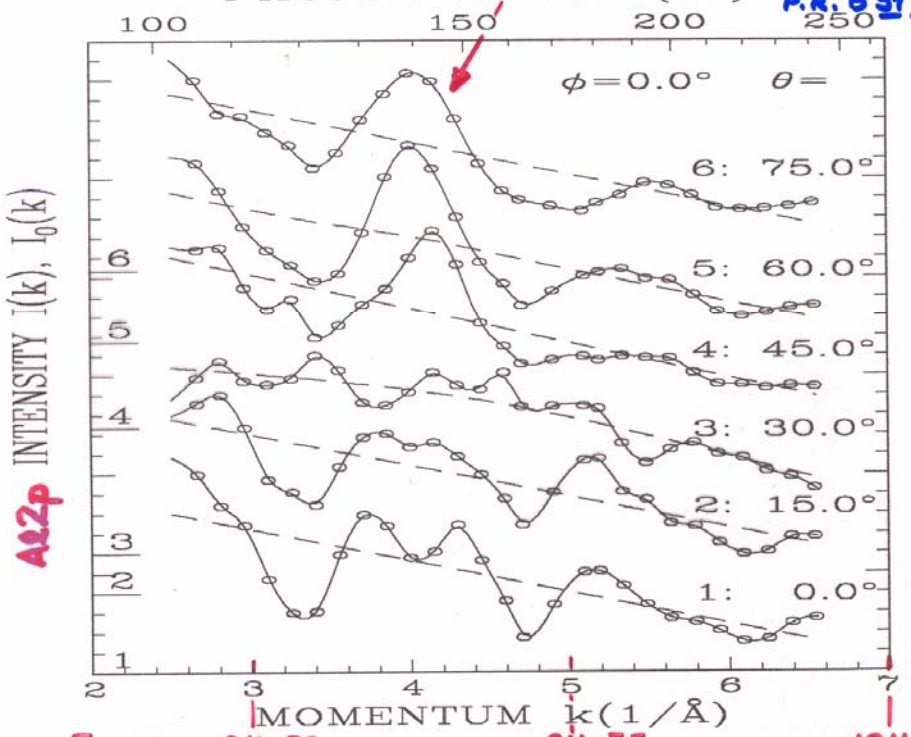

E_{kin}= 34 eV 94 eV 184 eV

Photoelectron diffraction: Simple single-scattering theory for s-subshell emission

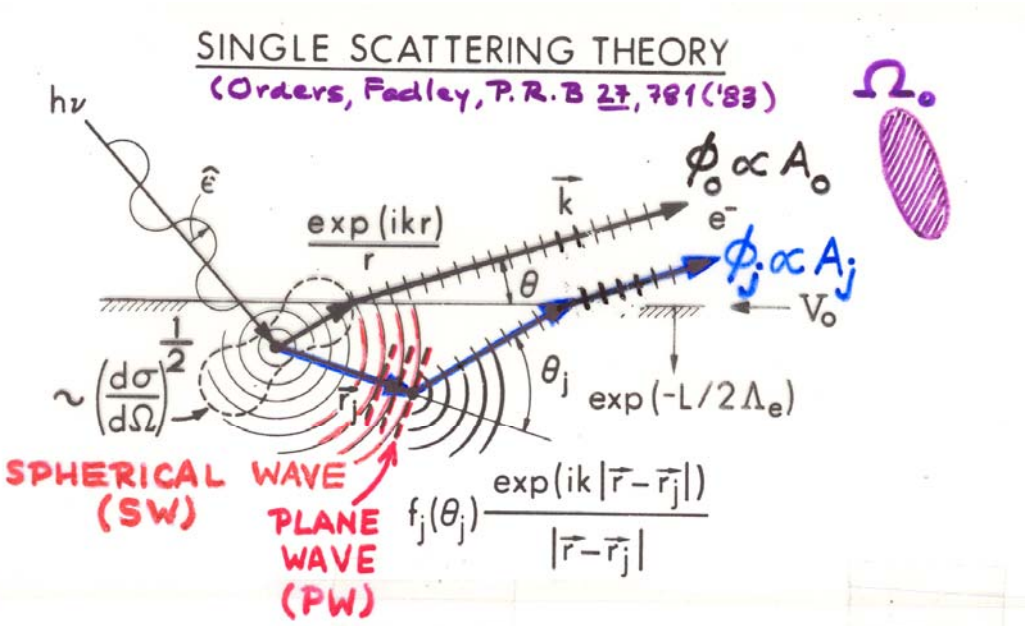

$$\chi(E \text{ or } \vec{k}) \propto \sum_{j\,(\text{CLUSTER})} \frac{F_j(k)}{F_0} \cos\left[kr_j(1-\cos\theta_j) + \Psi_j(\theta_j,k) \right]$$

Ω_0

ELASTIC e⁻–ATOM SCATTERING

PATH LENGTH DIFFERENCE (P.L.D.)

SCATTERING PHASE SHIFT

INELASTIC e⁻–e⁻ SCATTERING

DEBYE-WALLER

$$F_j(k) = (\hat{\varepsilon}\cdot\hat{r}_j)\frac{|f_j(\theta_j,k)|}{r_j} W_j(\theta_j,k) \exp(-L_j/2\Lambda_e)$$

= amplitude of scattered wave

$$F_0 = (\hat{\varepsilon}\cdot\hat{k}) \exp(-L_0/2\Lambda_e)$$

= amplitude of direct wave

"Study of Surface Structures…" Figure 3

FROM SINGLE-SCATTERING THEORY:

(E.G., P.R.B 22, 6085 ('80); P.R. B 27, 781 ('83))

$$I(\vec{k}) \propto \left|\phi_0 + \sum_j \phi_j\right|^2, \quad \sum_j \text{ ON FINITE CLUSTER},$$

$$\propto |\phi_0|^2 + \sum_j (\phi_0^* \phi_j + \phi_0 \phi_j^*) + \sum_j \sum_{j'} \phi_{j'}^* \phi_j,$$

IF $\phi_j \phi_{j'}^*$ SMALL W.R.T $\phi_0^* \phi_j + \phi_0 \phi_j^*$, A NECESSARY CONDITION FOR SIMPLE HOLOGRAPHY:

$$I(\vec{k}) \propto \underbrace{F_0^2}_{\| \; I_0} + 2F_0 \sum_j |F_j(\theta_j)| \cos\left[\underbrace{kr_j(1-\cos\theta_j)}_{\text{PATH LENGTH DIFFERENCE}} + \underbrace{\psi_j(\theta_j, k)}_{\text{SCATTERING PHASE}}\right]$$

$$\boxed{\chi(\vec{k}) = \frac{I(\vec{k}) - I_0}{I_0^{1/2}} \propto \left\{\sum_j |F_j(\theta_j)| \cos\left[kr_j(1-\cos\theta_j) + \psi_j(\theta_j, k)\right]\right\}}$$

WITH: $F_0 = (\hat{\varepsilon}\cdot\hat{k}) \exp(-L_0/2\Lambda_e)$

$= \text{amplitude of direct wave} = I_0^{1/2}$

$$|F_j(\theta_j)| = (\hat{\varepsilon}\cdot\hat{r}_j)\frac{|f_j(\theta_j)|}{r_j} W_j(\theta_j) \exp(-L_j/2\Lambda_e)$$

$= \text{amplitude of scattered wave}$

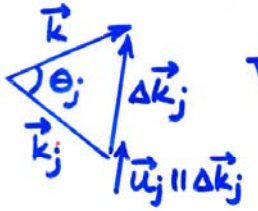

$$W_j = \exp(-\Delta k_j^2 \overline{u_j^2})$$

$$= \exp(-2k^2(1-\cos\theta_j)\overline{u_j^2})$$

LIKE EXAFS/SEXAFS, BUT THERE:

- ADD CENTRAL ATOM PHASE SHIFT δ_1
- $\psi_j \Rightarrow \pi$ FOR ALL SCATTERERS
- $\cos \Rightarrow \sin$ IN ANGLE INTEGRATION
- $\hat{\varepsilon}\cdot\hat{r}_j/r_j \Rightarrow \hat{\varepsilon}\cdot\hat{r}_j/r_j^2$ IN OUT/BACK PATHS

CALCULATION OF e^--ATOM SCATTERING FACTORS:

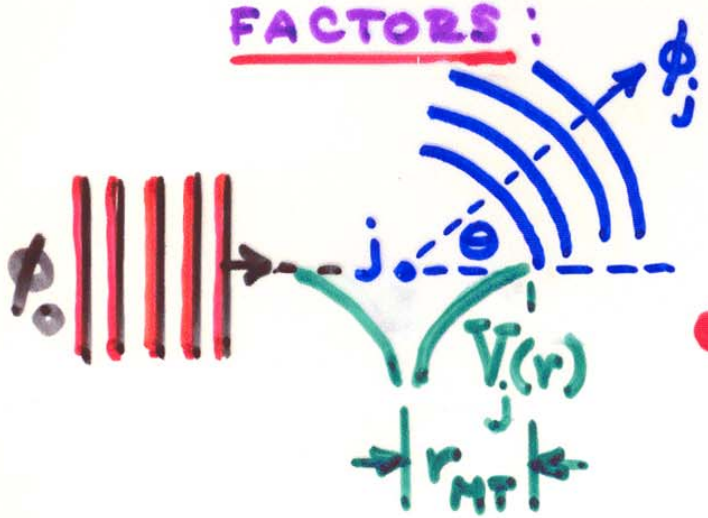

PLANE-WAVE SCATTERING:
PARTIAL-WAVE METHOD†

PHASE SHIFT

$$f_j^{PW}(\theta) = \frac{1}{k}\sum_{l=0}^{l_{max}} (2l+1)\, e^{i\delta_l} \sin\delta_l\, P_l(\cos\theta)$$

$$l_{max} \approx k r_{MT}$$

† ANY TEXTBOOK ON SCATTERING

ENERGY DEPENDENCE OF ELECTRON ELASTIC SCATTERING

$f(\theta) = |f(\theta)| e^{i\psi(\theta)}$

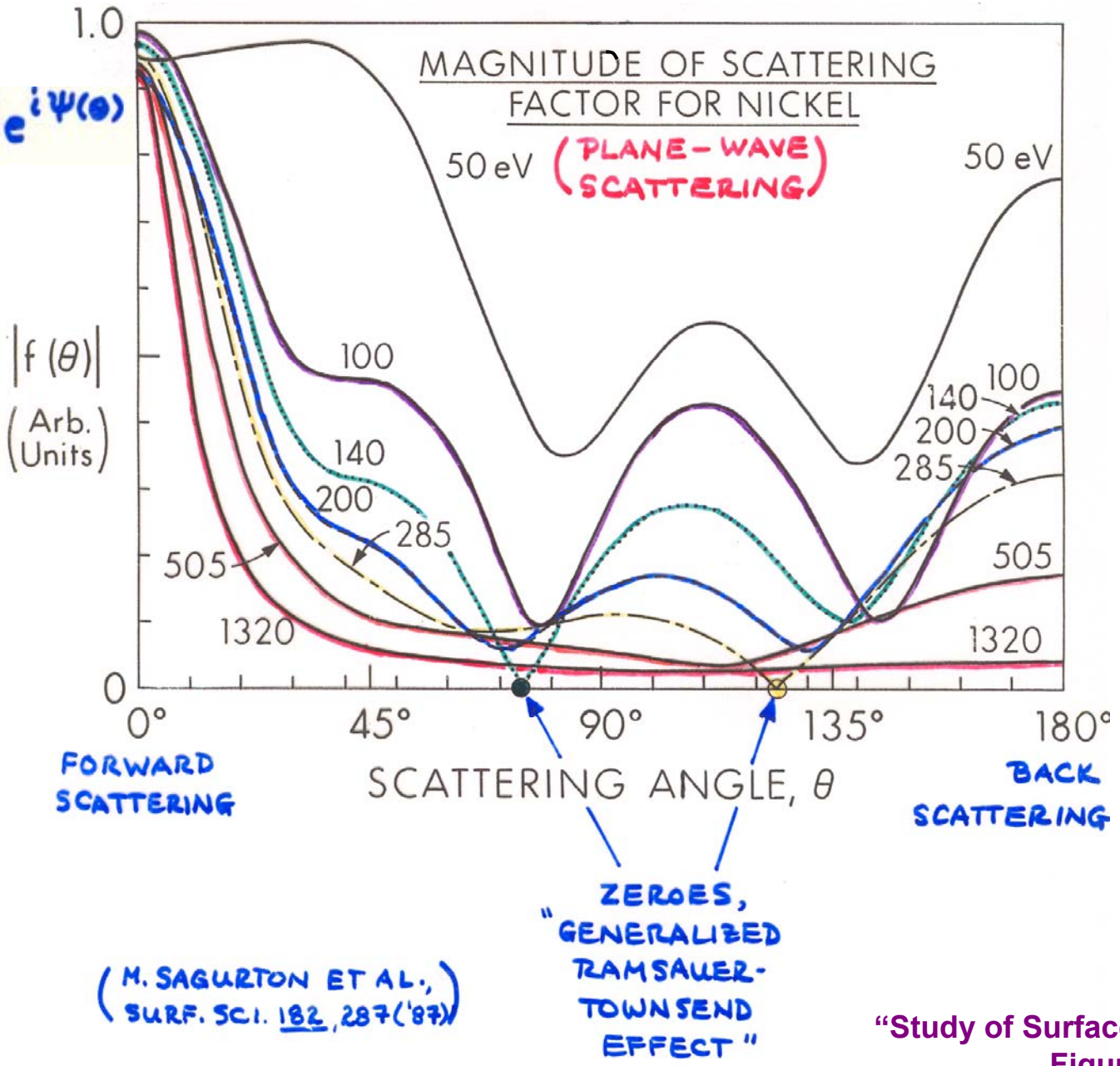

"Study of Surface Structures…"
Figure 2

ENERGY DEPENDENCE OF ELECTRON ELASTIC SCATTERING

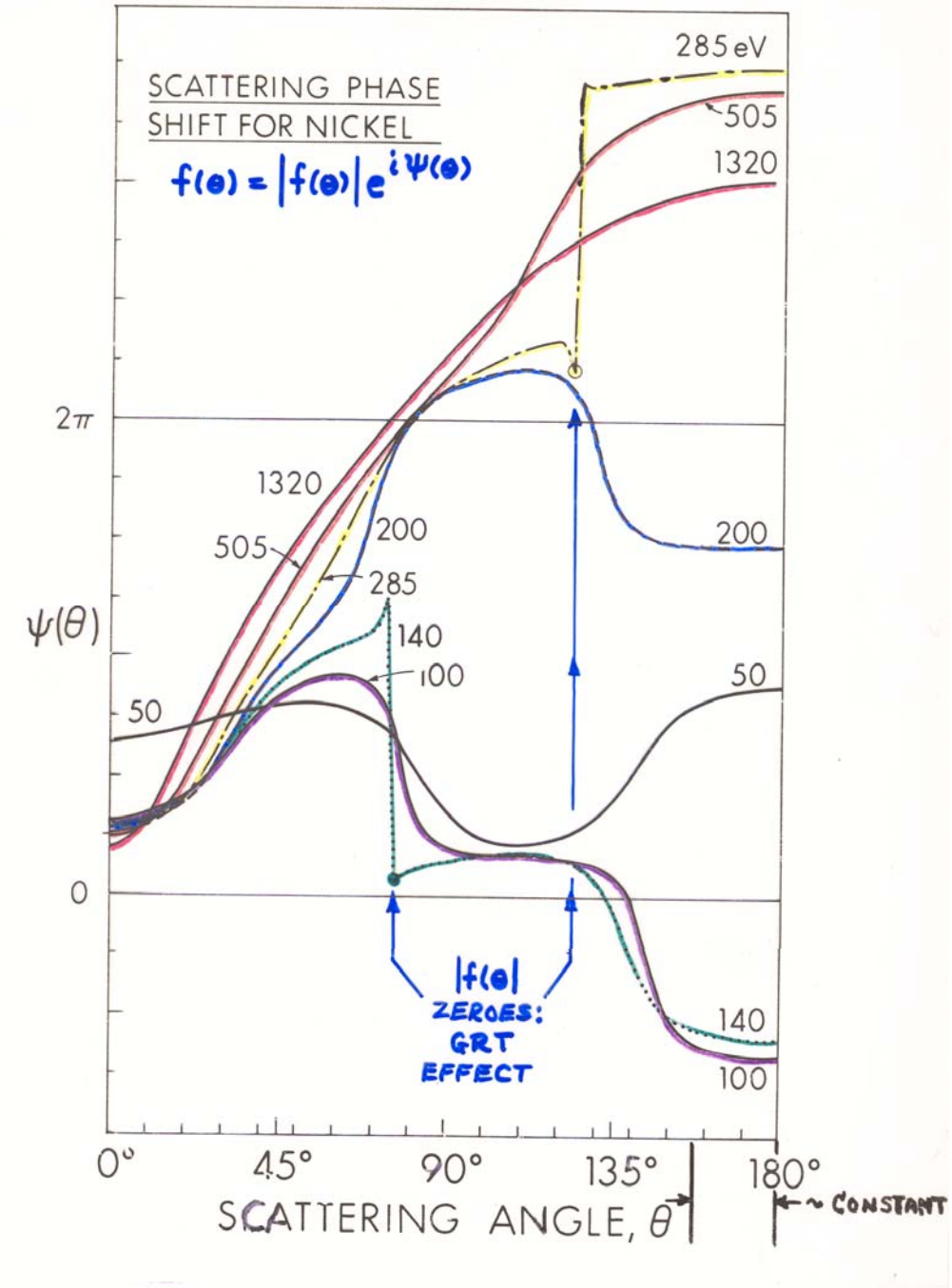

CALCULATION OF e^--ATOM SCATTERING FACTORS:

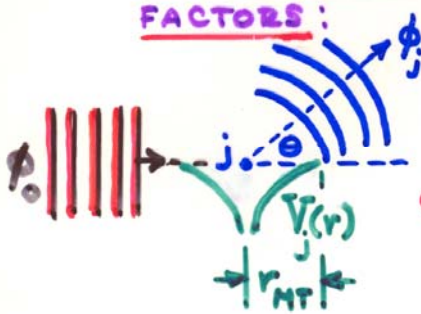

PLANE-WAVE SCATTERING: PARTIAL-WAVE METHOD†

$$f_j^{PW}(\theta) = \frac{1}{k}\sum_{\ell=0}^{\ell_{max}}(2\ell+1)e^{i\delta_\ell}\sin\delta_\ell P_\ell(\cos\theta)$$

(δ_ℓ: PHASE SHIFT)

$$\ell_{max} \approx kr_{MT}$$

† ANY TEXTBOOK ON SCATTERING

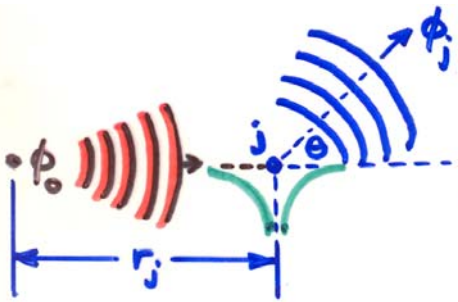

SPHERICAL-WAVE SCATTERING: REHR-ALBERS METHOD*

$$f_j^{SW}(\theta) = \frac{1}{k}\sum_{\ell=0}^{\ell_{max}}\left\{(2\ell+1)e^{i\delta_\ell}\sin\delta_\ell P_\ell(\cos\theta)\cdot \frac{[(\ell+1)C_{\ell+1}(kr_j)+\ell C_{\ell-1}(kr_j)]}{2\ell+1}\right\}$$

WITH:

$$C_\ell(kr_j) = \left[1+\frac{\ell(\ell+1)}{2(kr_j)^2}\right]e^{\frac{i\ell(\ell+1)}{2kr_j}}$$

* HUSTRE DE LEON ET AL., PHYS. REV. B 39, 5632 ('89)

- AND MORE ACCURATE MATRIX METHODS IN REHR, ALBERS, PHYS. REV. B41, 8139 (1990) + FRIEDMAN, FADLEY, J. ELECT. SPECT. 51, 689 (1990)

PW vs. SW scattering

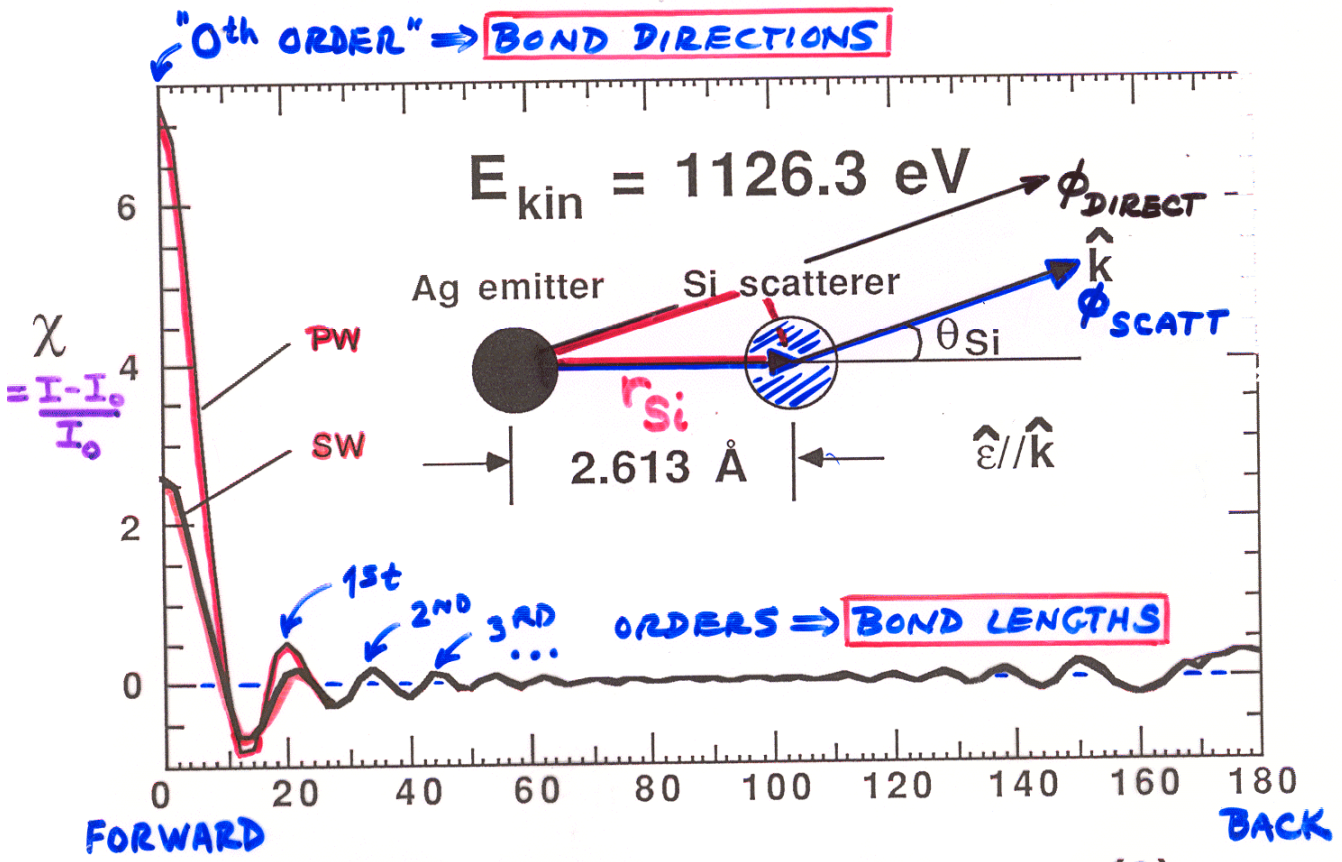

PATH LENGTH DIFFERENCE =

$$r_{Si}(1-\cos\theta_{Si})$$

ORDERS:

SCATTERING PHASE SHIFT

$$2\pi n = [k r_{Si}(1-\cos\theta_{Si}) + \psi_{Si}(\theta)]$$

Vibrational effects on diffraction

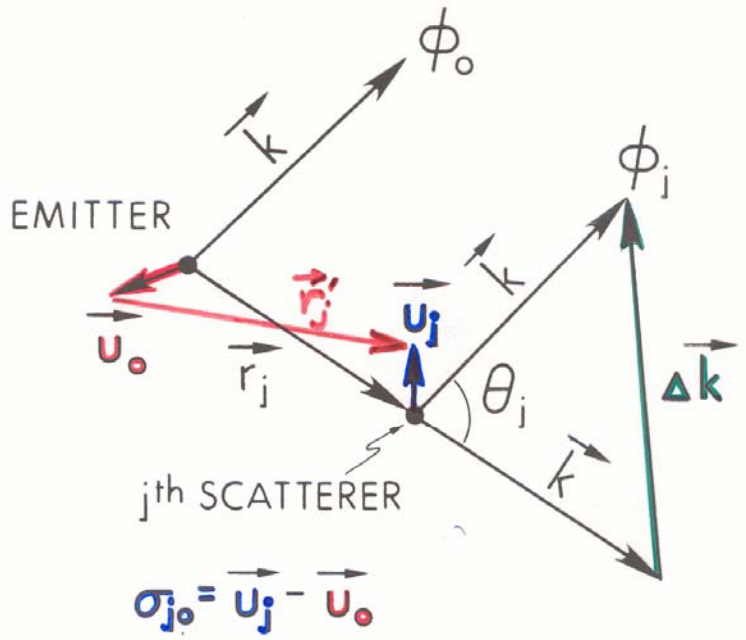

- DW FACTOR $= e^{-\frac{1}{2}\overline{(\Delta\vec{k}\cdot\vec{\sigma}_{jo})^2}} = e^{-\frac{1}{2}\Delta k^2\overline{\sigma_{jo,II}^2}}$
- $\vec{U}_j, \vec{U}_o$ UNCORRELATED:

  $DW = e^{-\frac{1}{2}\overline{(\Delta\vec{k}\cdot\vec{u}_j)^2}}\, e^{-\frac{1}{2}\overline{(\Delta\vec{k}\cdot\vec{u}_o)^2}}$
- $\vec{U}_j \approx \vec{U}_o$ IN DISTRIBUTION:

  $DW = e^{-\overline{(\Delta\vec{k}\cdot\vec{u}_j)^2}}$
- $\vec{U}_j$ ISOTROPIC:

  $DW = e^{-\Delta k^2\overline{u_j^2}} = e^{-2k^2(1-\cos\theta_j)\overline{u_j^2}}$ ← USUAL LEVEL

DECREASING ACCURACY

+ CORRELATED?

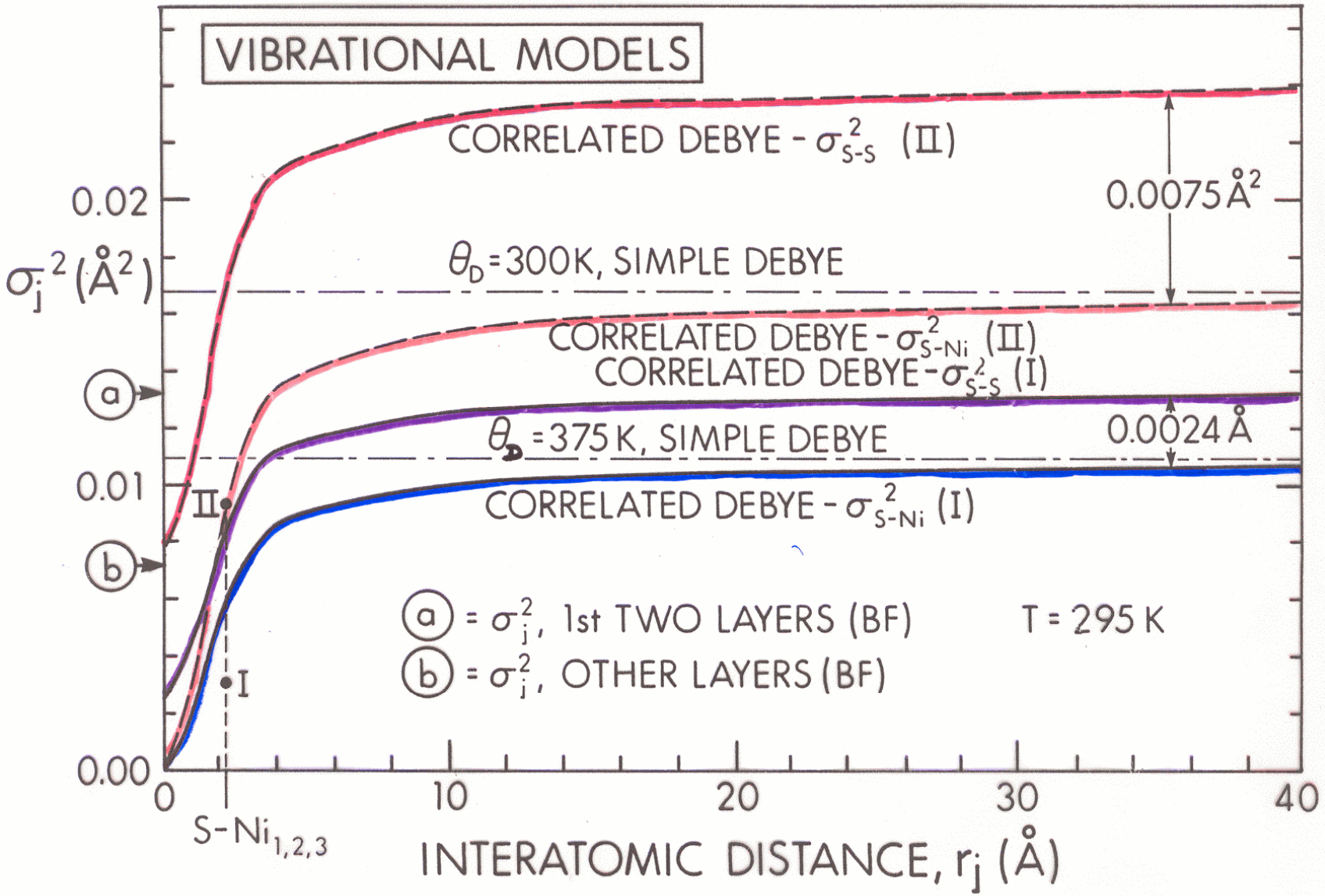

[SAGURTON, BULLOCK, FADLEY, SURF. SCI. 182, 287 (1987)]

Table 1 Debye temperature and thermal conductivity[a]

Li	Be											B	C	N	O	F	Ne
344	1440												2230				75
0.85	2.00											0.27	1.29				
Na	Mg											Al	Si	P	S	Cl	Ar
158	400	Low temperature limit of θ, in Kelvin										428	645				92
1.41	1.56	Thermal conductivity at 300 K, in W $cm^{-1}K^{-1}$										2.37	1.48				
K	Ca	Sc	Ti	V	Cr	Mn	Fe	Co	Ni	Cu	Zn	Ga	Ge	As	Se	Br	Kr
91	230	360.	420	380	630	410	470	445	450	343	327	320	374	282	90		72
1.02		0.16	0.22	0.31	0.94	0.08	0.80	1.00	0.91	4.01	1.16	0.41	0.60	0.50	0.02		
Rb	Sr	Y	Zr	Nb	Mo	Tc	Ru	Rh	Pd	Ag	Cd	In	Sn w	Sb	Te	I	Xe
56	147	280	291	275	450		600	480	274	225	209	108	200	211	153		64
0.58		0.17	0.23	0.54	1.38	0.51	1.17	1.50	0.72	4.29	0.97	0.82	0.67	0.24	0.02		
Cs	Ba	La β	Hf	Ta	W	Re	Os	Ir	Pt	Au	Hg	Tl	Pb	Bi	Po	At	Rn
38	110	142	252	240	400	430	500	420	240	165	71.9	78.5	105	119			
0.36		0.14	0.23	0.58	1.74	0.48	0.88	1.47	0.72	3.17		0.46	0.35	0.08			
Fr	Ra	Ac															

Ce	Pr	Nd	Pm	Sm	Eu	Gd	Tb	Dy	Ho	Er	Tm	Yb	Lu
						200		210				120	210
0.11	0.12	0.16		0.13		0.11	0.11	0.11	0.16	0.14	0.17	0.35	0.16

Th	Pa	U	Np	Pu	Am	Cm	Bk	Cf	Es	Fm	Md	No	Lr
163		207											
0.54		0.28	0.06	0.07									

[a] Most of the θ values were supplied by N. Pearlman; references are given the *A.I.P. Handbook*, 3rd ed; the thermal conductivity values are from R. W. Powell and Y. S. Touloukian, Science **181**, 999 (1973).

Case study: Determining the orientation of an adsorbed molecule from photoelectron diffraction at about 1 keV energy

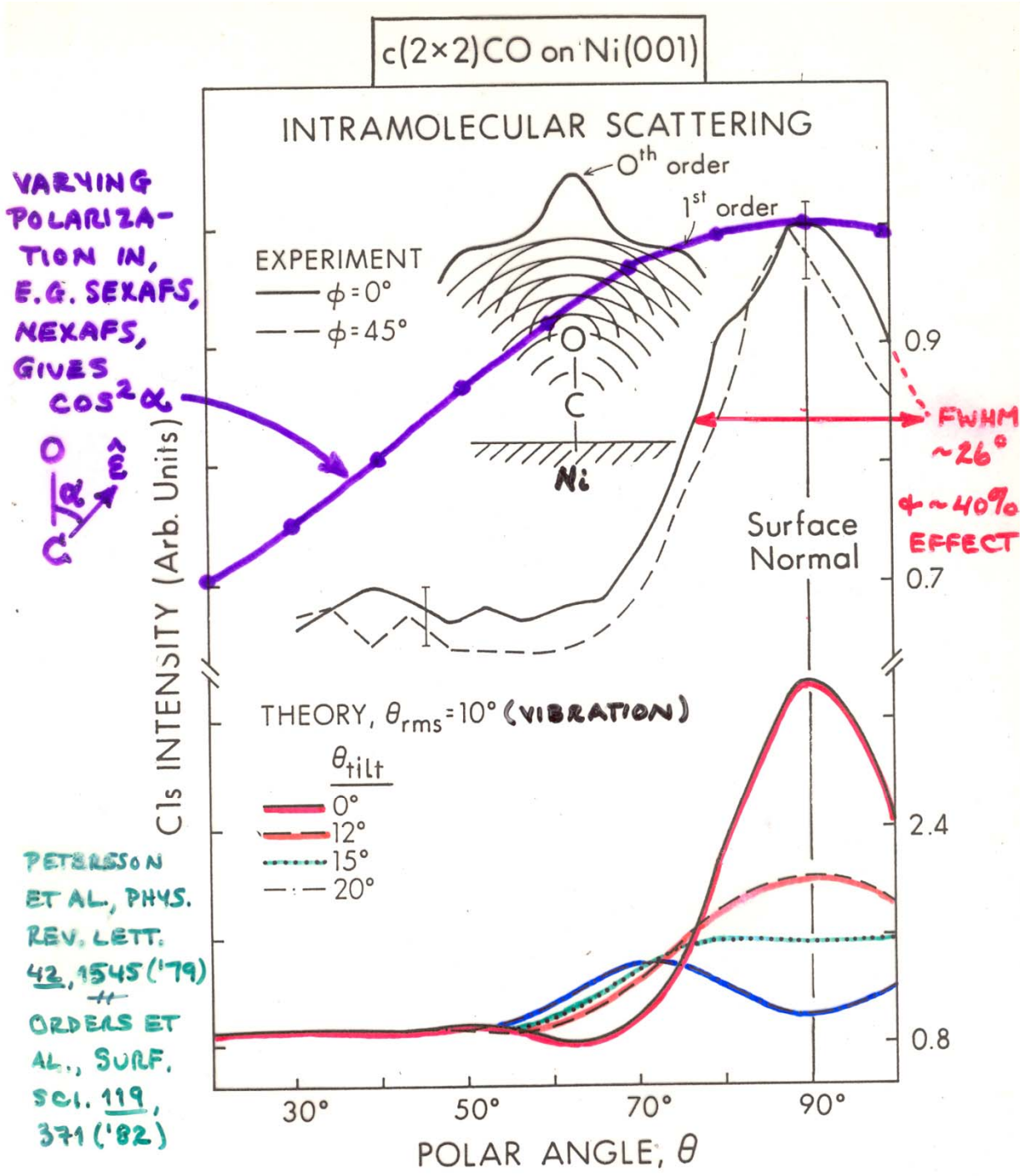

"Study of Surface Structures…"
Figure 8

TEMPERATURE-DEPENDENT ADSORBATE ORIENTATION

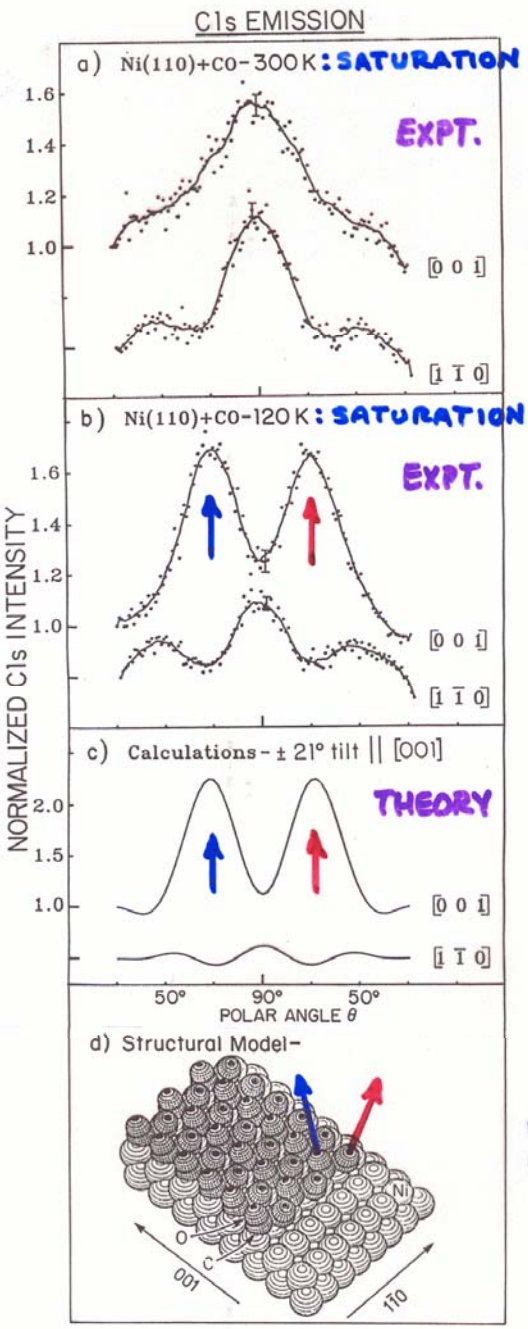

WESNER, BONZEL
COENEN, P.R.L.
60, 1045 ('88)

"Study of Surface Structures…"
Figure 12

ORIENTATION OF A HIGHLY TILTED MOLEC. ON SURFACE

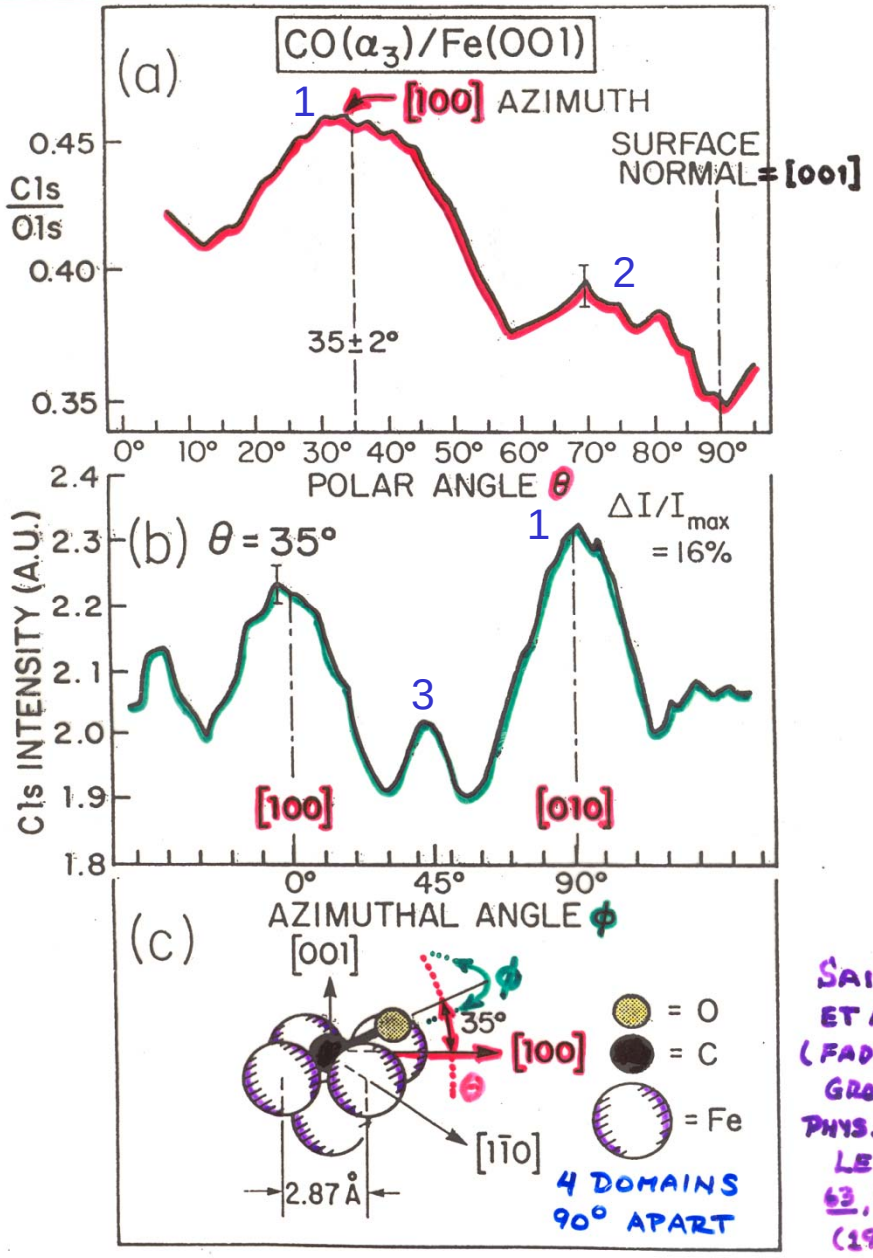

SAIKI ET AL. (FADLEY GROUP) PHYS. REV. LETT. 63, 283 (1984)

"Study of Surface Structures…"
Figure 9

CALCULATED E- INTENSITY
$CO(\alpha_3)/Fe(001)$

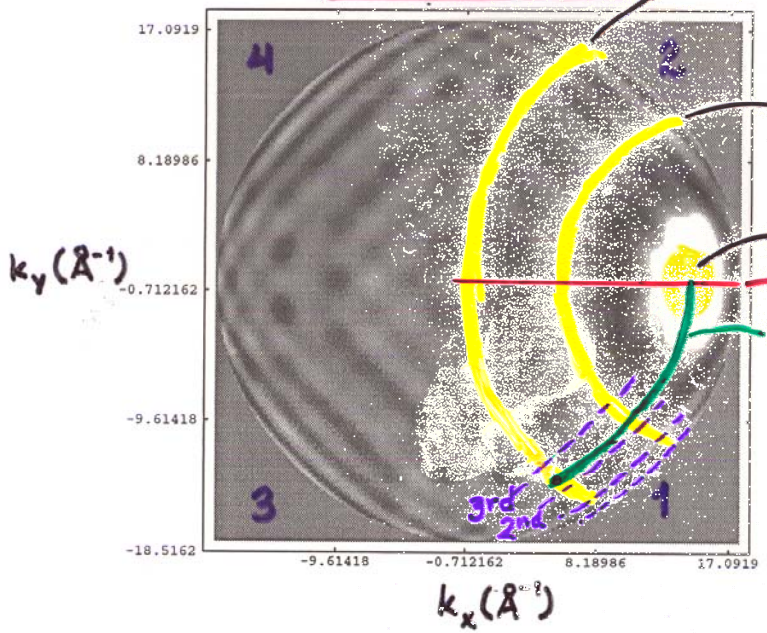

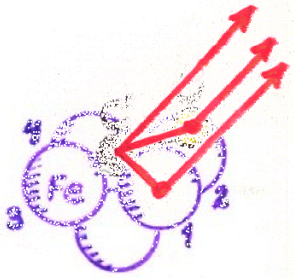

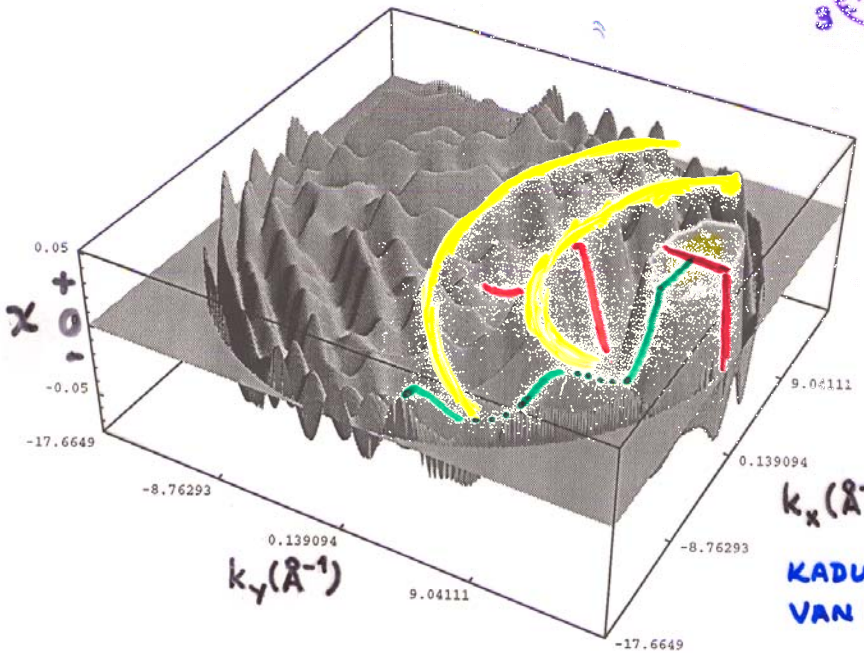

KADUWELA, BUDGE, VAN HOVE, FADLEY

Online calculation of photoelectron diffraction patterns:

EDAC output for CO/Fe(001)

Click on the figure to download data.

http://csic.sw.ehu.es/jga/software/edac/a.html

7 atoms:

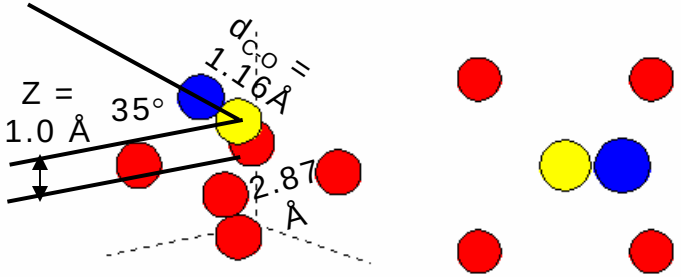

Left: representation of the cluster rocking around a line parallel to the *z* direction and passing by the **emitter (yellow atom)**. The dashed lines stand for the *xyz* axes. **Right:** top view of the cluster, where the *x*/*y* direction (not plotted) runs along the horizontal/vertical screen direction. Different atomic species have been assigned the colors **O**, **Fe**.

Oxygen 1st order diff. ring

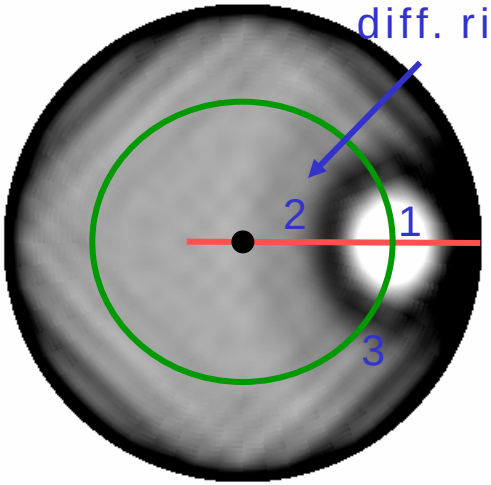

Polar scan of photoemission intensity (logarithmic scale). White/black regions correspond to high/low intensity. The orientation is the same as in the top-view of the cluster. The distance to the center of the figure is proportional to the polar angle θ. The polar angle range is (0.0, 89.0) (in degrees).

Parameters used in the calculation:

N=7 atoms
Iteration order=4
l_{max}=25
V_0=10.5 eV
Photoelecton energy=1202 eV
p-polarized light
z_0=1.435 Å
Recursion iteration method

X 4 domains rotated by 90°

Electron Diffraction in Atomic Clusters

for Core Level Photoelectron Diffraction Simulations

Created by F. Javier García de Abajo (CSIC and DIPC, San Sebastian, Spain)
in collaboration with M. A. Van Hove and C. S. Fadley (LBNL, Berkeley, and UCD, Davis, California)

This site allows performing on-line photoelectron diffraction calculations. Multiple scattering (MS) of the photoelectron is carried out for a cluster representing a solid or molecule. Select the corresponding parameters and click on the "Calculate" button below to perform the actual calculation and to produce a plot of the calculated data (a separate window pops out to display it). A numerical data table can be downloaded by clicking on the resulting plot. Click on the different parameter names in blue to see fuller explanations. Click on the "Preview Cluster" button to display the currently selected atomic cluster (but without performing a MS calculation) or the button "Download Cluster" to download the currently selected cluster. Notice that the scattering phase shifts and excitation radial matrix elements are calculated internally for each cluster configuration, so that the user does not have to provide them. Please, read the terms of use and the restrictions on input parameters before using this site for the first time.

Terms and conditions of use

Terms of use Restrictions on input parameters Password: ********

A password is only necessary for large computation times (click here for more details). Leave it blank otherwise.

Title (optional): CO/Fe(001)

Cluster definition

The cluster and the list of emitters are defined by a list of commands with the following format (click here or on the items of this list for further details):

atom symbol *x y z* layer symbol *x y z a b* α_1 α_2

surface symbol *x y z a* type emitter *x y z*

Fill in the text box with these commands according to the cluster specifications that you need. Some examples are provided by clicking here (you may cut and paste them to this page and modify them further).

```
atom O 0.95 0 1.66
atom C 0 0 1.0
surface Fe 1.435 1.435 0 2.87 bcc100
emitter 0 0 1.0
end
```

The cluster consists of a maximum of 7 atoms. (Warning: a finite number of atoms generally introduces symmetry breaking.)

The size of the cluster is determined by the distance d_{max} = 10 Å and the reference point x_0 = 0 Å, y_0 = 0 Å, z_0 = 0 Å.

See cluster shape for more details.

Plot cluster on output? (•) Yes ( ) No

Cluster shape: (•) Parabolic ( ) Spherical

Preview Cluster* Download Cluster*

Geometry of beam and analyzer

Incoming beam parameters (see figure)

Polar angle θ_i = 0 degrees

Azimuthal angle φ_i = 0 degrees

Polarization:
(•) p-polarization
( ) s-polarization
( ) RCP
( ) LCP

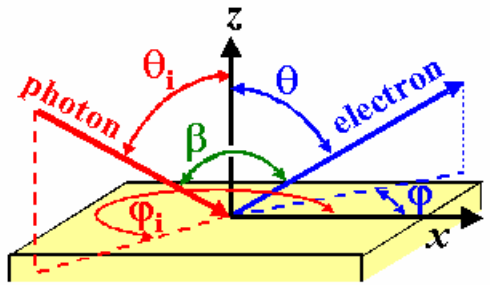

Schematic representation of the geometry

Mobility of cluster beam, and sample (click here for details):
(•) Only the sample moves with constant β = 90 degrees
( ) Only the analyzer moves
( ) Both the sample and the analyzer move

Energy and angle scanning parameters (see figure above)

The following entries will select the range of photoelectron energies and angles of emission.

Energy scans for a given emission angle can be chosen by selecting more than one energy of emission and only one polar angle and one azimuthal angle (the value of each angle is then taken as the lower limit of the selected angular range, and the value of the upper limits are disregarded). In this case, the output is a 1D plot with the photoelectron intensity as a function of photoelectron energy.

Electron energy range: 1 equally-spaced value(s) of the electron energy from 1202 eV to 1202 eV

Polar angle: 50 equally-spaced value(s) of the polar angle θ from 0 degrees to 89 degrees

Azimuthal angle: 61 equally-spaced value(s) of the azimuthal angle φ from 0 degrees to 360 degrees

Type of 2D angular representation: ○ Linear scale ◉ Logarithmic scale

Type of azimuthal of polar angular representation: ◉ Cartesian ○ Polar

Photoelectron detector half-width acceptance angle = 0 degrees. The photoelectron intensities are angle-averaged over a cone with half aperture given by this parameter.

Multiple scattering parameters

Internal code parameters

Maximum orbital quantum number l_{max} = 25

Scattering order = 4

Iteration method: ○ Jacobi (regular MS) ◉ Recursion

Additional solid parameters

Inner potential V_0 = 12.4 eV

Electronic edge z_0 = 1.435 Å

8.1 eV from band struct. + work function = 4.3 eV = 12.4 eV

Inelastic mean free path: either choose a fixed value = 17.8 Å

or (if that last entry is <0) use the TPP-2M formula with parameters ρ = 8.91 g/cm^3, N_v = 10, E_p = 35.45 eV, and E_g = 0 eV

Temperature (K) = 300 and Debye emperature (K) = 450

Table 4 Density and atomic concentration

The data are given at atmospheric pressure and room temperature, or at the stated temperature in deg K. (Crystal modifications as for Table 3.)

Atomic radius = r_{MT} = 0.5 n-n dist.

Average surface density = $\rho_S = (\rho_V)^{2/3}$

Density in g cm^{-3} (10^3kg m^{-3})
Concentration in 10^{22} cm^{-3} (10^{28} m^{-3})
Nearest-neighbor distance, in Å (10^{-10}m)

H 4K																	He 2K
0.088																	0.205 (at 37 atm)
Li 78K	Be											B	C	N 20K	O	F	Ne 4K
0.542	1.82											2.47	3.516	1.03			1.51
4.700	12.1											13.0	17.6				4.36
3.023	2.22												1.54			1.44	3.16
Na 5K	Mg											Al	Si	P	S	Cl 93K	Ar 4K
1.013	1.74											2.70	2.33			2.03	1.77
2.652	4.30											6.02	5.00				2.66
3.659	3.20											2.86	2.35			2.02	3.76
K 5K	Ca	Sc	Ti	V	Cr	Mn	Fe	Co	Ni	Cu	Zn	Ga	Ge	As	Se	Br 123K	Kr 4K
0.910	1.53	2.99	4.51	6.09	7.19	7.47	7.87	8.9	8.91	8.93	7.13	5.91	5.32	5.77	4.81	4.05	3.09
1.402	2.30	4.27	5.66	7.22	8.33	8.18	8.50	8.97	9.14	8.45	6.55	5.10	4.42	4.65	3.67	2.36	2.17
4.525	3.95	3.25	2.89	2.62	2.50	2.24	2.48	2.50	2.49	2.56	2.66	2.44	2.45	3.16	2.32		4.00
Rb 5K	Sr	Y	Zr	Nb	Mo	Tc	Ru	Rh	Pd	Ag	Cd	In	Sn	Sb	Te	I	Xe 4K
1.629	2.58	4.48	6.51	8.58	10.22	11.50	12.36	12.42	12.00	10.50	8.65	7.29	5.76	6.69	6.25	4.95	3.78
1.148	1.78	3.02	4.29	5.56	6.42	7.04	7.36	7.26	6.80	5.85	4.64	3.83	2.91	3.31	2.94	2.36	1.64
4.837	4.30	3.55	3.17	2.86	2.72	2.71	2.65	2.69	2.75	2.89	2.98	3.25	2.81	2.91	2.86	3.54	4.34
Cs 5K	Ba	La	Hf	Ta	W	Re	Os	Ir	Pt	Au	Hg 227	Tl	Pb	Bi	Po	At	Rn
1.997	3.59	6.17	13.20	16.66	19.25	21.03	22.58	22.55	21.47	19.28	14.26	11.87	11.34	9.80	9.31		
0.905	1.60	2.70	4.52	5.55	6.30	6.80	7.14	7.06	6.62	5.90	4.26	3.50	3.30	2.82	2.67	—	—
5.235	4.35	3.73	3.13	2.86	2.74	2.74	2.68	2.71	2.77	2.88	3.01	3.46	3.50	3.07	3.34		
Fr	Ra	Ac															
		10.07															
—	—	2.66															
		3.76															

Ce	Pr	Nd	Pm	Sm	Eu	Gd	Tb	Dy	Ho	Er	Tm	Yb	Lu
6.77	6.78	7.00		7.54	5.25	7.89	8.27	8.53	8.80	9.04	9.32	6.97	9.84
2.91	2.92	2.93	—	3.03	2.04	3.02	3.22	3.17	3.22	3.26	3.32	3.02	3.39
3.65	3.63	3.66		3.59	3.96	3.58	3.52	3.51	3.49	3.47	3.54	3.88	3.43
Th	Pa	U	Np	Pu	Am	Cm	Bk	Cf	Es	Fm	Md	No	Lr
11.72	15.37	19.05	20.45	19.81	11.87								
3.04	4.01	4.80	5.20	4.26	2.96	—	—	—	—	—	—	—	—
3.60	3.21	2.75	2.62	3.1	3.61								

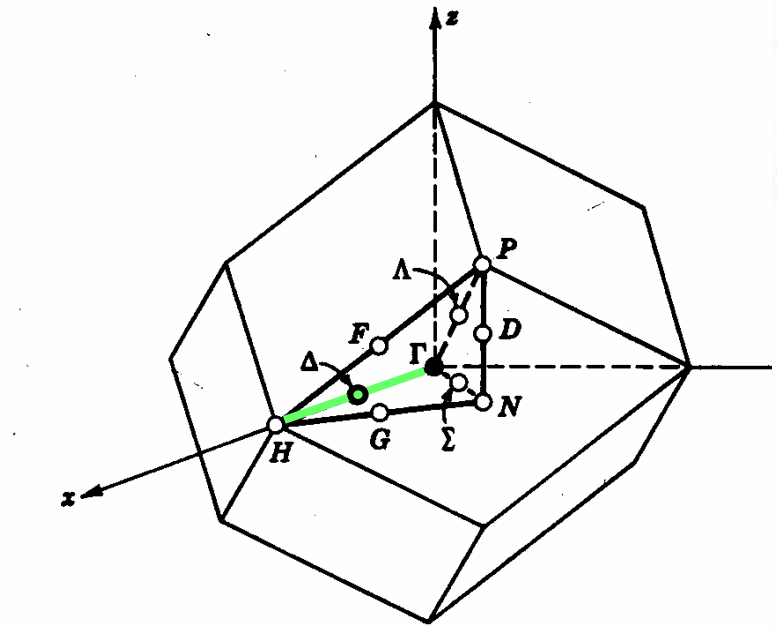

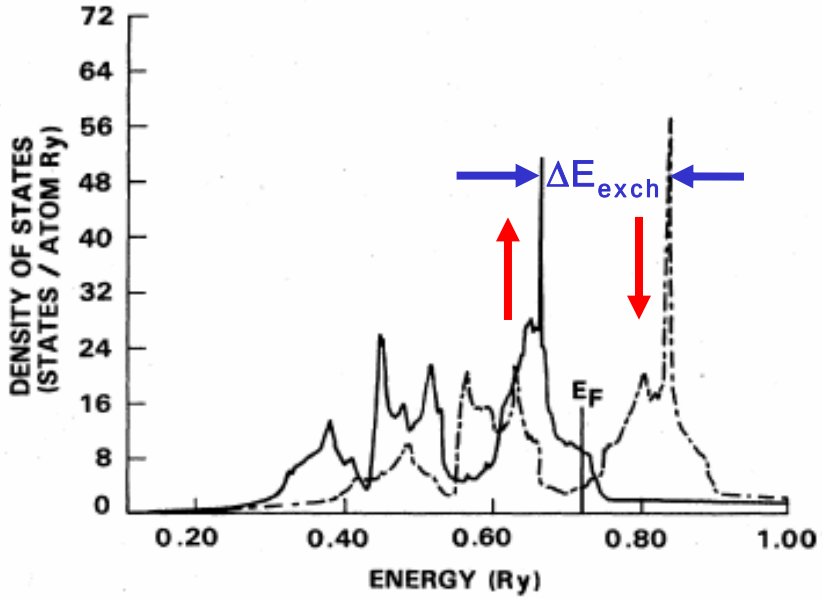

FIG. 4. Density of states at the equilibrium lattice constant of Fe for majority- (solid line) and minority- (broken line) spin states.

Hathaway et al., Phys. Rev. B 31, 7603 ('85)

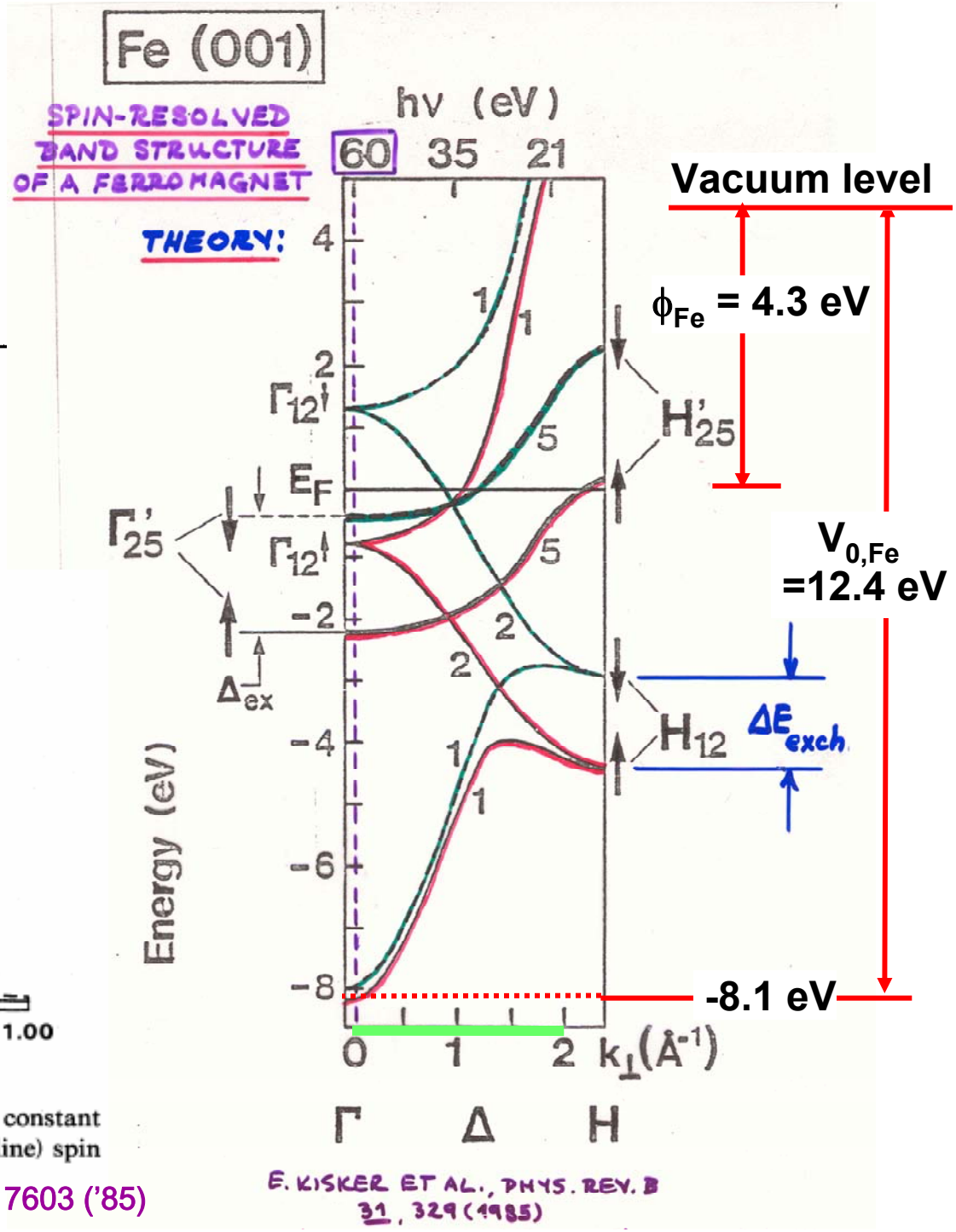

Initial core-state quantum numbers

Radial matrix elements:
- (•) Automatic: core level (e.g. 1s, 2s, 2p, etc.) = [1s]
- ( ) Manual: l_0=[0], R_{l0+1}=[1.0], δ_{l0+1}=[0.0], R_{l0-1}=[0.0], δ_{l0-1}=[0.0]

[Calculate*] [Download Input File**] [Reset***]

COMPUTATION TIME: the CPU time needed for the calculation using the default cluster and input parameters (use Reset to recover default input) is 1.24 seconds on a Pentium III @ 733 MHz. This gives a time scale to estimate the computation time for other input parameters, keeping in mind that it scales like $\sim (n_{scat} - 1)\, N^2\, (l_{max}+1)^3$, where N is the number of atoms in the cluster and n_{scat} is the scattering order. For reference, the default values are N=48, l_{max}=6, and n_{scat}=2, for which the above number is $7.9\ 10^5$.

IMPORTANT: READ THESE LINES BEFORE RUNNING THE CODE FOR THE FIRST TIME.

***The results will be plotted on a separate window.**

****The input file can be used to run the code locally, for which a copy of the code is needed. This can be obtained from F. Javier García de Abajo. An online version of the input-file manual is also available here.**

*****Reset all input values (including cluster specification) to the original settings.**

For comments/questions/suggestions, please contact F. Javier García de Abajo at jga@sw.ehu.es

CO/Fe(001)—Effect of CO height z above first Fe plane

2 atoms: Z = ∞

7 atoms: 1.0 Å

0.5 Å

0.0 Å

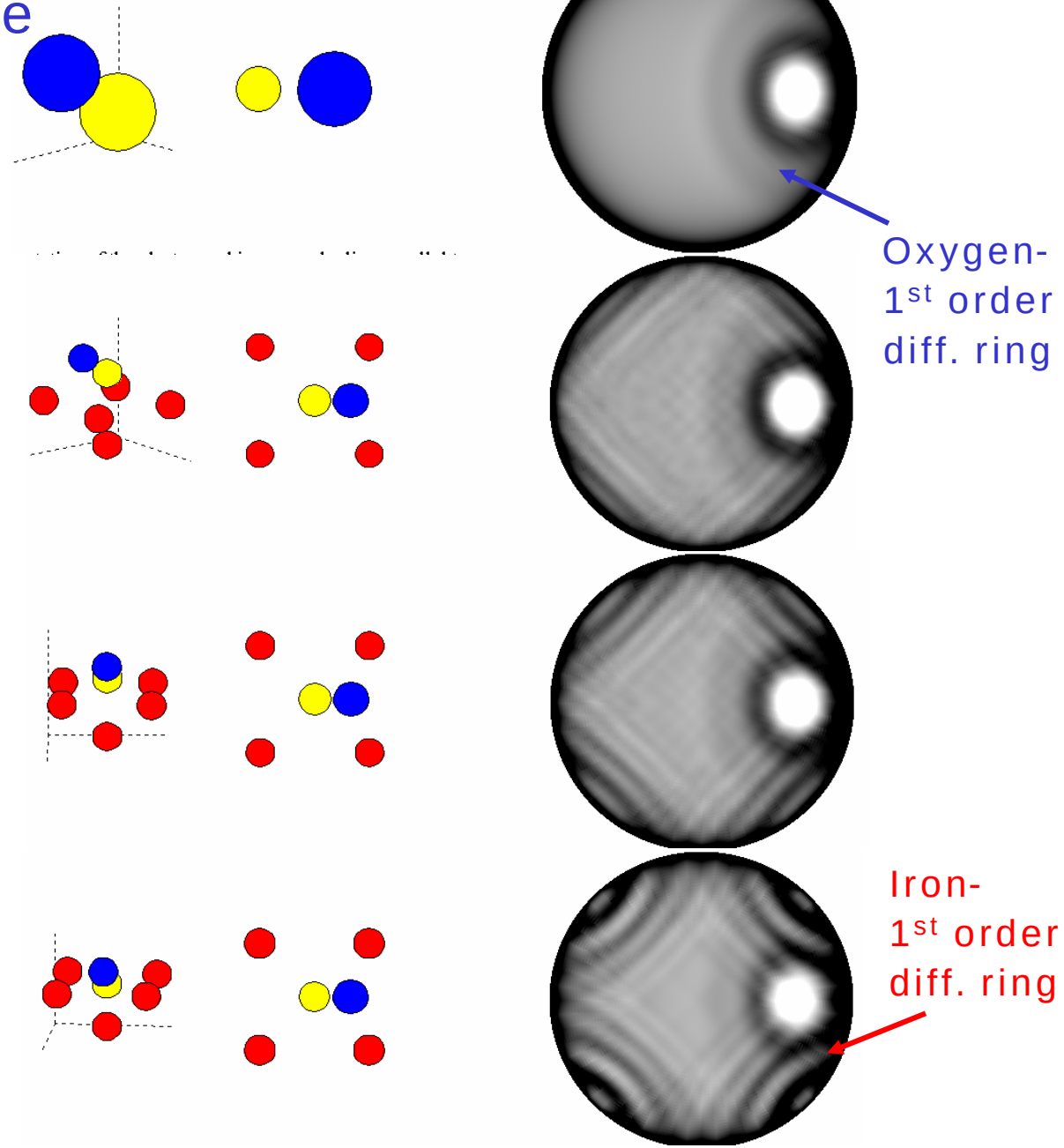

Oxygen-1st order diff. ring

Iron-1st order diff. ring

CO/Fe(001)—Effect of CO bond dist.

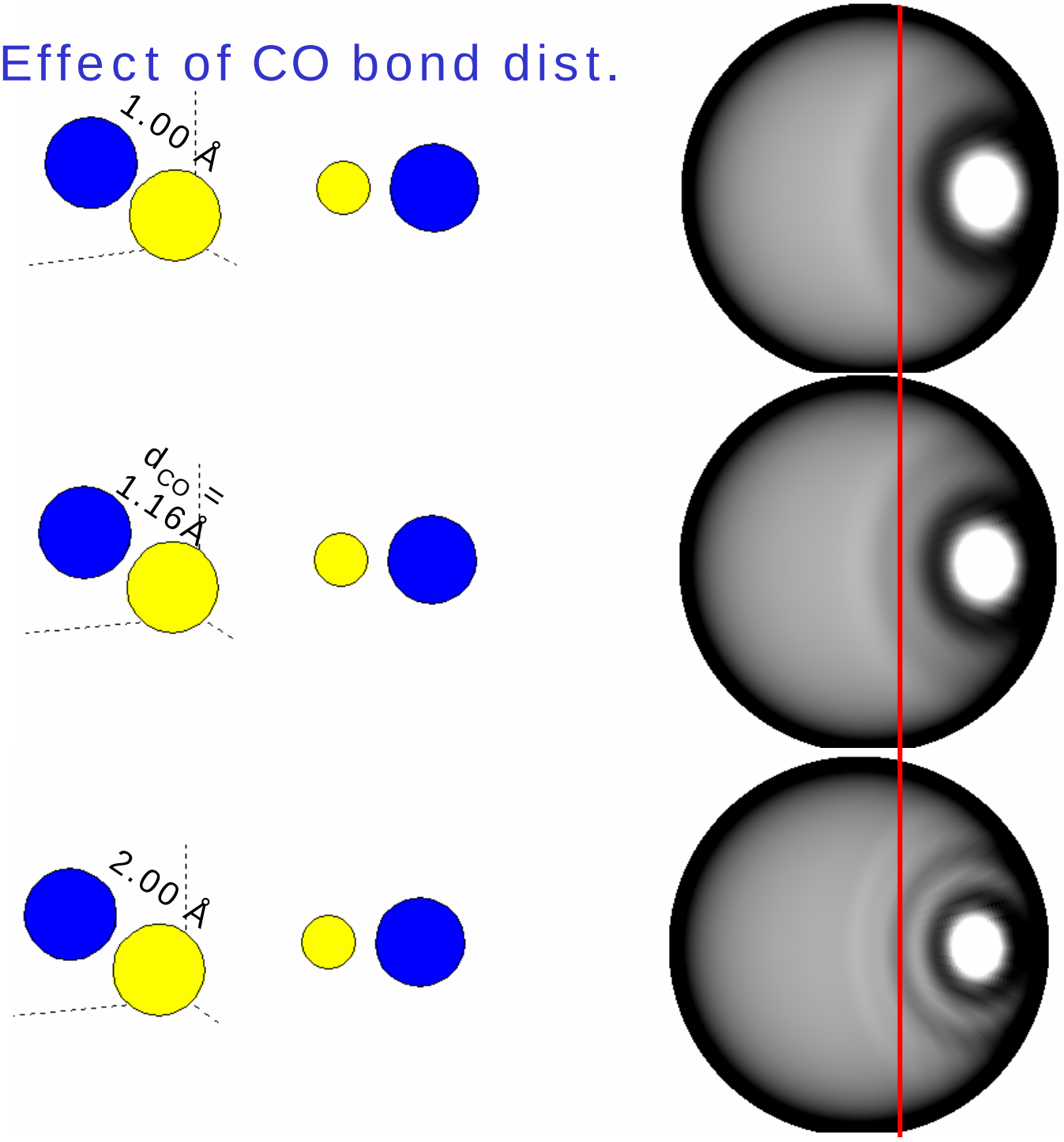

CO/Fe(001)—Effect of cluster size

19 atoms:

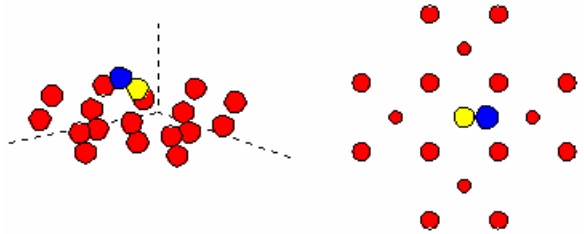

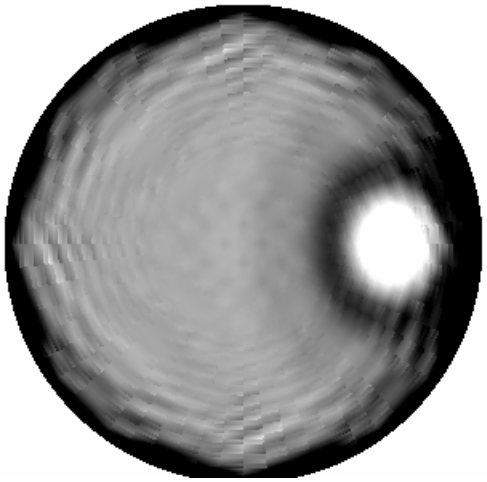

31 atoms:

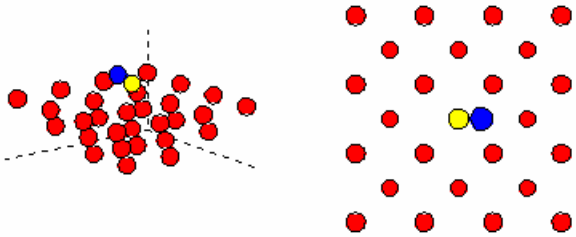

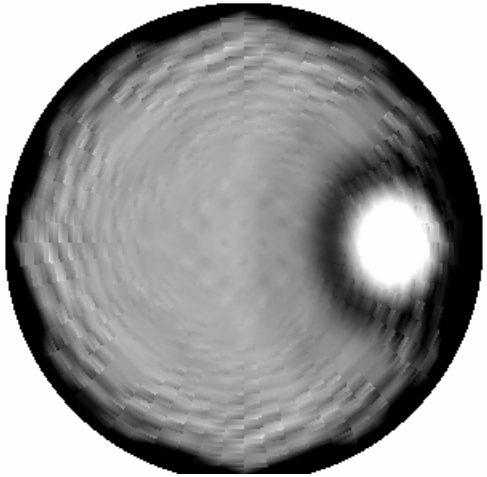

19 ≈ 31, AND SO “CONVERGED” AT 19 OR LESS

CO/Fe(001)—Effect of scattering order

Single scattering:

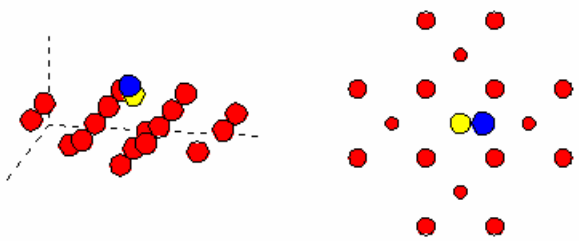

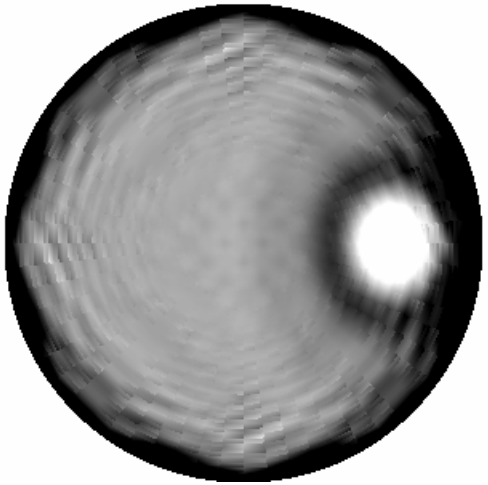

Fourth order scattering:

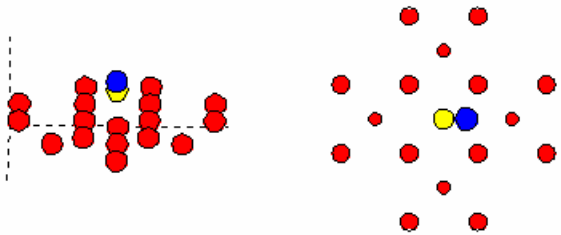

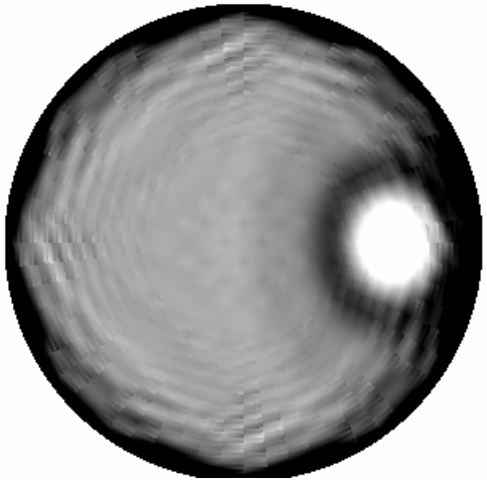

APPROX. CONVERGED AT SINGLE—FOR THIS PARTICULAR PROBLEM ONLY!

Effect of varying the polarization?: C 1s emission from CO

E_{kin} = 200 eV

Linear p polarization:

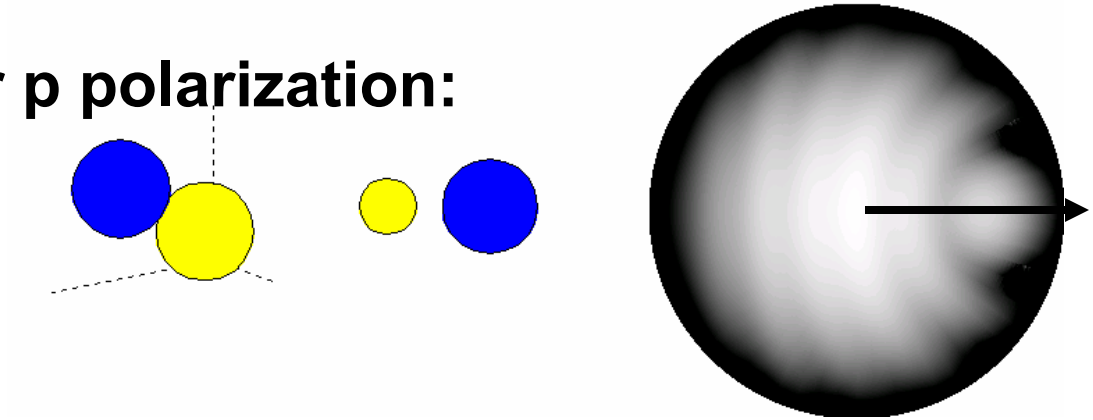

Right circular polarization:

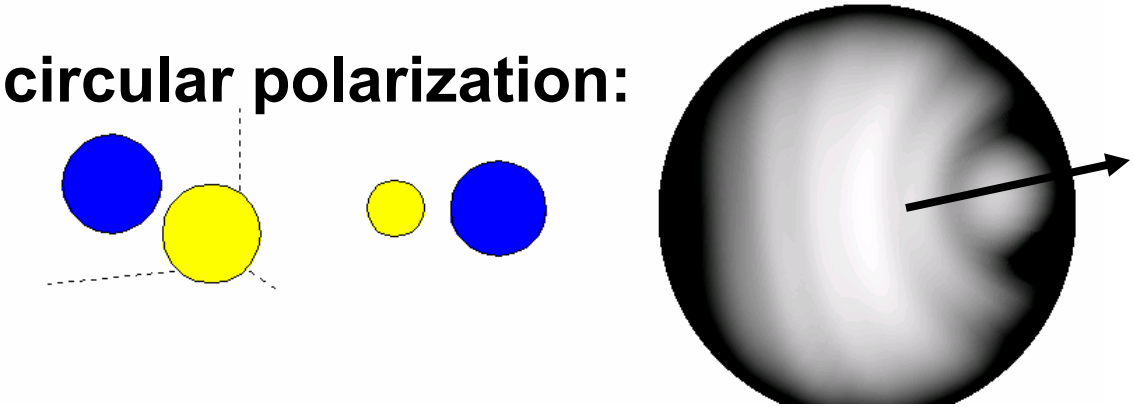

Left circular polarization:

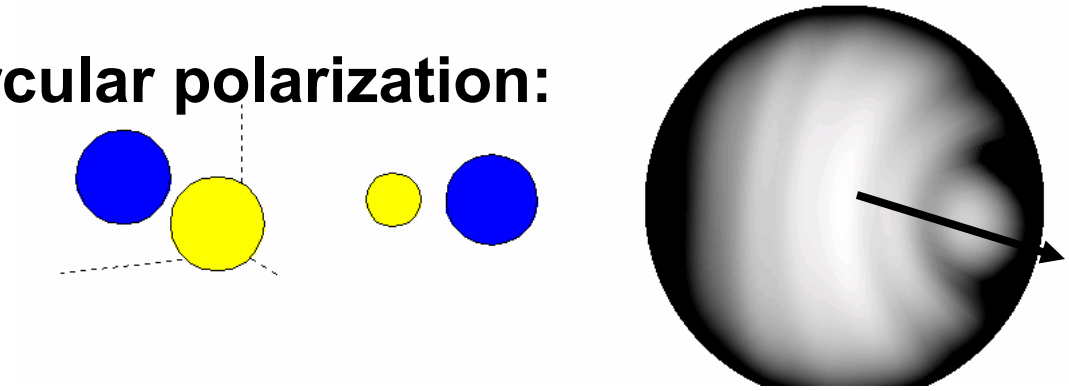

Circular dichroism in angular distributions (CDAD)—more later

4-atom Fe nearest-neighbor chain along [110]—Effect of scattering order

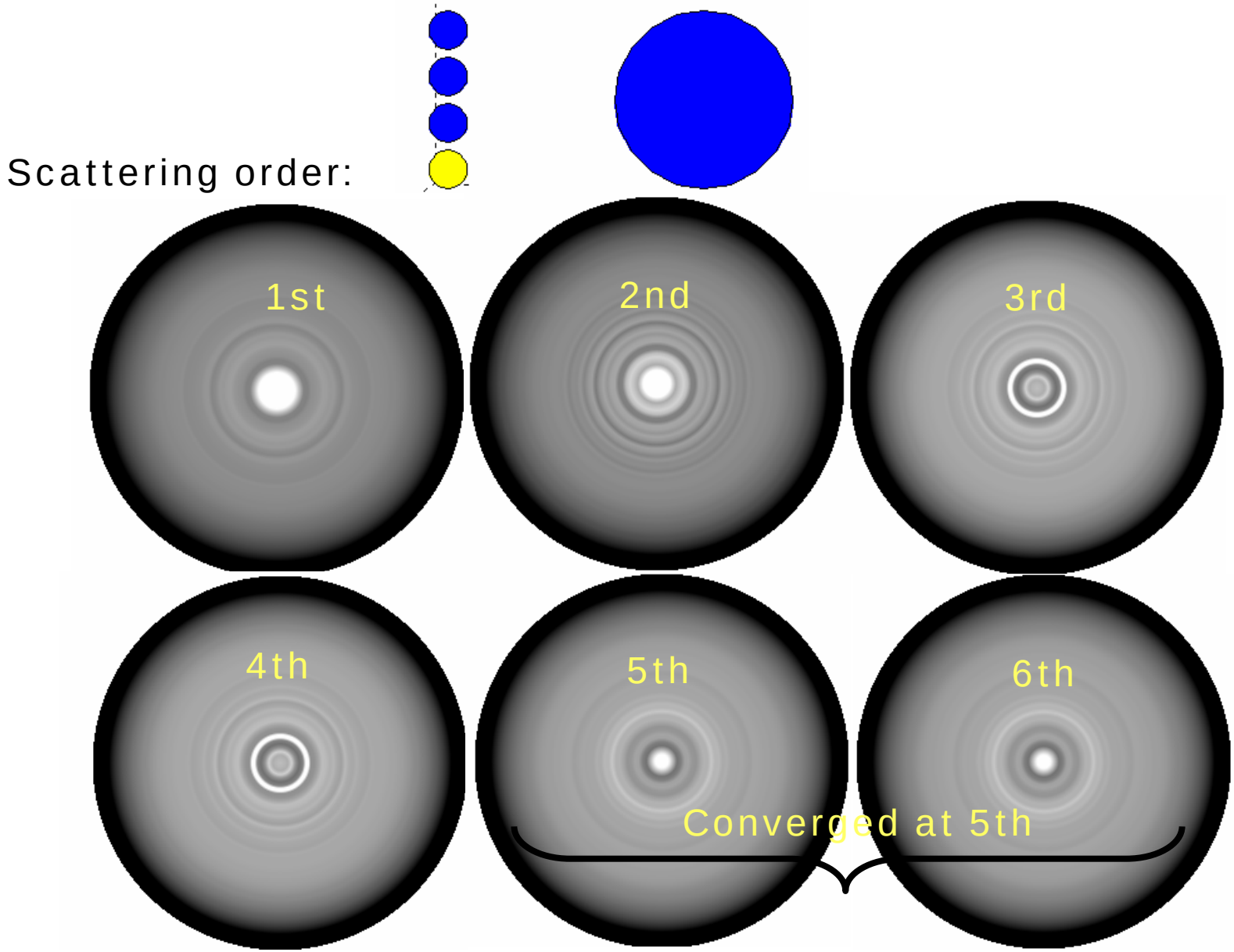

Cu nearest-neighbor chains along [110]—Effect of scattering order

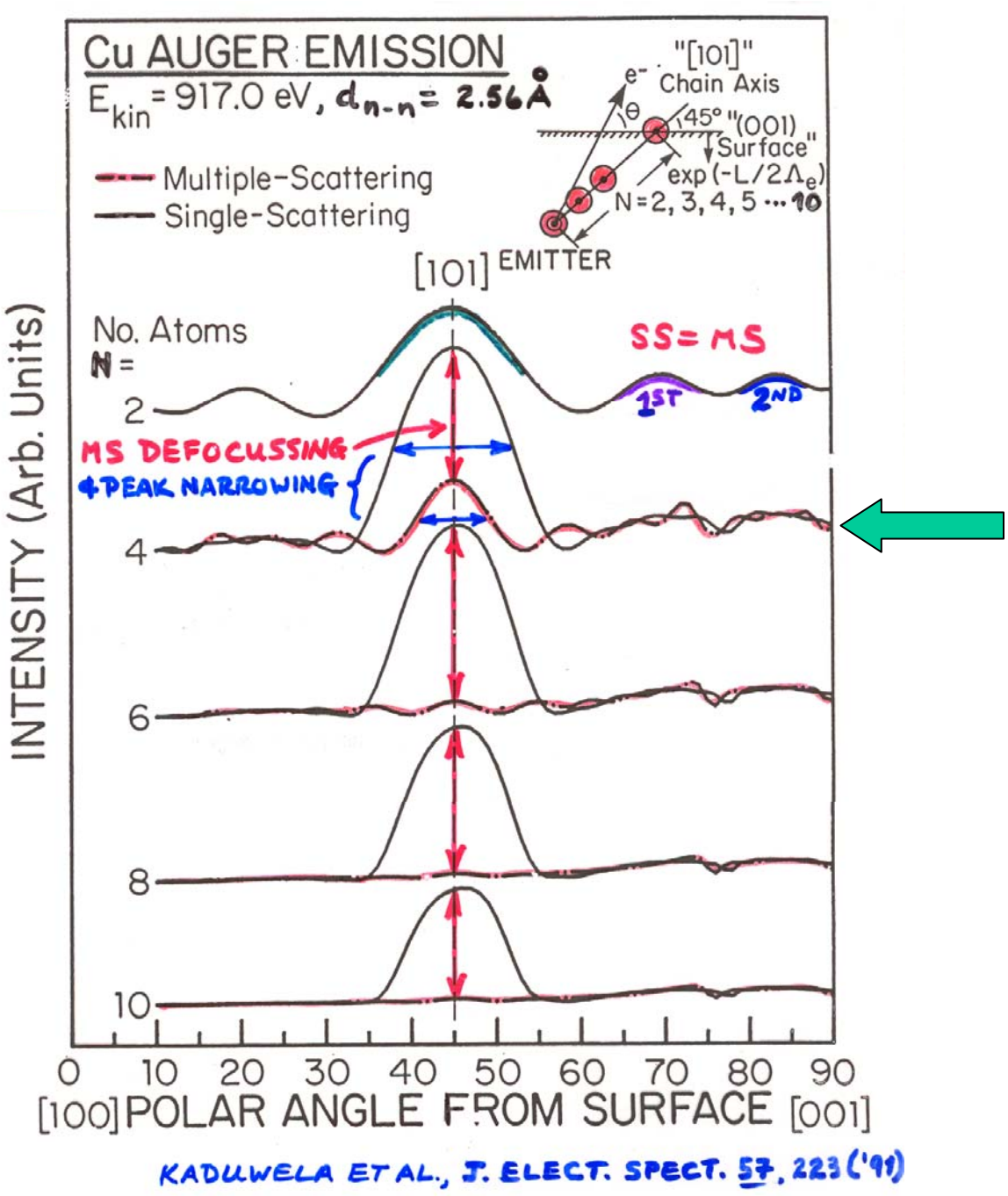

Plus cf. Figs. 6 and 7 in C.F., "The Study of Surface Structures by Photoelectron Diffraction and Auger Electron Diffraction"

Photoelectron Intensities From Different Surfaces
(Stereographic Projection)

Ni(001):Ni 2p at 636 eV

fcc
(001)

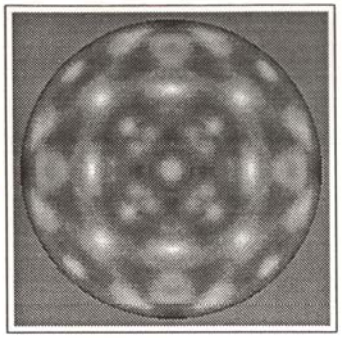

THEVUTHASAN
ET AL.

Ru(0001):Ru 3d at 1206 eV

hcp
(0001)

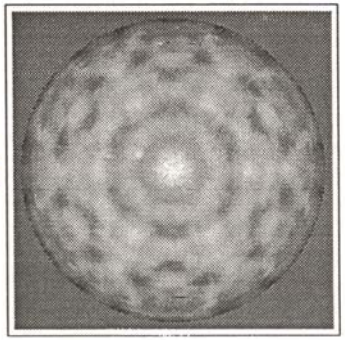

THEVUTHASAN
ET AL.

HOPG: Graphite (0001): C 1s at 946 eV

textured

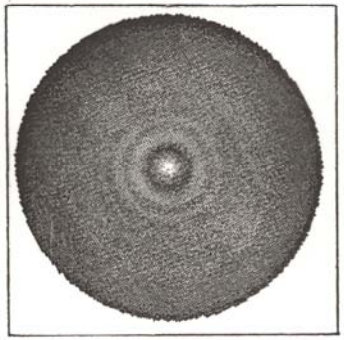

OSTERWALDER
ET AL.

Fingerprint identification of short-range atomic structure and symmetry

- Some growth modes:

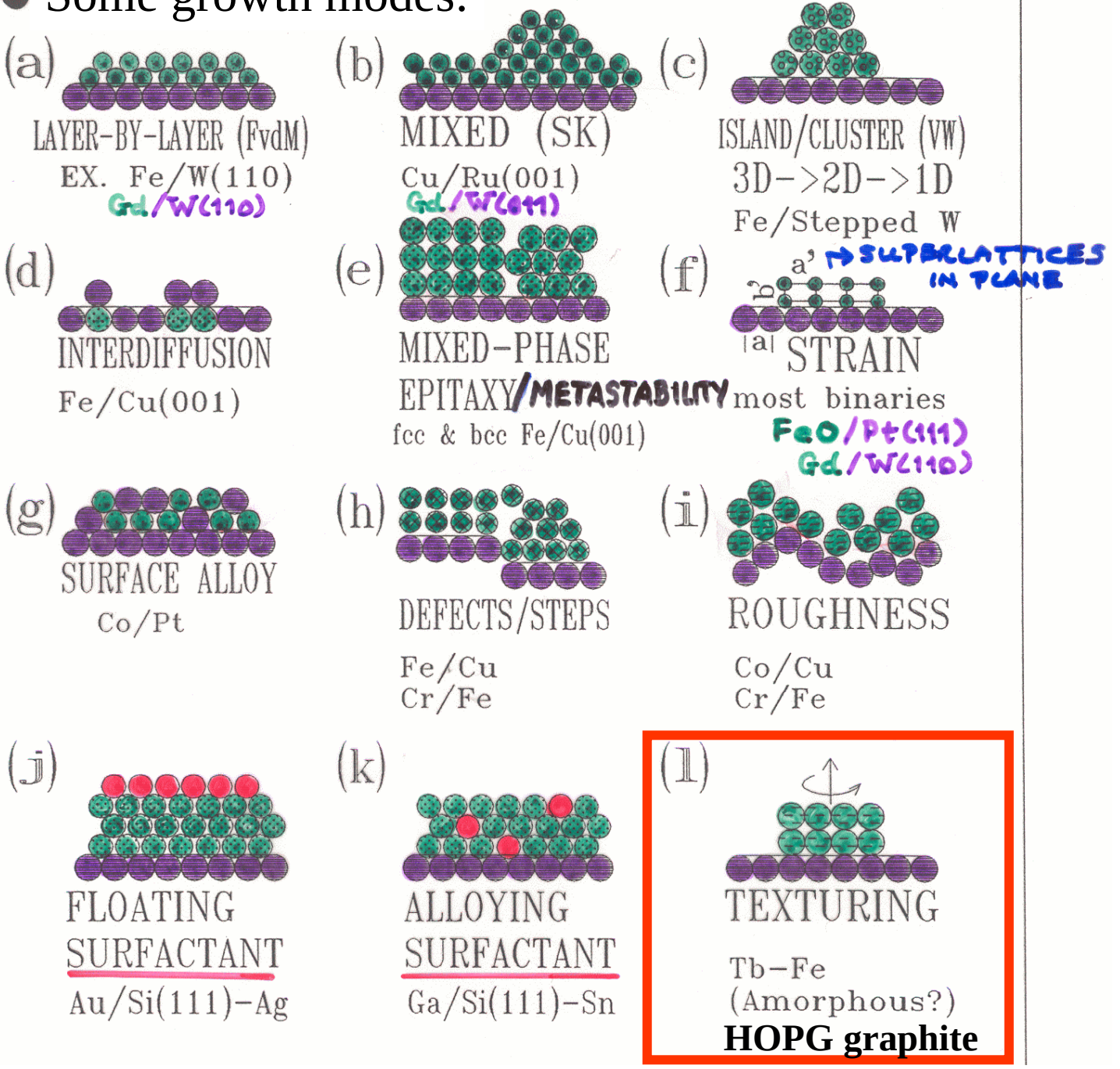

Photoelectron diffraction from W(110) interface atoms beneath an Fe overlayer

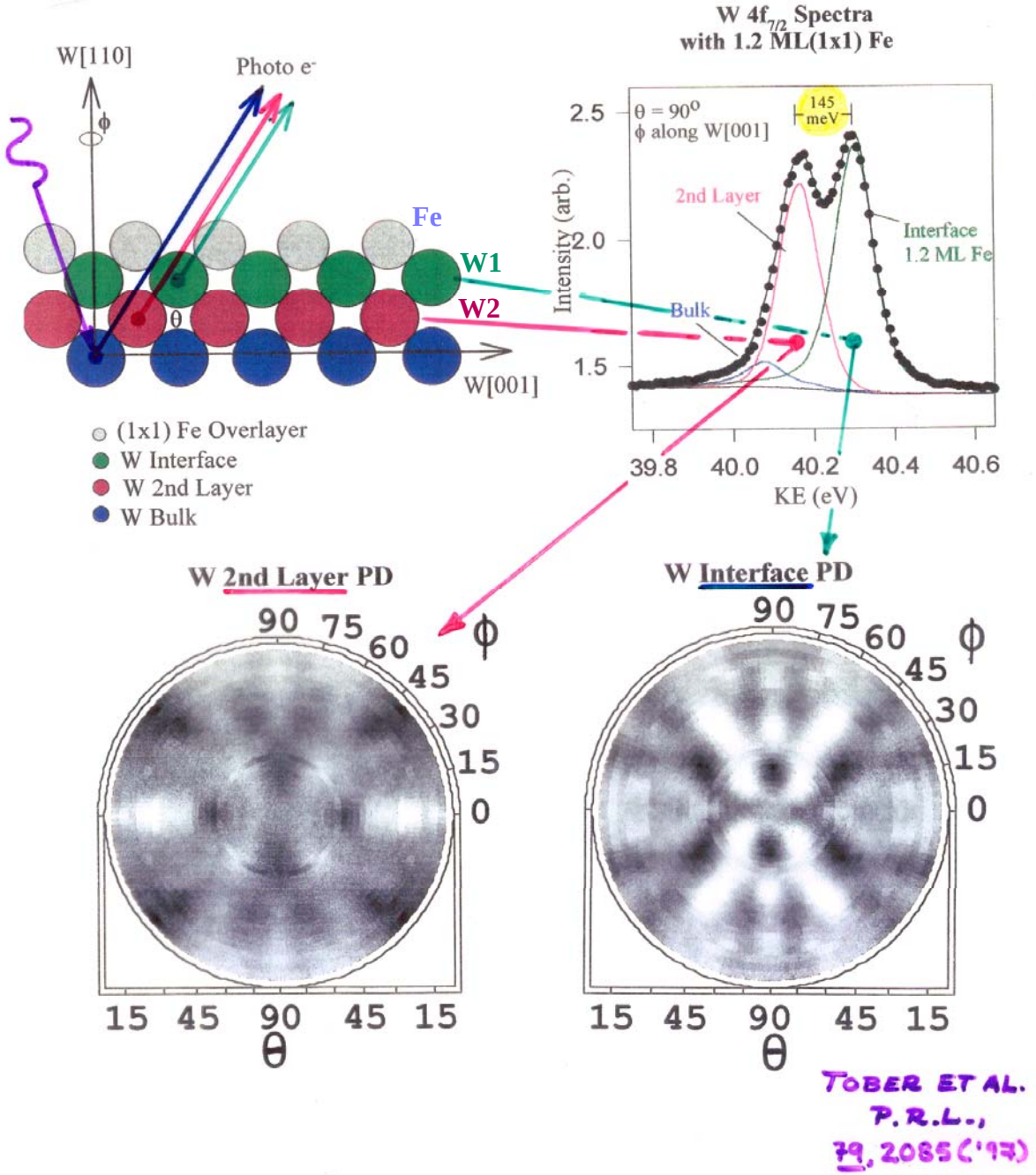

Fe on W(110): Determination of structure by expt./theory comparison

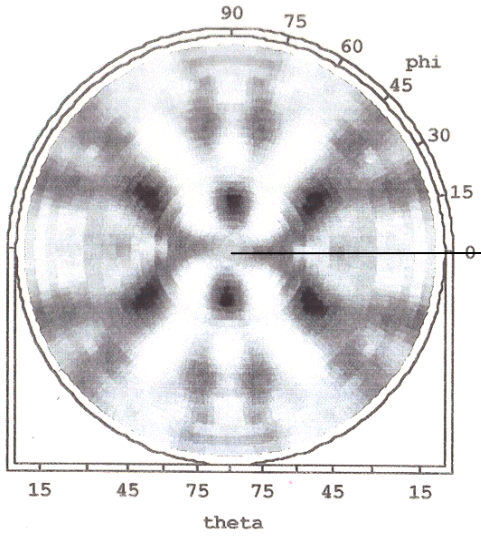

W $4f_{7/2}$
Interface Diffraction

Experiment

$h\upsilon$ = 70 eV
E_{kin} = 40 eV

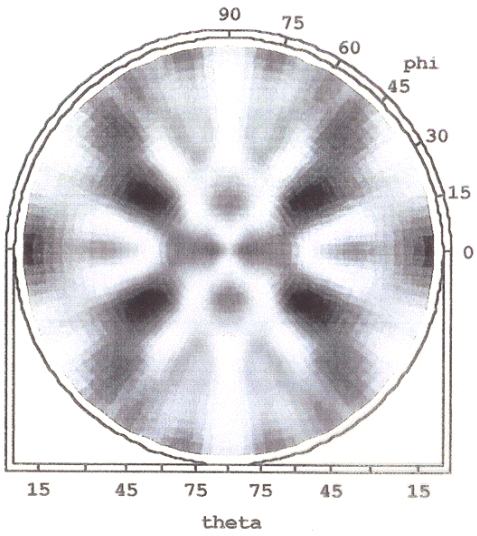

W $4f_{7/2}$
Interface Diffraction

Multiple Scattering
Theory
(110 atom cluster)

E_{kin} = 40 eV
Z_{Fe} = 2.165 Å

(Bridge Site)

↳ ~ CONTINUES BULK W STRUCTURE

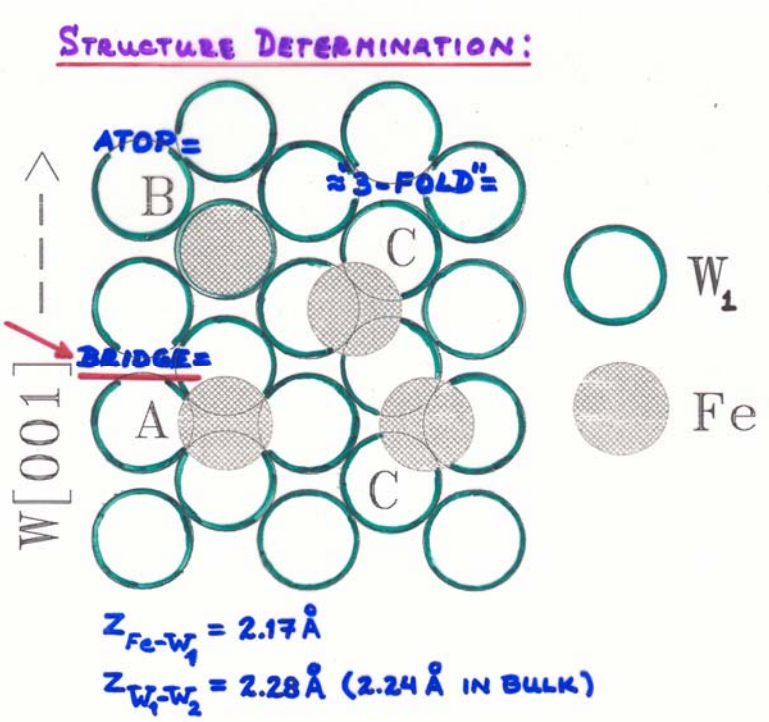

Clean W(110) 4f Surface Peak: R-Factor Analysis

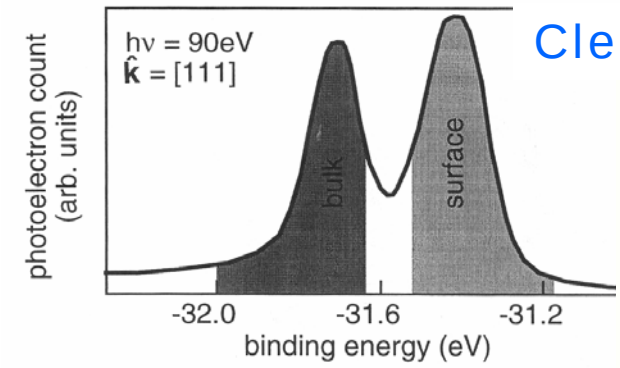

Expt.

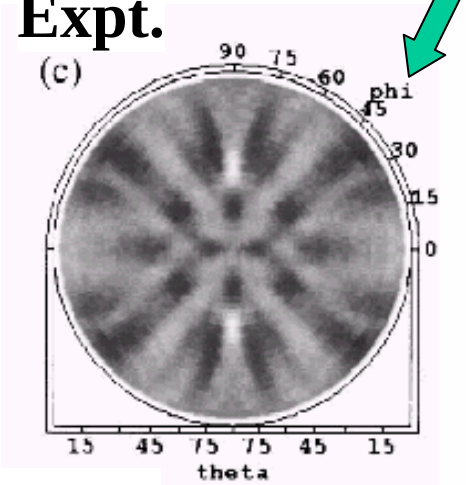

Theory

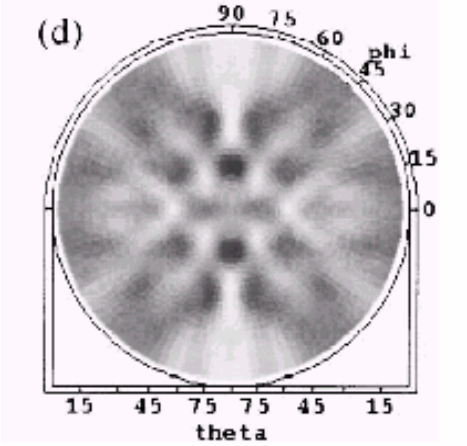

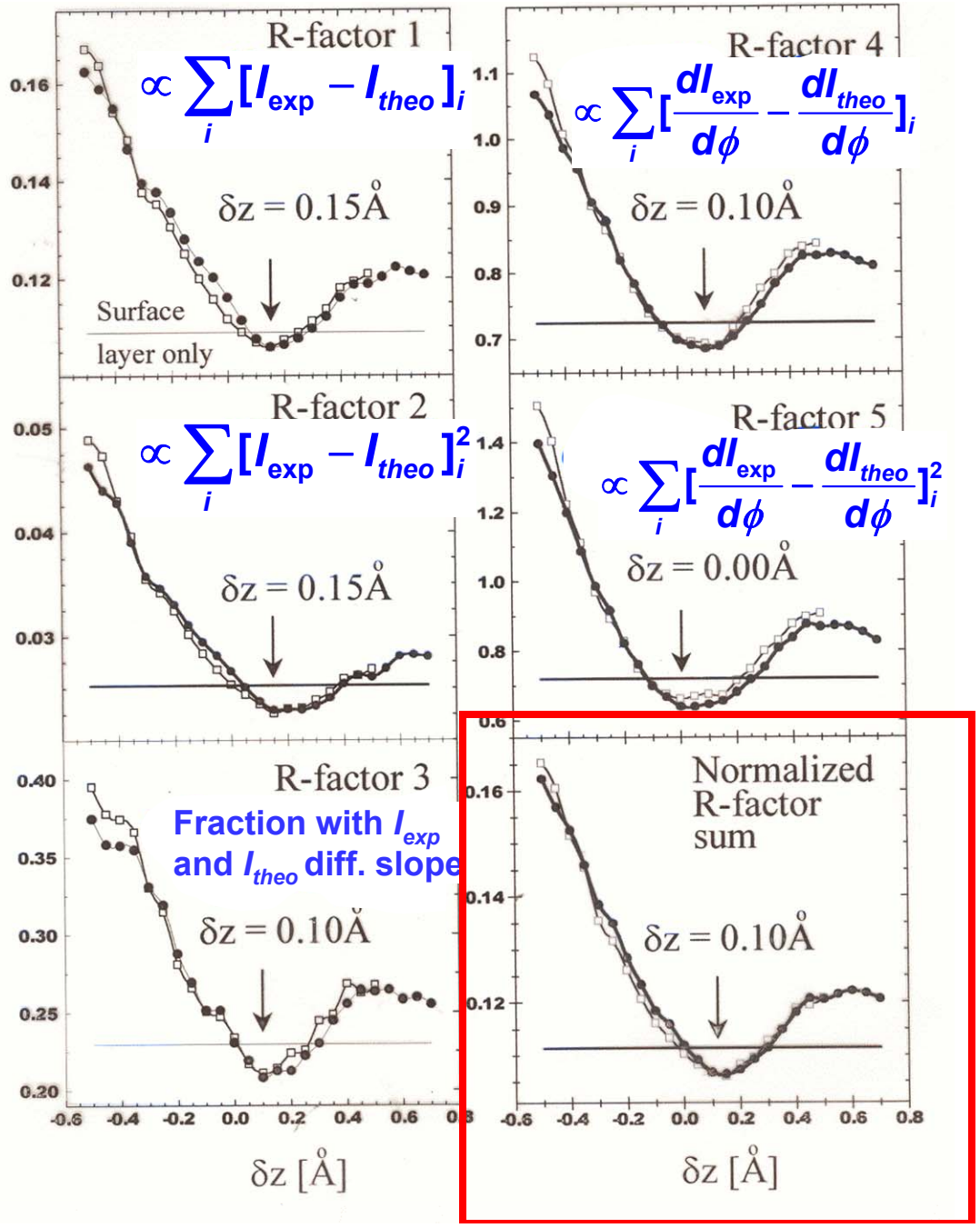

PHOTOELECTRON SPECTRA

OXIDIZED SILICON

CHEMICAL SHIFTS OF CORE LEVELS

EXACTLY WHAT IS STRUCTURE OF INTERFACE? NEED STATE-SPECIFIC STRUCTURAL INFORMATION!

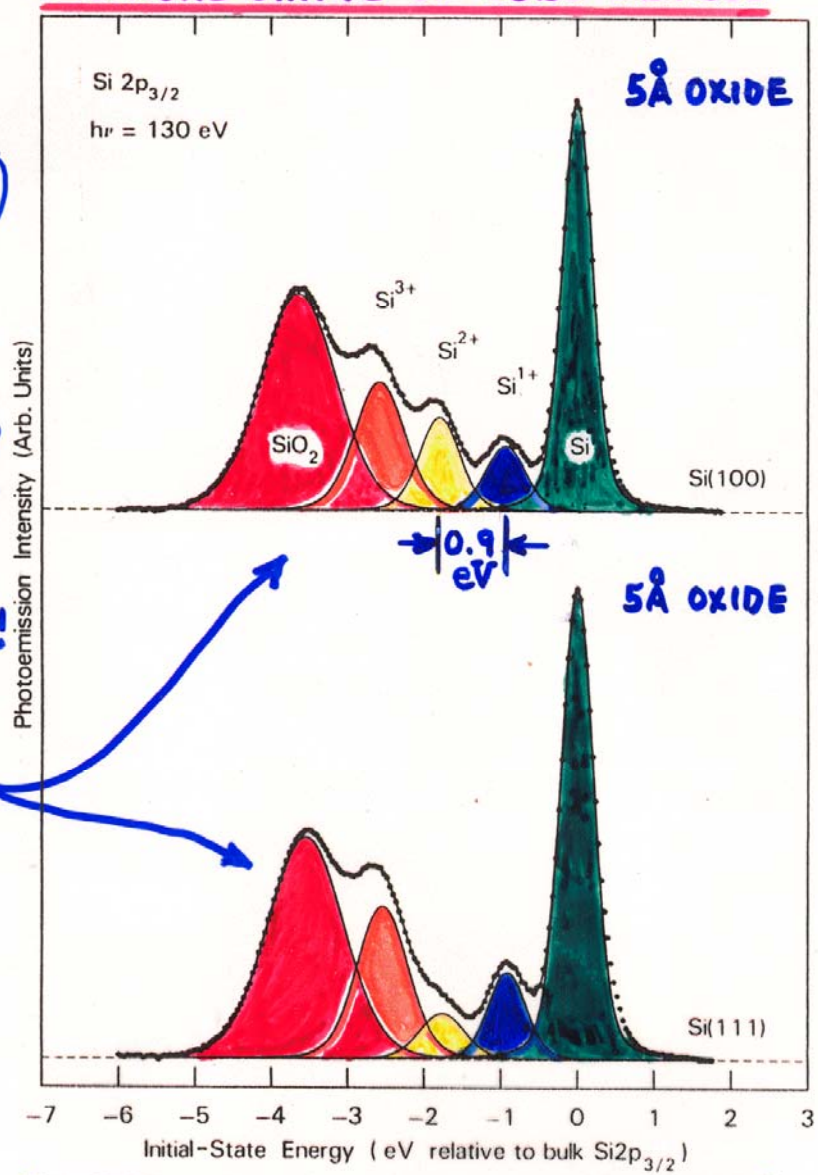

HIMPSEL ET AL., PHYS. REV. B, 38, 6084('90)

Case study: Interface structure of SiO_x/SiO_2

(Westphal et al.)

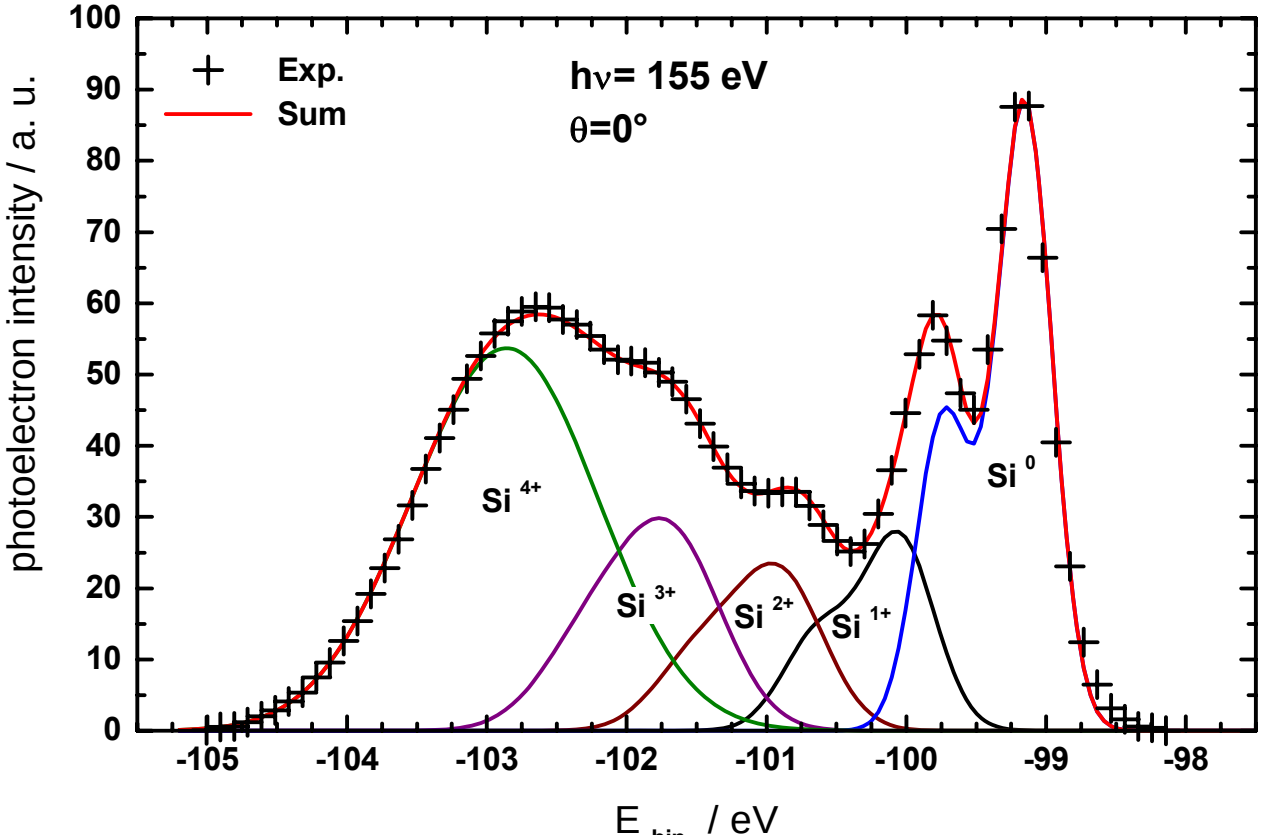

Spin-orbit-splitting	**0.58 eV**
Si^0 width	**0.48 eV**
Si^{1+} shift / width	**0.9 / 0.59 eV**
Si^{2+} shift / width	**1.74 / 0.72 eV**
Si^{3+} shift / width	**2.46 / 0.84 eV**
Si^{4+} shift / width	**3.54 / 1.42 eV**

F.J. Himpsel et al, Phys. Rev. B 38 (1988) 6084

S. Dreiner et al. (Westphal group), Phys. Rev. Lett. 86, 4068 (2001)

Experimental diffraction patterns for SiO_2/Si(100)

3000 L

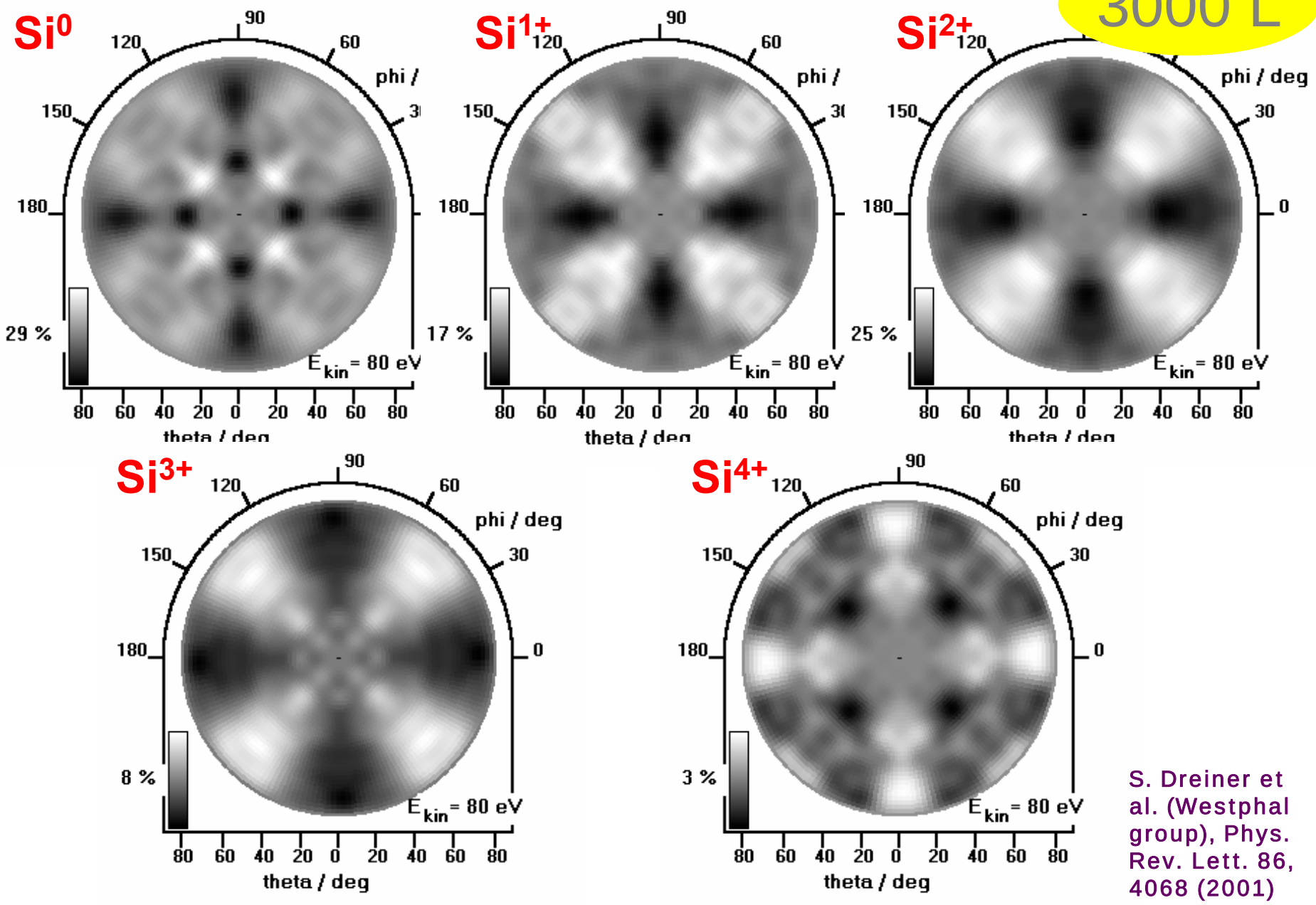

S. Dreiner et al. (Westphal group), Phys. Rev. Lett. 86, 4068 (2001)

Structure determination by R-factor analysis: $SiO_x/Si(100)$

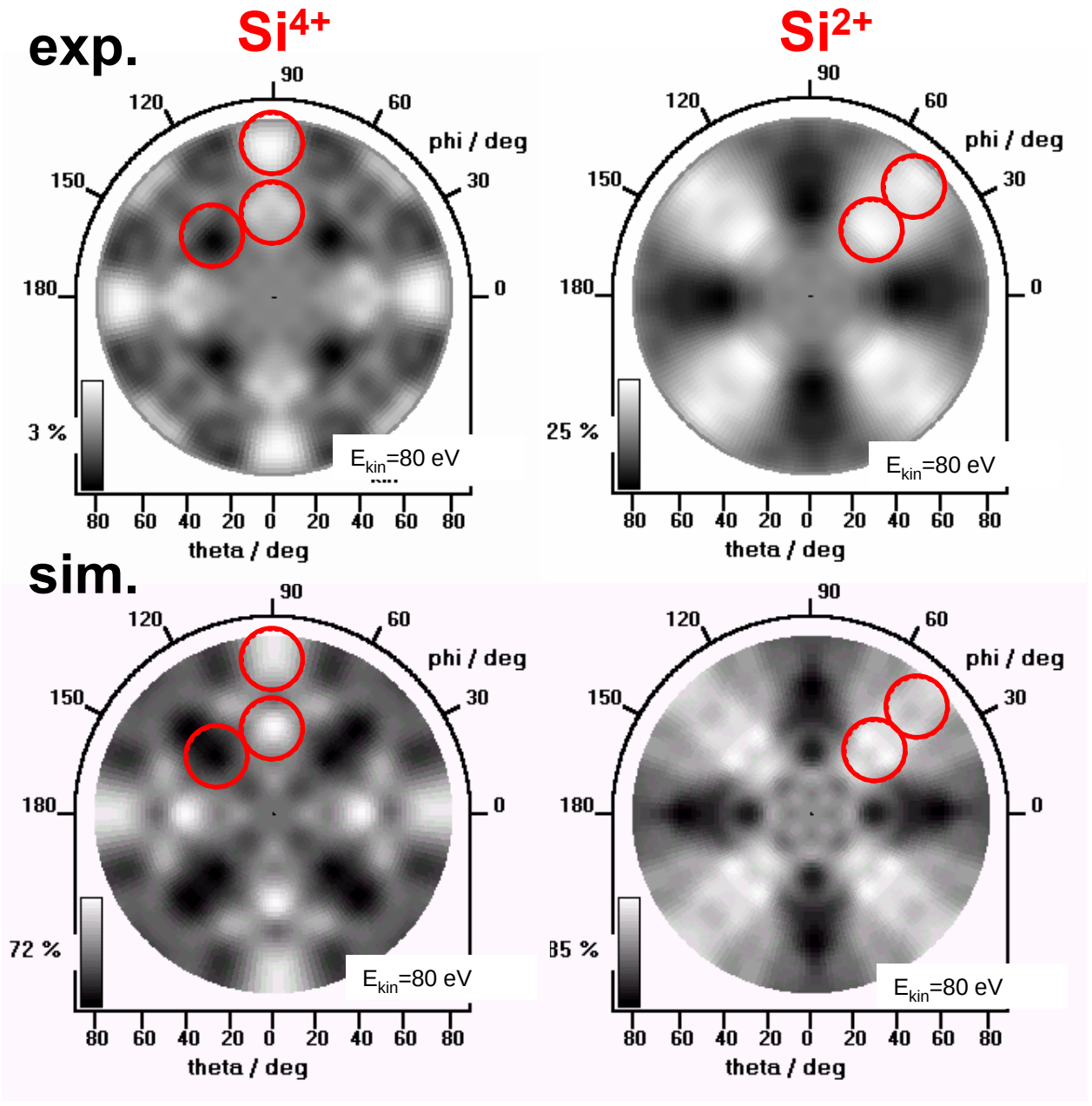

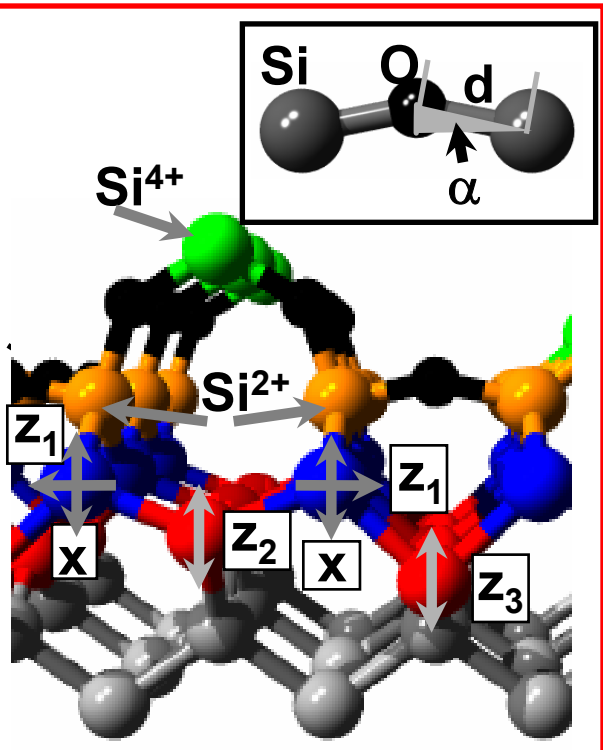

d [Å]	1,82 ± 0,02
α [°]	20 ± 1
x [Å]	0,18 ± 0,02
z_1 [Å]	-0,01 ± 0,02
z_2 [Å]	0,5 ± 0,02
z_3 [Å]	-0,27 ± 0,02
R-Faktor	0,14

Phys. Rev. Lett. 86, 4068 (2001)

+ Assignment of additional Si$^{\alpha}$- and Si$^{\beta}$-components

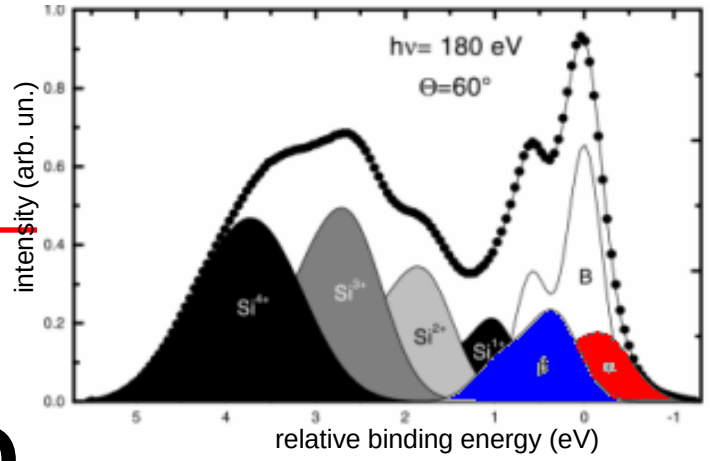

SiO_2

Si-bulk

S. Dreiner et al. (Westphal group)

Some Comple-mentary Surface Structure Probes

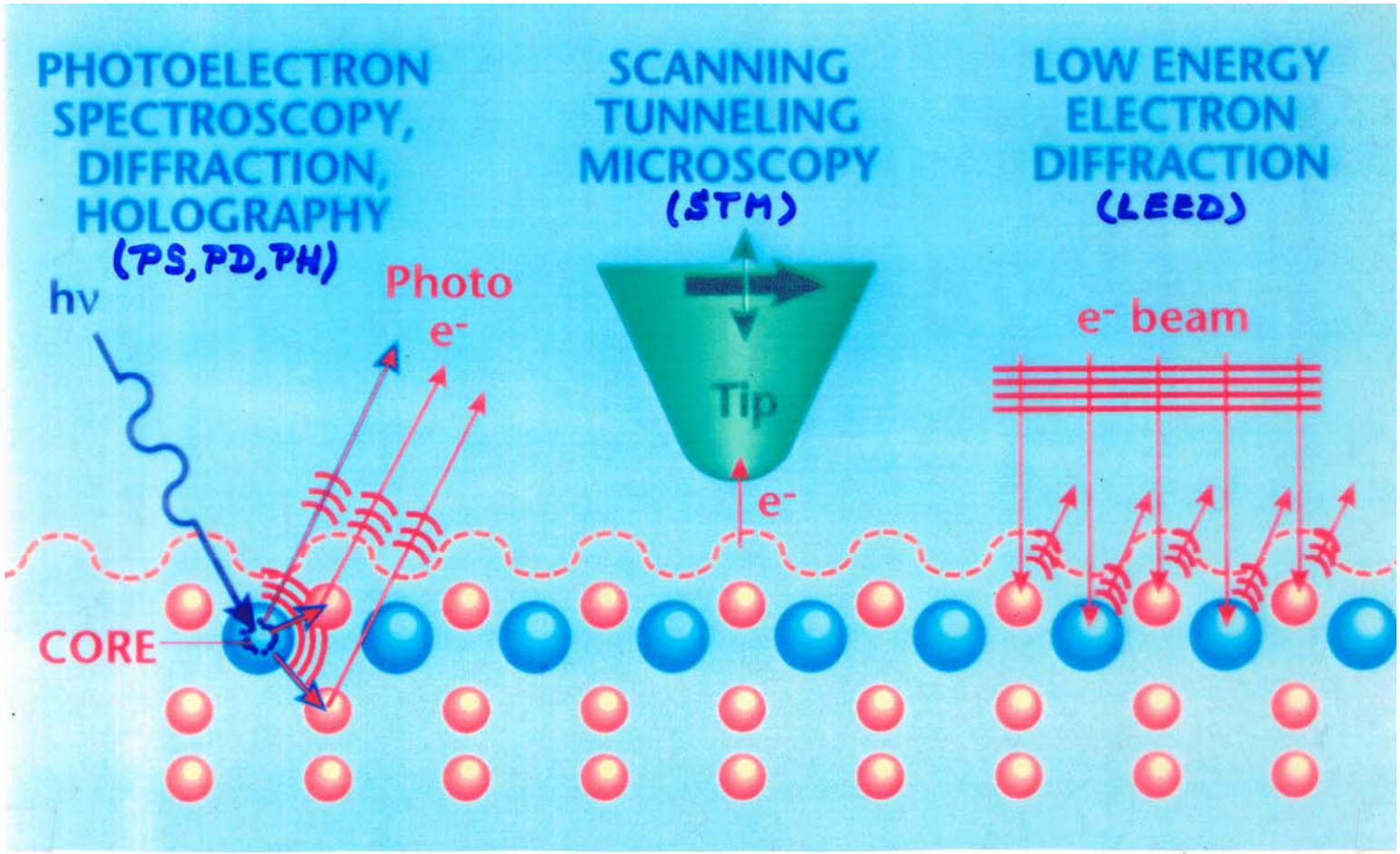

-Type of order:	Short (< 10Å)	Short, long and disorder	Long (> 100Å)
-Atom & site specific:	Yes	No	No
-Sensing depth:	5-40Å	Mostly surface D.O.S.	5-20Å
-Lateral resolution:	1 mm^2 to $(300Å)^2$	Single atom	1 mm^2 to 1 $micron^2$

Case study: 1 ML of FeO on Pt(111): A combined LEED, STM, XPD study

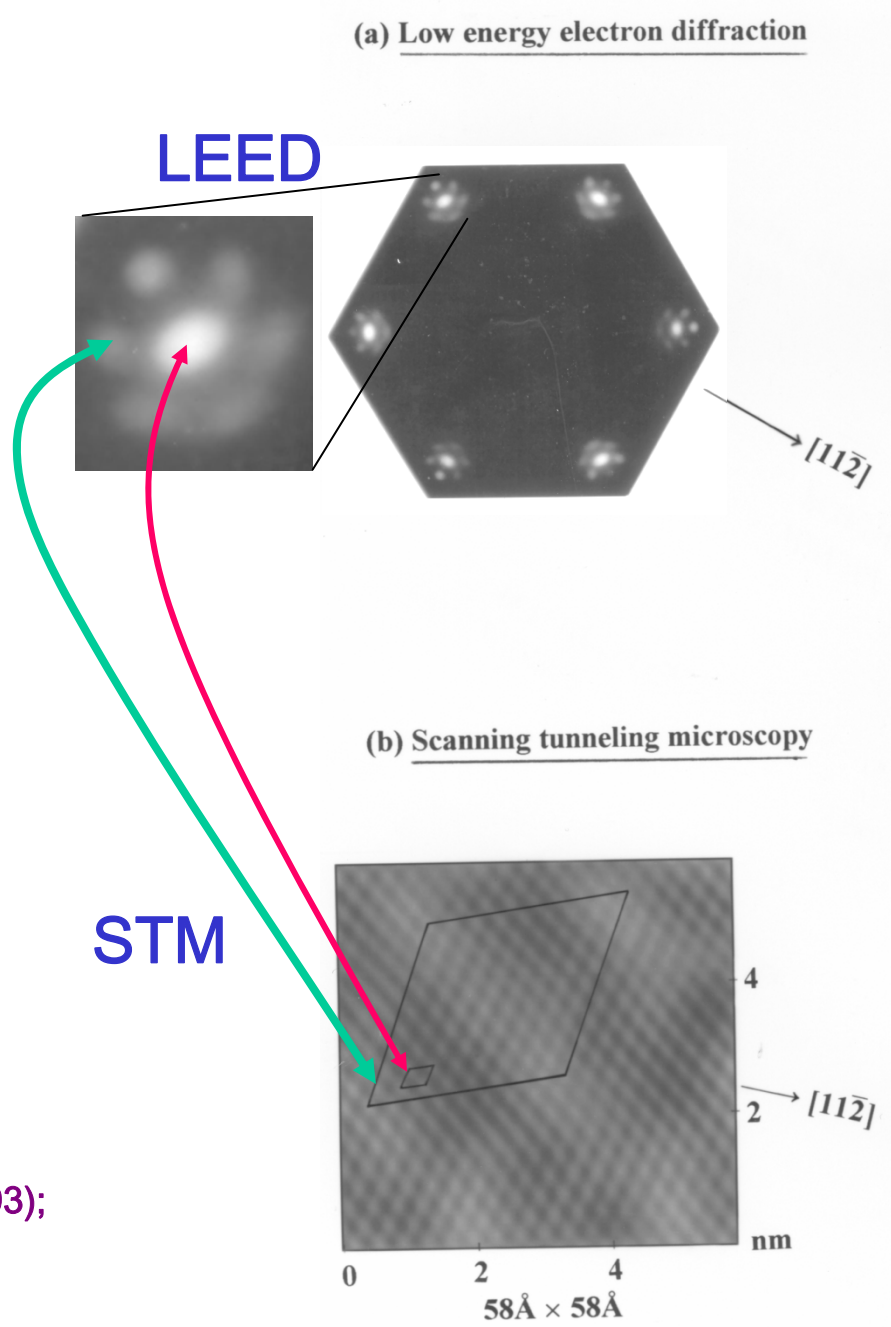

Galloway et al., Surf. Sci. 198, 127 ('93);
J. Vac. Sci. Tech. A12, 2302 ('94).
Y.J. Kim et al.,
Phys. Rev. B 55, R 13448 ('97);
Surf. Sci. 416, 68 ('98)

1 ML of FeO on Pt(111): Structural model from LEED and STM

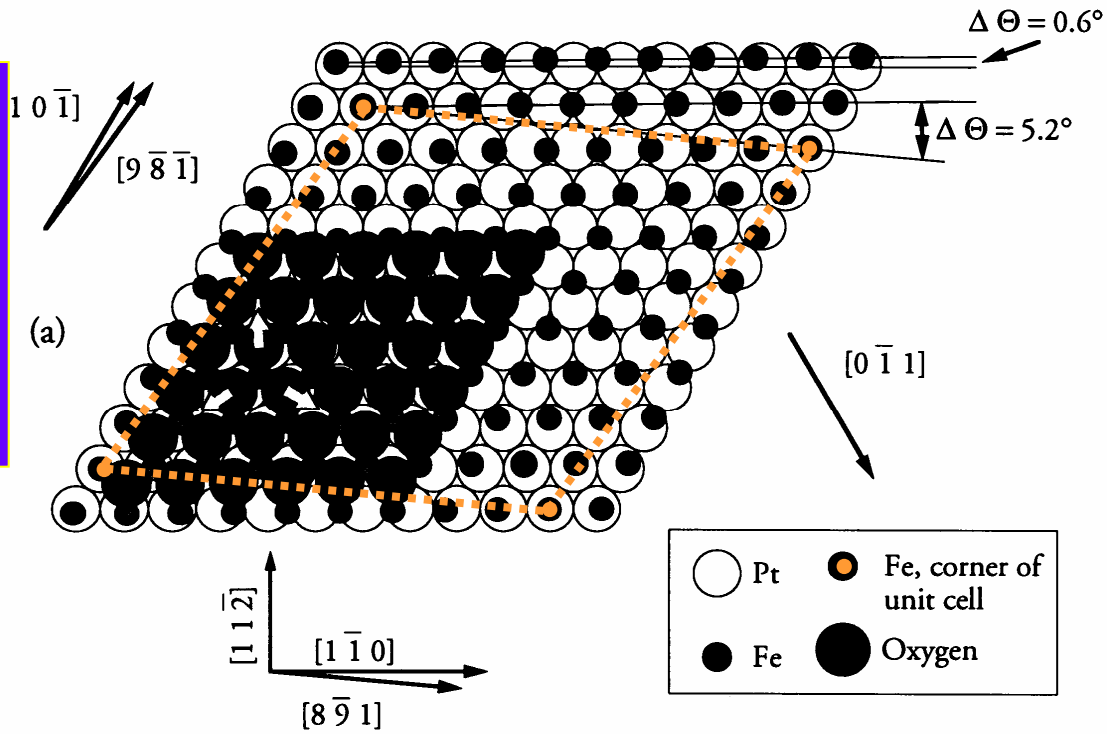

Remaining Questions:

-Is Fe or O on top?

-Fe-O interlayer spacing?

-Fe-O orientation?

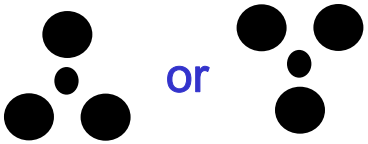

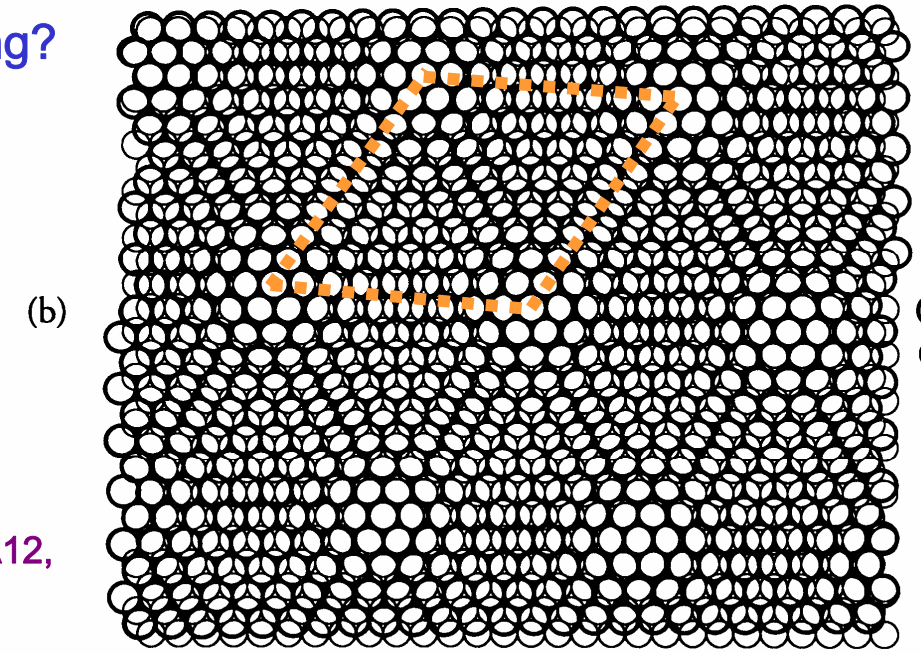

Superlattice or Moiré structure

Galloway et al., Surf. Sci. 198, 127 ('93); J. Vac. Sci. Tech. A12, 2302 ('94).

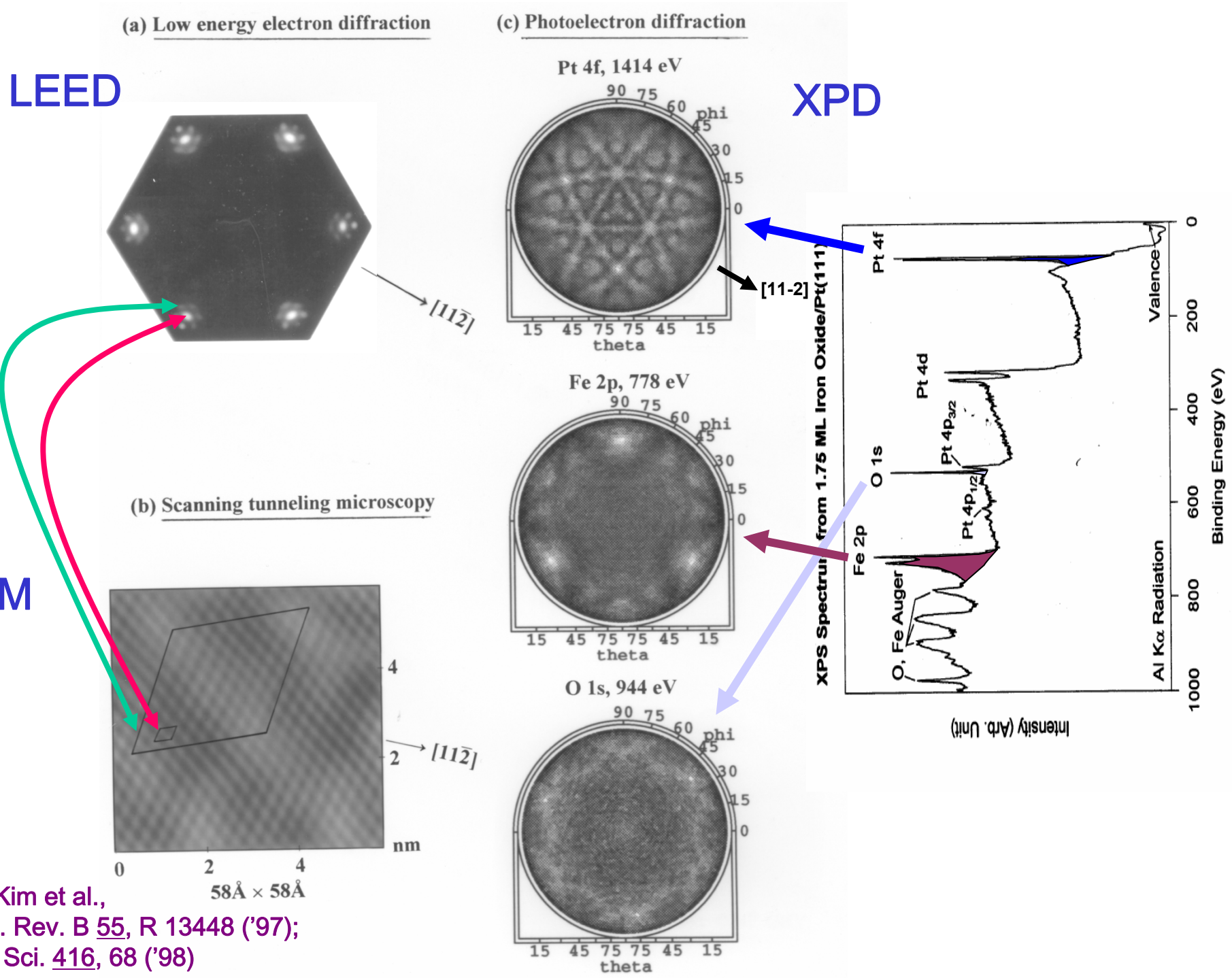

Y.J. Kim et al.,
Phys. Rev. B 55, R 13448 ('97);
Surf. Sci. 416, 68 ('98)

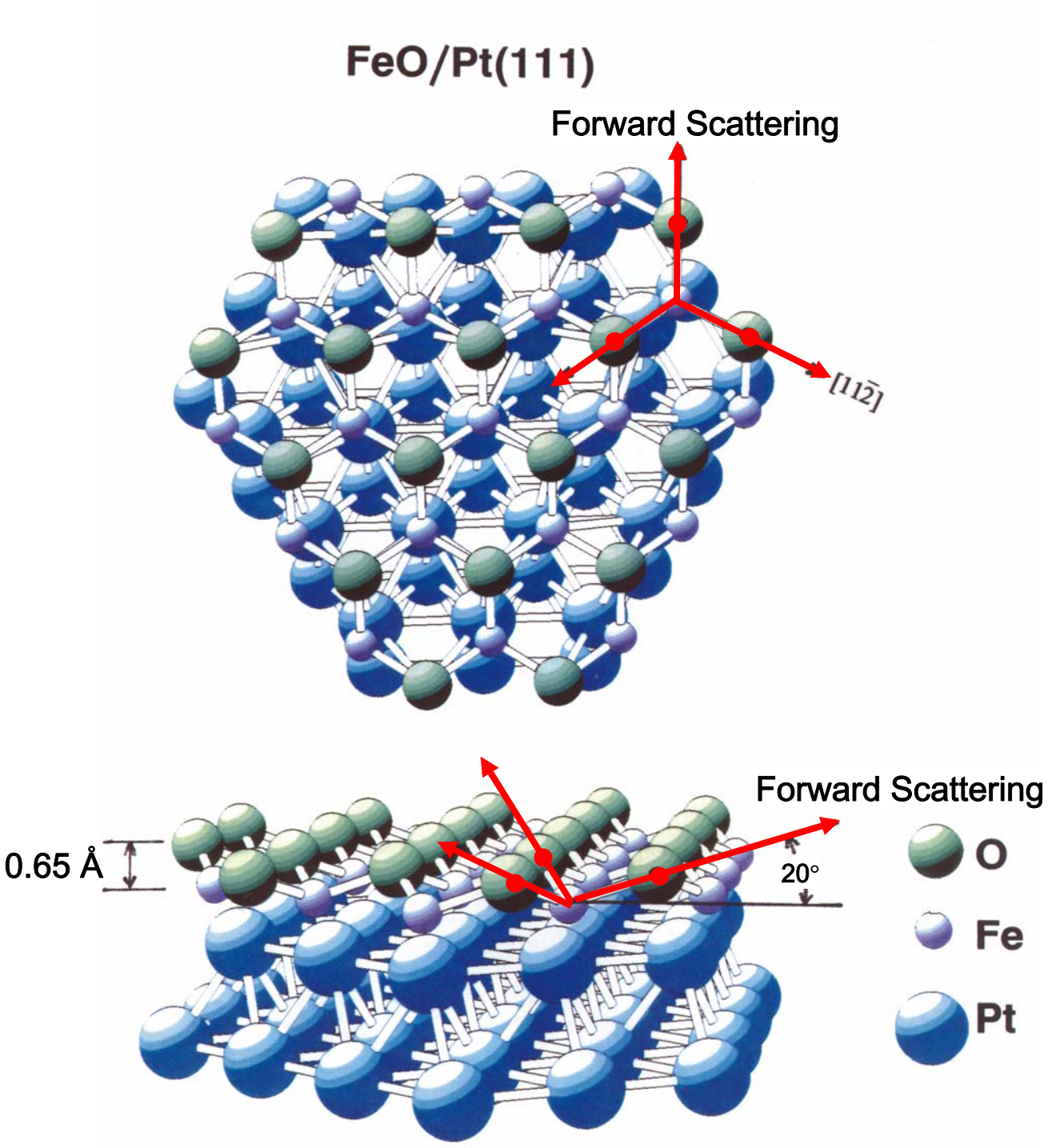
FeO/Pt(111)
Forward Scattering
[11$\bar{2}$]
Forward Scattering
0.65 Å
20°
O
Fe
Pt

X-ray Photoelectron Diffraction: Fe 2p from 1ML FeO on Pt(111)

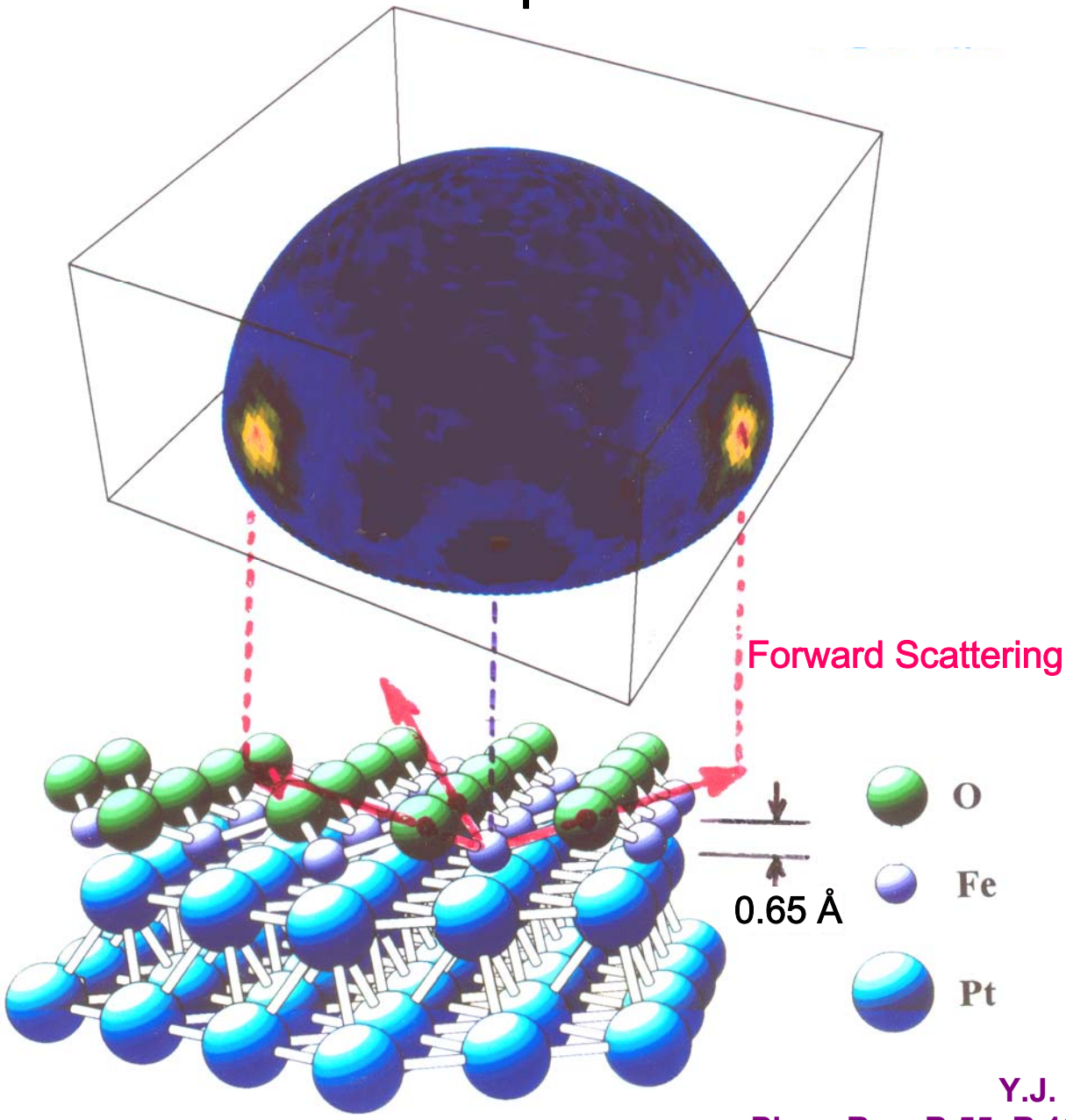

Y.J. Kim et al.
Phys. Rev. B 55, R 13448 ('97)

Permits selecting favored domain of growth—2nd layer Pt effect

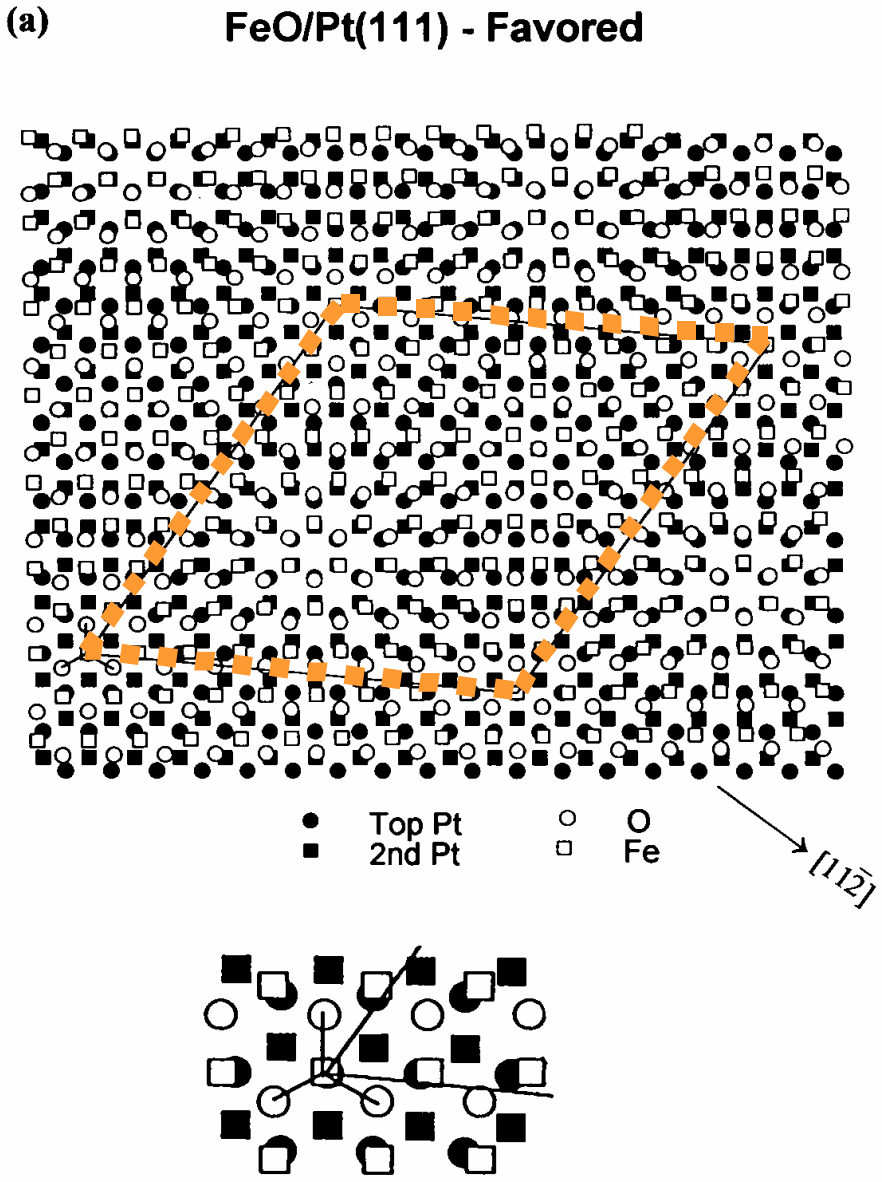

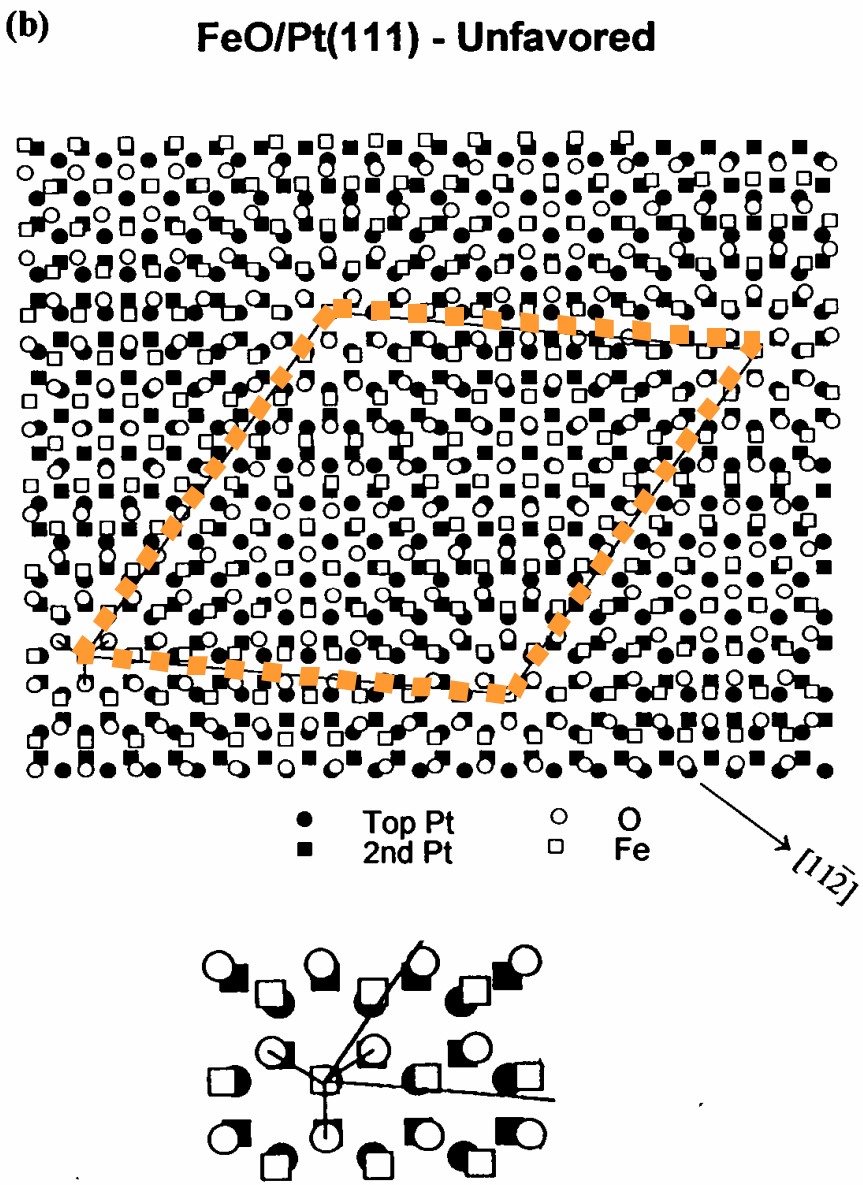

SCANNED-ENERGY PHOTOELECTRON DIFF.

$(\sqrt{3}\times\sqrt{3})$ AL ON Si(111)

* 41 diffraction curves χ taken from Al 2p
* $\theta = 0 \sim 70°$, $\varphi = 0 \sim 60°$

} ~1100 DATA POINTS

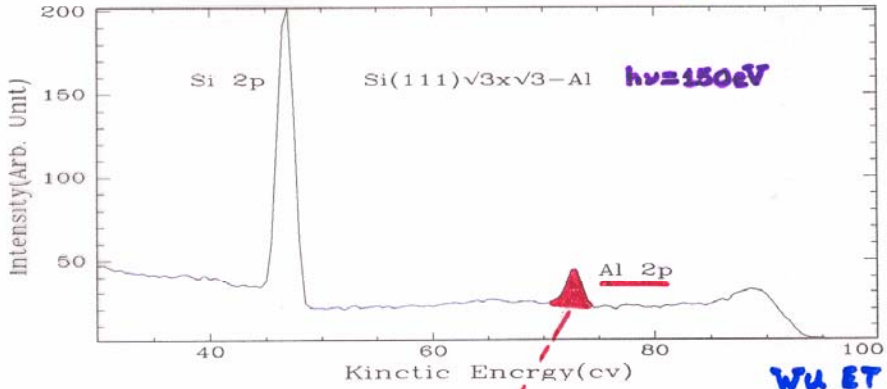

WU ET AL., P.R.L. 71, 261('93) P.R.B 51, 14549('95)

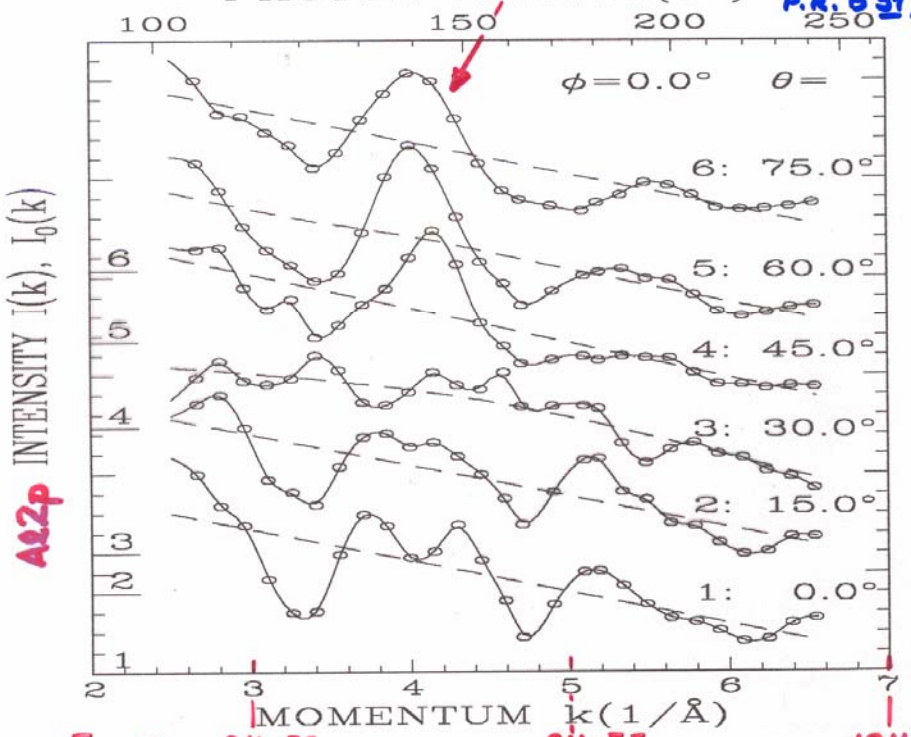

E_{kin}= 34 eV 94 eV 184 eV

Photoelectron diffraction: Simple single-scattering theory for s-subshell emission

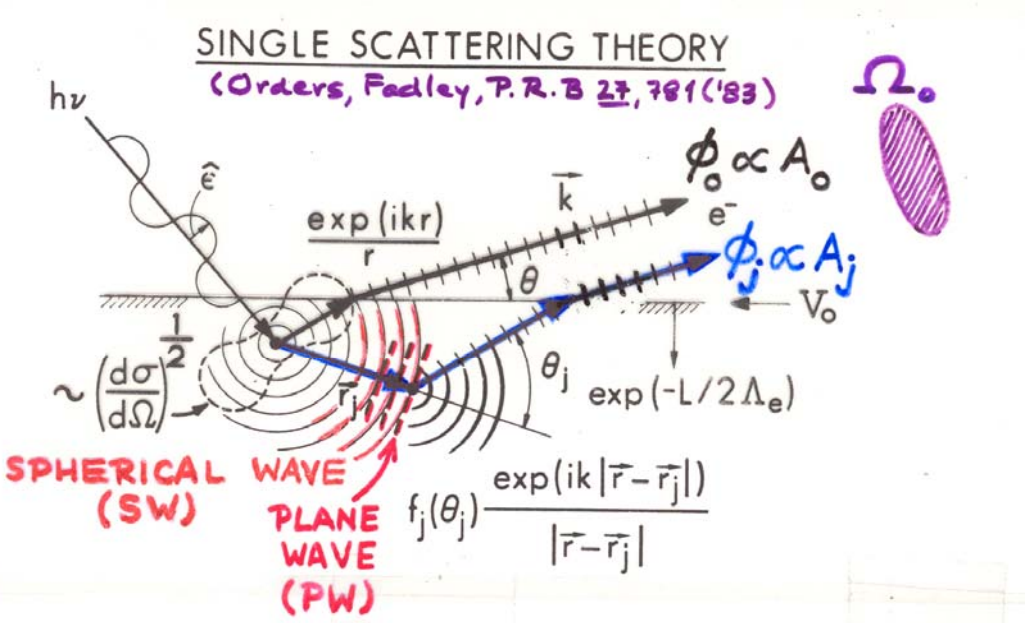

$$\chi(E \text{ or } \vec{k}) \propto \sum_{j\,(\text{CLUSTER})} \frac{F_j(k)}{F_0} \cos\left[k r_j (1-\cos\theta_j) + \Psi_j(\theta_j, k) \right]$$

PATH LENGTH DIFFERENCE (P.L.D.)

SCATTERING PHASE SHIFT

ELASTIC e⁻–ATOM SCATTERING

DEBYE-WALLER

INELASTIC e⁻–e⁻ SCATTERING

$$F_j(k) = (\hat{\varepsilon}\cdot\hat{r}_j)\frac{|f_j(\theta_j,k)|}{r_j} W_j(\theta_j,k) \exp(-L_j/2\Lambda_e)$$

= amplitude of scattered wave

$$F_0 = (\hat{\varepsilon}\cdot\hat{k}) \exp(-L_0/2\Lambda_e)$$

= amplitude of direct wave

∴ FOURIER TRANSFORM OF $\chi(k) \Rightarrow$ PEAKS AT ~ P.L.D. $= r_j(1-\cos\theta_j)$

PATH-LENGTH DIFF'S. FROM FOURIER TRANSFORMS*

c(2x2)S/Cr(001): 45° off normal

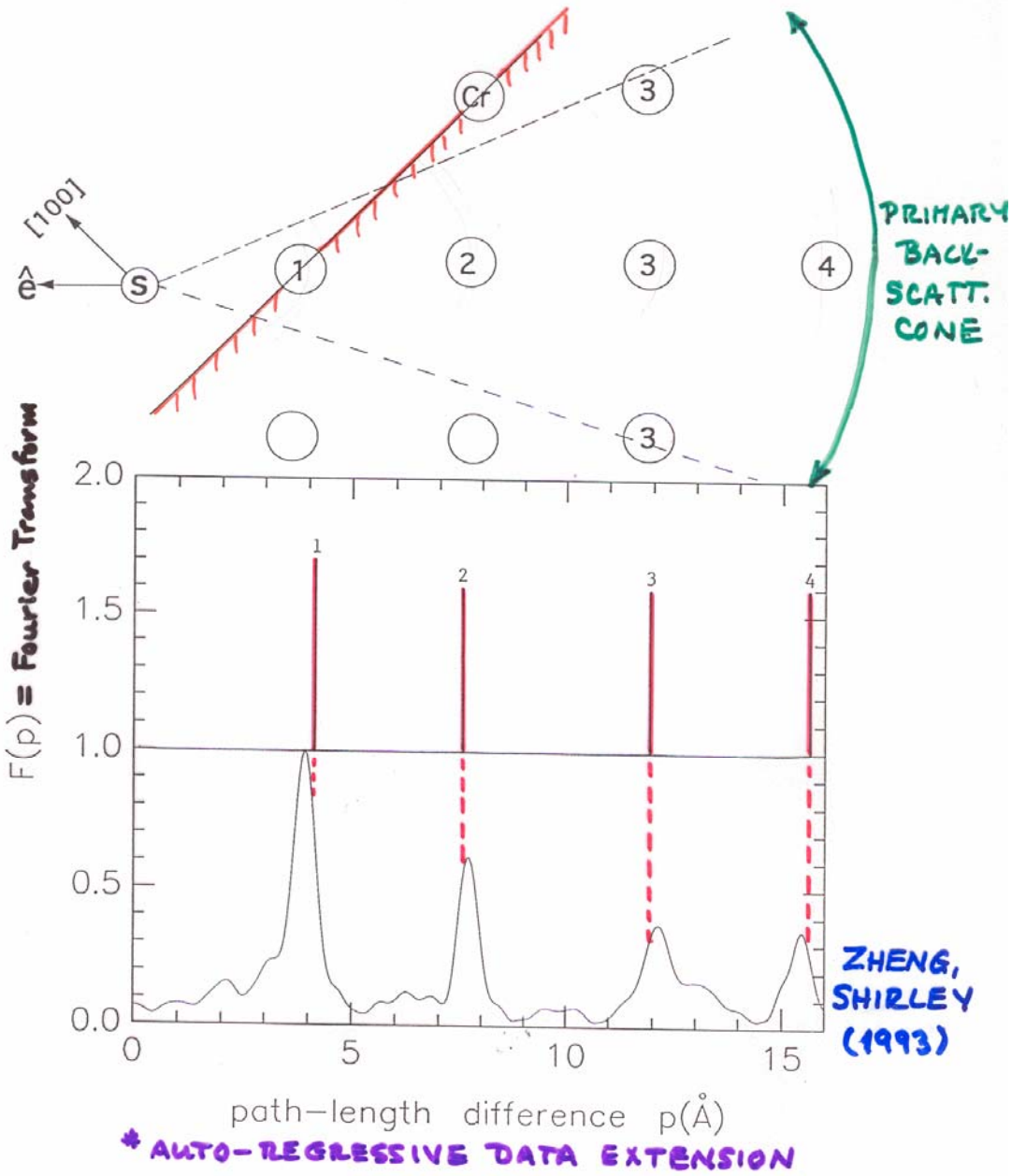

ZHENG, SHIRLEY (1993)

* AUTO-REGRESSIVE DATA EXTENSION

Outline

Surface, interface, and nanoscience—short introduction

Some surface concepts and techniques→photoemission

Synchrotron radiation: experimental aspects

Electronic structure—a brief review

The basic synchrotron radiation techniques:
more experimental and theoretical details

Core-level photoemission:

X-ray optical effects on intensities

Valence-level photoemission

Microscopy with photoemission

PHOTOELECTRON INTENSITIES—THE 3-STEP MODEL

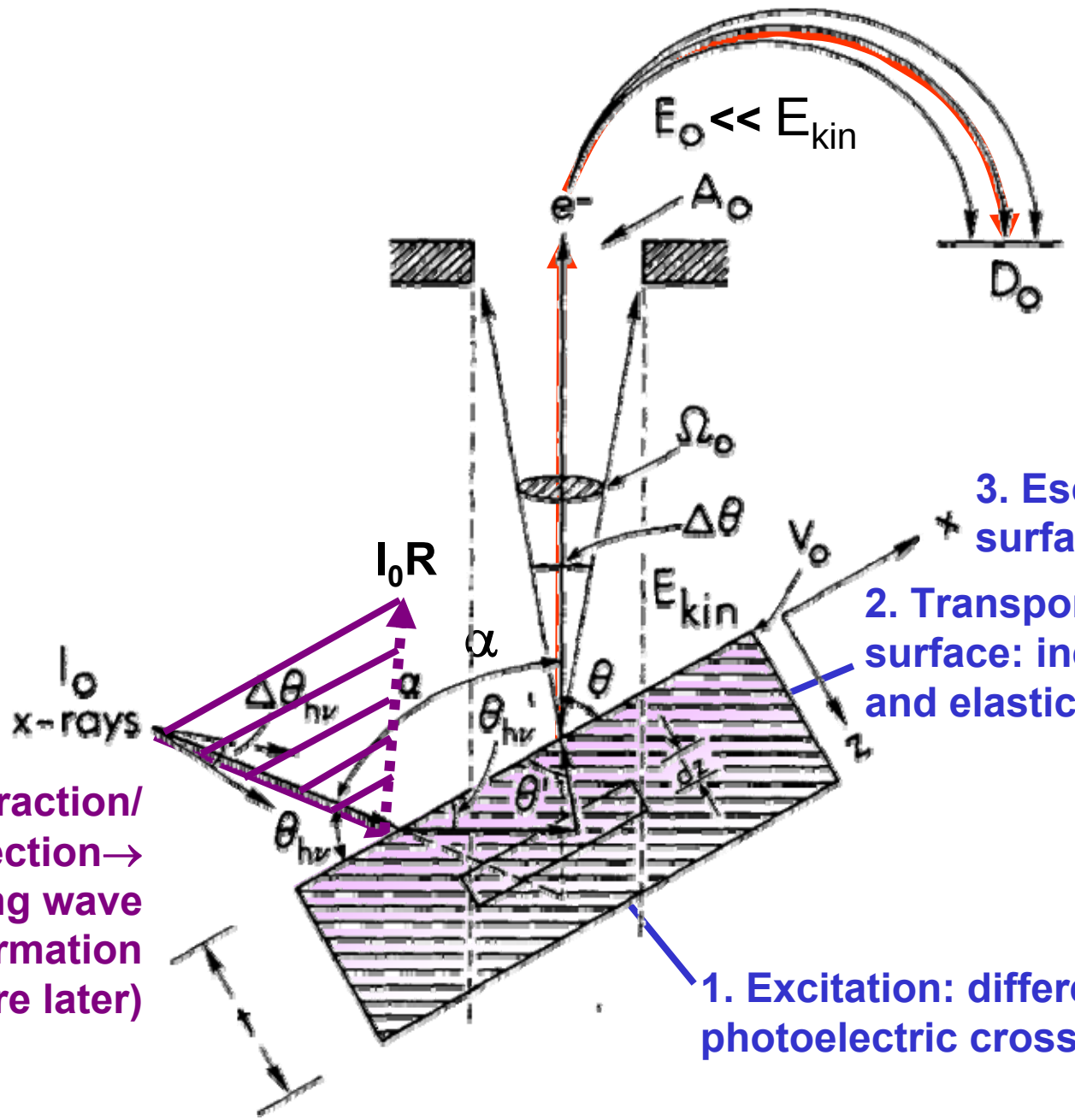

3. Escape across the surface barrier (V_0)

2. Transport to the surface: inelastic (Λ_e) and elastic ($f(\theta)$) scattering

+X-ray refraction/ reflection→ standing wave formation (more later)

1. Excitation: differential photoelectric cross section ($d\sigma/d\Omega$)

Some basic measurements:

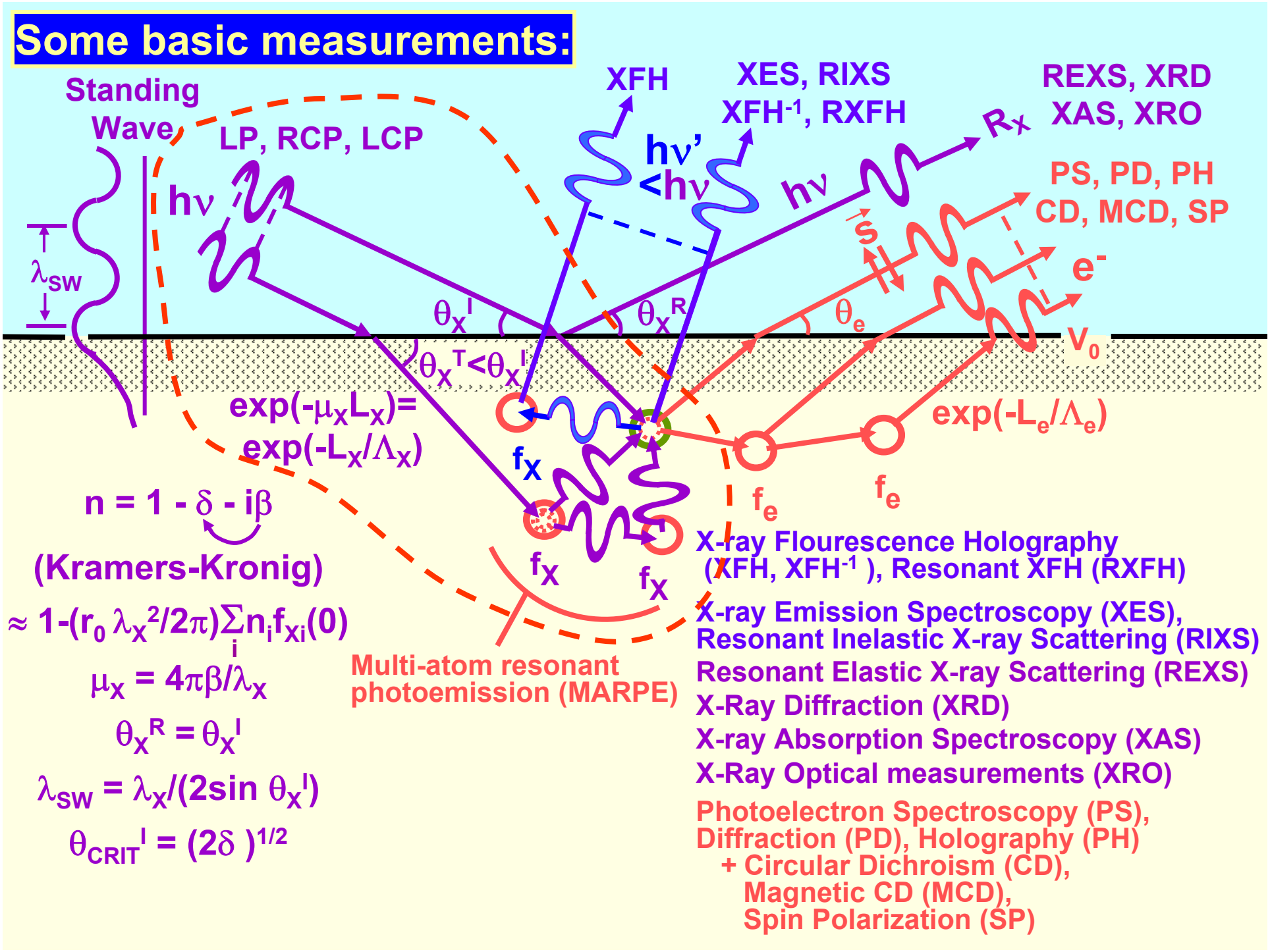

A LITTLE X-RAY OPTICS

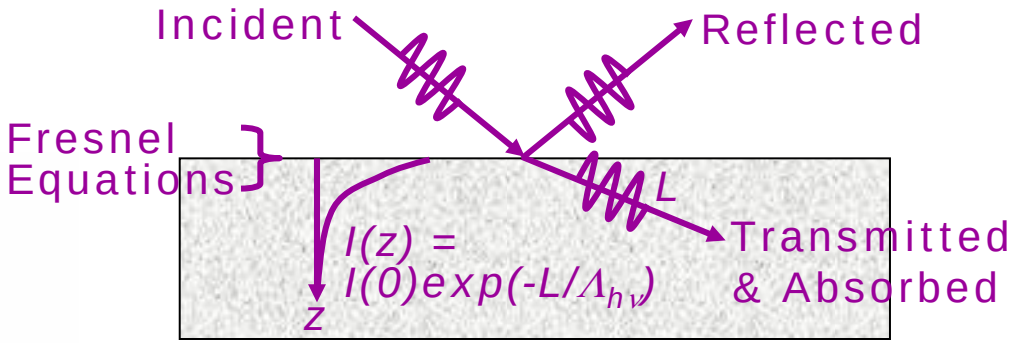

(E.G. See pp. 1-38, 1-44, 5-18-5-19 in X-Ray Data Booklet)

Index of refraction = n = 1 - δ - iβ

δ = + no. = refractive decrement << 1 (Sometimes negative through absorption resonances)

β = + no. = absorptive decrement << 1

δ and β linked by Kramers-Kronig transform

n also = 1 – $(r_e/2\pi)\lambda_{h\nu}^2 \Sigma n_i f_i$(0=fwd. scatt.)

r_e = classical electron radius
$= e^2/4\pi\varepsilon_0 m_e e^2 = 2.817 \times 10^{-15}$ m
$\lambda_{h\nu}$ = x-ray wavelength

n_i = no. i atoms per unit volume

f_i = x-ray scattering factor for ith type of atom, in forward direction

Exponential absorption length = $l_{abs} = \lambda_{h\nu}/(4\pi\beta) = \Lambda_{h\nu}$

θ_{CRIT} = critical grazing angle at which reflectivity begins ($R \approx 0.20$)
$= [2\delta]^{0.5}$

Online data and calculations at:
http://www-cxro.lbl.gov/optical_constants/

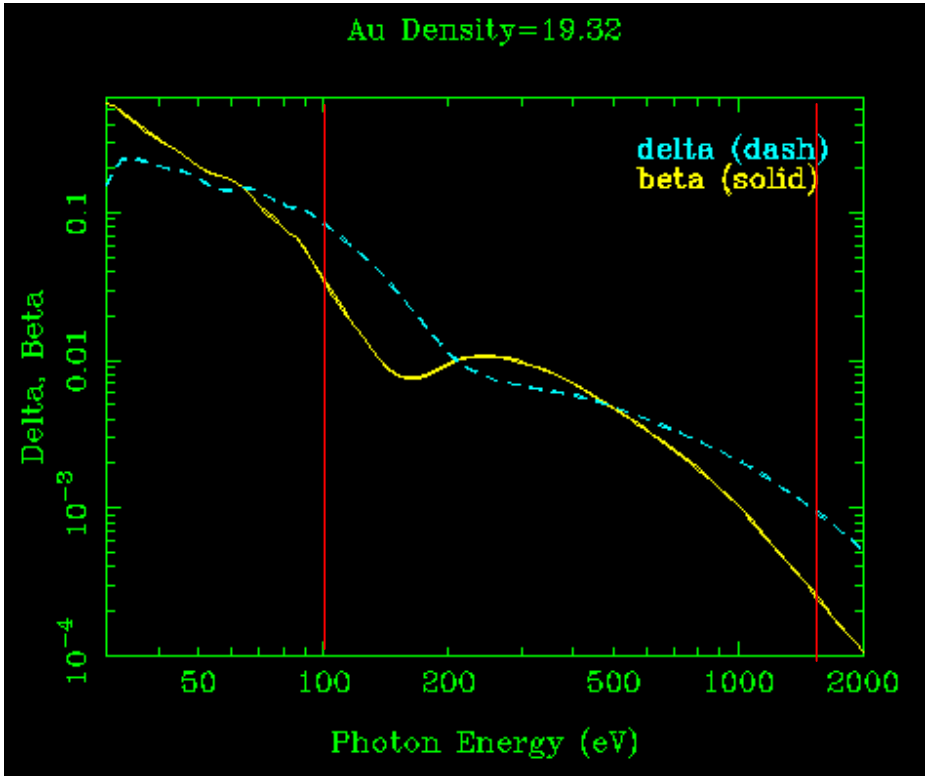

X-ray scattering factor:
$f_i = Ref_i + i(Imf_i)$

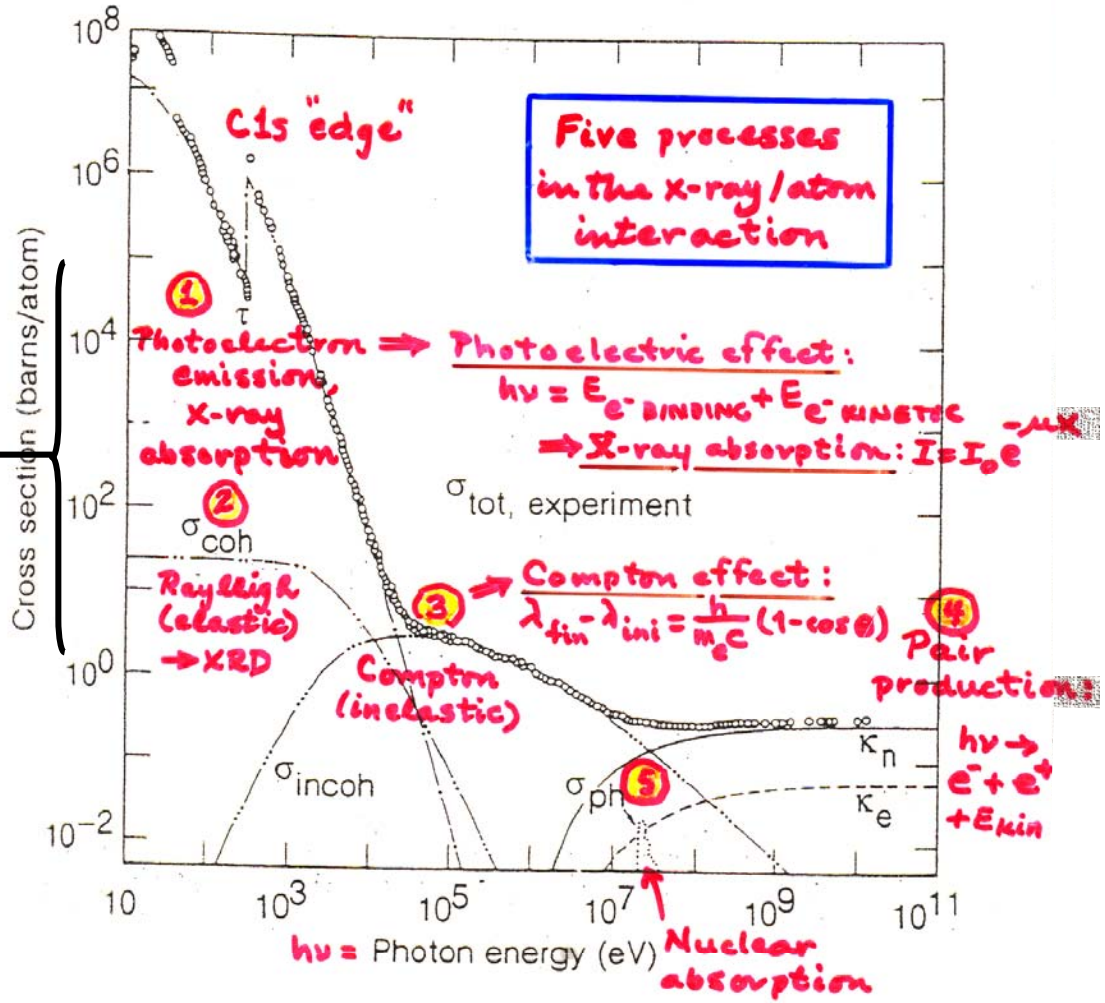

Fig. 3-1. *Total photon cross section σ_{tot} in carbon, as a function of energy, showing the contributions of different processes: τ, atomic photo-effect (electron ejection, photon absorption); σ_{coh}, coherent scattering (Rayleigh scattering—atom neither ionized nor excited); σ_{incoh}, incoherent scattering (Compton scattering off an electron) κ_n, pair production, nuclear field; κ_e, pair production, electron field; σ_{ph}, photonuclear absorption (nuclear absorption usually followed by emission of a neutron or other particle). (From Ref. 5; figure courtesy of J. H. Hubbell.)*

http://www-cxro.lbl.gov/optical_constants/

Website

X-Ray Interactions with Matter

Contents

These pages utilize *JavaScript*, but the decaffeinated versions are still available.

Reference

B.L. Henke, E.M. Gullikson, and J.C. Davis. *X-ray interactions: photoabsorption, scattering, transmission, and reflection at E=50-30000 eV, Z=1-92*, Atomic Data and Nuclear Data Tables Vol. **54** (no.2), 181-342 (July 1993).

By Eric Gullikson. Please direct any comments to EMGullikson@lbl.gov

SOME X-RAY OPTICAL EFFECTS: REDUCED PENETRATION DEPTHS AND INCREASED REFLECITIVITY AT GRAZING INCIDENCE ANGLES

θ_{CRIT} = Grazing angle at which reflectivity begins ($R \approx 0.20$)

$= [2\delta]^{0.5}$

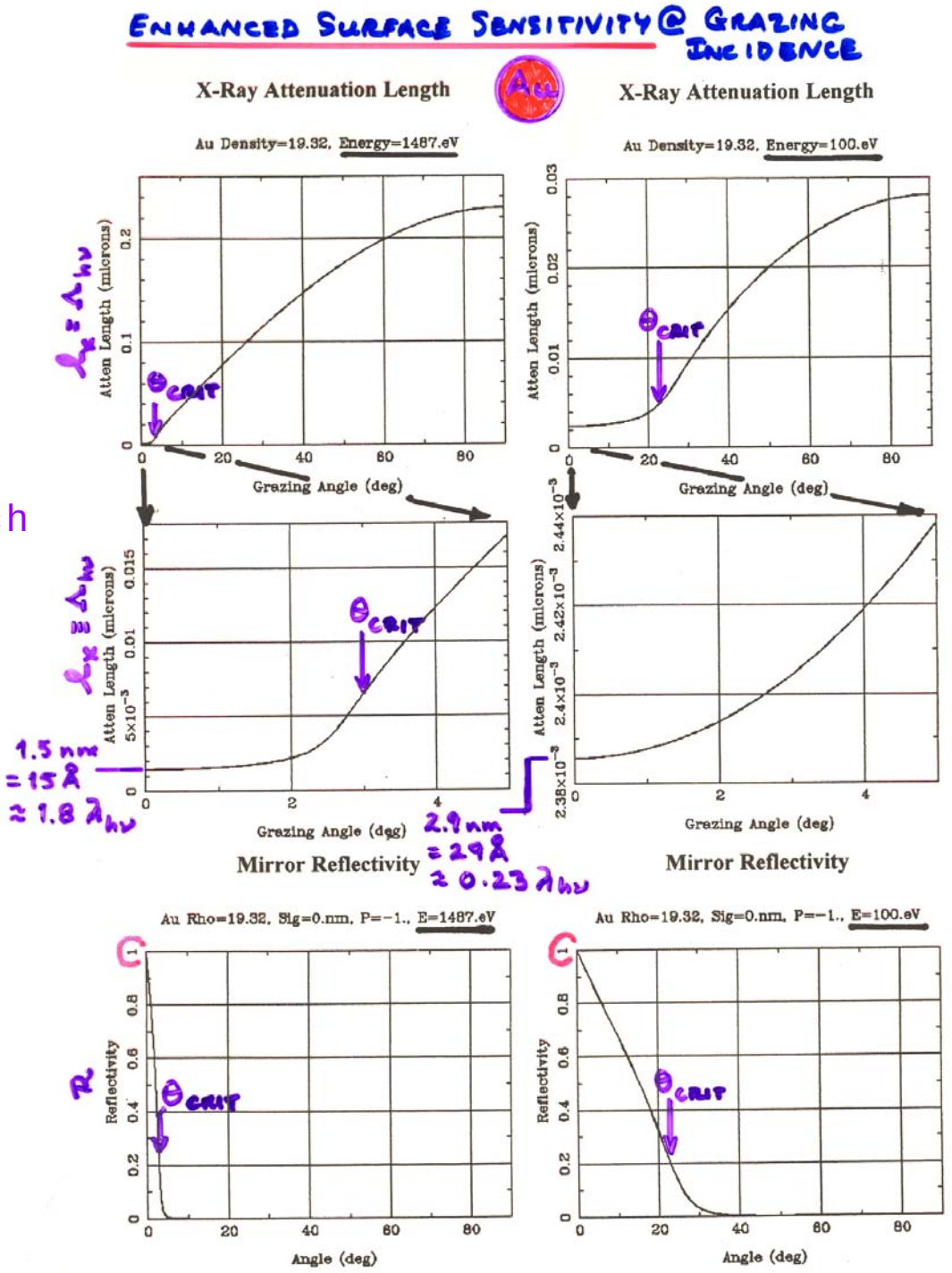

Optical constants through Mn 2p edges of MnO—
Web data <u>without absorption peaks</u>

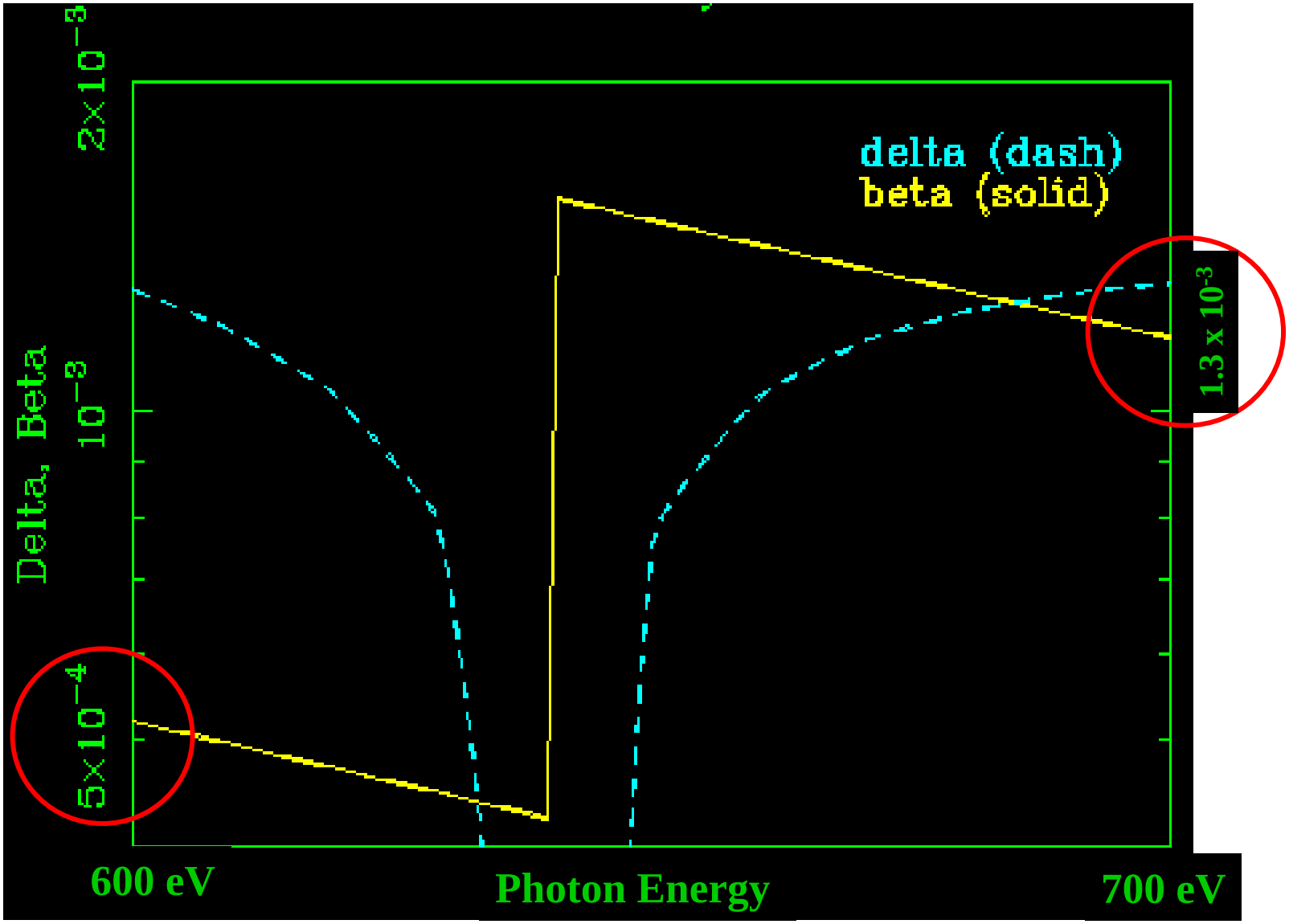

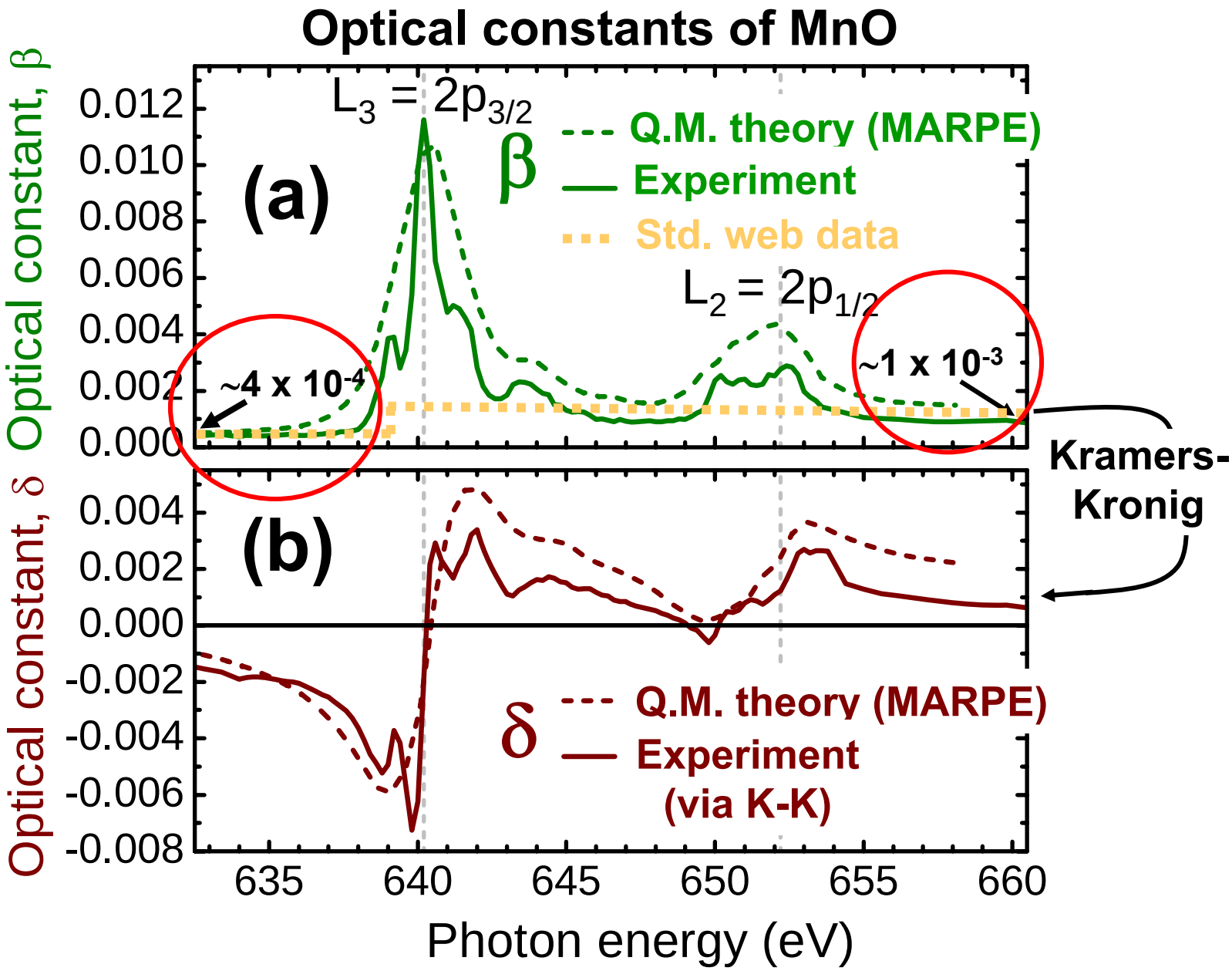
Optical constants of MnO
Optical constant, β
Optical constant, δ
0.012
0.010
0.008
0.006
0.004
0.002
0.000
L3 = 2p3/2
(a)
β
Q.M. theory (MARPE)
Experiment
Std. web data
L2 = 2p1/2
~4 x 10-4
~1 x 10-3
Kramers-Kronig
(b)
0.004
0.002
0.000
-0.002
-0.004
-0.006
-0.008
δ
Q.M. theory (MARPE)
Experiment
(via K-K)
635
640
645
650
655
660
Photon energy (eV)

X-ray optical effects through core resonances:

(a)

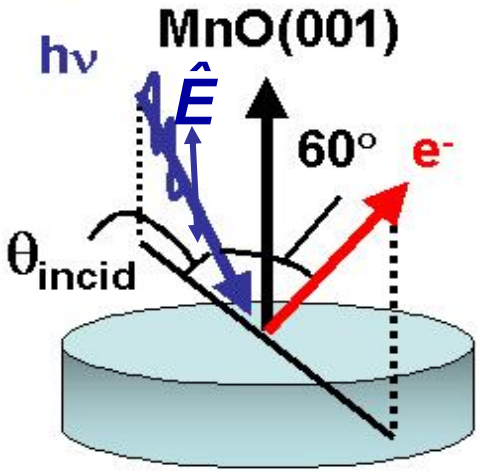

(b)

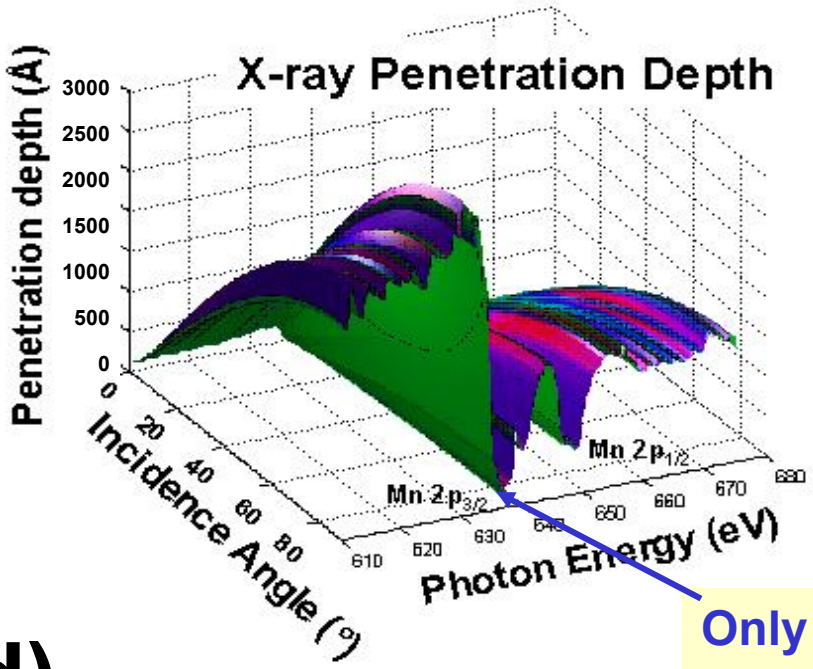

Only approx. 130 Å at normal incidence

(c)

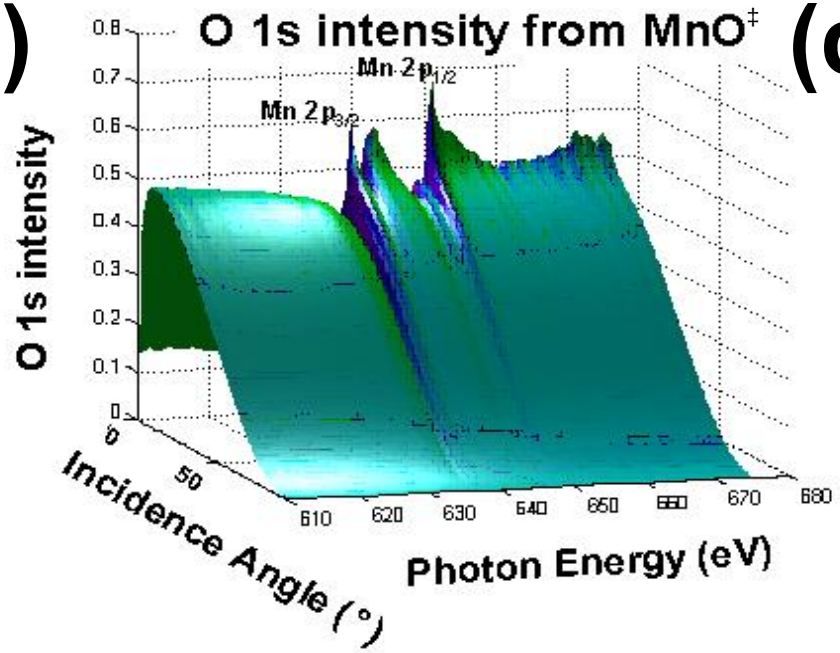

(d)

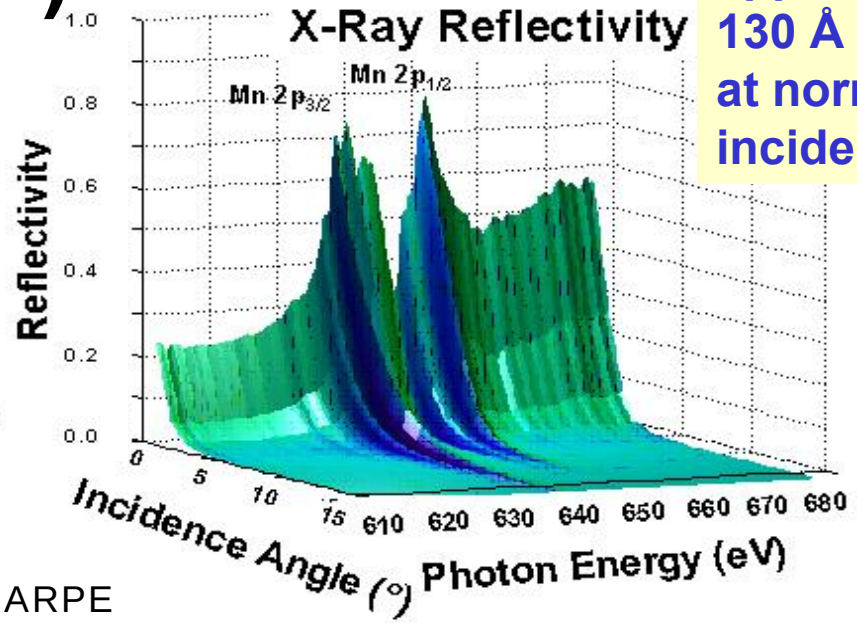

‡Aka Multi-Atom Resonant Photoemission = MARPE

Outline

Surface, interface, and nanoscience—short introduction

Some surface concepts and techniques→photoemission

Synchrotron radiation: experimental aspects

Electronic structure—a brief review

The basic synchrotron radiation techniques

Core-level photoemission
X-ray optical effects on emission→
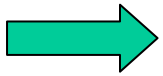
Use of standing waves to probe buried interfaces

Valence-level photoemission

Microscopy with photoemission

Standing wave formation:

$I_{SW}(|E^2|) \propto |\phi_{inc} + \phi_{refl}|^2$
$= |\phi_{inc}|^2 + \underbrace{\phi_{inc}\phi_{refl}^* + \phi_{inc}^*\phi_{refl}}_{\text{SW modulation}} + |\phi_{refl}|^2$

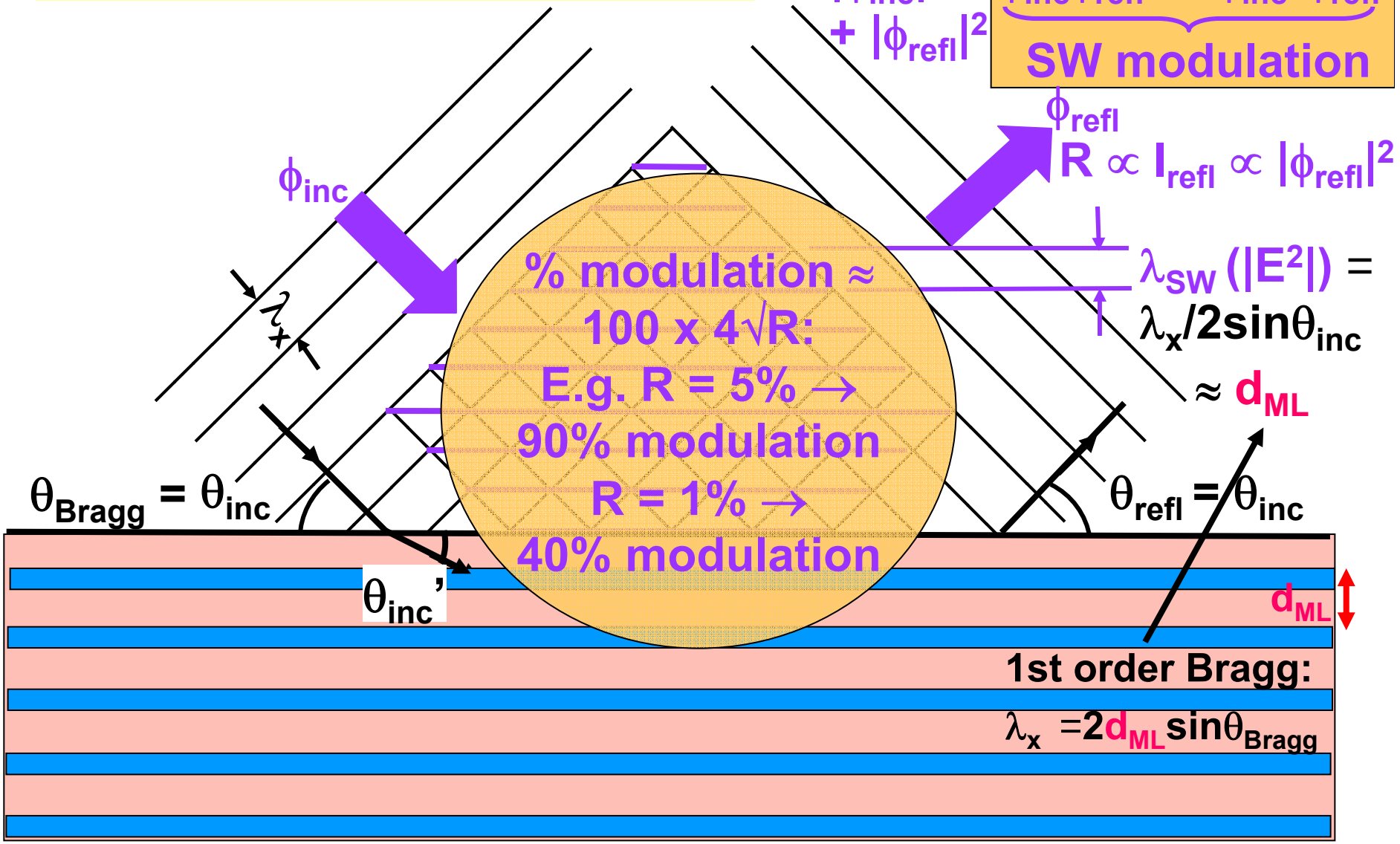

Periodic atomic planes: $d_{ML} \leq$ ~5 Å--Si(111)—≤3.74Å, LaB_{66}(001) --≤23.52Å→5.88Å, mica—10.0 Å; or Synthetic multilayers: $d_{ML} \approx$ ~20-40 Å

Standing wave formation in reflection from a surface, or single-crystal Bragg planes[+], or a multilayer mirror

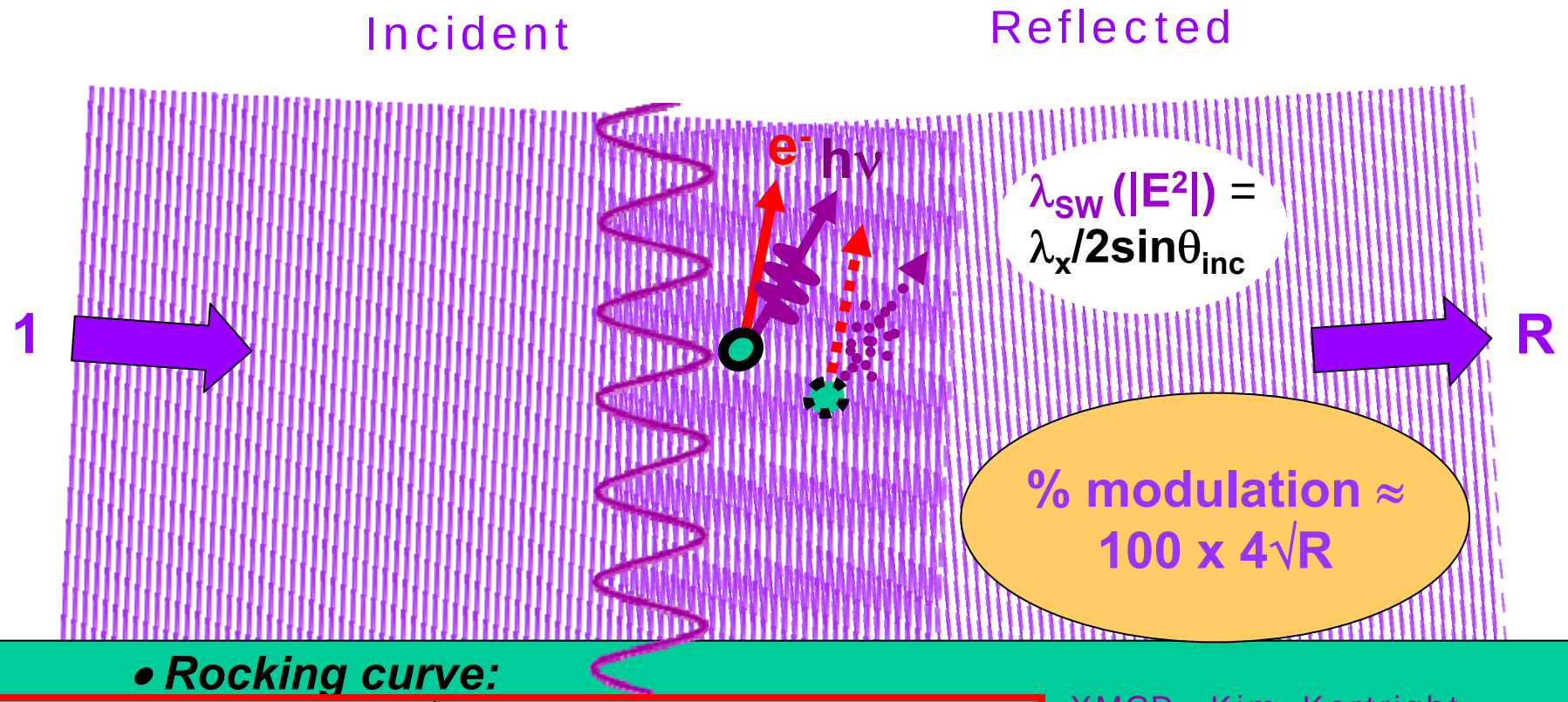

- ***Rocking curve:***

$$I(\theta_{inc}) \propto 1 + R(\theta_{inc}) + 2\sqrt{R(\theta_{inc})}\, f \cos[\varphi(\theta_{inc}) - 2\pi P]$$

XMCD—Kim, Kortright, PRL 86, 1347 (2001)

- ***Energy scan:***

$$I(h\nu) \propto 1 + R(h\nu) + 2\sqrt{R(h\nu)}\, f \cos[\varphi(h\nu) - 2\pi P]$$

with: f = coherent fraction of atoms, P = phase of coherent-atom position

- ***Phase scan with wedge-shaped sample ("Swedge" method):***

[+]Standing waves via Bragg reflection of hard x-rays: Batterman, Phys. Rev A 133, 759 (1964)

PHOTOELECTRON (OR X-RAY EMISSION) INTENSITIES AND COMPOSITION

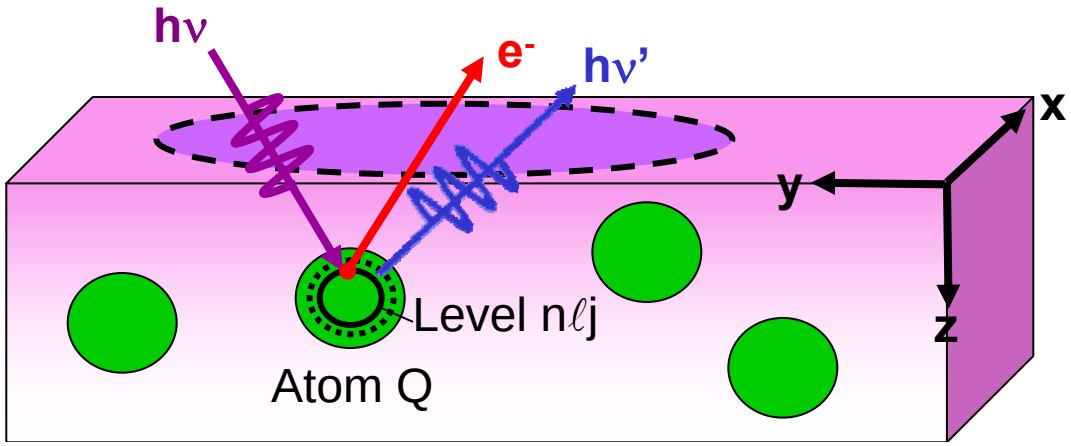

$$I(Qn\ell j) =$$

$$C\int_0^{\infty} |\vec{E}(x,y,z)|^2 \rho_Q(x,y,z) \frac{d\sigma_{Qn\ell j}(h\nu)}{d\Omega} exp\left[-\frac{z}{\Lambda_{e(x)}\sin\theta}\right] \Omega(h\nu,x,y)dxdydz$$

$|\vec{E}(x,y,z)|^2$ = *x-ray intensity, incl. standing wave modulation*

$\rho_Q(x,y,z)$ = *density of atoms Q* $\rightarrow$ *quantitative analysis*

$\frac{d\sigma_{Qn\ell j}(h\nu)}{d\Omega}$ = *differential photoelectric (or x – ray emission) cross section for subshell* $Qn\ell j$

$\Lambda_{e(x)}$ = *inelastic attenuation length for electrons or x – rays*

$\Omega(h\nu,x,y)$ = *spectrometer acceptance solid angle*

X-ray Optical Calculations :

Calculating XRO effects on spectroscopy--Yang

- n (hν) =
1 -δ (hν) + iβ(hν)

-variable polarization

-multiple reflection/ refraction

-exact treatment of interlayer intermixing a/o roughness

-electric field at i-th layer:

$$|E_{SW,i}(z)|^2 = |E_i^+(z) + E_i^-(z)|^2$$

Photoemission:

-differential cross section

-inelastic attenuation

-surface refraction

X-ray emission:

-fluorescence yield

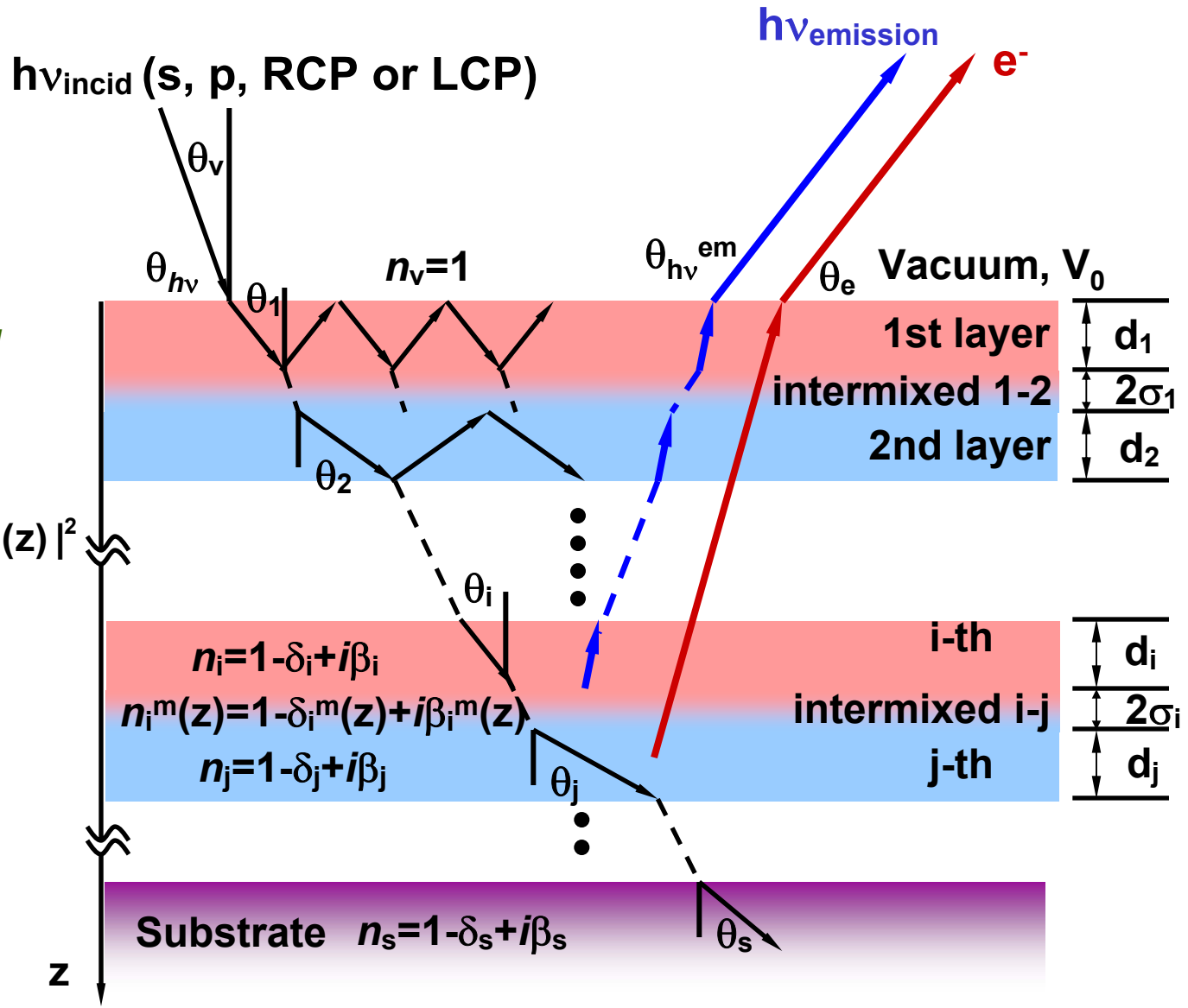

Multilayer PS, XES--S.-H. Yang et al., Surf.Sci.Lett. 461, L557 ('00); J.Phys.C.M. 14, L406 ('02)

Standing Wave Behavior During a Rocking Curve Scan—Emission Intensity from a Surface Atom/Nanolayer

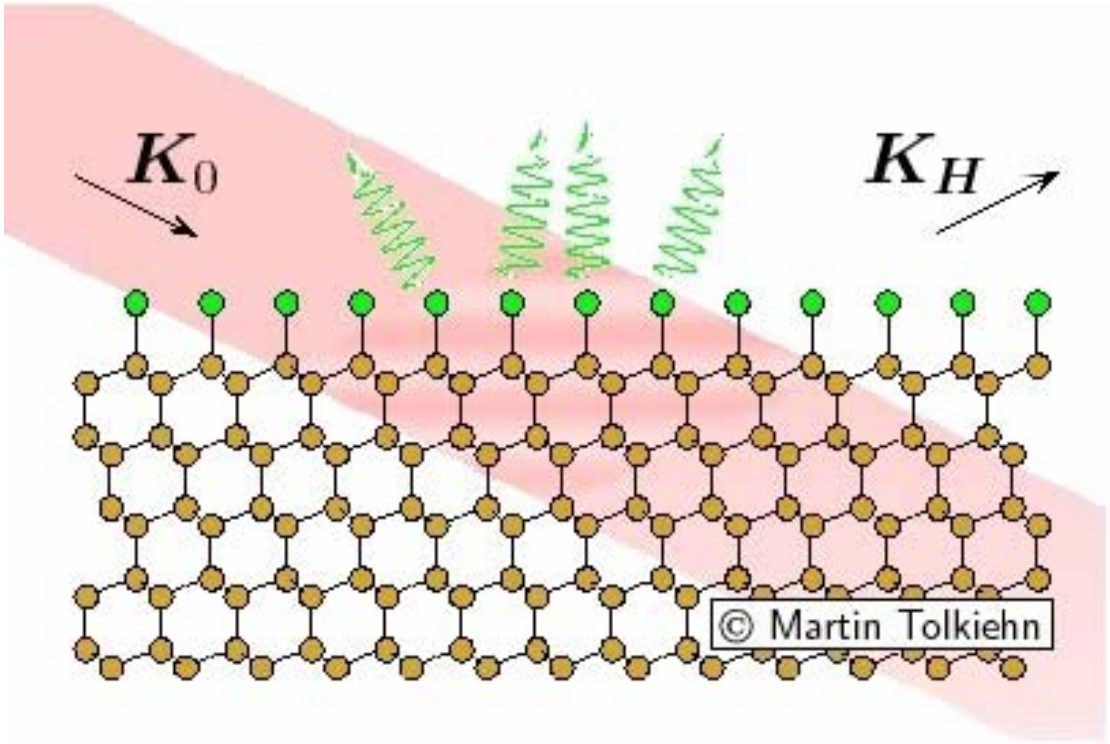

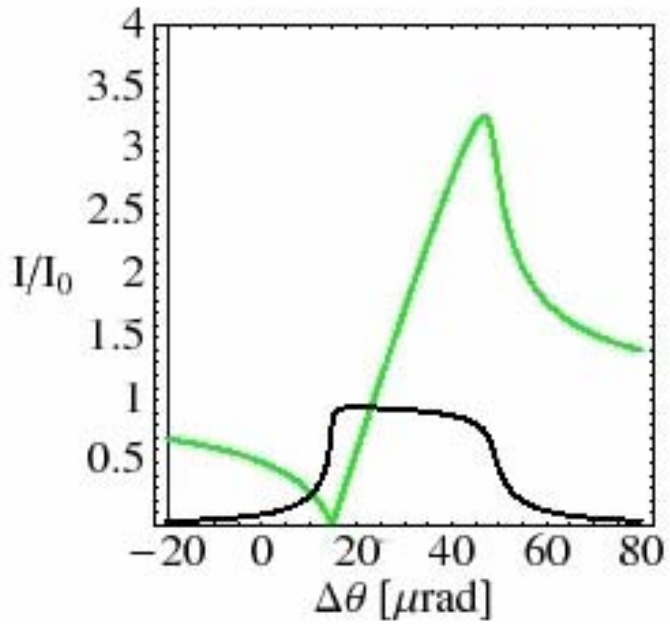

With thanks to Martin Tolkiehn, Diamond
Dimitri Novikov, Hasylab

Various Forms of Rocking Curves—Vertical Shift of Emitter/Nanolayer Position

Reflectivity

Emission intensity profile at different vertical heights

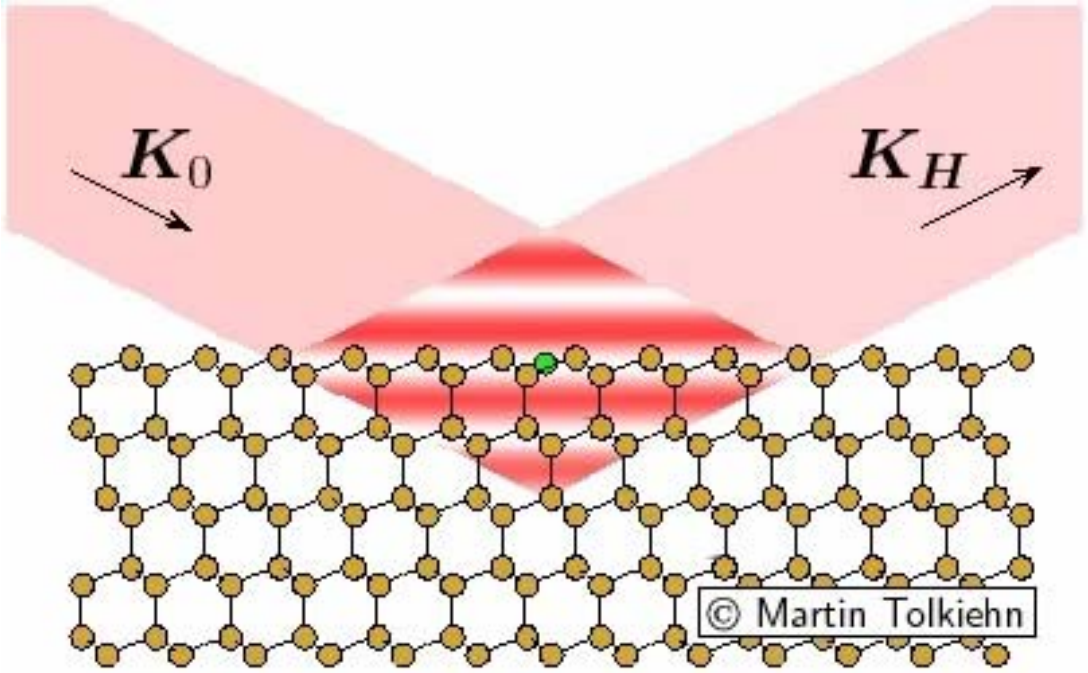

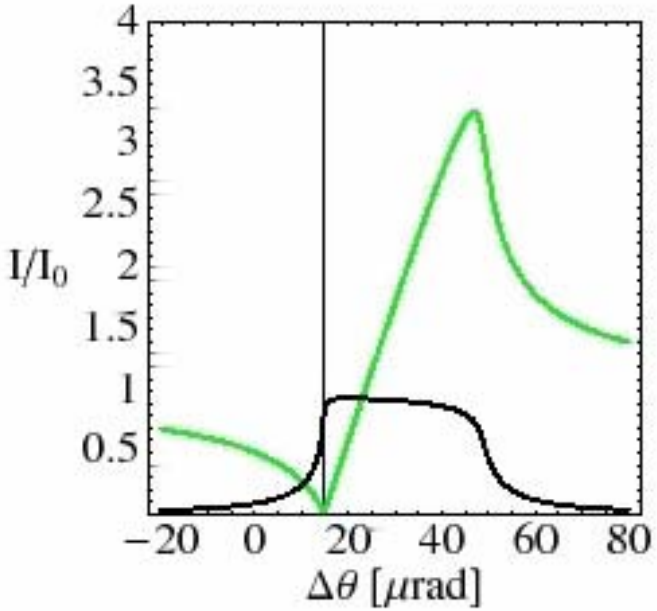

With thanks to Martin Tolkiehn, Diamond
Dimitri Novikov, Hasylab

Standing wave formation in reflection from a surface, or single-crystal Bragg planes[+], or a multilayer mirror

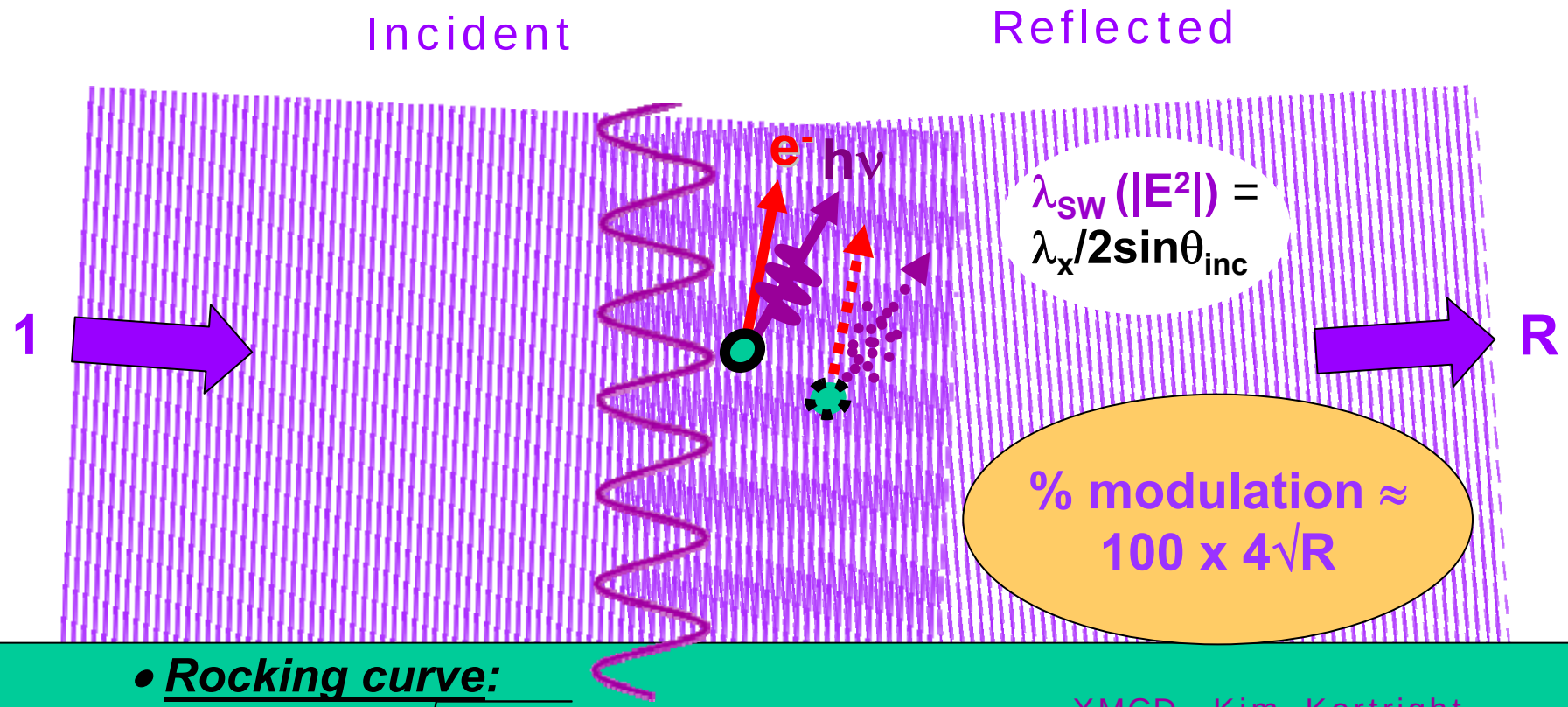

- ***Rocking curve:***

$$I(\theta_{inc}) \propto 1 + R(\theta_{inc}) + 2\sqrt{R(\theta_{inc})}\, f \cos[\varphi(\theta_{inc}) - 2\pi P]$$

XMCD—Kim, Kortright, PRL 86, 1347 (2001)

- ***Energy scan:***

$$I(h\nu) \propto 1 + R(h\nu) + 2\sqrt{R(h\nu)}\, f \cos[\varphi(h\nu) - 2\pi P]$$

with: f = coherent fraction of atoms, P = phase of coherent-atom position

- ***Phase scan with wedge-shaped sample ("Swedge" method):***

[+]Standing waves via Bragg reflection of hard x-rays: Batterman, Phys. Rev A 133, 759 (1964)

PROBING BURIED INTERFACES WITH SOFT X-RAY STANDING WAVES:

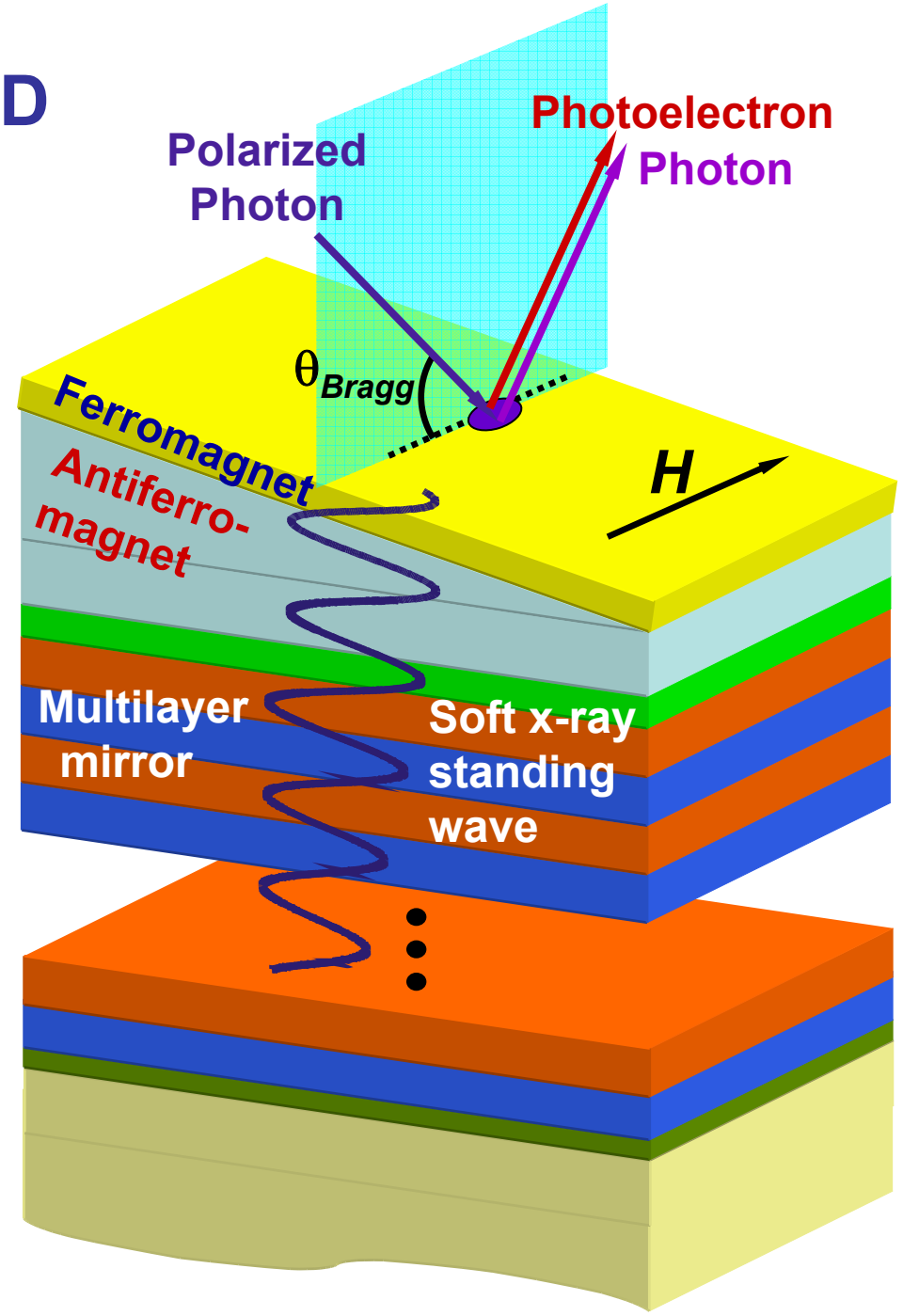

PROBING BURIED INTERFACES WITH SOFT X-RAY STANDING WAVES:

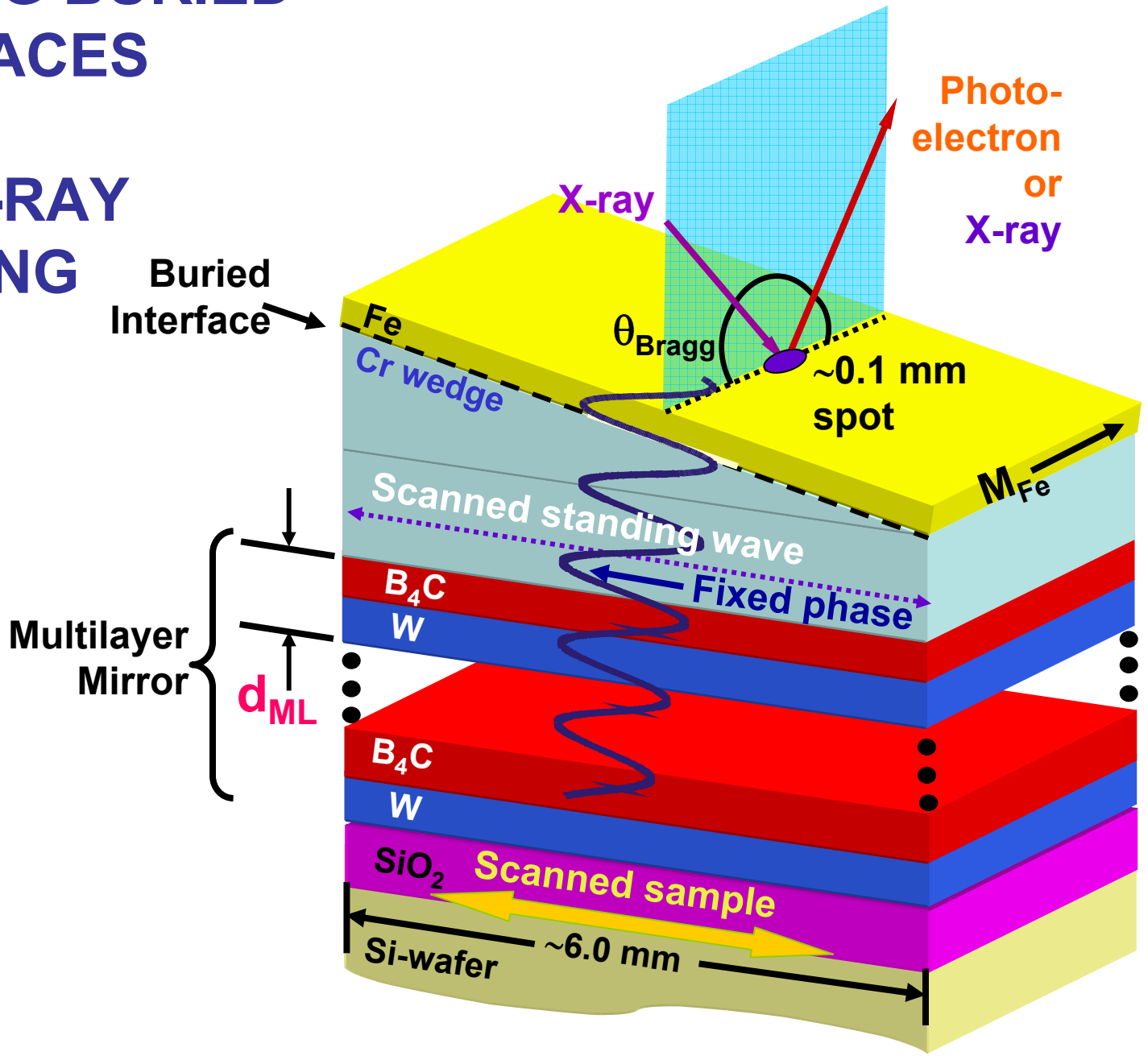

PROBING BURIED INTERFACES WITH SOFT X-RAY STANDING WAVES:

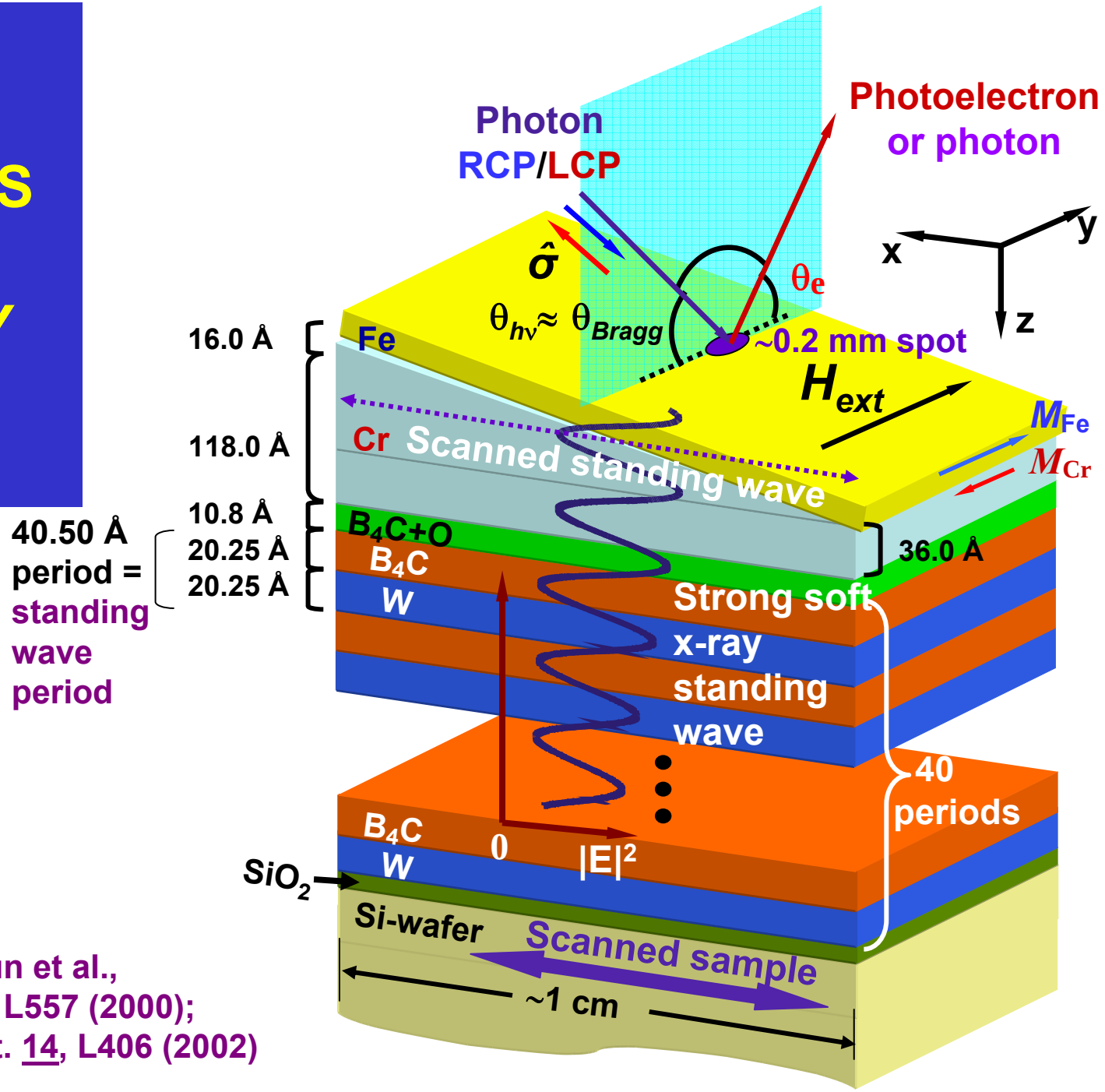

S.-H. Yang. B.S. Mun et al.,
Surf. Sci. Lett. 461, L557 (2000);
J. Phys. Cond. Matt. 14, L406 (2002)

TRANSMISSION ELECTRON MICROSCOPY IMAGE FOR Fe/Cr/MULTILAYER SWG
(Synthesis-CXRO, and Imaging-NCEM, LBNL)

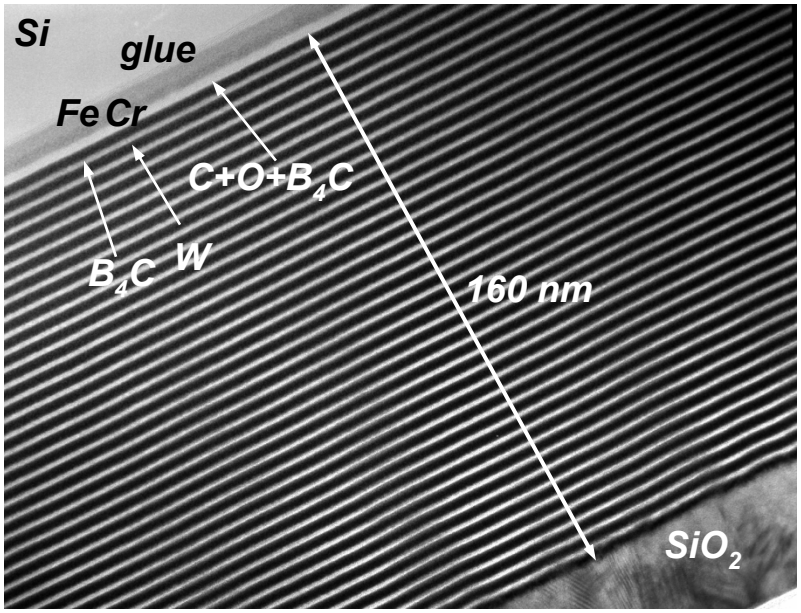

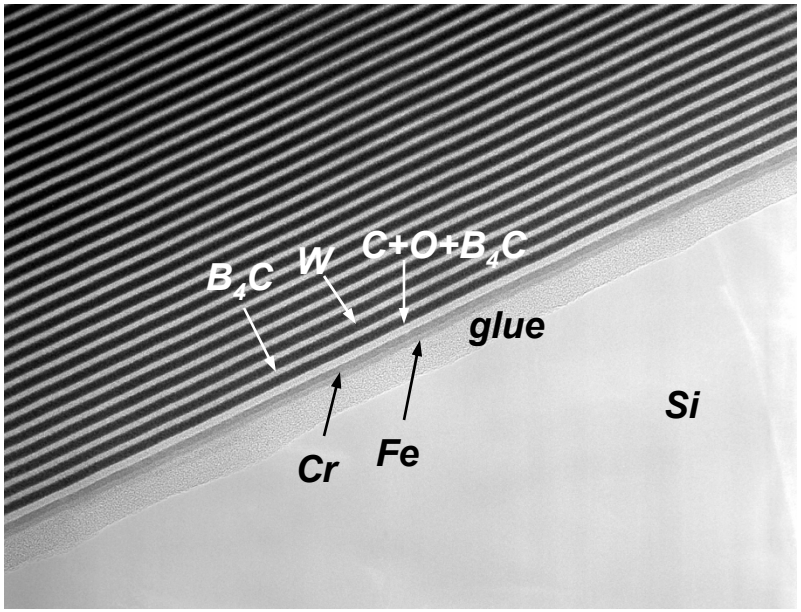

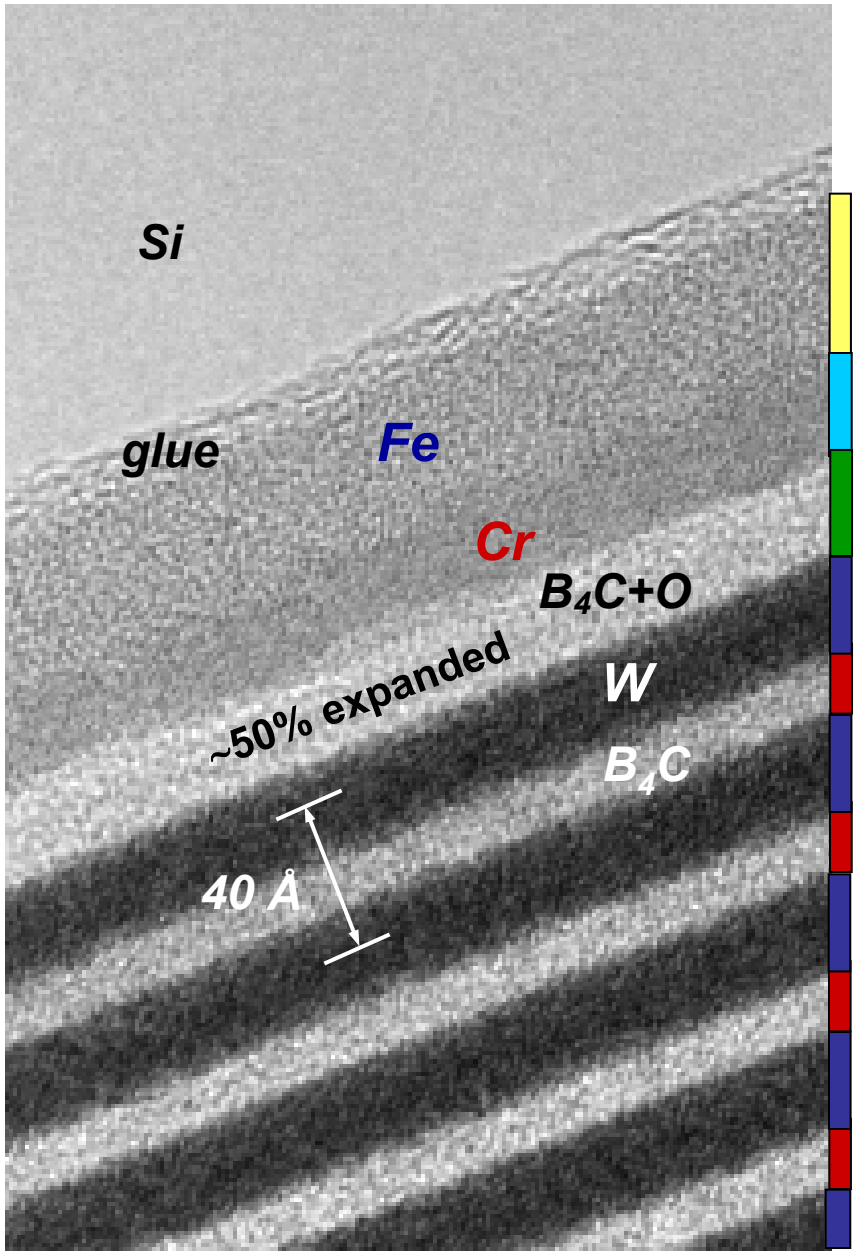

Experimental + Calculated Photoemission Yield Ratio I(Fe 3p)/I(Cr 3p) from Fe/Cr wedge on standing-wave multilayer

Sample pos'n. scan-- Standing wave scan

Sample angle scan-- Rocking curves

Sample angle scan → Rocking curves

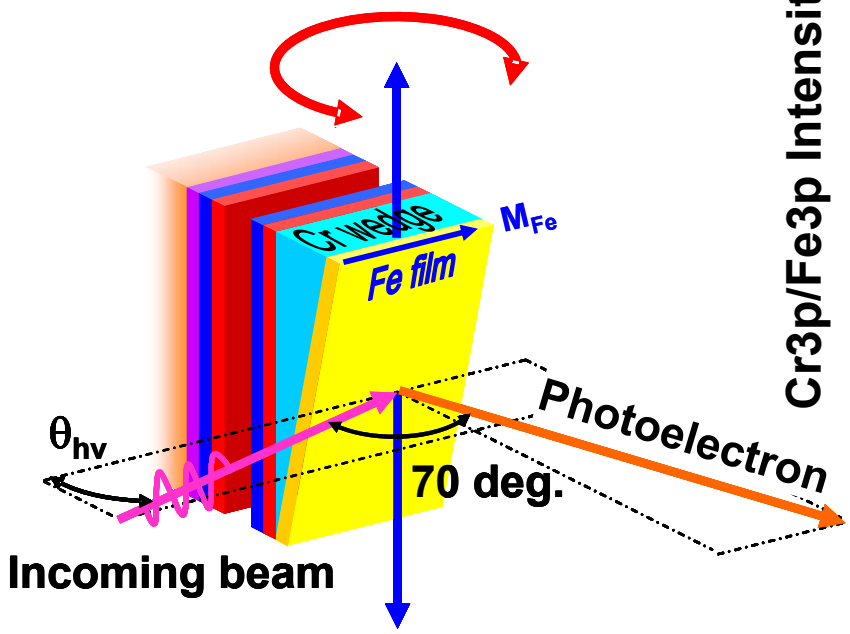

Sample position scan → Cr Thickness & Standing Wave Scan

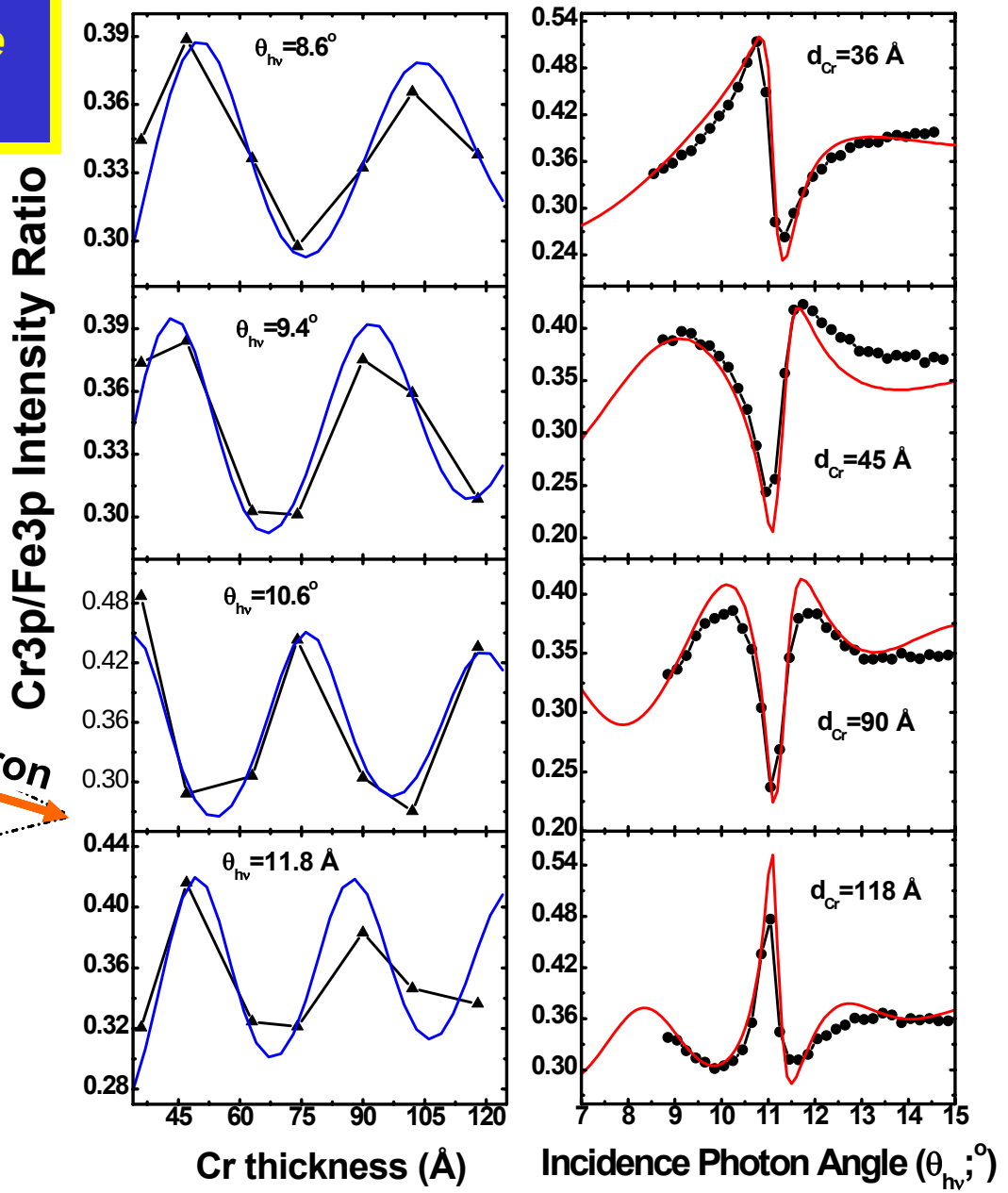

Cr magnetization Is antiparallel to Fe; systematic variation of MCD strengths vs d_{cr}

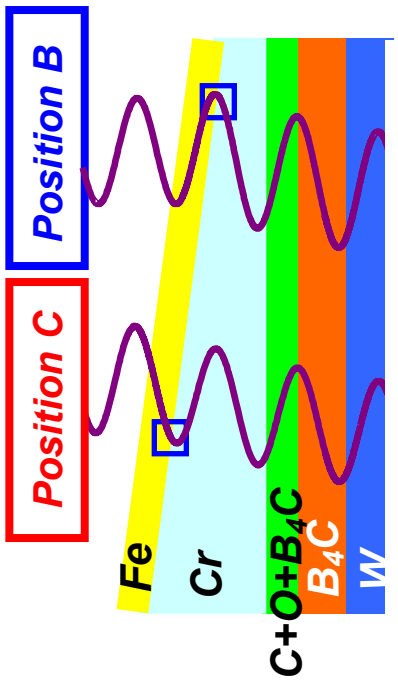

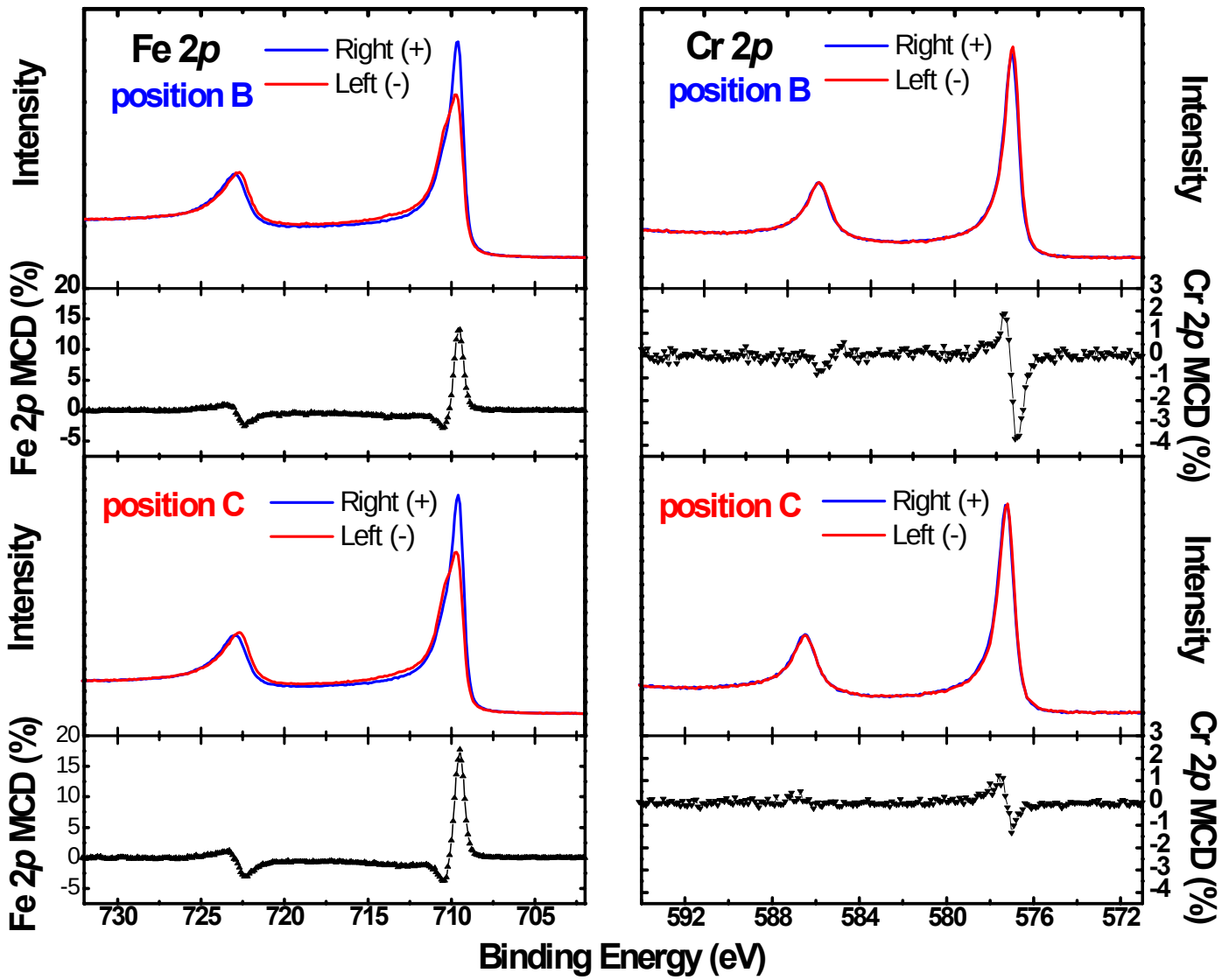

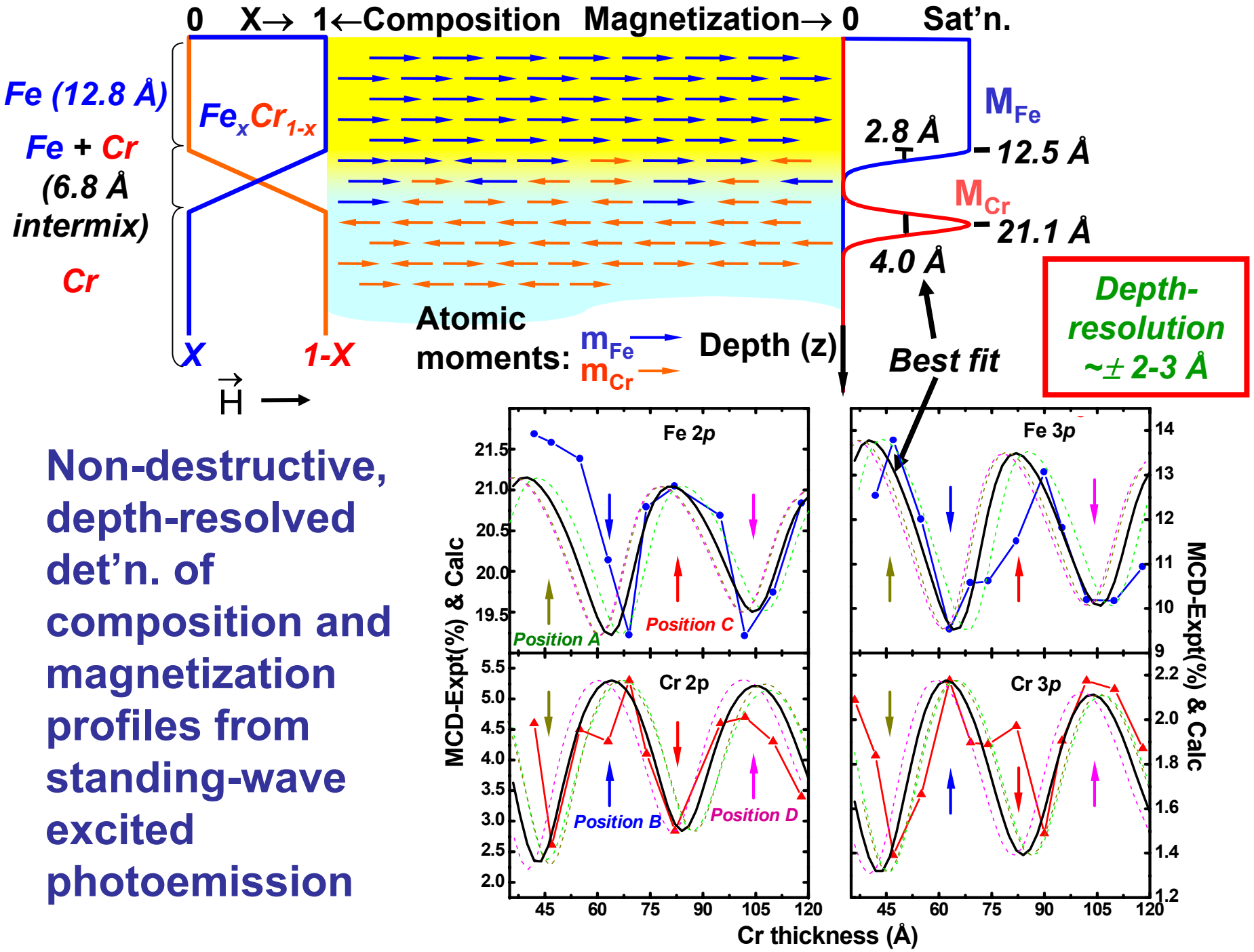

Non-destructive, depth-resolved det'n. of composition and magnetization profiles from standing-wave excited photoemission

Standing-Wave Excited Spectroscopy--Future Possibilities

- Other material pairs in multilayer (B_4C/W, Al_2O_3/Pt,…) + epitaxial multilayers → epitaxial samples
- Smaller periods (to ~25-30 Å) → smaller SW period, better resolution
- Lower $h\nu_{inc}$ →higher Bragg angles→perpend. component of M
- X-ray emission→ deeper layers, more sensitivity to SW position

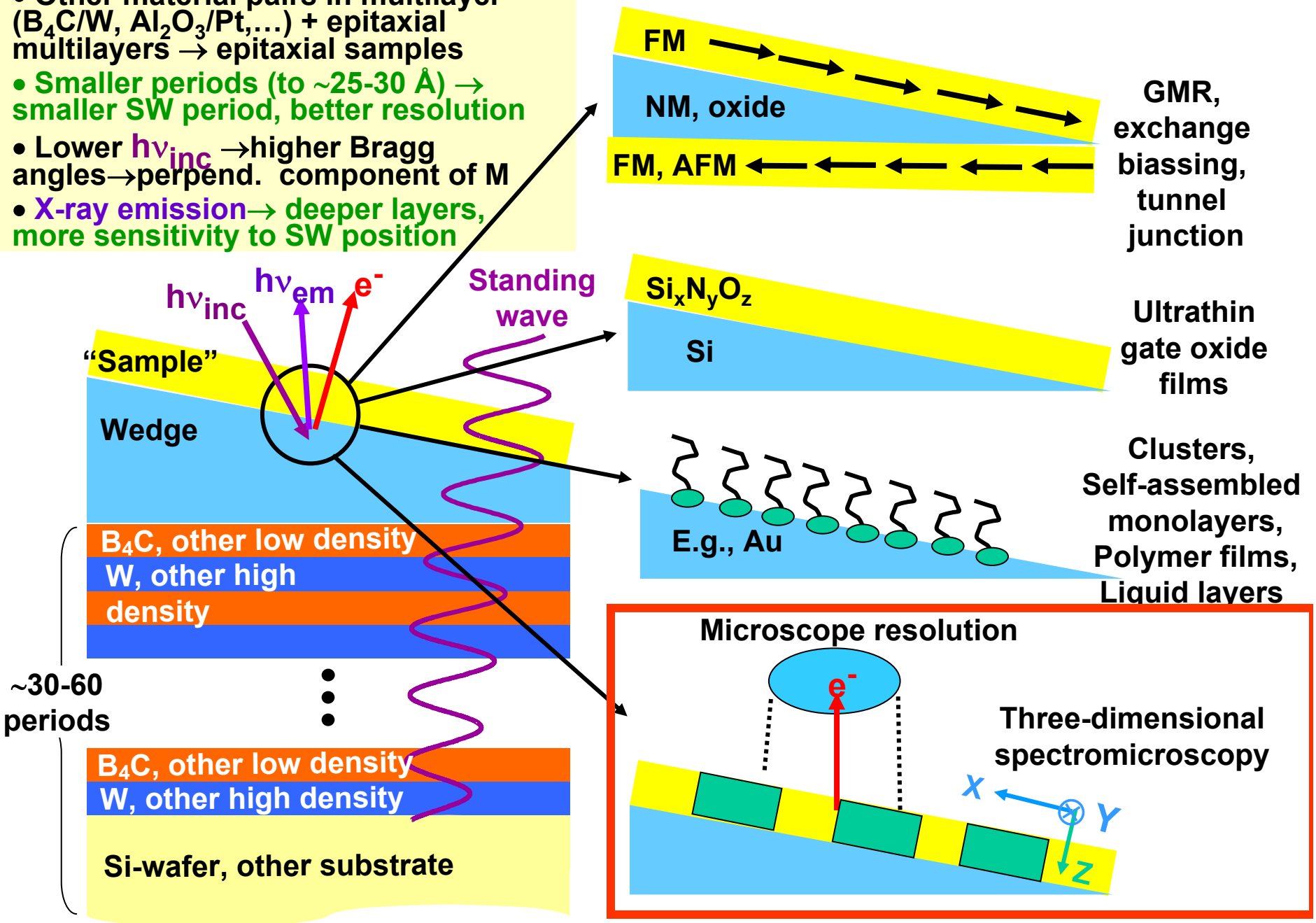

First observation of standing wave effects in a photoelectron microscope

Elmitec SP-PEEM—BESSY, Berlin

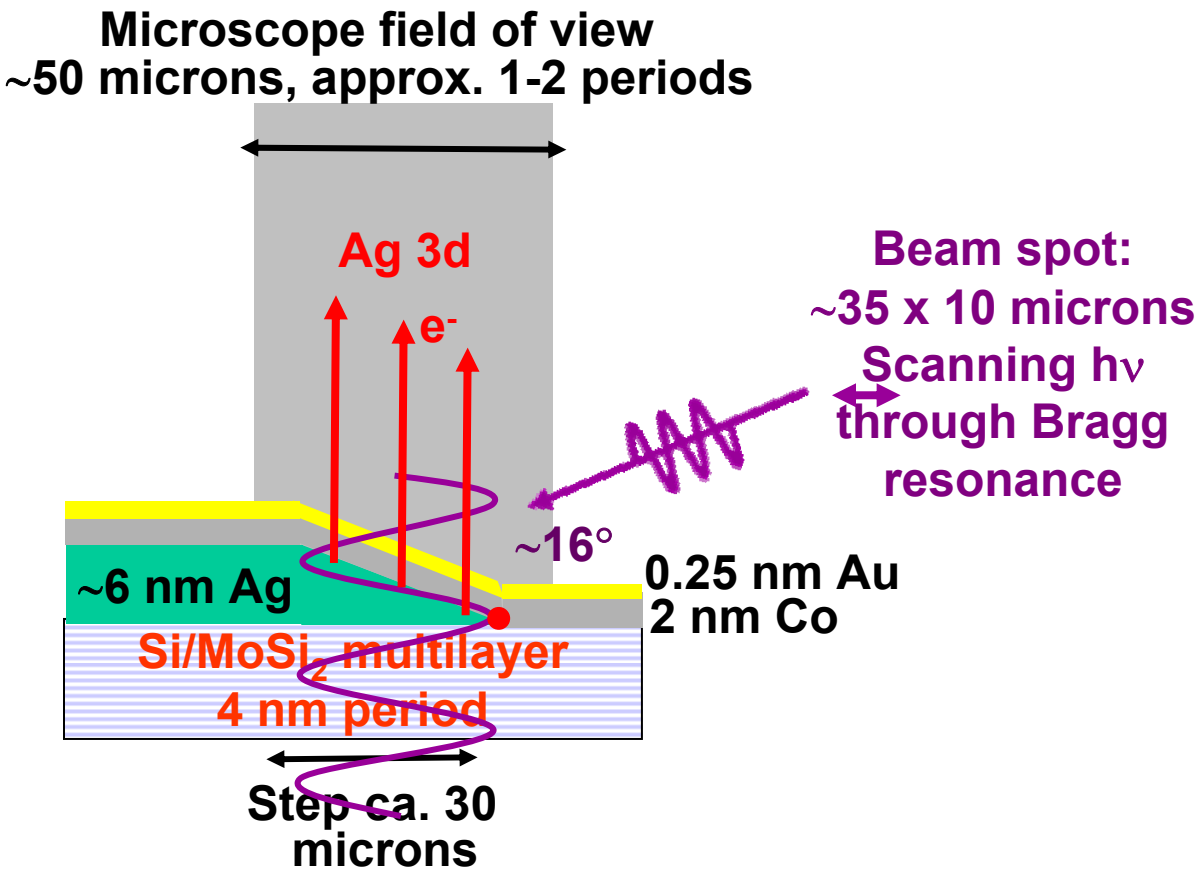

F. Kronast, H. Dürr, BESSY
D. Buergler, R. Scheiber,C. Schneider, Jülich CF

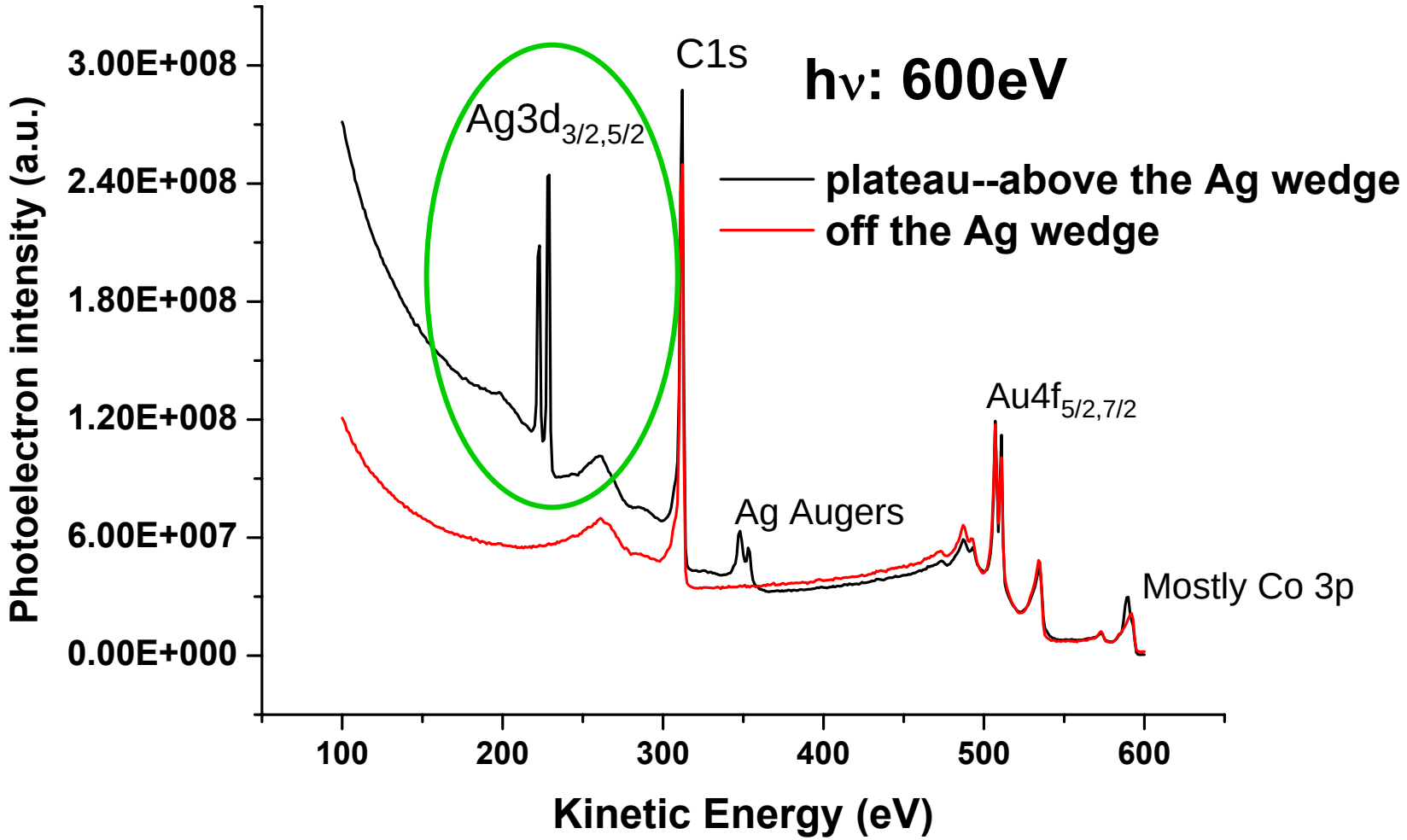
Photoelectron intensity (a.u.)
3.00E+008
2.40E+008
1.80E+008
1.20E+008
6.00E+007
0.00E+000
100
200
300
400
500
600
Kinetic Energy (eV)
Ag3d3/2,5/2
C1s
hν: 600eV
plateau--above the Ag wedge
off the Ag wedge
Au4f5/2,7/2
Ag Augers
Mostly Co 3p

Movie:
Ag 3*d* intenstity moving along the wedge while scanning over the Bragg energy

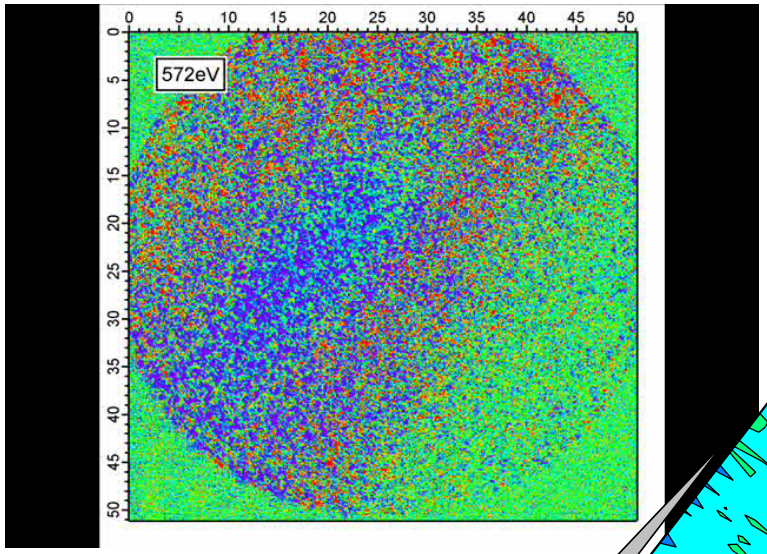

PEEM image of the Ag wedge (normalized Ag 3*d* intensity)

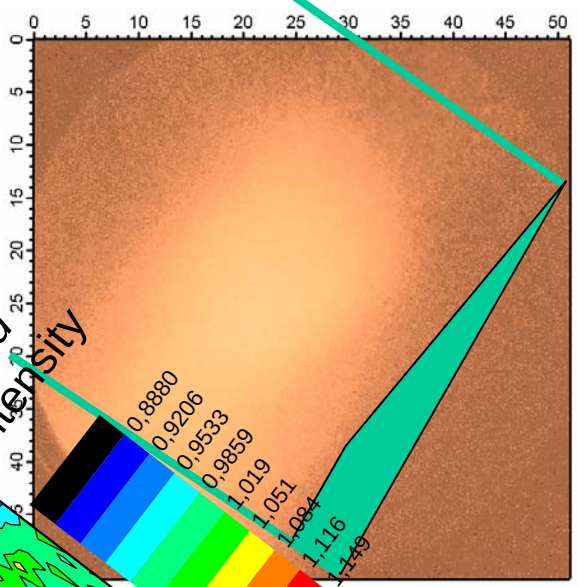

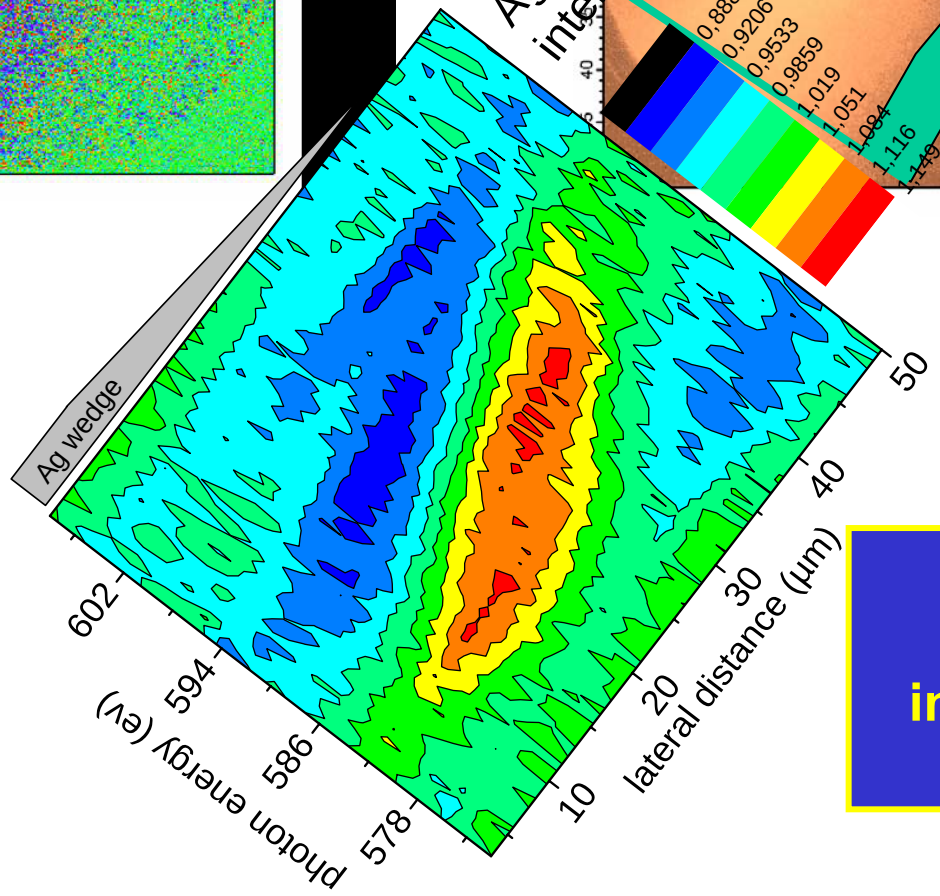

Standing wave effects in a photoelectron microscope

Outline

Surface, interface, and nanoscience—short introduction

Some surface concepts and techniques→photoemission

Synchrotron radiation: experimental aspects

Electronic structure—a brief review

The basic synchrotron radiation techniques:
more experimental and theoretical details

Core-level photoemission:
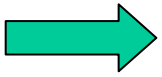
photoelectron (and x-ray fluorescence) holography

Valence-level photoemission

Microscopy with photoemission

CLASSIC OPTICAL HOLOGRAPHY:

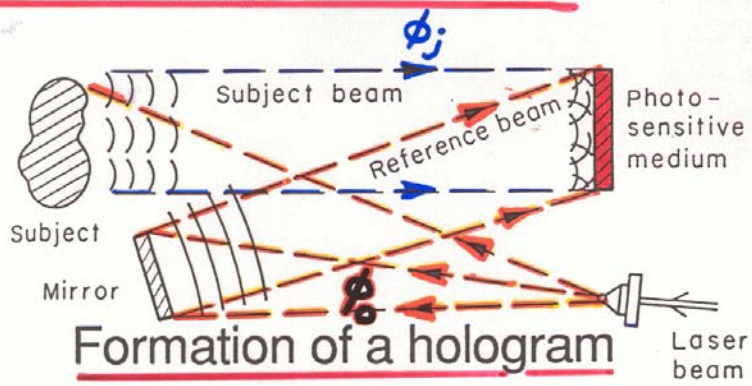

Formation of a hologram

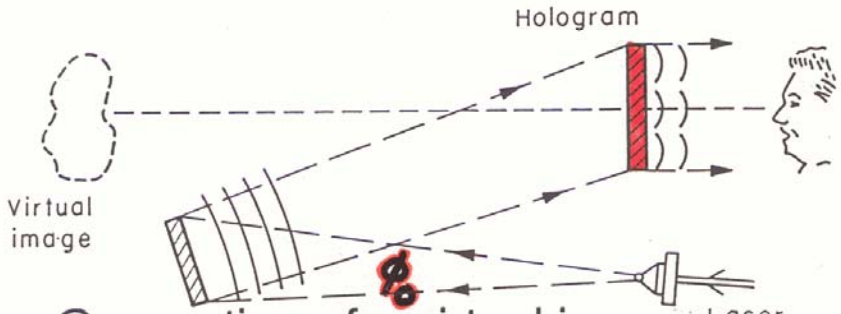

Generation of a virtual image

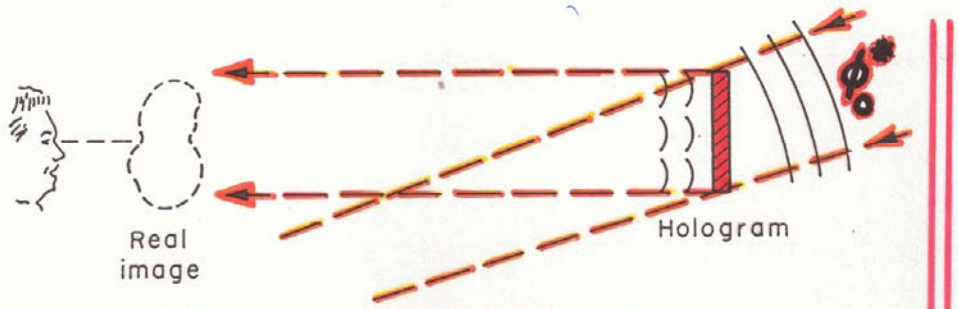

Generation of a real image

⇒ In electron emission holography, reference is outgoing spherical & conjugate is incoming spherical

Photoelectron diffraction→ holography: Element-specific short-range atomic structure

FORWARD SCATT. = "OTH ORDER" → **Bond & Low-Index Directions**

HIGHER ORDERS → **Bond Lengths & Atomic Positions**

→**Holographic fringes**

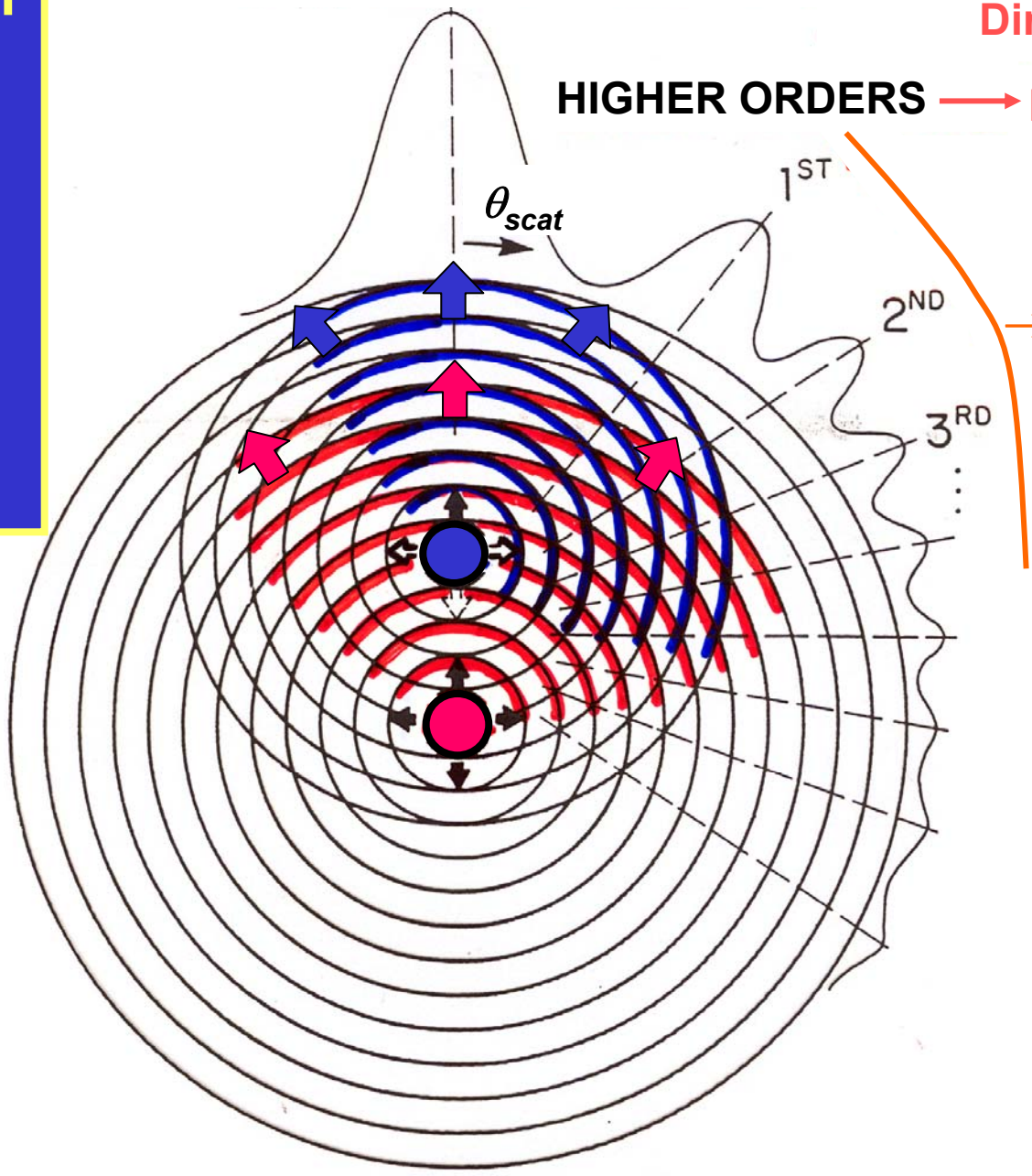

Principles of photoelectron and x-ray fluorescence holography:

(a) Inner source holography -direct:

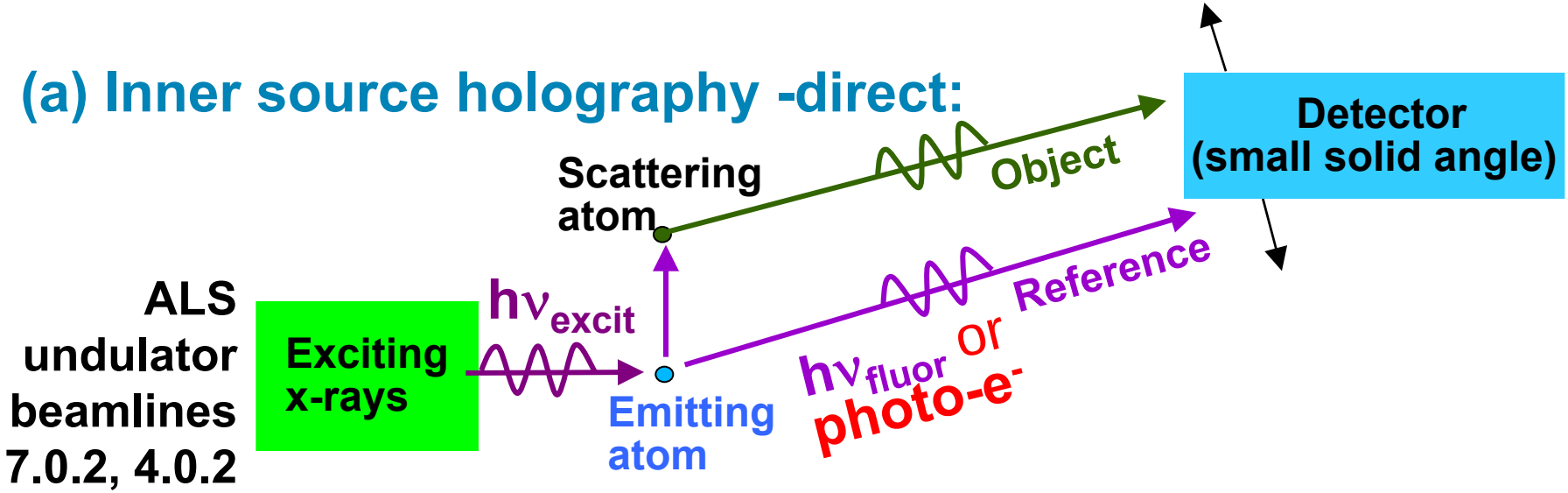

Recent overviews:
G. Faigel and M. Tegze, Rep. Prog. Phys. 62, 355 (1999)
Adams et al., Phys. Stat. Sol. (b) 215, 757 (1999)
C.S.F., M.A Van Hove, et al., J. Phys. B Cond. Matt. 13, 10517 (2001)

The basic imaging ideas
(Gabor; Helmholtz-Kirchoff; Wolf; Szöke; Barton-Tong)

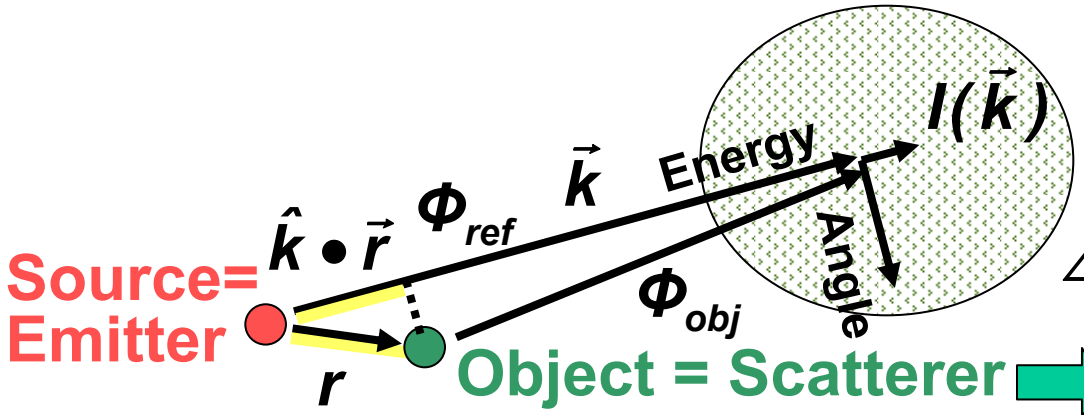

$k = 2\pi/\lambda$

3D sampled region:

$\Delta k_x \times \Delta k_y \times \Delta k_z$

Resolution:

$\Delta x \approx 1/\Delta k_x$

$\Delta y \approx 1/\Delta k_y$

$\Delta z \approx 1/\Delta k_z$

Phase difference between Φ_{ref} and $\Phi_{obj} = \vec{k} \bullet \vec{r} - kr$

$$I(\vec{k}) = \left|\Phi_{ref}(\vec{k}) + \Phi_{obj}(\vec{k})\right|^2$$

Holographic interference

$$= \left|\Phi_{ref}(\vec{k})\right|^2 + \left[\Phi_{ref}^{*}(\vec{k})\Phi_{obj}(\vec{k}) + \Phi_{ref}(\vec{k})\Phi_{obj}^{*}(\vec{k})\right] + \left|\Phi_{obj}(\vec{k})\right|^2$$

$$Hologram: \quad \chi(\vec{k}) = \frac{I(\vec{k}) - I_0}{I_0} = \frac{I(\vec{k}) - \left|\Phi_{ref}(\vec{k})\right|^2}{\left|\Phi_{ref}(\vec{k})\right|^2}$$

Weak, ~isotropic scattering, no phase shift

Holographic image:

$$U(\vec{r}) = \left|\iiint \chi(\vec{k}) \exp[i\vec{k} \bullet \vec{r} - ikr]\, d^3k\right|$$

(Usual phase problem)

Inside-source PH-first adsorbate: S/Ni(100)

Typical S emitter
$h\nu$ = 1486.6 eV→
E_{kin} = 1327 eV

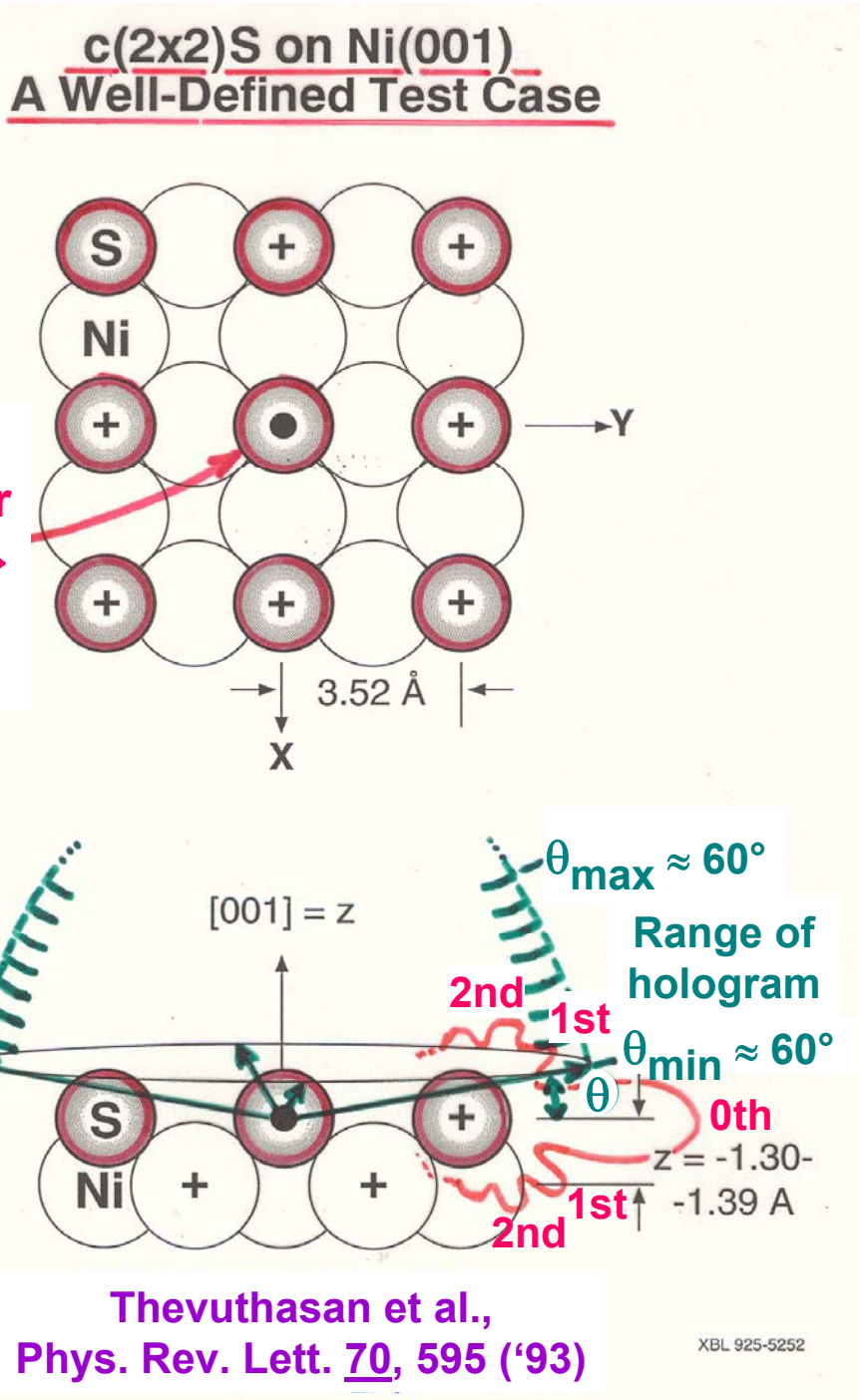

Thevuthasan et al.,
Phys. Rev. Lett. 70, 595 ('93)

Holograms: S/Ni(001)

Experiment

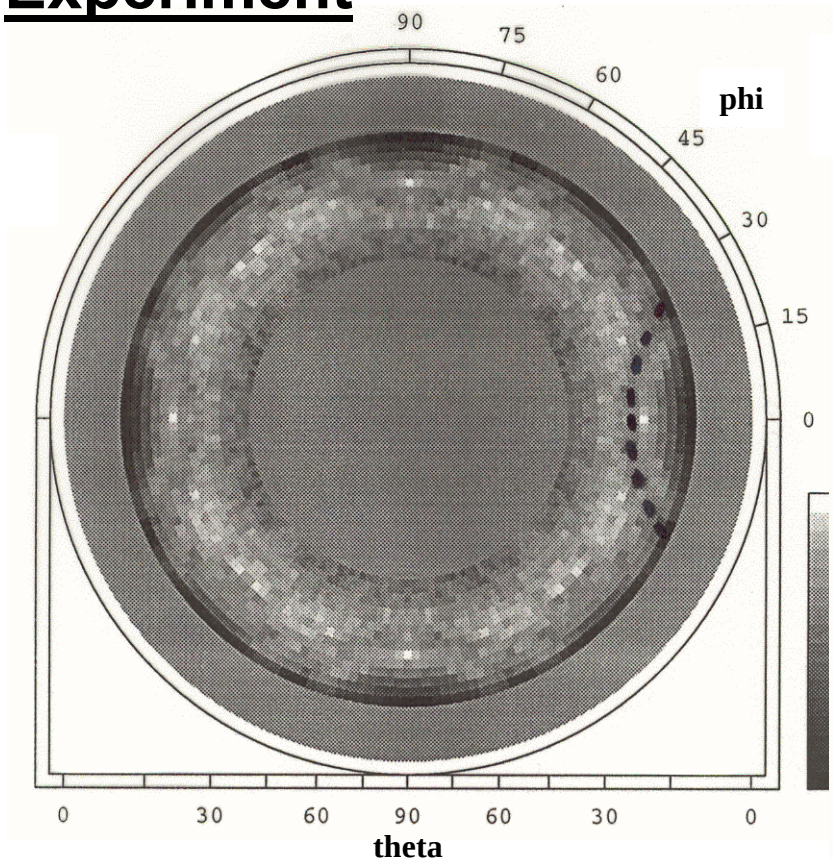

Theory

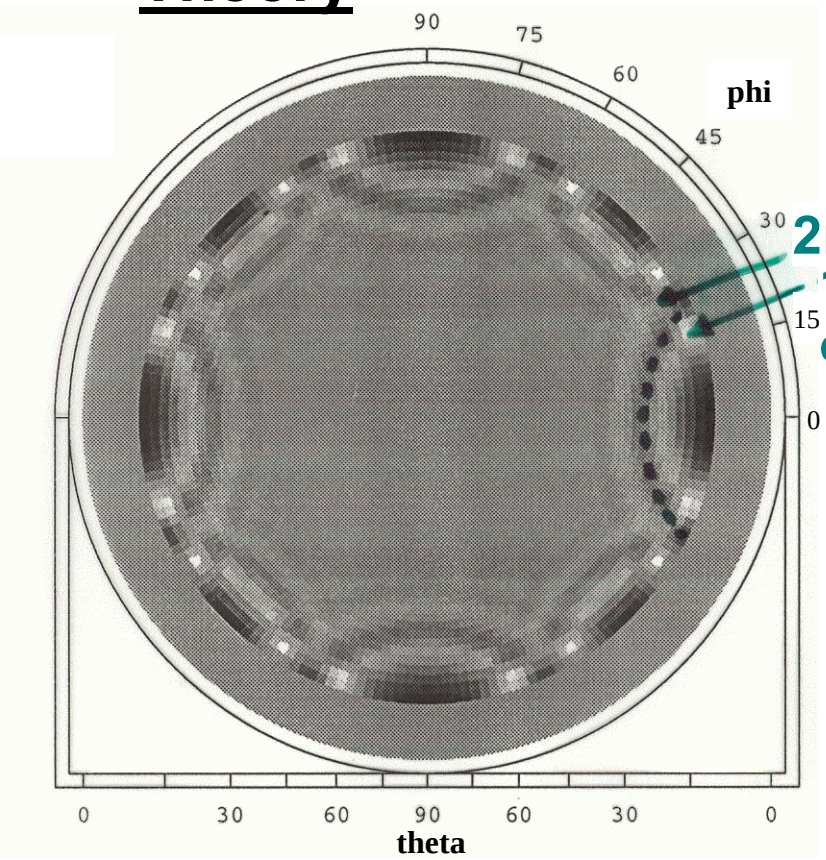

Holographic Images: S/Ni(001)

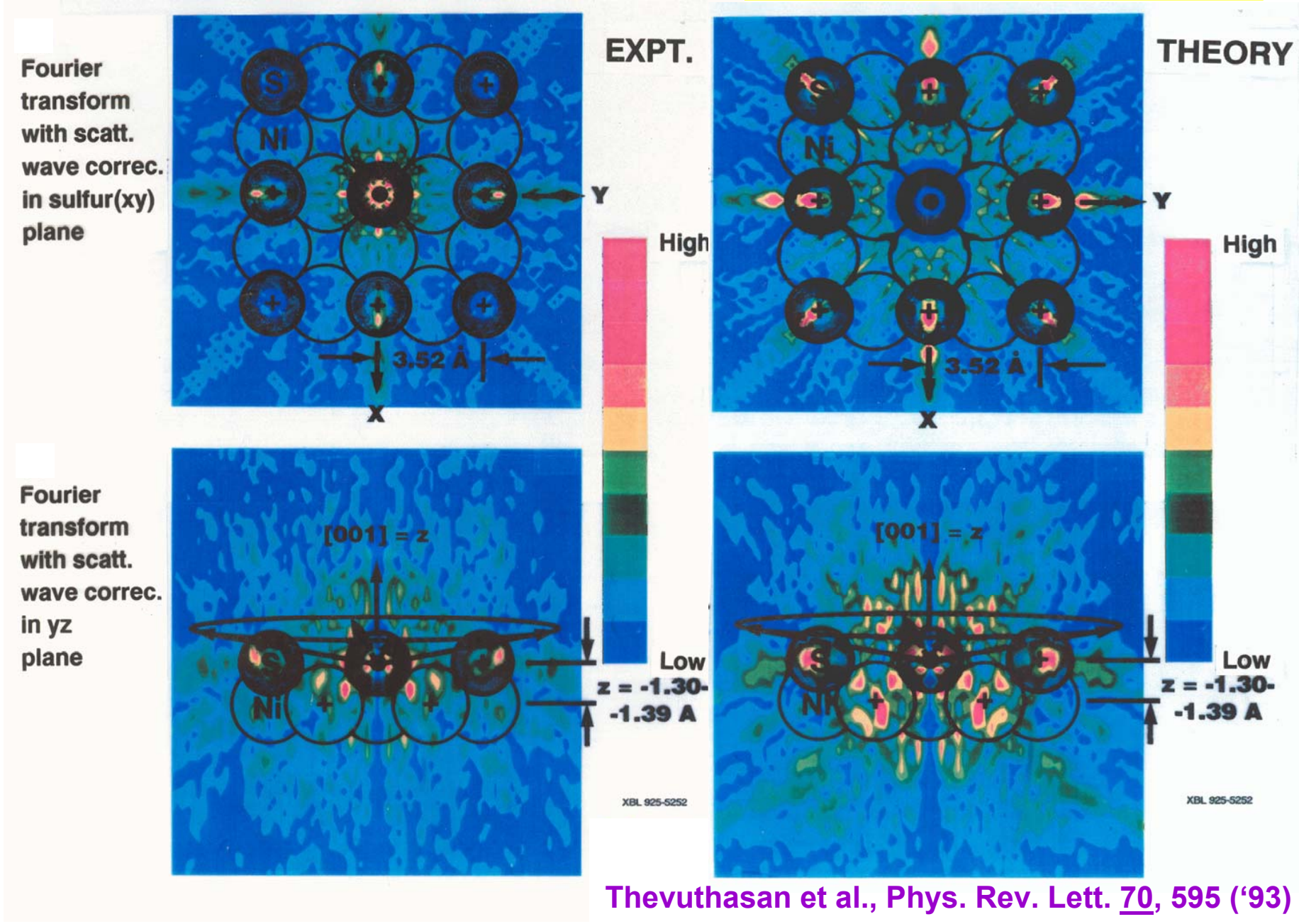

Thevuthasan et al., Phys. Rev. Lett. 70, 595 ('93)

Derivative photoelectron holography: As and Si emission from As/Si(111):

$$U(\vec{r}) = \left| \iiint \chi(\vec{k}) \exp[i\vec{k}\cdot\vec{r} - ikr]\, d^3k \right|$$

$$\text{with } \chi = \frac{I(\vec{k}) - I_0}{I_0}$$

and $I(\vec{k})$ from int egration of log arithmic derivative

$$L(h\nu, \hat{k}) = \frac{I(h\nu + \delta, \hat{k}) - I(h\nu - \delta, \hat{k})}{\left[I(h\nu + \delta, \hat{k}) + I(h\nu - \delta, \hat{k}) \right] \delta}$$

$$I(\vec{k}) \equiv I(k, \hat{k}) = A \int L(h\nu, \hat{k}) d^3k$$

Luh, Miller, Chiang, PRL 81, 4160 (1998)

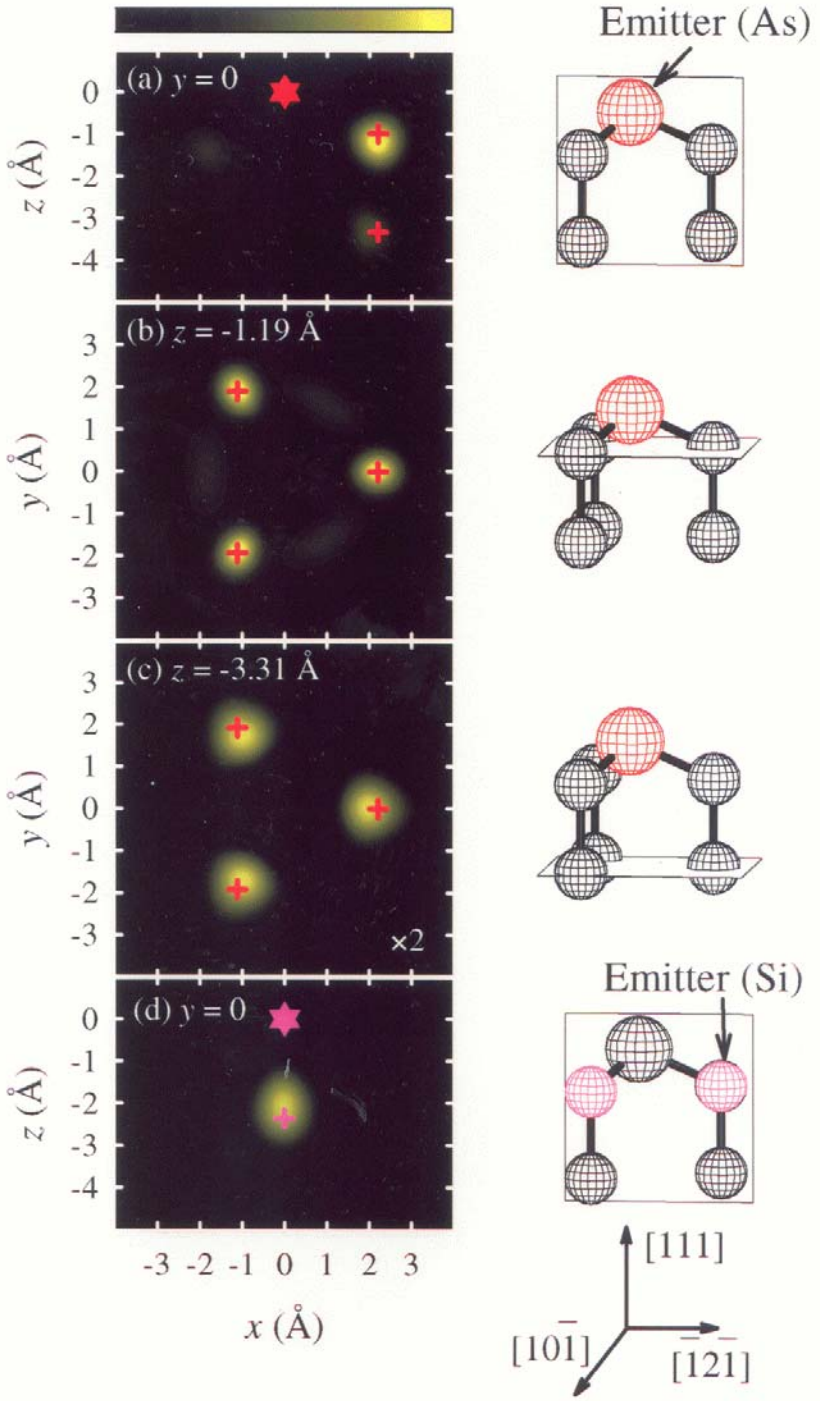

Single-atom holograms

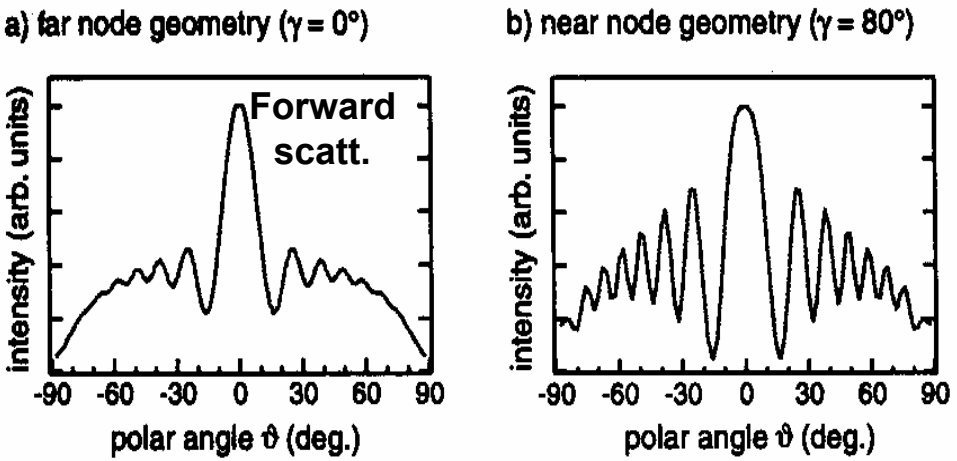

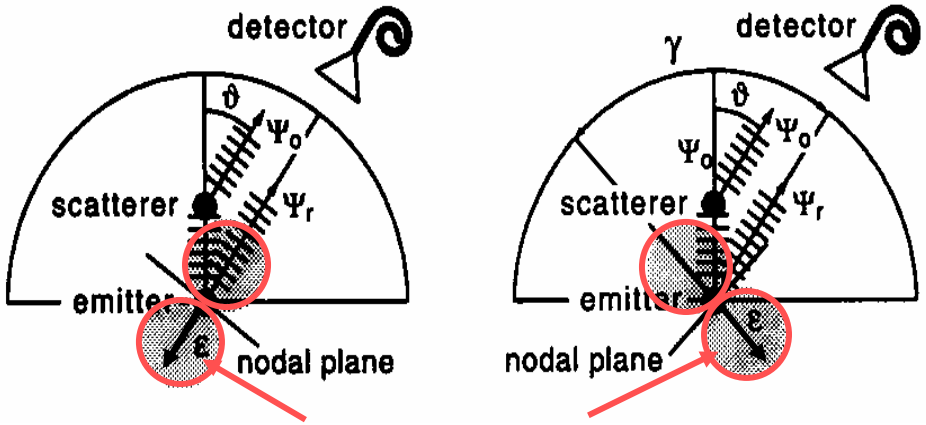

$$M(\vec{k},\vec{r}) \propto \sqrt{\text{photoe}^- \text{ cross sec.}} = \hat{\varepsilon}\bullet\hat{k}$$

Wider et al. PRL
86, 2337 (2001)

Near-node photoelectron holography: Al 2s emission from Al(111)

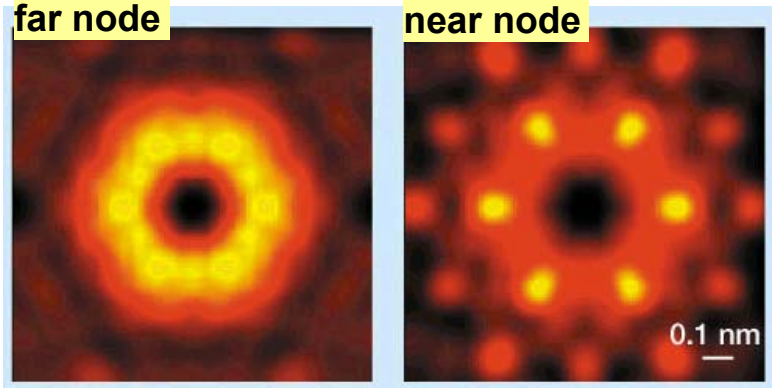

Images around
typical Al emitter

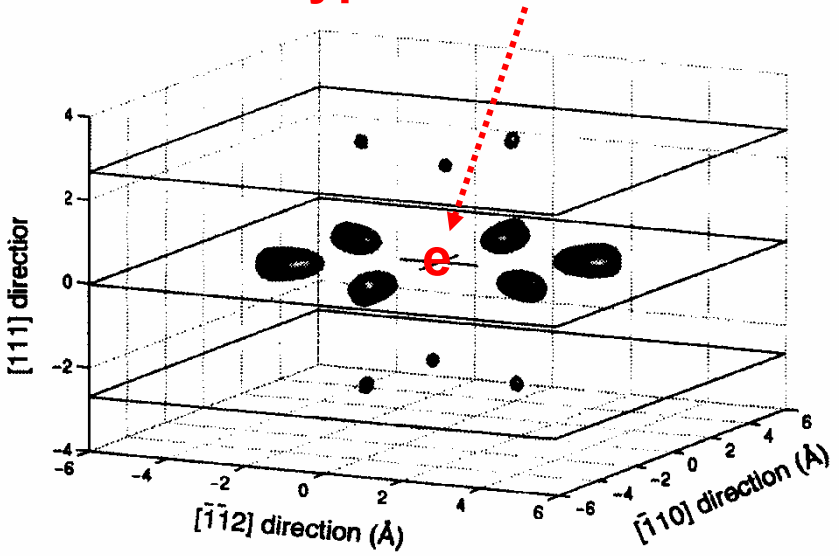

Cu 3p-Cu(001)-- differential photoelectron holography

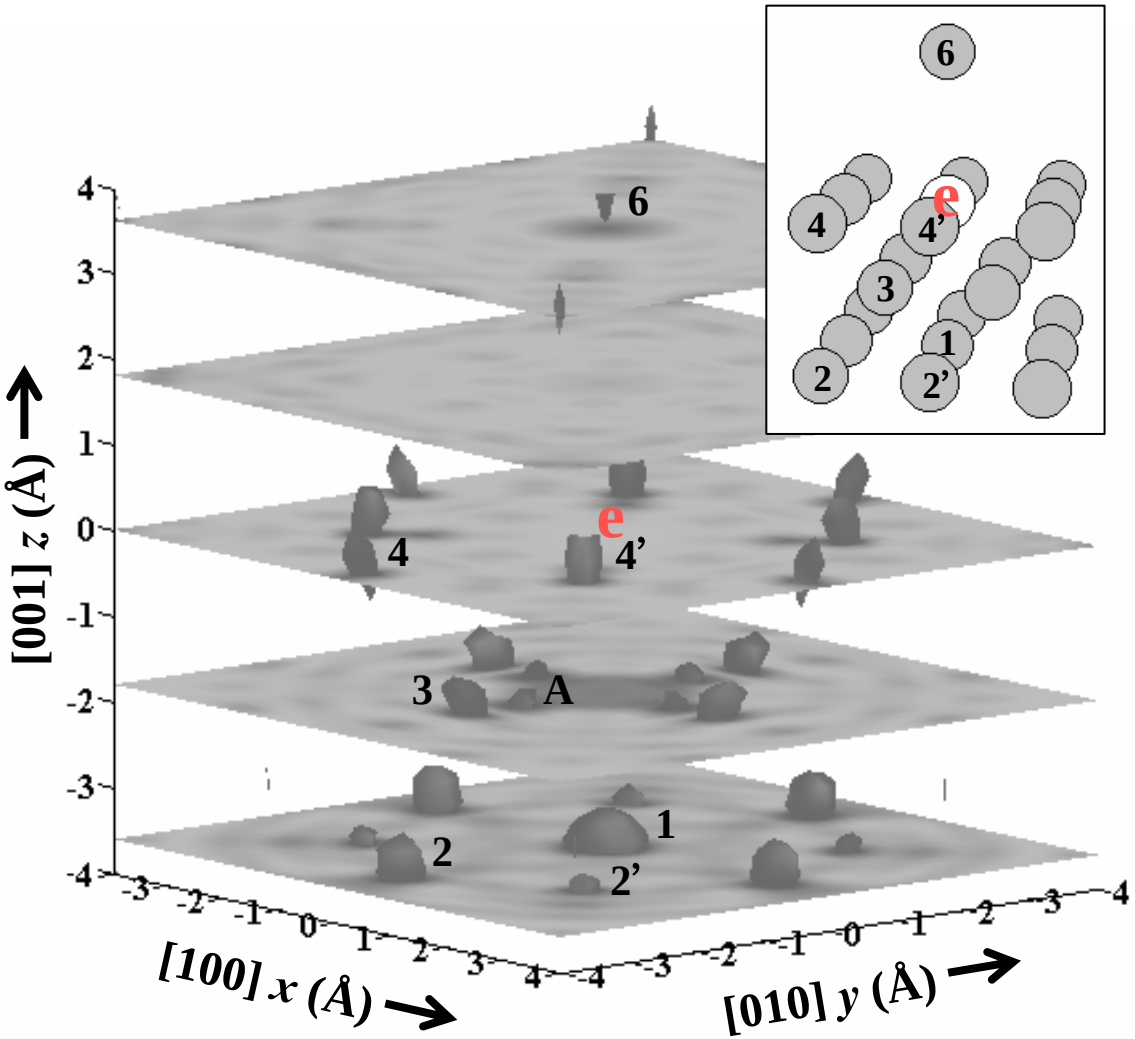

Imaging of back, side, (and fwd.) scattering atoms
(Omori et al., PRL 88, 055504 ('02) and
animations at http://electron.lbl.gov/marchesini/dph)

Principles of photoelectron and x-ray fluorescence holography:

(a) Inner source holography -direct:

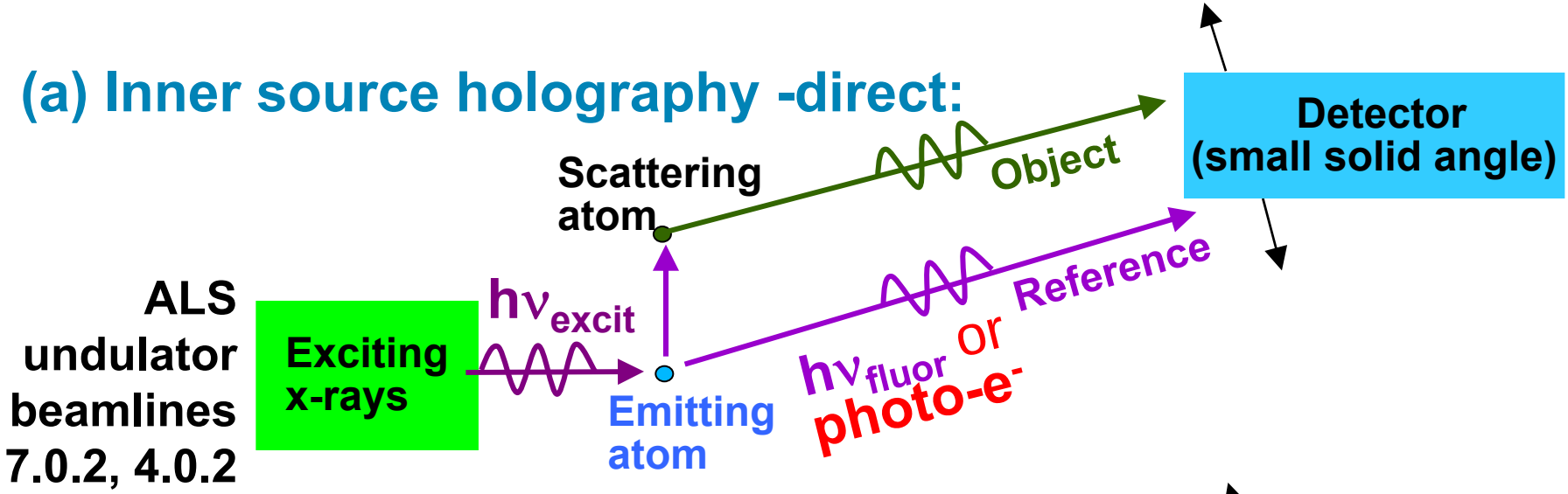

(b) Inner detector holography-inverse:

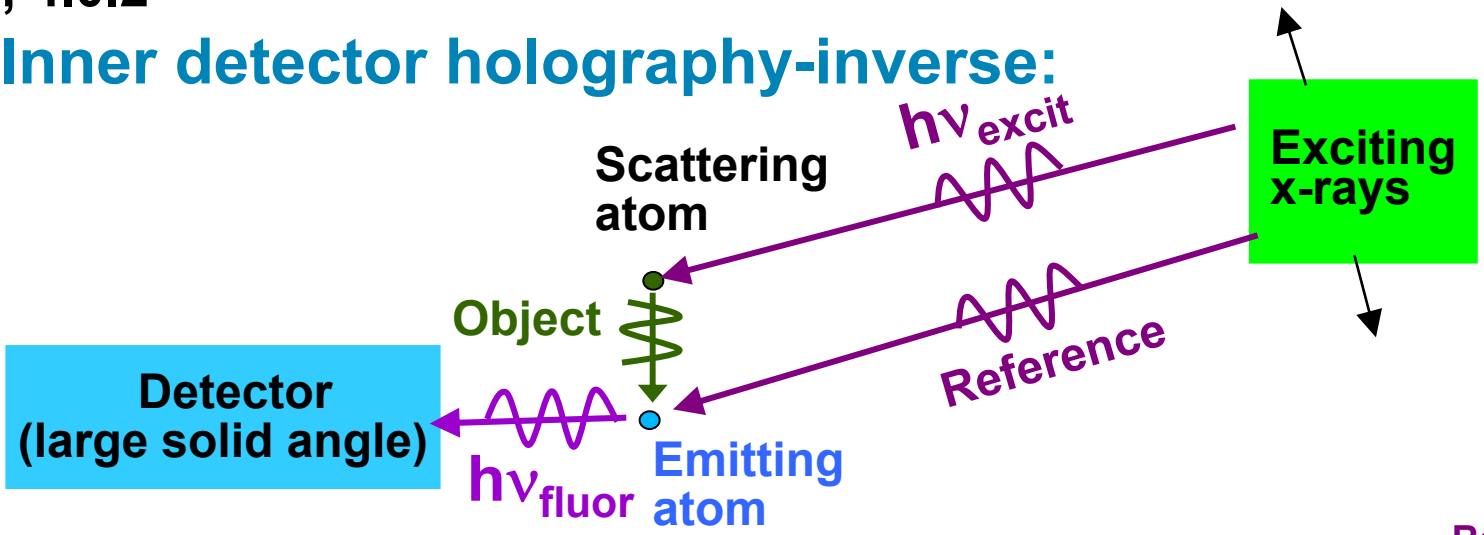

Recent overviews:
G. Faigel and M. Tegze, Rep. Prog. Phys. 62, 355 (1999)
Adams et al., Phys. Stat. Sol. (b) 215, 757 (1999)
C.S.F., M.A Van Hove, et al., J. Phys. B Cond. Matt. 13, 10517 (2001)

Inside-source XFH--the first experiment:

$SrTiO_3$ (100) sample
Mo x-ray tube
Excitation of Sr Kα
@ 14.1 keV with
Mo Kα @ 17.4 keV
Approx. 2 months
data accumulation
10^{10} photons counted
over 2400 pixels in θ , ϕ

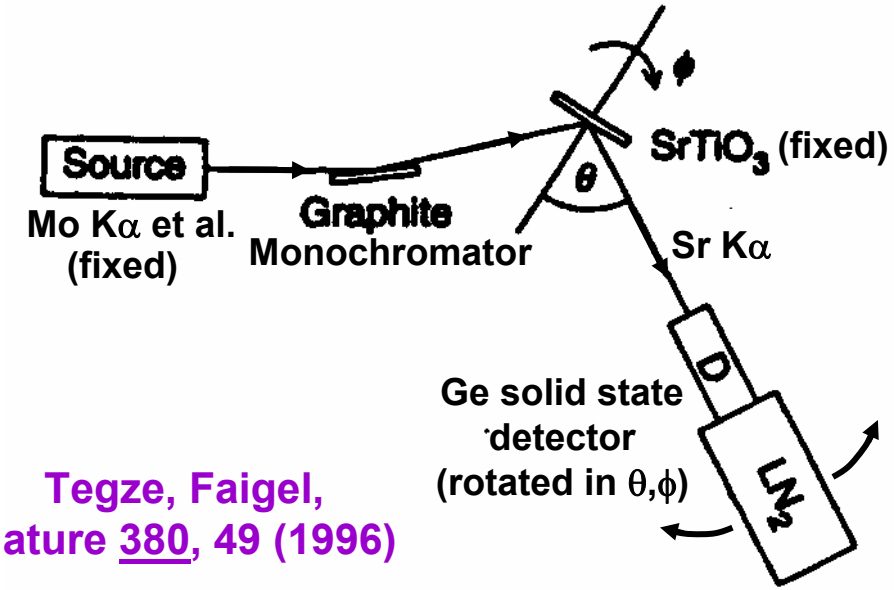

Tegze, Faigel,
Nature 380, 49 (1996)

Symmetrized

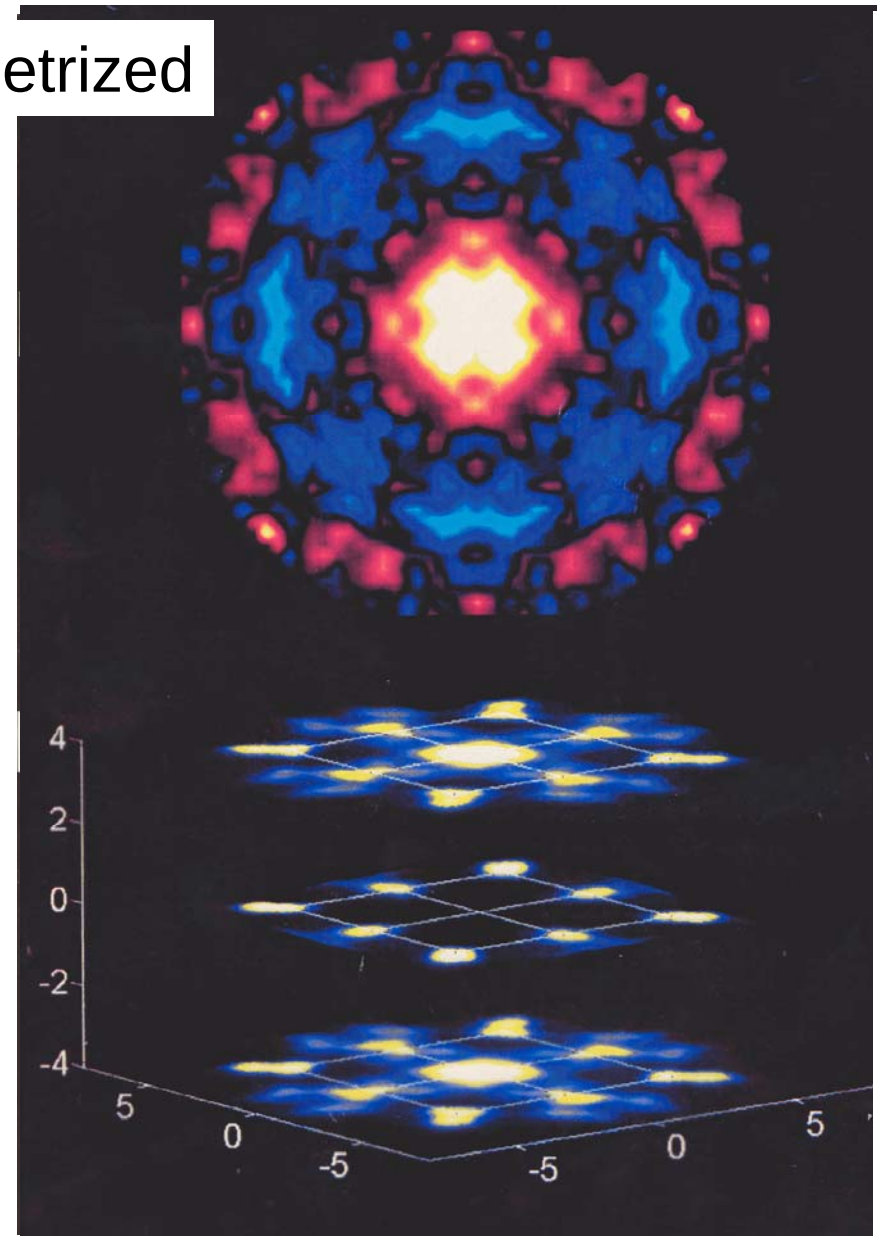

Inside-detector XFH--the first experiment:

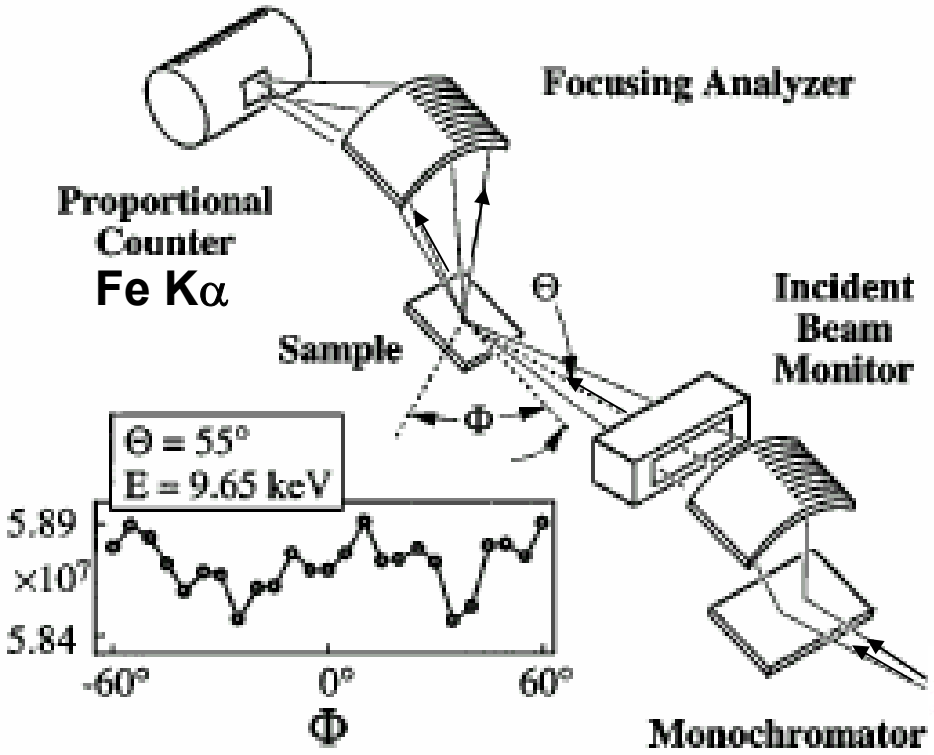

$$\frac{\Delta I}{I_0} \approx 0.5\ \%$$

Gog et al. PRL 76, 3132 (1996)

Images of Fe_2O_3

Can be multi-energy→ "MEXH"

Resolution much worse in perpendicular plane:

$$\Delta k_x = \Delta k_y >> \Delta k_z$$

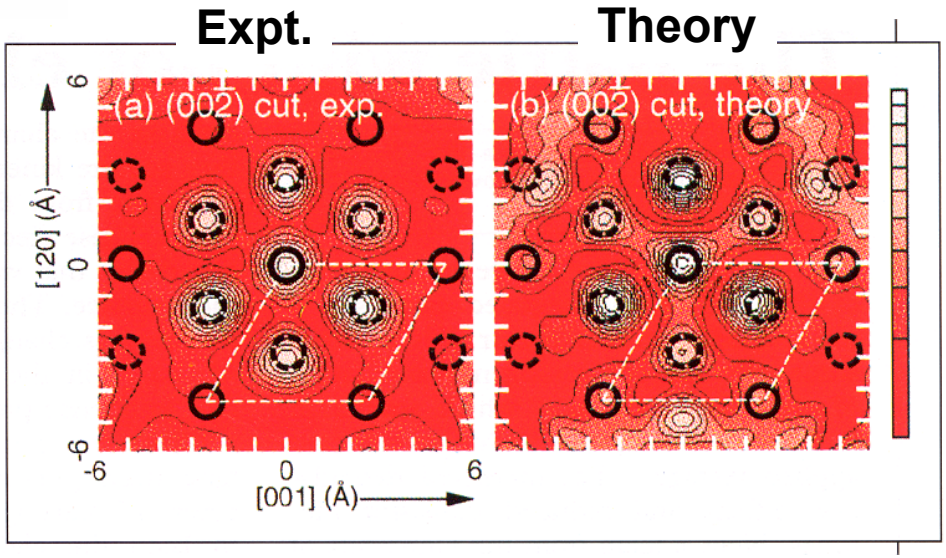

XFH at ESRF: CoO(111)

Inside source:
hν = 6.92 keV

Inside detector:
hν = 13.86 keV

Multi-energy transform

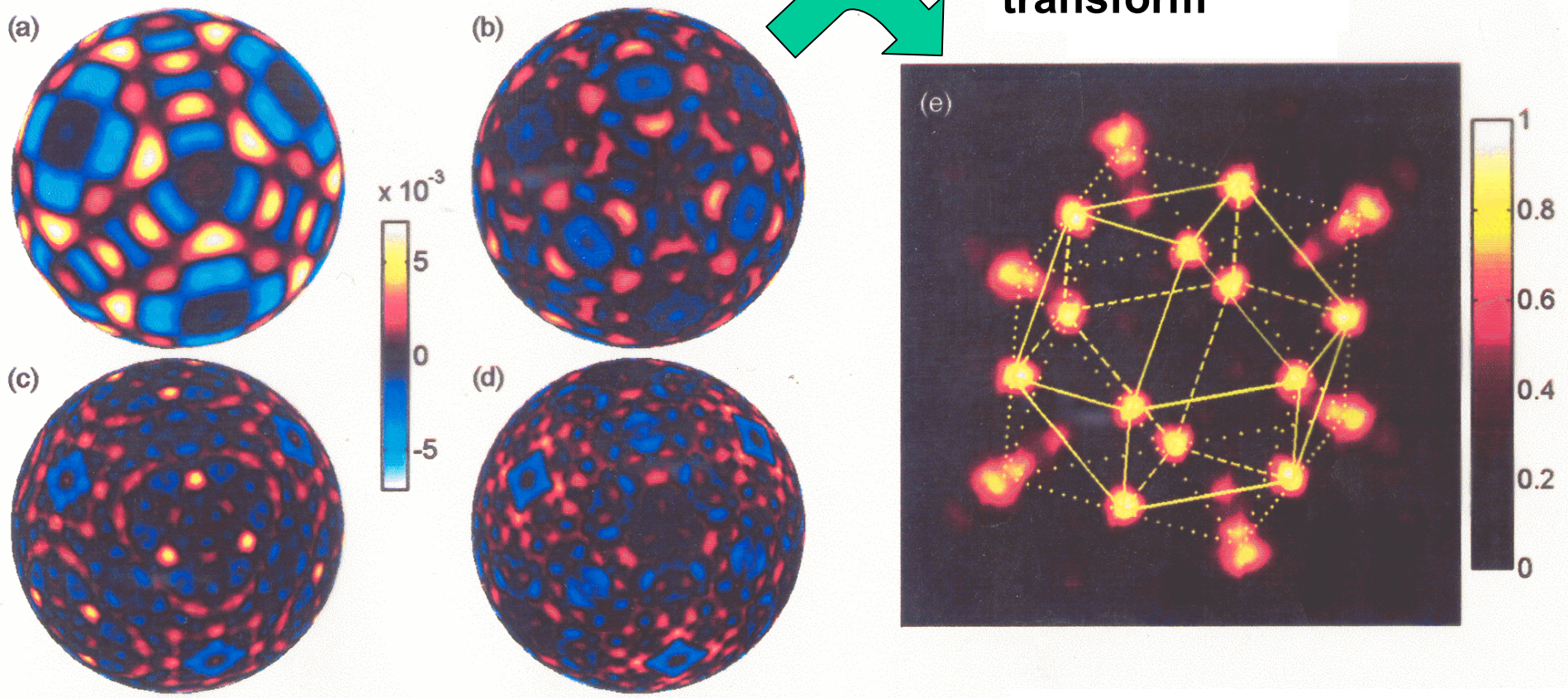

Inside detector:
hν = 17.44 keV

Inside detector:
hν = 18.92 keV

Tegze, Faigel, Marchesini et al.,
Phys. Rev. Lett. 82, 4847 ('99)

Multi-Energy Inside-Detector X-Ray Holography of NiO

Full hologram with Kossel lines

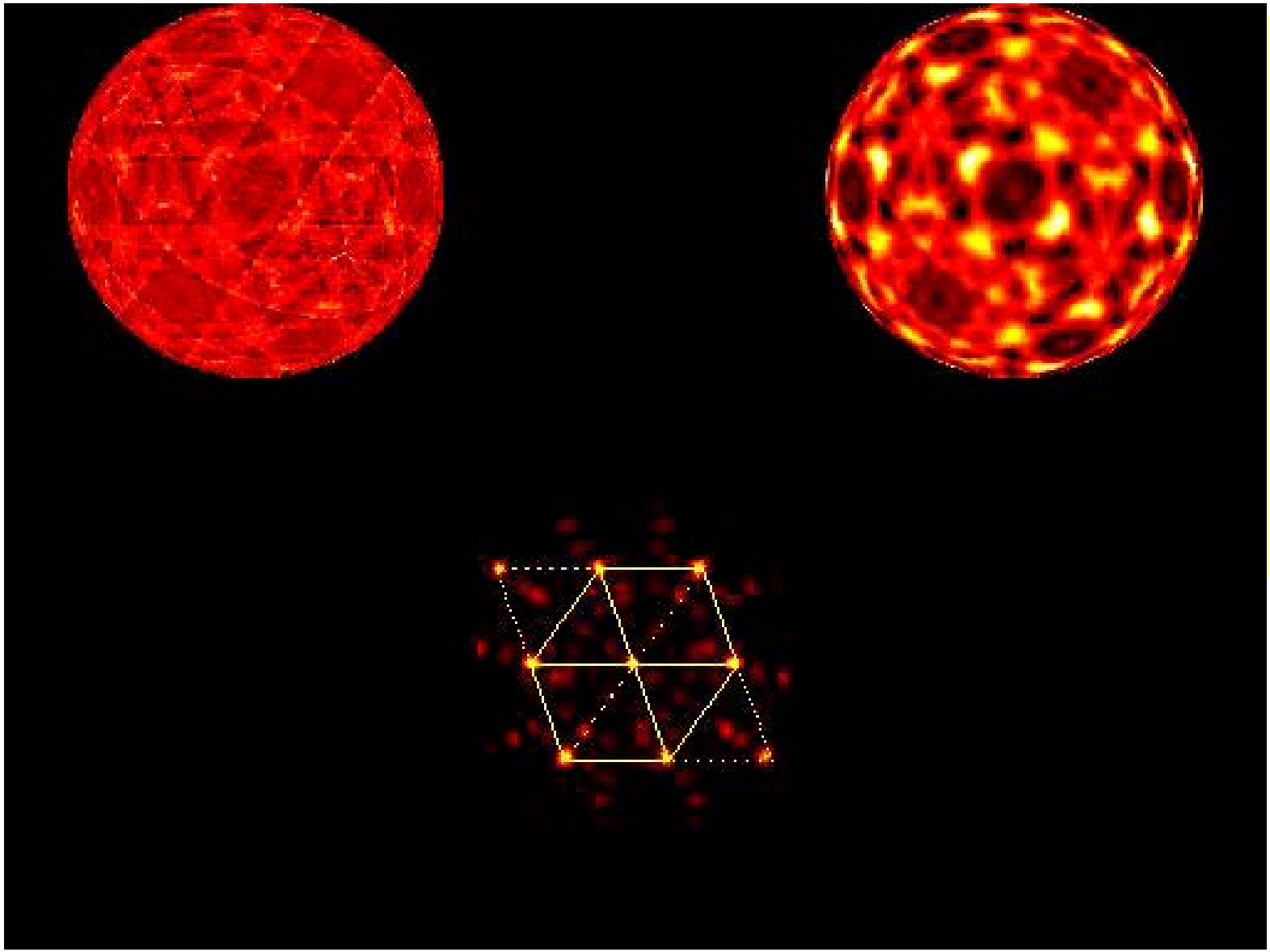

Smoothed hologram →short-range structure

Ni and weaker O images

Marchesini et al., Nature 407, 38 (2000)

XFH at ESRF: some highlights

Imaging light atoms:
Nature 407, 38 (2000)

- **O around Ni in NiO**
- **~150 O and Ni atoms imaged**

Inside detector-
Ni Kα Hologram

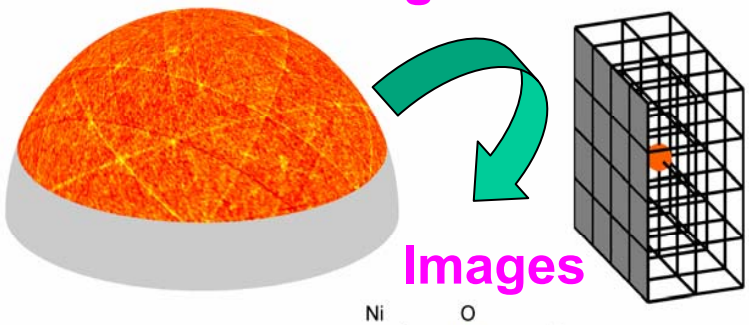

Images

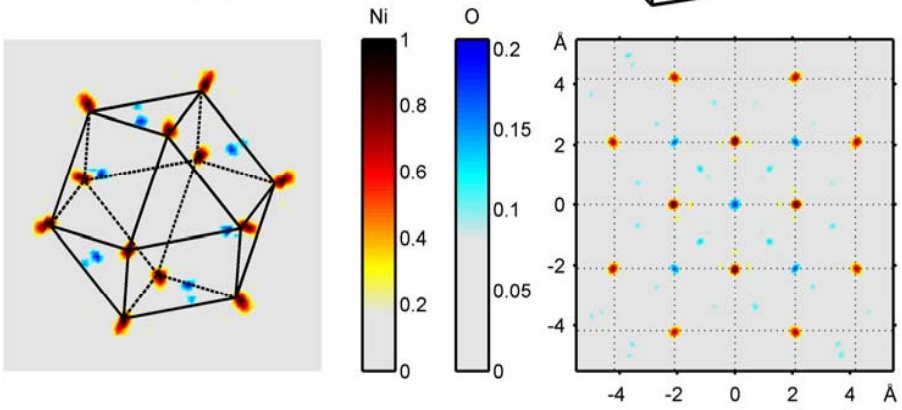

Imaging a quasicrystal:
Phys. Rev. Lett. 85, 4723 (2000)

- **method works without true periodicity**
- **neighbors around Mn in MnAlPd**
- **image of average atomic distribution**

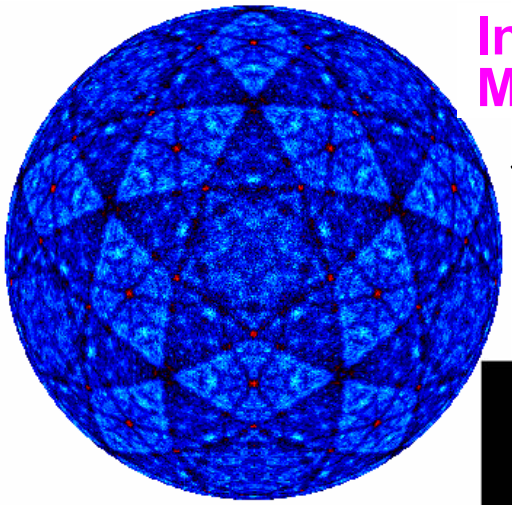

Inside detector-
Mn Kα Hologram

Image